QUATERNARY GEOLOGY OF HOWARD'S PASS AND APPLICATIONS TO DRIFT PROSPECTING

by

Derek G. Turner
B.Sc., University of Victoria, 2005

THESIS SUBMITTED IN PARTIAL FULFILLMENT OF
THE REQUIREMENTS FOR THE DEGREE OF

MASTER OF SCIENCE

In the
Department of Earth Sciences

SIMON FRASER UNIVERSITY

Fall, 2008

APPROVAL

Name: **Derek Glen Turner**

Degree: **Master of Science**

Title of Thesis: **Quaternary Geology of Howard's Pass and Applications to Drift Prospecting**

Examining Committee:

Chair: _____

Dr. James A. MacEachern
Associate Professor of Earth Sciences

_____

Dr. Brent C. Ward
Senior Supervisor
Associate Professor of Earth Sciences

_____

Mr. Jeffery D. Bond
Supervisor
Surficial Geologist, Yukon Geological Survey

_____

Dr. Lionel E. Jackson Jr.
Supervisor
Quaternary Geologist, Geological Survey of Canada

_____

Dr. Victor M. Levson
External Examiner
Quaternary Geologist, British Columbia Ministry of Energy, Mines and Petroleum Resources

Date Defended/Approved: August 6th, 2008 _____

ABSTRACT

The Quaternary geology of Howard's Pass was studied by creating a 1:50 000-scale terrain inventory map of the area and examining the ice-flow history of the region. Four stages of ice flow occurred in Howard's Pass during the late Wisconsinan McConnell glaciation. The first stage is marked by ice growth from local cirques. During the second stage, an ice divide developed east of the Nahanni River, with ice flowing southwest across Howard's Pass. During continued ice sheet growth in stage 3, the ice divide either migrated or a second divide grew to the southwest in the Logan Mountains and ice flowed northward across the study area. Stage 4 is marked by deglaciation and topographically controlled ice-flow. This last phase of ice-flow is the most important for drift prospecting in the valley bottoms. Conversely, drift transport directions at higher elevation are likely remnant from earlier stages of ice-flow. To investigate the potential of till and mobile-metal-ion geochemistry for drift prospecting in Howard's Pass, a survey was conducted over a known deposit. The promising results from this survey suggest that these are possible tools for future exploration in other drift-covered areas of Howard's Pass.

Keywords: Drift prospecting; Quaternary stratigraphy; Ice-flow history; Terrain inventory mapping; MMI geochemistry; Terrestrial cosmogenic nuclides

DEDICATION

This thesis is dedicated to the memories of my father, Ralph Turner, and my friend, Geoff Bradshaw. Both were inspirations and are deeply missed.

ACKNOWLEDGEMENTS

First, I would like to thank Selwyn Resources Ltd. for their support in all aspects of the work. Without their help, this project would have been impossible. Next, a special thank you to Dr. Brent Ward and Mr. Jeffrey Bond. Their guidance, patience and encouragement were essential to the project and have made me a better researcher. My other committee member, Dr. Lionel Jackson, and my external examiner, Dr. Vic Levson, made significant contributions to improving the quality of the following work. This gratitude is extended to Dr. John Gosse and Dr. Beth McClenahan, whose interest in my work and help with the interpretation of the terrestrial cosmogenic nuclide dating and geochemistry, respectively, is much appreciated.

Funding for this project was in part provided by the Natural Sciences and Engineering Research Council of Canada (NSERC) through an Industrial Postgraduate Scholarship. Funding was also supplied by the Northern Scientific Training Program (NSTP). The Yukon Geological Survey not only supported this research financially, but also logistically and intellectually. The environment they provide encourages inexperienced scientists to pursue their interest in Yukon geology. My thanks are also extended to the numerous field assistants, including Kristy Long and Jennifer Owen, who put up with me on long, hot traverses in difficult conditions.

Finally, thank you to Jillian Evers, Julia Turner and Brennen Cross. Their love and patience has inspired me and kept me motivated through all the challenges along the way. While any amount of truth obtained in this thesis is shared with all those mentioned above, all errors remain the sole possession of the author.

TABLE OF CONTENTS

LIST OF FIGURES

LIST OF TABLES

1 INTRODUCTION

The glacial history of Howard's Pass is significant both academically and practically. As a source area for the Selwyn lobe of the northern Cordilleran Ice Sheet (CIS), knowledge of the dynamics and style of deglaciation has important implications. The inferred proximity of a major ice divide contributes to the academic significance of the area.

Understanding the ice-flow history of the study area is also vital for continued drift prospecting used to find new mineralized zones. Tracing geochemical anomalies in glacially transported sediments requires examination of the intensity and direction of late Wisconsinan ice-flow. In addition, ongoing infrastructure development in the area has been negatively affected by a lack of suitable aggregate resources and an incomplete understanding of potential hazards.

To address these issues, a M.Sc. project was designed as a joint collaboration between Simon Fraser University, the Yukon Geological Survey and Selwyn Resources Ltd., formerly Pacifica Resources Ltd. The following research questions were proposed:

1. What is the glacial history of Howard's Pass, including the sequence of ice growth and decay, and the position of the nearby ice divide?
2. Can surficial geology and glacial history be used to aid infrastructure development and drift prospecting in Howard's Pass?

To answer these questions, the following objectives were set for the project:

1. Reconstruct the ice-flow and pattern of deglaciation.

2. Map the distribution of surficial sediments over the claim block that encompasses the deposits in the study area.
3. Locate and characterize the surficial materials useful for mining development.
4. Provide an alternative to standard exploration soil geochemistry methods by conducting a Mobil Metal Ion geochemistry case study over a known deposit.
5. Identify any potential terrain hazards in the area, such as debris flow fans and avalanche tracks.

This chapter will introduce the study area by describing the physiography, regional and local bedrock geology and significance of the area for interpreting the regional Quaternary history of the northern Cordilleran Ice Sheet.

1.1 Physiography

The study area lies in the Selwyn Mountains on the border between Yukon and Northwest Territories and encompasses parts of NTS 105I and J (Fig. 1.1). It is surrounded by the Nahanni River Valley and the Sappe Range to the east, the Logan Mountains to the south and the Pelly River Valley to the west (Fig. 1.2). The study area straddles the continental divide with the Pelly River flowing west to the Yukon River, and the Nahanni River flowing east to the Mackenzie River. This study area is informally termed Howard's Pass and all further uses of this term refer to the study area defined by the approximate boundaries stated above.

High peaks with exposed bedrock and moderate to steep valleys characterize Howard's Pass. In the Pelly River drainage, broad river valleys oriented east-west contrast with narrower tributary valleys running north-south. The highest peaks in the area lie above 2500 m and the lowest elevation is 800 m in the Nahanni River Valley. Local relief is in the order of 600 m. Cirques are common throughout the study area and those facing north typically contain rock glaciers. The closest glaciers are in the Itsi Range to the north.

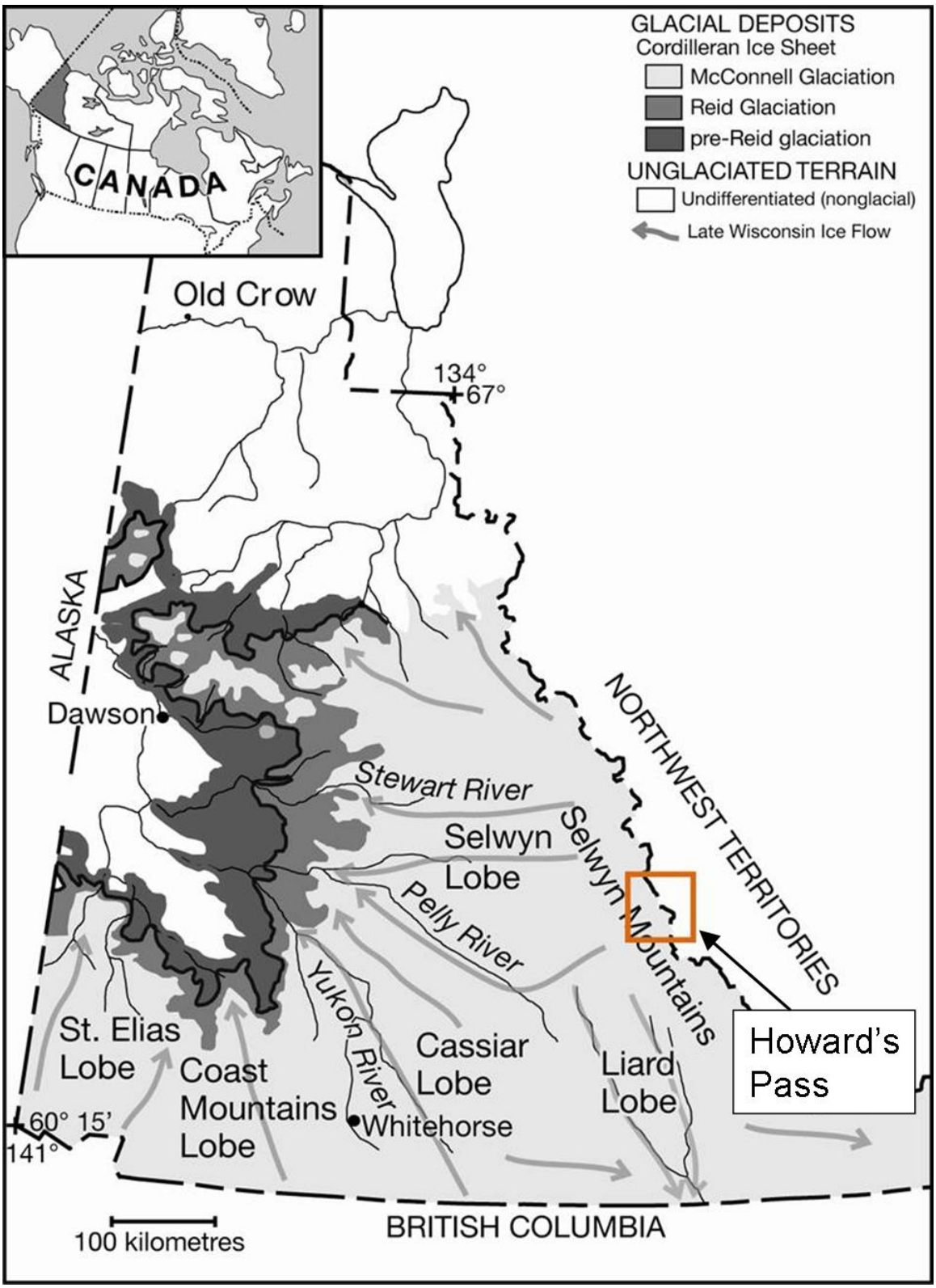

Figure 1.1 Location map of the Howard's Pass study area (see square) in context with late Wisconsinan ice lobes and glacial extents of Yukon Territory (modified from Duk-Rodkin, 1999; Ward *et al.*, 2007). The study area encompasses parts of 105I and J.

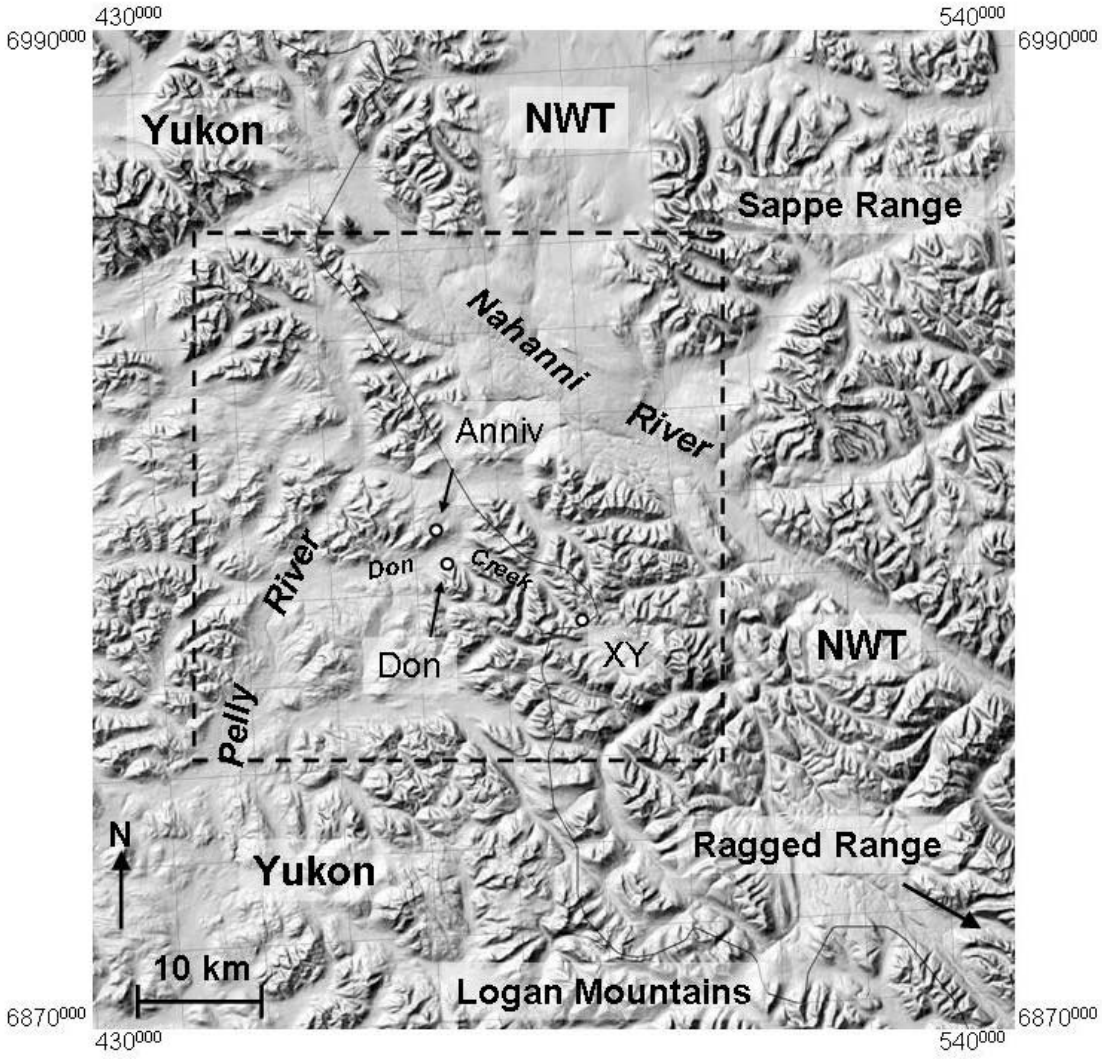

Figure 1.2 Physiography of Howard's Pass with the locations of Anniv, Don and XY camps. The dashed box represents the approximate study area boundary. The thin black line is the border between Yukon and Northwest Territories. The coordinates are in UTM NAD 83.

1.2 Bedrock Geology

Howard's Pass lies within the central part of the Selwyn Basin, a Palaeozoic fault-controlled depocentre formed from the Late Proterozoic to the Mississippian (Fig. 1.3; Goodfellow, 2007). The basin is bounded by the Mackenzie, MacDonald and Cassiar carbonate platforms to the northeast, southwest and south, respectively (Gordey, 1981; Goodfellow, 2007). The Selwyn Basin formed

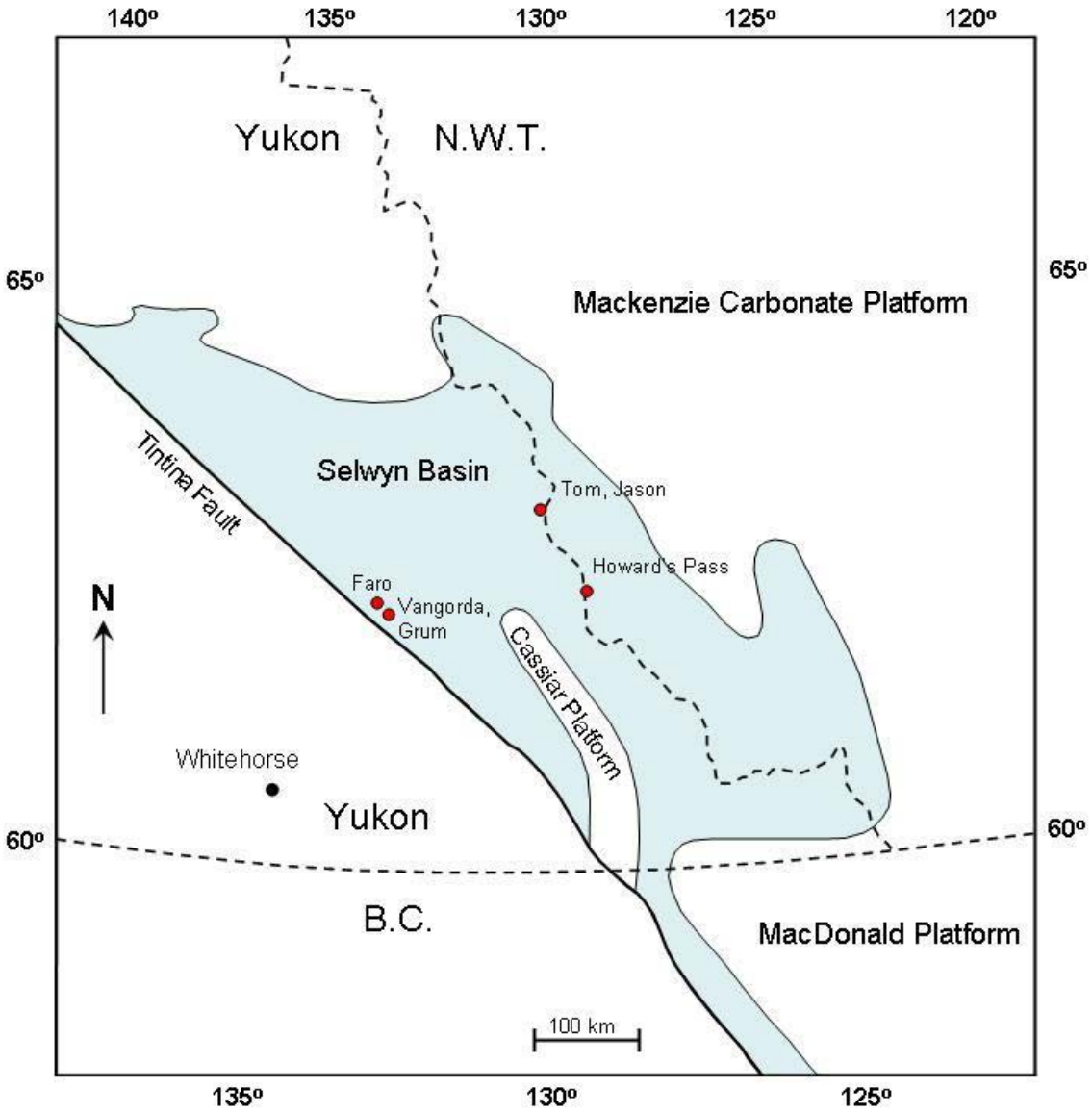

Figure 1.3: Location of of the Selwyn Basin and surrounding carbonate platforms including the locations of the Palaeozoic-aged deposits mentioned in the text (modified from Goodfellow, 2007).

during continental rifting of the western margin of North America during the Late Proterozoic, and was reactivated as an extensional back-arc basin in the Palaeozoic (Nelson *et al.*, 2002).

The Selwyn Basin has the world's third largest SEDEX resources, with 12 major Palaeozoic-aged deposits with proven reserves (Goodfellow, 2007). These deposits include the Faro, Tom, Jason, Vangorda and Grum (Fig. 1.3). These deposits formed at intersections between extensional and translational faults and contain syn-rift permeable clastics and volcanics, and post-rift impermeable shales and carbonates.

The deposits in Howard's Pass comprise a 35 km long string. These include the established XY and Anniv deposits, as well as the Don, H.C., O.P., Brodel, Abbey and Pelly North deposits newly discovered by Selwyn Resources Ltd. (Fig. 1.4). These small deposits likely formed from a single event during the Early Silurian (Goodfellow, 2007). Their basin-conforming morphology, weak zonation, low aspect ratio (extent/thickness) and delicate laminated sulphides suggest that these deposits formed vent-distally as brines (Goodfellow, 2007; Goodfellow and Lydon, 2007).

The multiple smaller deposits in Howard's Pass are estimated to host between 87 (Pearson *et al.*, 2004) to 120 million tonnes (Goodfellow and Lydon, 2007) of indicated mineral resources, with an additional 215 (Pearson *et al.*, 2004) to 250 million tonnes (Morganti, 1979) of inferred ore. The estimated Zn and Pb concentrations are 5 % and 2 %, respectively (Goodfellow and Lydon, 2007). The size and metal content of the deposits in Howard's Pass put them in the top 10 percentile globally, resulting in their group classification as a giant deposit (Singer, 1995; Goodfellow, 2007).

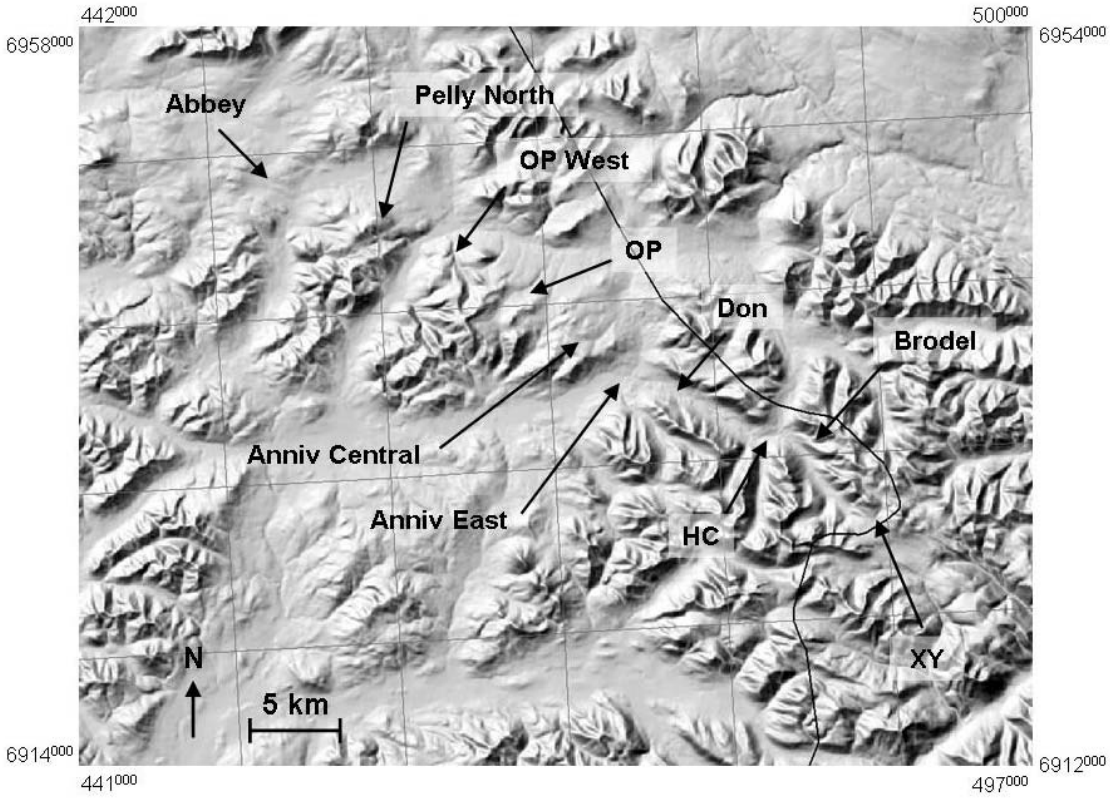

Figure 1.4 Major deposit locations in Howard's Pass. The thin black line is the border between Yukon and the Northwest Territories.

The stratigraphy in the Howard's Pass area represents over 200 million years. The basement rocks are Precambrian Windermere Supergroup clastics. These are overlain by Cambrian-Ordovician Rabbitkettle Formation basinal carbonates, Ordovician-Devonian Road River Group cherts and shales, and Devonian-Mississippian Earn Group clastics (Fig. 1.5; Morganti, 1979; Goodfellow, 2007). The Road River Group is separated into five informal members (Morganti, 1979), including the locally named "Active Member" that contains black cherty bedded and laminated sulphides (Goodfellow *et al.*, 1986).

Mineralization in the Selwyn Basin resulted from subsidence of grabens and discharge of metaliferous fluids onto the sea floor. These fluids reacted with H_2S in an anoxic bottom layer in 2nd and 3rd order basins (Morganti, 1979; Goodfellow, 2007). Although seawater recharge maintained the convection of

metaliferous fluids in the Selwyn Basin for over 200 million years, mineralization in Howard's Pass formed in less than 15 million years during the Early Silurian. There is considerable secondary Holocene Zn mineralization in mosses surrounding springs in Howard's Pass. These typically contain hemimorphite, smithsonite and wurtzite (Jonasson *et al.*, 1983; Goodfellow, 1989).

The nearest sizable intrusives in Howard's Pass are the Central Nahanni Pluton and the O'Grady Batholith (Fig. 1.5; Gordey, 1981). Both of these members of the Selwyn Plutonic Suite are located approximately 20 km east of Howard's Pass, across the Nahanni River. The closest large pluton to the west is over 100 km away.

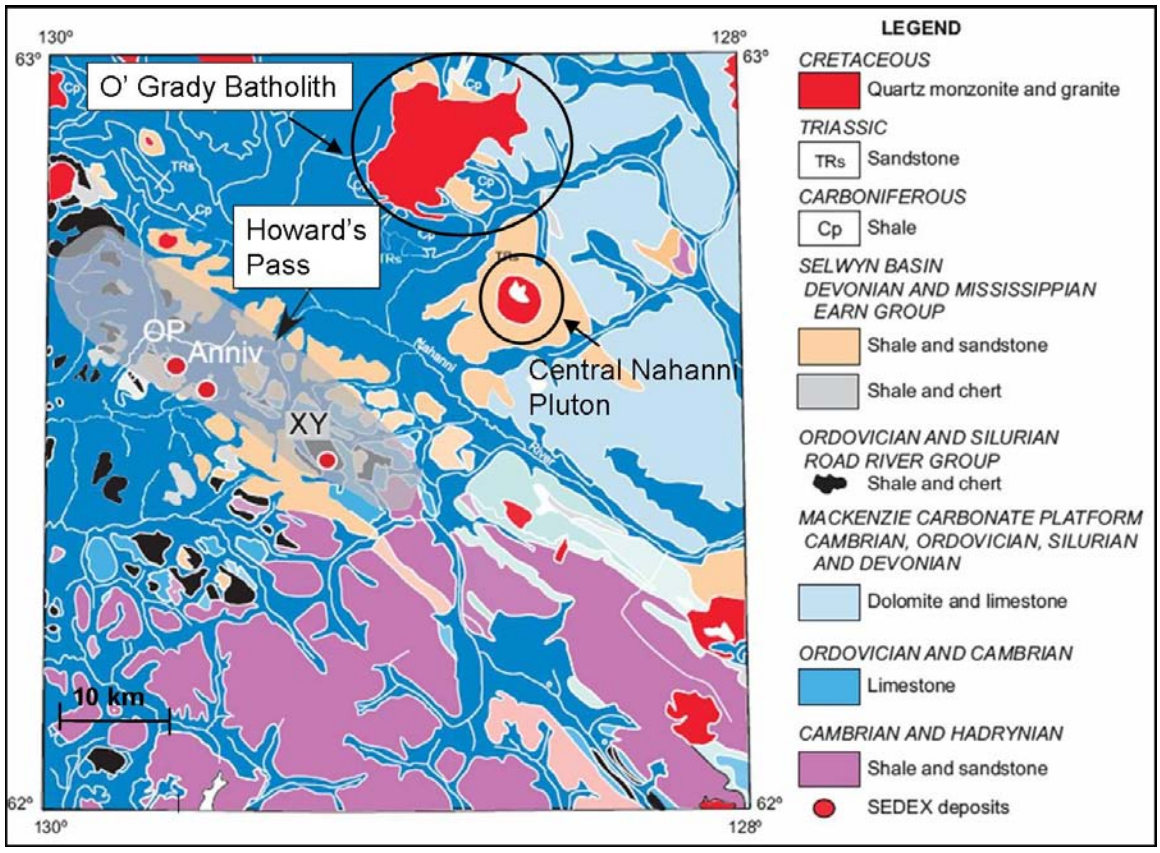

Figure 1.5 Bedrock geology map of Howard's Pass study area. Batholiths highlighted to the northeast are the likely sources of granodiorite erratics found across Howard's Pass, see chapter 4 (modified from Gordey, 1981).

1.3 Regional Quaternary Geology

Multiple glaciations covered Yukon throughout the Late Pliocene and Pleistocene (Jackson *et al.*, 1991; Froese *et al.*, 2000). Bostock (1966) initially proposed four glaciations in Yukon. He called these the McConnell, Reid, Klaza and Nansen. However, discriminating between deposits older than the Reid is difficult. This led Hughes *et al.* (1969) to group all glaciations before the Reid as pre-Reid. In the mountainous Howard's Pass area, only McConnell deposits have been observed (e.g. Jackson, 1982).

Growth of the northern Cordilleran ice sheet (CIS) in the late Wisconsinan was likely similar to the four-phase model for the southern CIS presented by Kerr (1934) and expanded by Davis and Matthews (1944). This model proposes that initially, local alpine ice grew and created small ice fields at high elevations (alpine phase). With increased precipitation and lower temperature, these ice fields coalesced and covered mountain ranges (intense alpine phase). As glaciers from these ice fields extended into nearby lowlands, topographically dependent ice masses formed, covering most of the Cordilleran landscape (mountain ice sheet phase). The last phase involved ice thickening in non-mountainous interiors and extending over bordering mountains (continental ice sheet phase).

The northern CIS initiated from local cirque accumulation (Bond, 2004, 2007). Unfortunately, most landforms created during this early phase were eroded by subsequent ice-flows. Evidence is therefore limited to exposures with well-preserved stratigraphy. In the western Pelly Mountains, Bond (2007) found data suggesting alpine ice travelled at least 16 km from its source area before coalescing with the Cassiar lobe. Similarly, other data gathered from the eastern margin of the Pelly Mountains suggest alpine ice coalesced with the Selwyn lobe (Plouffe and Jackson, 1992; Bond and Kennedy, 2005).

At the onset of glacial maximum (Davis and Matthews' mountain ice sheet phase), the maximum thickness of the northern CIS varied across its extent, but was likely over 2000 m thick in the source area and topped most mountain peaks (Jackson, 1989; Bond, 2007). Despite the thickness of the northern CIS, ice-flow was dominantly topographically dependent. Ice-flow indicators throughout southern Yukon demonstrate that ice flowed along major valleys and around neighbouring mountain massifs (Jackson et al., 1991). However, Bond (2007) found aligned landforms above 1650 m in the Pelly Mountains, suggesting ice-flow over these mountains was largely topographically unconstrained. This indicates that glacial flow dynamics varied along with ice thickness across the ice sheet.

During glacial maximum, the northern CIS consisted of multiple, distinct ice lobes (Fig. 1.6; Jackson et al., 1991, Duk-Rodkin, 1999). These lobes were centred in the Eastern Coast Ranges and the St. Elias, Cassiar and Selwyn mountains. The location of these ice centres allowed for the development of a major ice divide extending from the Cassiar Mountains to the Selwyn Mountains (Fig. 1.6). Ice flowing from this divide extended as lobes into the surrounding lowlands (Jackson *et al.*, 1991; Bond, 2007). The Eastern Coast Ranges lobe flowed northwest between the St. Elias lobe and the Cassiar lobe (Jackson *et al.*, 1991). The Liard lobe spread east from the Cassiar Mountains and south from the Selwyn Mountains, filling the Liard Lowlands (Klassen, 1987; Dyke, 1990a). Ice flowing west from the Cassiar Mountains created the Cassiar lobe. This lobe was diverted northwest by the Eastern Coast Ranges lobe, where it coalesced with the Selwyn lobe. Although both the Cassiar and Selwyn lobes overran the Pelly Mountains (Jackson *et al.*, 1991; Ward and Jackson, 1992; Bond, 2007), the northern CIS was likely not thick enough to reach the continental ice sheet phase before deglaciation (Jackson *et al.*, 1991).

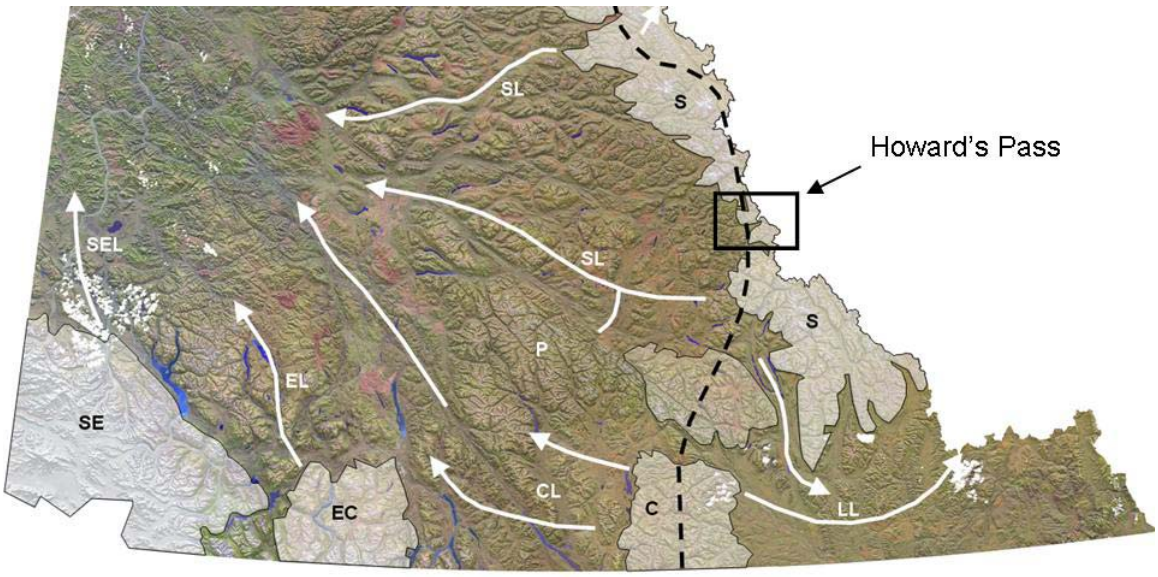

Figure 1.6 Ice-flow in the northern Cordillera during the late Wisconsinan (modified from Jackson *et al.*, 1991). Highlighted polygons are areas of major ice accumulation. SE = St. Elias Mountains, EC = Eastern Coast Mountains, P = Pelly Mountains, C = Cassiar Mountains, S = Selwyn Mountains, SEL = St. Elias lobe, EL = Eastern Coast Ranges lobe, CL = Cassiar lobe, LL = Liard lobe, SL = Selwyn lobe. Dashed line is the location of an inferred ice divide at last glacial maximum.

The Selwyn Mountains were the largest centre of ice accumulation in the northern CIS during the late Wisconsinan (Klassen, 1987; Dyke, 1990a). Ice flowed from the Selwyn divide southeast into the Liard Lowlands, where it was deflected east by ice from the Cassiar Mountains, and coalesced into the Liard lobe (Dyke, 1990a). Ice also extended east from this divide into the Mackenzie Mountains, but was far more limited than ice spreading west (Ford, 1976; Jackson, 1989, Duk-Rodkin and Huntley, 2006). Westerly flowing ice from the Selwyn Mountains travelled over 300 km, creating the Selwyn lobe (Jackson 1989; Jackson *et al.*, 1991).

After initial thinning and frontal retreat, deglaciation of the northern CIS generally occurred by wholesale starvation and downwasting of the ice surface (Jackson, 1989; Jackson *et al.*, 1991). This is similar to Fulton's (1991) model of deglaciation for the entire CIS, with thinning and increased topographic influence culminating in stagnation. Evidence for this includes the continuation of

stagnation features between cirques and valley floors (Jackson, 1987). These features have been observed at elevations up to 1830 m, indicating a rapid rise in the firn line to above this height (Jackson, 1989). Widespread stagnation only required a minor change in firn line given the gentle slope of the Selwyn lobe (cf. Duk-Rodkin *et al.*, 1986). Due to this stagnation, recessional moraines are typically only observed in the northern CIS within a few kilometres of the former glacial margins (Jackson *et al.*, 1991).

In contrast to the regional stagnation model, a more classical frontal retreat deglacial model was presented by Dyke (1990a) for the Francis Lake area, in the Ragged Range and Logan Mountains (Fig. 1.2). Ice in this area formed a complex pattern of ice lobes and alpine ice. Following ice expansion south and coalescence with the Liard lobe, ice retreated north up the Frances and Hyland river valleys (Dyke, 1990a). This retreat left multiple lateral and end moraines, suggesting that this lobe remained active during deglaciation. Jackson *et al.* (1991) attributed this style of deglaciation to the high elevation and precipitation associated with the Ragged Range.

There is also evidence of re-advances during deglaciation of the Cassiar lobe. In the Pelly Mountains, glaciolacustrine sediments and meltwater channels at the continental drainage divide that follows the territorial border indicate that the ice margin migrated east across the divide during deglaciation (Bond, 2007). This was followed by reactivation of the local glaciers depositing moraines within three kilometres of their source (Bond, 2007). Other examples of late Wisconsinan re-advances in central Yukon have been described by Plouffe and Jackson (1992) and Ward and Jackson (1992). The contrast between these examples of dynamic equilibrium with frontal retreat and re-advances, and stagnation in the source areas similar to Fulton's (1991) model, suggests deglaciation differed across the northern CIS.

2 TERRAIN INVENTORY MAPPING

Terrain inventory maps have open legends that incorporate the surficial geology, surface expression, texture and geomorphological processes of delineated polygons. They are designed to provide background information and have many possible derivative applications. For this project, the Terrain Classification System for British Columbia (Howes and Kenk, 1997) was used, with a few minor modifications. This map is useful for understanding the glacial history of Howard's Pass, and provides valuable information for drift prospecting and infrastructure development associated with mineral exploration in the area. This chapter contains descriptions of the different elements of the map and highlights materials of interest for mineral exploration and development.

2.1 Previous Work

The map area encompasses all of 105I/11 and 12, and portions of 105I/05, 06, 07, 10 and 105J/08, 09 (Fig. 2.1). No detailed (>1:100 000-scale) mapping has been completed in 105I or any adjacent map sheet. Prior 1:125 000-scale terrain mapping completed by Jackson (1982) for all of 105I accompanied a report on the terrain conditions and Quaternary history of the Nahanni Map Sheet (105I). The surficial geology and terrain conditions were investigated in 105J by Jackson and Morison (1984), Jackson *et al.*, (1993a-c), Jackson (1993a), in 105G by Jackson (1986a, 1993b-e) and in 105H by Dyke (1990b-e). In addition, glacial limits were mapped in 105O and P, and 95E by Duk-Rodkin (2001a,b).

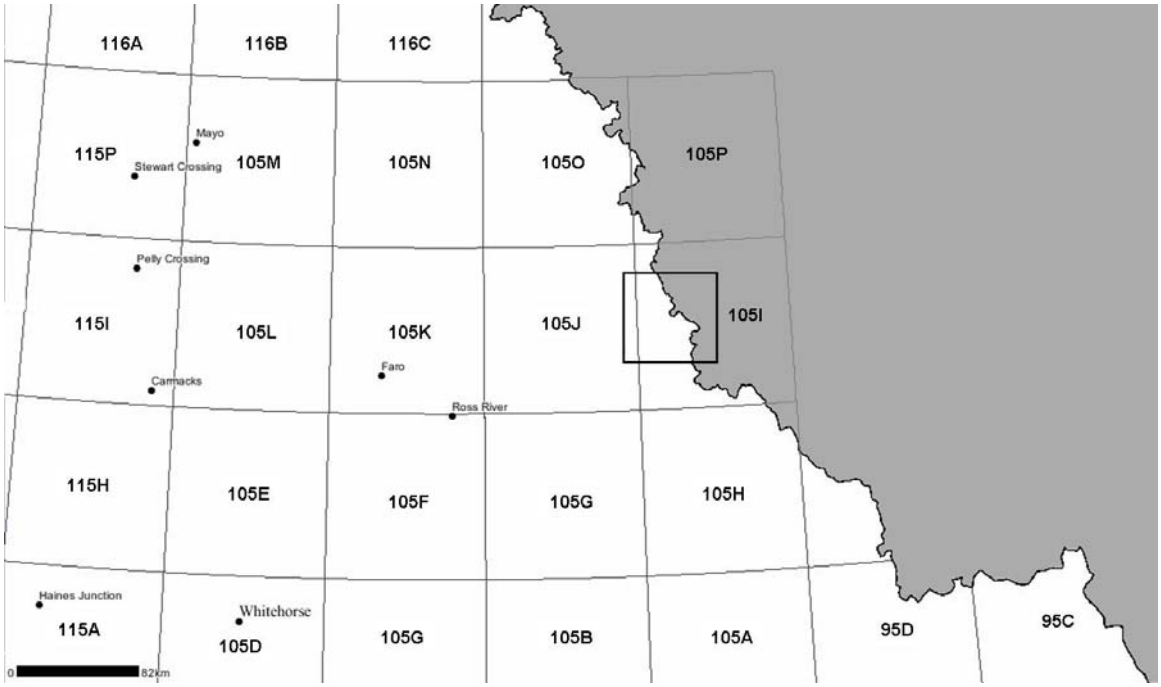

Figure 2.1 National Topographic Map grid for southeastern Yukon Territory. The black square highlights the study area, encompassing portions of 105I and J.

2.2 Methodology

A 1:50 000-scale terrain inventory map was created for Howard's Pass based on 2004 1:40 000-scale air photos. The map area boundaries were based largely on areas of academic interest and the needs expressed by Selwyn Resources Ltd. Pre-typing for this map commenced in June, 2006. Polygons were delineated for areas of similar surficial materials, expressions and geomorphological processes. During pre-typing, some common processes, such as permafrost and creep, were only identified where they were unusually prevalent or hazardous. Three boundary types were utilized during pre-typing: solid lines delineated defined boundaries, dashed lines indicated inferred boundaries, and dotted lines marked assumed boundaries. This was later reduced to two boundary types, defined and inferred, during the digitizing process.

The pre-typing continued during the 2006 field season in conjunction with helicopter and ground-based field verifications. Information gathered from 152

stations during the 2006 field season was used to refine the map during the subsequent winter. This map was then field checked at 154 stations during the 2007 field season. Soil pits dug using shovels were examined for material type, texture and lithology. Where possible, thicknesses and stratigraphic relations were also noted. Multiple large stratigraphic sections added valuable information and are described in Chapter 3.

Following completion of the mapping, the air photos were sent to Aero Geometrics Ltd. in Vancouver, B.C. for digitizing. Shape-files were produced containing polygons and on-site symbols. The associated terrain information for each polygon was manually entered by the senior author using ArcGIS and Global Mapper software. Shannon Mallory at the Yukon Geological Survey completed the final map layout. Polygons were assigned a colour based on the dominant surficial material. The map is included as Appendix A in paper format and as Appendix B in CD format.

2.3 Map Legend

Each delineated polygon on the terrain inventory map was given a terrain symbol. These symbols are composed of composite letters used to describe the texture, surficial material, surficial expression and geomorphological processes that describe the terrain in a polygon. The following descriptions of the different components of the terrain symbol are based on Howes and Kenk (1997), the Resource Inventory Committee Guidelines and Standards to Terrain Mapping in British Columbia (1996) and Jackson (1986b), but were modified specifically to comply with Yukon Geological Survey standards. The only major modification was the order of the texture labels. The B.C. guidelines suggest listing these textures in increasing prevalence, whereas this map lists them with the most dominant texture first.

2.3.1 Texture

The texture was only specified in polygons that were field checked. It refers to the size, rounding and sorting of the grains in a material. In the map area, the grain sizes range from clay to boulder (Table 2.1). Rounding ranges from well-rounded to angular. Sorting refers to the distribution of grain sizes in the material. Both roundness and grain size are indicated on this map with different combinations of texture symbols. For example, angular clasts between 2 to 256 mm are rubble (r), whereas well-rounded clasts of the same range in grain size are gravel (g).

Similarly, sorting is indicated by combining several different texture symbols. For example, a mixture of silt (z), sand (s) and mixed fragments (d) is very poorly sorted and is a diamicton. Comparatively, a polygon with only one textural symbol is considered well-sorted. Texture symbols are listed before the surficial materials in order of decreasing significance.

Table 2.1 Textures used in the terrain inventory map to indicate the size, shape and sorting of sediment grains in a surficial material.

Texture	Symbol	Description
Blocks	a	Angular grains >256 mm
Boulders	b	Rounded grains >256 mm
Cobbles	k	Rounded grains between 64 - 256 mm
Pebbles	p	Rounded grains between 2 - 64 mm
Sand	s	Grains between 0.0625 - 2 mm
Silt	z	Grains between 0.002 - 0.0625 mm
Clay	c	Grains <0.002 mm
Mixed Fragments	d	Mixed round and angular grains >2 mm
Angular Fragments	x	Mixed angular grains >2 mm
Gravel	g	Mixed rounded grains >2 mm
Rubble	r	Angular grains between 2 - 256 mm

2.3.2 Surficial Material

Surficial materials are the non-lithified sediments found in an area (Table 2.2). This includes all materials that have been eroded, transported or deposited. Bedrock was also identified where it was exposed at the surface or was covered by a thin sediment veneer (<20 cm). To simplify the mapping, surficial materials comprising approximately <10% of a polygon were not included in the terrain symbol. In polygons with multiple surficial materials, these materials are listed in the terrain symbol in order of decreasing aerial extent and influence, separated by one or two slashes (/ or //). One slash denotes that the material to the left is more extensive than the one to the right, whereas two slashes indicate that the material to the left is considerably more extensive than the one to the right (Howes and Kenk, 1997). A maximum of three surficial materials were allowed for one polygon. Where one material lies stratigraphically above another, a back-slash (\) was used to separate the two units, with the overlying material on the left. The materials are described below from youngest to oldest.

Table 2.2 Surficial material types, their depositional environments and descriptions. Surficial materials are used in a terrain inventory map to indicate the primary non-lithified material(s) in a polygon.

Surficial Material	Symbol	Depositional Processes and Descriptions
Organic	O	Accumulations of vegetative matter >1 m thick
Fluvial	F	In and adjacent to modern streams or rivers
Colluvium	C	Down-slope, gravity-driven, rapid or slow processes
Glaciofluvial	FG	Deposited directly by glacial meltwater
Glaciolacustrine	LG	Deposition into a lake in contact with a glacier
Morainal	M	Deposited by primary or secondary processes controlled by glacial ice
Bedrock	R	Bedrock outcrops or is covered by <10 cm of sediment

2.3.2.1 Bedrock

The bedrock surficial material label was used for areas where bedrock outcrops or is covered by a thin veneer of sediment (<20 cm). The dominant lithologies in

the map area are carbonates of the Rabbitkettle Formation, cherts and shales of the Road River Group, and Earn Group clastics (Gordey, 1981). Bedrock outcrops occur mostly on steep slopes at high elevations. However, in several areas outcrops occur as hummocks and ridges in valley bottoms. The high fracture density in the local bedrock results in frequent slow and rapid mass movements, such as rock falls and translational slides. Because of the probability of creep, highly fractured bedrock outcrops are not recommended for foundation material.

2.3.2.2 Morainal

Morainal material describes diamicts and poorly-sorted gravels deposited by primary glacial processes such as lodgement, deformation and melt-out, or secondary glacial processes dominated by gravity and water (Dreimanis, 1989; Hicock, 1990). Thus, this term applies to all types of till including flow tills, which are not directly deposited by glacial ice.

Till is widespread throughout the map area, occurring as thick deposits on valley bottoms and blankets and veneers on gentle to moderate slopes. In some valley bottoms, till comprises hummocky and undulating ice-stagnation terrain. Most of the map area was likely covered in thick deposits of till during late Wisconsinan glaciation. However, subsequent erosion has removed or covered some of this till cover. Lateral moraines composed of till are scattered throughout the map area on the walls of narrow valleys. End moraines are typically found within a few kilometres of cirques (Fig. 2.2). Moraines are indicated on the map as on-site symbols.

Till in Howard's Pass is generally poorly-sorted, sandy-silt diamicton (Fig. 2.3a), but ranges in grain size distribution (Fig. 2.4) and clast lithology. The amount of consolidation also varies, with some tills being loose and others being overconsolidated. Overall, the tills in the study area have a high density, contain abundant striated clasts and are regionally extensive. In a few locations, the till

was likely subject to Fe, Mn and $CaCO_3$ cementation (Fig. 2.5). Till locally contains segregated ice lenses, so infrastructure development on north-facing or organic-mantled slopes should proceed with caution. Although it typically has a coarse-grained matrix (Fig. 2.4), in some locations the till is more clay-rich. These deposits are more suitable for bulk fill and as an impermeable liner for tailing ponds.

2.3.2.3 Glaciofluvial

Glaciofluvial materials are deposited directly by glacial meltwater. These deposits likely formed in the study area supra-, en- or subglacially, as well as ice marginally in pro and lateral meltwater channels. Glaciofluvial sediments typically

Figure 2.2 Lateral (dashed line) and end moraines (solid lines) in a tributary valley to Don Creek. There are few end moraines observed in the map area, although others are observed in cirques immediately to the north. The lateral moraine is typical of most of the moraines in the map area. These are mapped as on-site symbols.

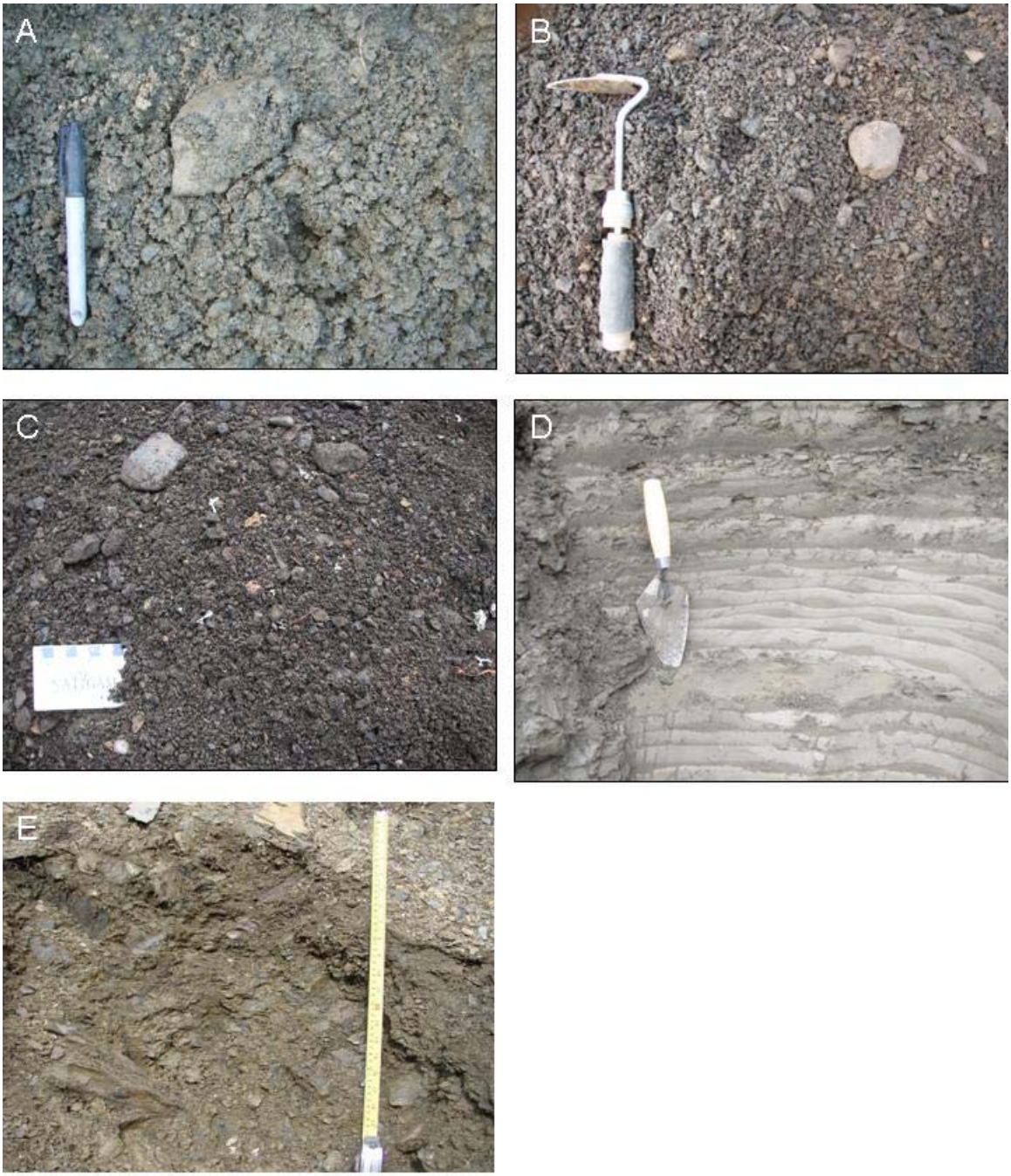

Figure 2.3 Textures of various surficial materials in Howard's Pass: a) Typical till composed of a diamict with 15-20% clasts and a sandy-silt matrix; b) High aggregate quality glaciofluvial material with resistive sedimentary clasts and granodiorite erratics; c) Low aggregate quality glaciofluvial material with dominantly non-resistive shale clasts (scale card = 9 cm); d) Glaciolacustrine material with climbing ripples composed of interlaminated clay, silt and sand; e) Colluvium derived from the physical weathering of bedrock and transportation down-slope, (tape = 50 cm).

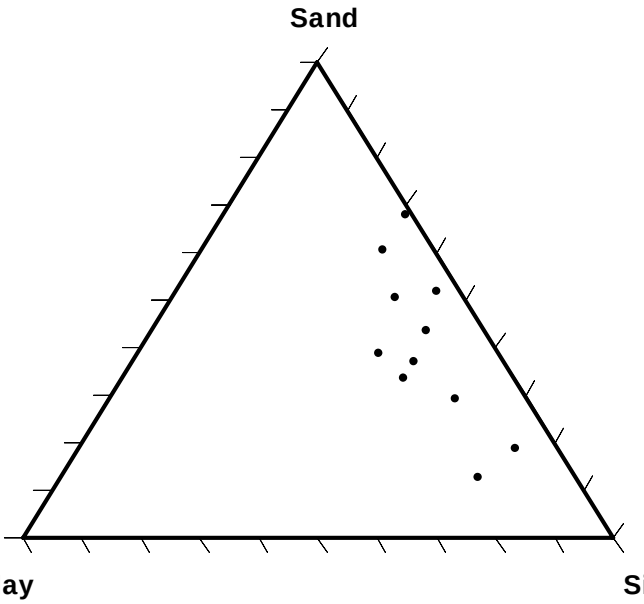

Figure 2.4 Ternary plot of the sand-silt-clay fraction of 11 tills collected in Howard's Pass. The lack of clay suggests short transport distances for these samples and possibly reflects glaciofluvial source material.

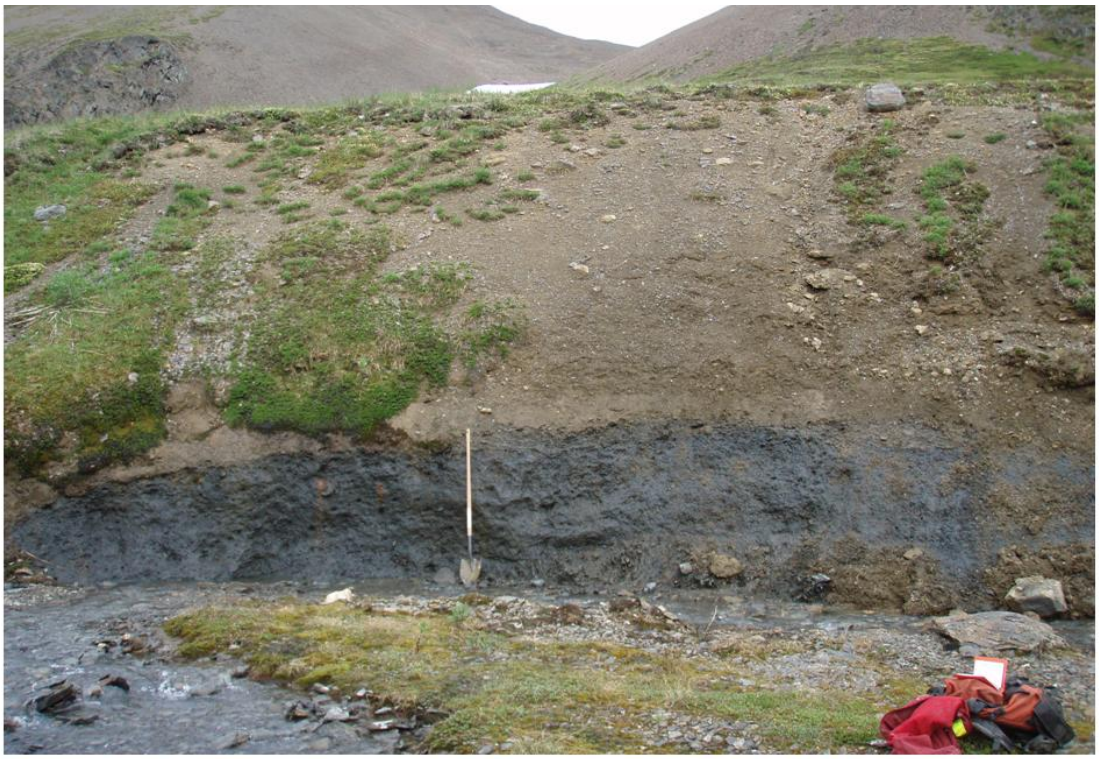

Figure 2.5 Cemented till underlying an unconsolidated till near XY camp. The jet black colour and the chemistry of the nearby streams indicate the cement is Manganese oxide. The lower till is black and difficult to penetrate with a pick. The shovel is 1.5 m high.

consist of moderately to well-sorted, well-rounded, massive to well-stratified sand and gravel, but can vary locally depending on the transport distance (Fig. 2.3b). For example, ice-marginal glaciofluvial deposition likely resulted in poorly-sorted, massive deposits relative to distal glaciofluvial sediment.

In Howard's Pass, glaciofluvial deposits are concentrated on valley sides and bottoms where they comprise terraces, kames and eskers ranging from a few metres to tens of metres in depth. Terraces are common at the confluence of tributaries into larger valleys such as the Don Creek Valley and the Nahanni River Valley. The presence of kame-and-kettle topography composed of glaciofluvial material suggests deposition associated with buried ice and is indicative of ice stagnation (Fig. 2.6). Eskers are also found scattered across the map area, but are concentrated in the Don Creek Valley and near the Nahanni River.

The quality of the glaciofluvial material as an aggregate resource differs across the map area, but is generally good. Some gravel consists of poorly-indurated shales that break down easily and result in poor aggregate material (Fig. 2.3c). Gravels that are more mature and contain more indurated clasts result in more high-quality aggregate material. Well-drained glaciofluvial deposits result in few segregated ice lenses, making them good locations for roads and other infrastructure.

2.3.2.4 Glaciolacustrine

Glaciolacustrine materials are deposited in standing water on, in, under or beside a glacier. The largest known glaciolacustrine deposit near the study area is in the Nahanni Valley north of the map boundary and was interpreted by Jackson (1987) as forming during deglaciation. In Howard's Pass, glaciolacustrine sediments are rare. They are mostly restricted to small tributary valleys or adjacent to glaciofluvial ridges and hummocks. An example of this is in the Don

Figure 2.6 Kame terrace in a tributary to the Don Creek Valley. The surface is heavily kettled from the melting of buried ice blocks. This terrace was mapped as FGt-H.

Creek Valley, where a large slump exposed interbedded and interlaminated silt, clay and fine-grained sand (Fig. 2.7) adjacent to a large esker system. The geomorphic relationship between the eskers and these deposits, and paleocurrent measurements of starved sand ripples in the section indicate that this material was deposited from the eskers to the west, likely into a shallow lake formed between the eskers and the valley side during deglaciation.

Glaciolacustrine sediments consist of stratified sand, silt and clay (Fig. 2.3d). Their low permeability, poor drainage and high *in situ* moisture content can result in ice lenses that melt and cause large slumps. The previously described slump in the Don Creek Valley is an example of this. However, the low permeability of glaciolacustrine materials makes them excellent liner material for tailing ponds.

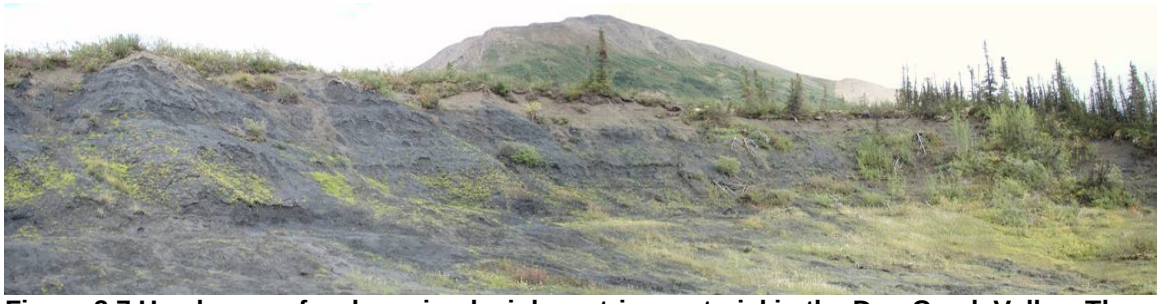

Figure 2.7 Headscarp of a slump in glaciolacustrine material in the Don Creek Valley. The slump was probably caused by melting of ice lenses following exposure from river erosion. The scarp is ~8 m high.

2.3.2.5 Fluvial

Fluvial materials are transported and deposited by modern streams and rivers running throughout Howard's Pass. They typically consist of stratified sand and gravel with well-sorted and well-rounded clasts. Most of these deposits are limited to small floodplains, terraces and fans, but can be substantial in the larger rivers such as the Pelly and the Nahanni. Floodplains are generally poor sites for development despite favourable foundation conditions. This is due to potential flooding, especially from ice jams during break-up. Many smaller streams transporting sediment down mountain-sides develop fans in valley bottoms.

These features may contain useful aggregate materials, but they are also prone to hazards such as debris flows, debris floods and rapid channel avulsions.

2.3.2.6 Colluvium

Colluvium is material that was transported and directly deposited by down-slope, gravity-driven processes. It is common in the map area, but differs dramatically in formation time and location. Some materials formed by rapid processes, such as rock falls, debris flows and avalanches, are deposited within tens of seconds and are typically found on steep or moderate slopes. Some of these failures were large enough to fill valleys and alter drainage (Fig. 2.8). Conversely, slow processes associated with permafrost, like solifluction and creep, occur on gentle slopes (Fig. 2.9); rock glaciers are present in most north-facing cirques (Fig. 2.10). Although water and ice are not the dominant transporting agents for

Figure 2.8 A large failure (white dashed outline) in a tributary valley south of XY camp. This failure likely blocked the valley and changed the local drainage. This failure was mapped as colluvium.

Figure 2.9 Solifluction lobes on a north-facing slope as an example of periglacial mass movement processes. These features were marked either as Cb-S or as Cb-Z if cryoturbation or nivation also occur on the slope.

colluvium, they play important roles in determining the type of process and the resulting sediment texture.

The texture and composition of colluvium varies more than any other material in Howard's Pass, depending on the parent material and the mechanism and distance of transport. For example, materials derived from a glaciofluvial source likely contain well-rounded, well-sorted clasts of diverse lithology. Comparatively, colluvium derived from physically weathered bedrock will be angular and poorly-sorted (Fig. 2.3e). The most common form of colluvium in the map area is a mix of colluviated till and bedrock, resulting in a silt diamict with a mix of angular, local bedrock and sub-rounded erratic clasts. Thus, the utility of colluvium as aggregate material also differs across the map area. In some areas, colluvium can be used as fill material. However, due to the hazards commonly associated

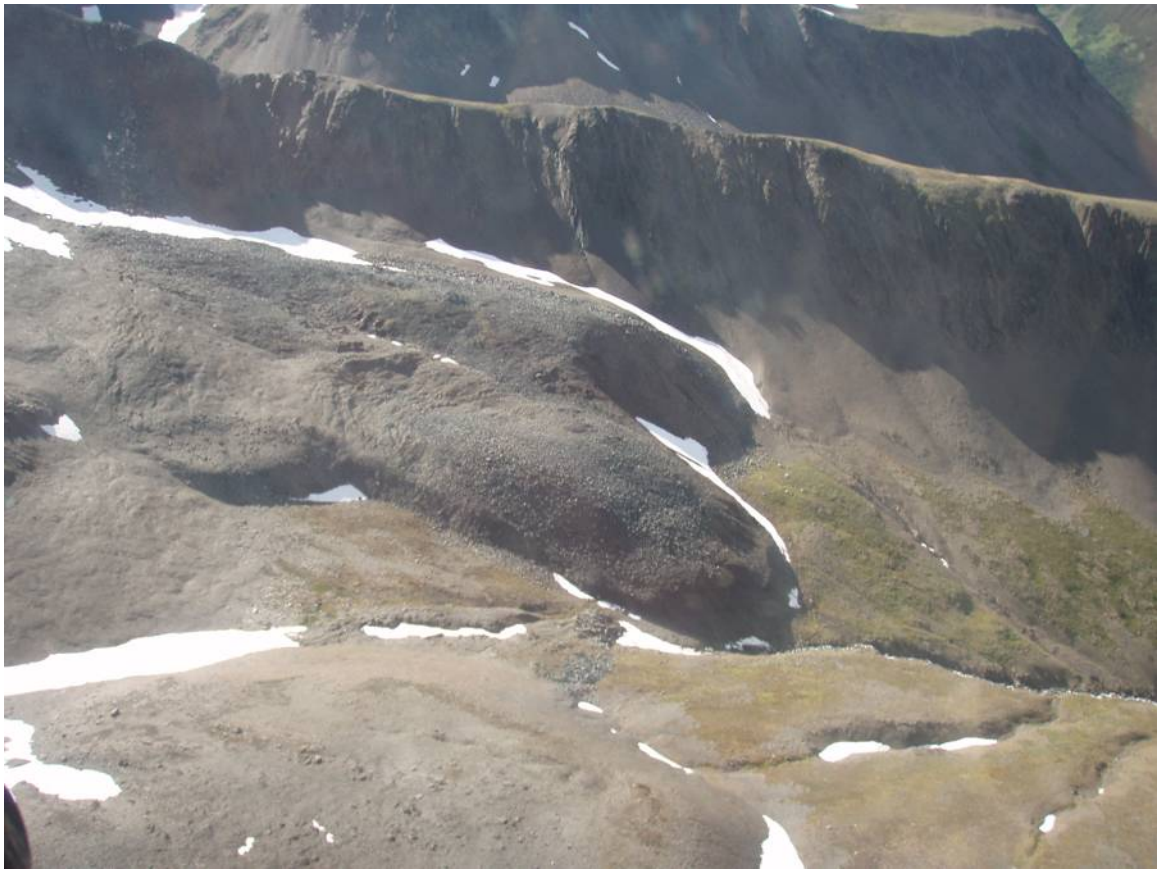

Figure 2.10 Rock glaciers such as this are common in north-facing cirques. Some extend to valley bottoms and are over a kilometre in length. Rock glaciers were mapped as Cb-ZFg. The surrounding bedrock slopes were mapped as Rs-Rb and the colluviated slopes were mapped as Ck-Rb.

with this material, sites with colluvium are not recommended for infrastructure development.

2.3.2.7 Organic

Organic deposits are accumulations of vegetative matter thicker than one metre. They are usually found in floodplains, areas of shallow permafrost, and other locations with poor drainage. Abundant small tussocks throughout the map area may indicate active ground ice in organic materials (Fig. 2.11). Their susceptibility to freeze-thaw processes and their compressibility make organic sediments a poor foundation material.

Organic deposits near Zn-rich streams and springs are highlighted by bright green mosses (Fig. 2.12; Jonasson *et al.*, 1983; Goodfellow, 1989). The high chemical exchange capacity of these mosses has concentrated the zinc to create secondary Zn minerals such as hemimorphite, smithsonite and wurtzite (Jonasson *et al.*, 1983). The distinct green colour comes from the development of a water-resistant protective coating on the moss in response to the high metal contents (Lee *et al.*, 1984).

Figure 2.11 Tussocks of fine-grained material in a depression between esker ridges. These features may have formed from active ground ice in organic deposits. This depression would be mapped as Ob-Z but was too small to be a separate polygon. Backpack is 70 cm long.

Figure 2.12 Zn-rich moss accumulated from streams and springs running through mineralized bedrock zones. The green colour results from a water resistant coating developed on the moss due to the high metal content of the water.

2.3.3 Surficial Expression

Surface expression refers to the 3-D shape of a landform. Four broad categories of surficial expression were used: slope indicators, thin material cover, thick material cover, and complex expressions (Table 2.3). These are grouped according to the relationship between the thickness of the material and the influence of the underlying material on the topography of the polygon. Slope indicators (p, j, a, k, s) denote the steepness of the slope. Thin material expressions (b, v, w) indicate relatively shallow sediments, with the surface topography being controlled by the underlying material, usually bedrock. Thick material expressions (u, h, m, r) are thick enough that they control their own surface expression, independent of the underlying material. Complex expressions (f, c, t) are non-planer and/or multi-directional and are independent of the underlying bedrock. In polygons with multiple surface expressions, they are listed in the terrain symbol in order of decreasing influence. Because terrain inventory maps do not provide interpretations of terrain stability for every polygon, only processes that were identified as potential hazards were included on the map.

2.3.4 Geomorphological Processes

Geomorphological processes are mechanisms of weathering, erosion and deposition that alter surficial materials and landforms (Howes and Kenk, 1997). Processes affecting the map area vary in frequency and magnitude from long-term, centimetre-scale changes in permafrost levels, to rapid changes such as debris flows capable of damaging infrastructure (Table 2.4). This diversity of geomorphological processes reflects the different ways the landscape is continuously adjusting. This is evident on gentle slopes where mass movements, such as creep, are common in association with the active layer. Conversely, steeper slopes have abundant debris flows and rock slides, which are caused by shorter-term climatic events.

Table 2.3 Surficial expressions used in the terrain inventory map to indicate the 3-D shape of the landform.

	Expression	Symbol	Description
Slope Indicators	Plain	p	0-3^{o}
	Gentle Slope	j	4-15^{o}
	Moderate Slope	a	16-26^{o}
	Moderately Steep Slope	k	27-35^{o}
	Steep Slope	s	>35^{o}
Thin Materials	Blanket	b	>1 m
	Veneer	v	<1 m
	Mantle of Variable Thickness	w	Varies between 0 and >1 m
Thick Materials	Undulating Topography	u	Non-linear features with slopes <15^{o}
	Hummocky	h	Non-linear features with slopes >15^{o}
	Rolling Topography	m	Linear features with slopes <15^{o}
	Ridges	r	Linear features with slopes >15^{o}
Complex Expressions	Fan	f	Fan-shaped and <15^{o}
	Cone	c	Fan-shaped and >15^{o}
	Terrace	t	Level area with slopes above and below

Identifying and classifying mass wasting processes is especially important for infrastructure development in the map area. The range in types of mass wasting processes and their associated hazards necessitates their distinction with process qualifiers (Table 2.5). Five qualifiers were used for this map, four of which distinguish types of rapid mass movements (R). These qualifiers allow the user to evaluate more accurately the level of hazard of developing the areas where mass wasting processes are active.

Processes that were common across the map area were not always labelled on the map to reduce redundancy. For this reason, only polygons with excessive or especially hazardous geomorphological processes are labelled with the appropriate geomorphological processes. This is most notable for avalanches,

Table 2.4 Geomorphological processes present in the study area and indicated on the terrain map.

Process	Symbol	Description
Snow avalanche	A	Rapid down-slope movement of snow, ice and incorporated materials
Meltwater channelling	E	Erosion by glacial meltwater
Slow mass movements	F	Slow mass movement of surficial materials down-slope
Kettled	H	Depressions created from the melting of buried ice
Irregular sinuous channel	I	Single channel with irregular bends
Meandering channel	M	Single channel with regular and repeated bends
Rapid mass movement	R	Rapid mass movement of surficial materials down-slope
Solifluction	S	Slow down-slope movement of saturated, non-frozen material
Gullying	V	Incision of varying slope on valley sides
Permafrost processes	X	Processes resulting from growth or decay or permafrost
Periglacial processes	Z	Combination of solifluction and other periglacial processes

Table 2.5 Processes qualifiers used in the terrain inventory map to provide details on rapid (R) and slow (F) mass movement processes.

Process Qualifier	Symbol	Description
Rockfall	Rb	Falling and rolling bedrock
Debris Flow	Rd	Rapid flow of saturated surficial material
Rock Slide	Rr	Sliding masses of disintegrated bedrock
Debris Slide	Rs	Sliding masses of surficial material
Rock Creep	Fg	Slow movement of debris by periglacial processes

which are abundant on steep slopes throughout the map area, especially during the spring when melting snow packs are more mobile (Fig. 2.13). Other common geomorphological processes include periglacial and permafrost. The difference between these two processes is subtle. For this map, periglacial processes include cryoturbation, nivation and solifluction (Howes and Kenk, 1997). Alternatively, permafrost processes are controlled by permafrost aggradation or degradation Their absence on the map should not be interpreted as a lack of avalanche hazard, but should instead be interpreted as high hazard on most steep slopes across the map area. As permafrost is common in the map area, permafrost processes are more frequent than periglacial processes.

2.3.5 On-Site Symbols

Glacial landforms are indicated on the map with a combination of terrain polygon symbols and on-site symbols. The on-site symbols used on the map are described below in detail as they are useful for understanding the glacial history of the area and can be important for infrastructure development. On-site symbols include both erosional (cirques, streamlined bedrock, meltwater channels, striations and rat tails) and depositional (eskers and moraines) features.

All the cirques observed in the area were likely active in the late Wisconsinan, although many of them were also active during cold periods in the Holocene. Most of the cirques in the map area are north-facing, and many contain active rock glaciers. Jackson (1982) observed that cirques are frequent above 1520 m

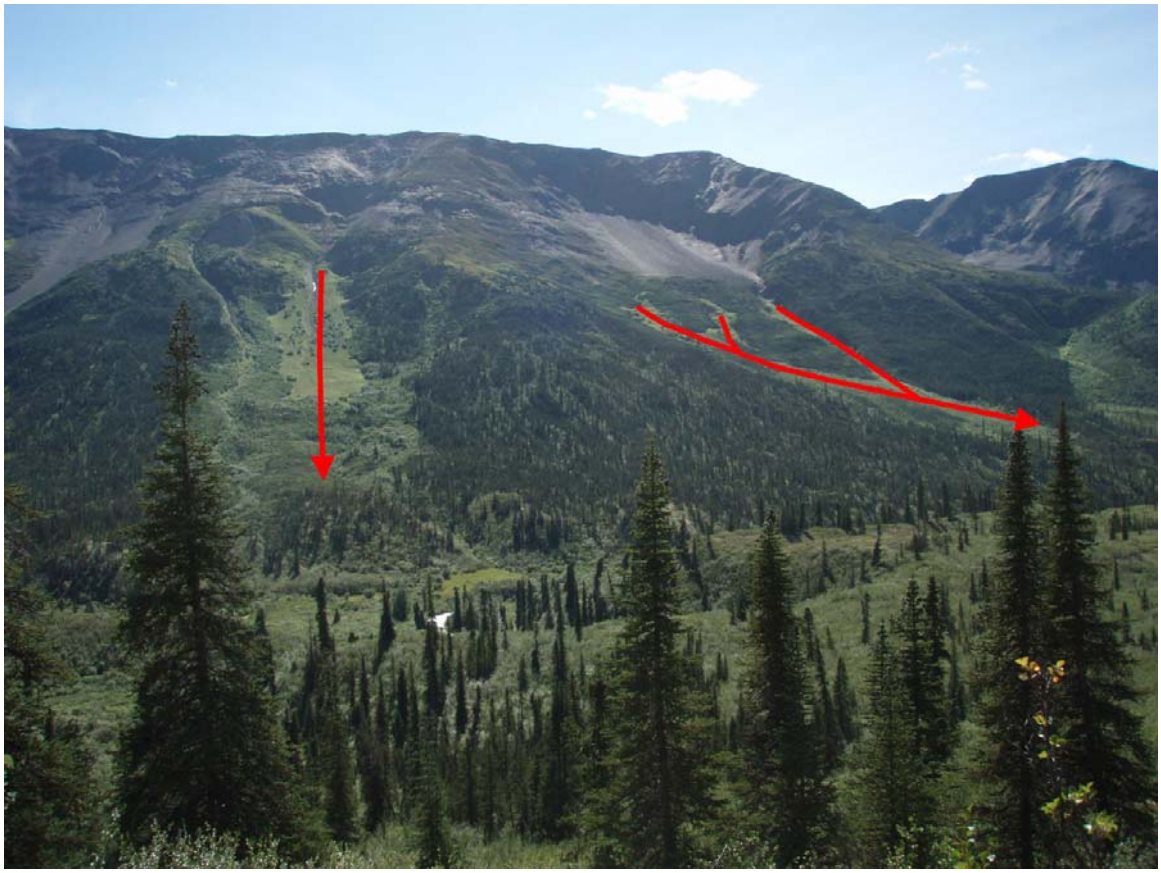

Figure 2.13 Avalanche and debris flow tracks on the side of Don Creek Valley. The pattern of vegetation in these tracks indicates multiple recent events.

in Howard's Pass, with the freshest cirques occurring above 1830 m in the Ragged Range to the southeast.

Streamlined bedrock features are eroded subglacially. Although their formation remains controversial (e.g. Boulton, 1987; Shaw *et al.*, 1989), they are reliable ice-flow indicators. Because of the thick sediments that cover most valley floors, these forms were mainly observed in the Nahanni Valley and west of the Pelly River. None were observed at high elevations, likely due to the fissility of the bedrock in these locations.

Two types of meltwater channels were observed incised into bedrock or surficial sediments in the map area. Lateral channels eroded by ice-contact glacial meltwater provide an indication of the slope and ice-marginal position of the

glacier (Fig. 2.14). Pro-glacial meltwater channels are formed as meltwater exits the front of a glacier. Although both types were observed, lateral meltwater channels are more abundant. In addition, many meltwater channels were mapped flowing down-slope. These were identified as meltwater channels because of their large size in relation to present stream flow.

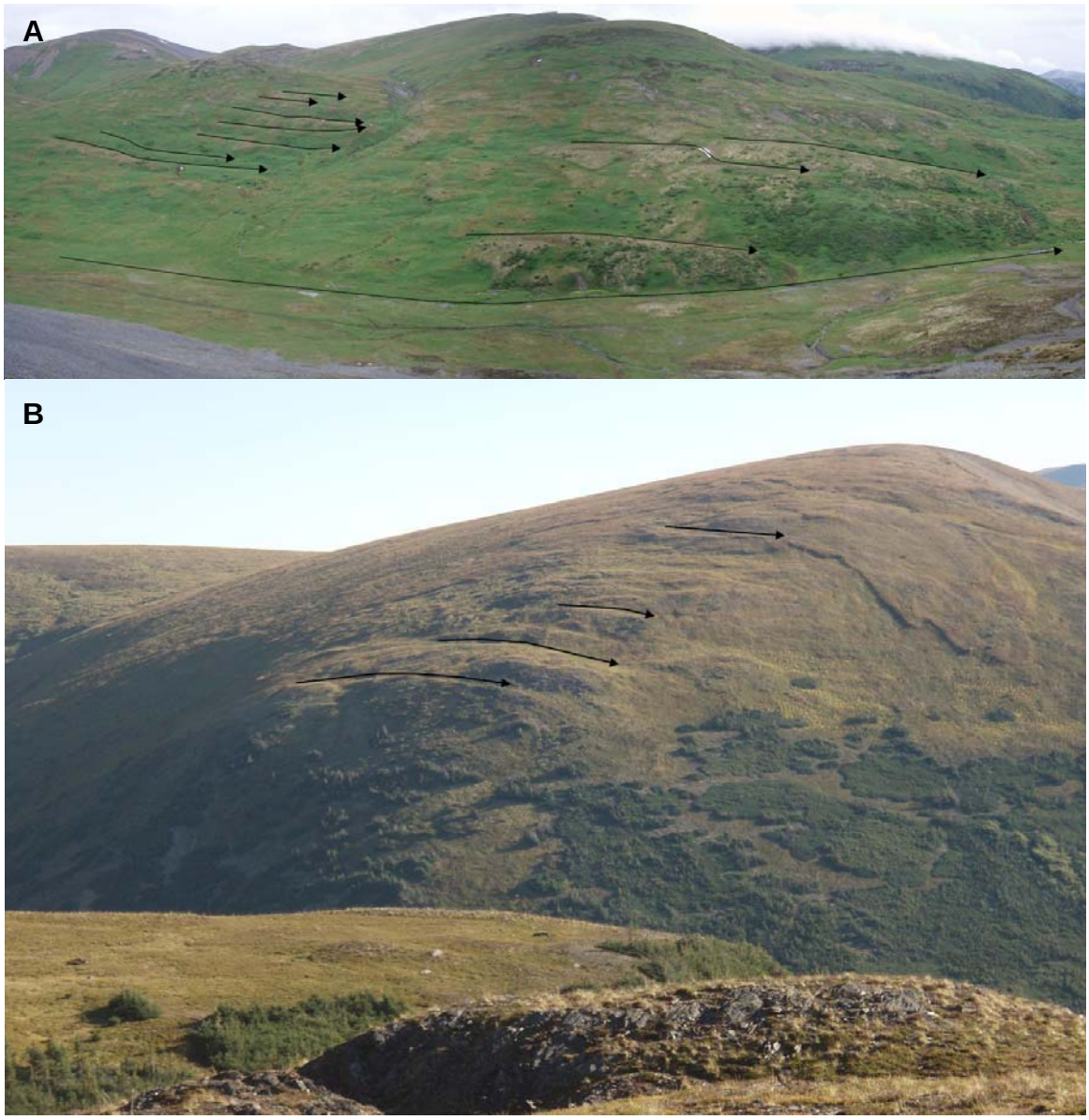

Figure 2.14 a) Meltwater channels north of XY camp; b) meltwater channels in the southeast of the map area. These features are common on valley walls. The ones pictured here formed laterally on the glacial margin. Arrows indicate interpreted meltwater flow directions.

Striations and rat tails are small-scale, linear erosional features that act as reliable ice-flow indicators. Striations are formed from abrasion of bedrock surfaces by ice-transported debris. They are typically bidirectional ice-flow indicators, although some forms show unidirectional ice-flow orientations. Rat tails are formed from differential erosion around relatively resistant bedrock surfaces and are good unidirectional indicators of ice-flow. In the map area. Resistant chert clasts in Earn Group conglomerates provided the best rat tails. Both striations and rat tails were observed across the study area.

Eskers in the map area are concentrated in the bottoms of major east-west valleys. They typically exceed five metres in height and can extend for over 15 km in length (Fig. 2.15). Esker sedimentology and stratigraphic relationships with underlying units in the Don Creek Valley indicate that they formed sub-glacially during waning ice-flow (see Chapter 3).

Figure 2.15 Eskers oriented from east to west in the Don Creek Valley. These eskers formed subglacially during late-stage ice-flow (see Chapter 3). Paleoflow directions in eskers (arrows) were interpreted from morphology and paleocurrent measurements.

Few moraines were observed in Howard's Pass. They are mostly lateral moraines on the slopes of narrow valleys, although some occur in wider valleys. End moraines are confined to within cirques and were likely formed during minor late glacial or Holocene re-advances.

2.4 Summary

A 1:50 000-scale terrain inventory map was constructed for the map area to help infrastructure development and to provide information on glacial dynamics. The terrain symbols used to describe the delineated polygons include descriptions of the texture and type of surficial materials, in addition to the surficial expressions and geomorphological processes. These data are included in the back pocket as Appendix A and in CD form in Appendix B.

The map was based on the digitized terrain information entered into ArcGIS software. The different colours used on this map reflect the primary surficial material of each polygon. This map is therefore useful for determining the aerial extent of the different surficial materials in the map area. Seven types of surficial material were recognized in the map area: bedrock, morainal (till), glaciofluvial, glaciolacustrine, colluvium, organic and fluvial.

Till is the most aerially extensive material in the map area. It typically occurs as veneers and blankets on gentle to moderate slopes. In areas of lower relief, till deposits are thicker and have expressions that are more complex. Most of the map area was likely covered in till following late Wisconsinan glaciation. Subsequent erosion at high elevations and deposition in valley bottoms have stripped or buried some of this till cover.

The next most extensive surficial materials are colluvium and bedrock. These materials are commonly found in close association on moderate to steep slopes and at high elevations. However, because of the prevalence of active permafrost

in the map area, many moderate to gentle slopes have solifluction lobes and other deposits of active colluvium than can adversely affect infrastructure development. Other hazardous mass wasting processes commonly found on colluvium and bedrock slopes in the map area include avalanches, rock falls, rock slides, debris slides and debris flows.

The other types of surficial materials are mostly restricted to valley bottoms. Many of the larger valleys are filled with thick glaciofluvial deposits with thin accumulations of fluvial material. Glaciofluvial materials range from a few metres to tens of metres in depth. The quality of these deposits as aggregate resources depends on their clast size and lithology. Fortunately, their abundance in the valleys currently being developed makes them an easily accessible construction material. Fluvial materials are restricted to modern floodplains, terraces, fans and cones. Although fluvial materials may be extensive enough to be a source of aggregate in the largest valleys in the map area, flooding, migrating channels and the presence of protected fish habitat make them unsuitable locations for aggregate extraction or infrastructure development.

Other material types that are concentrated in the valley bottoms include organic and glaciolacustrine deposits. Although organic deposits are common throughout the map area, they are limited in depth from a few metres to less than a metre. These deposits are poorly-drained and commonly contain segregated ice lenses, making them highly unstable as a foundation. Similarly, glaciolacustrine deposits are limited in the map area and can have ice lenses. However, their low permeability makes glaciolacustrine materials useful as tailing pond liner.

3 QUATERNARY STRATIGRAPHY

Investigating Quaternary exposures is useful for this study for two reasons. First, these sections provide thicknesses and relationships between different surficial materials and expressions. This is useful for drift prospecting as the type of survey used depends on the thickness of the material type (see section 5.3). Second, knowledge of the stratigraphy of the study area gives important information on ice-flow dynamics and chronology. Unfortunately, datable material such as tephras or organic remains were not observed in the sections in Howard's Pass. However, these sections do provide insight into depositional environments and ice-flow directions. In particular, measurements of clast orientations in till were useful for interpreting late-stage ice-flow directions.

The Quaternary exposures observed in Howard's Pass are described in this chapter in three sections – river exposures, esker sedimentology, and data recovered from drill cores. The river sections are scattered throughout the study area and reveal a similar stratigraphy with till overlying glaciofluvial sand and gravel. These sections, like elsewhere in Yukon (e.g. Levson, 1992), are typically restricted to valleys perpendicular to later ice-flow. Recent road cuts through eskers in the Don Creek Valley that lie stratigraphically above these two units allowed the description, interpretation and correlation of seven facies. Nearby, 19 drill holes preserving Quaternary sediments provided valuable stratigraphic data that was otherwise inaccessible. Stratigraphic logs of all of the sections are illustrated in Appendix C.

3.1 Methodology

During the summer of 2006 and 2007, numerous Quaternary sections exposed by river erosion and road construction were investigated throughout Howard's

Pass (Fig. 3.1). At each of these exposures, sections were measured, sketched and photographed. Their colour, texture, structure, contacts between units, consolidation and any other important features were also described. Separate units were assigned to different material types and samples were collected for grain-size analysis (Fig. 2.4) and archiving with the Geological Survey of Canada.

Where possible, measurements of the down-plunge orientations of long-axes of clasts in till (till fabrics) and glaciofluvial material (paleoflows) were made to help deduce depositional flow directions. These measurements were analyzed by calculating the three normalized eigenvalues and the associated eigenvectors of their 3-D distributions (Hicock *et al.*, 1996), following the approach used by Andrews and Shimizu (1966). Of the three, the primary eigenvalue (S_1) and eigenvector best represent the down-plunge orientation of clast long-axes in the case of till fabrics, and down-dip for paleoflow measurements. Because clasts are deposited with their down-plunge directions oriented reverse to flow direction, flow direction is 180^o from the primary eigenvector. The eigenvalues and plots for this study were calculated using StereoNett Version 2.46, a shareware utility created by Johannes Duyster at the Institut fur Geologie, Ruhr-Universitat-Bochum, in Bochum, Germany.

Eigenvalue analysis on its own is insufficient to accurately analyze till fabric data for interpretations of ice-flow directions. In addition, the modality classification suggested by Hicock *et al.* (1996) was used to help distinguish different types of till. This method combines eigenvalues analysis with visual examination of Schmitt equal-area, lower-hemisphere projections of long-axes fabrics to classify measurements as unimodal cluster, spread unimodal, bimodal cluster, spread bimodal or polymodal (Hicock *et al.*, 1996). Generally, fabrics with high primary eigenvalues and unimodal cluster or spread unimodal plots represent basal tills. However, Hicock *et al.* (1996) stress that this classification is still limited and is not a complete representation of all subglacial depositional environments. Fabric

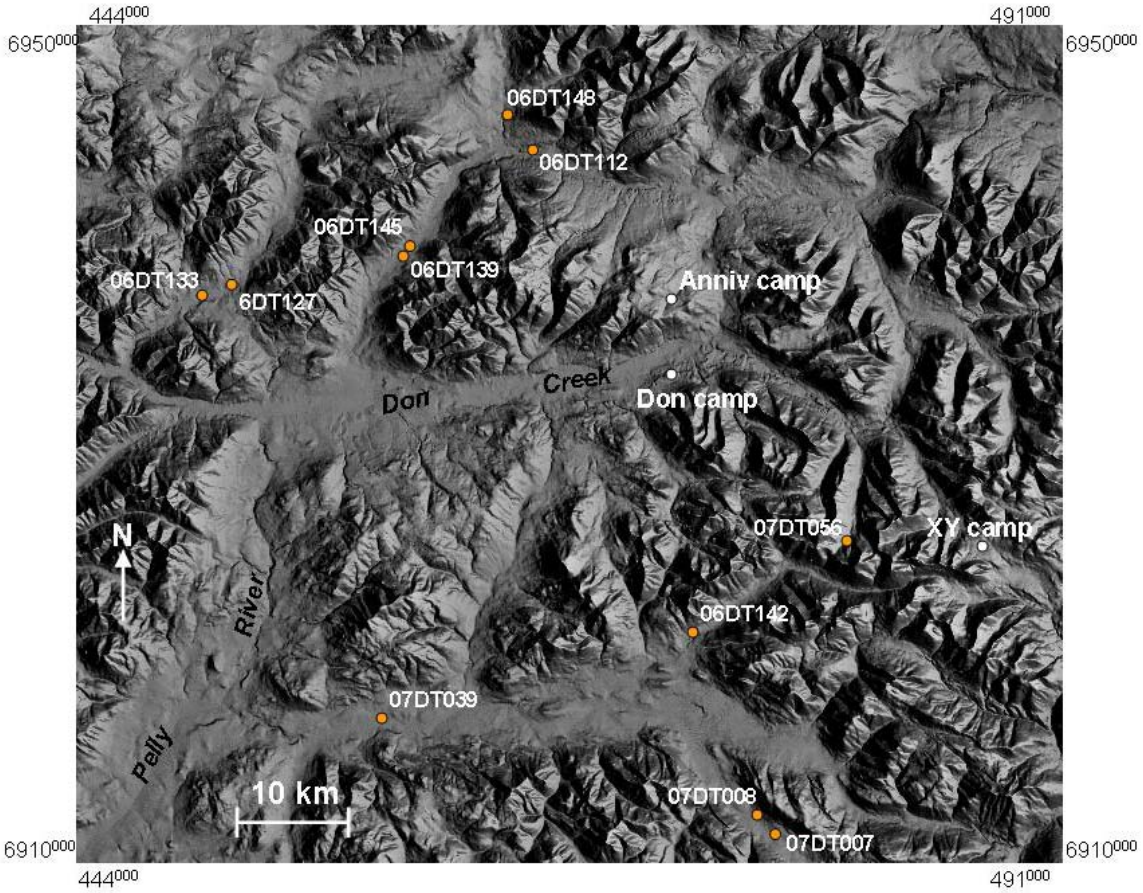

Figure 3.1 Location map of river sections in Howard's Pass. Most of these sections have similar stratigraphy, with a thin till cap overlying thick glaciofluvial sand and gravel.

measurements were therefore augmented by examination of clasts for striations, lee-end fractures, keels and any other evidence of glacial erosion.

Drill core logged from 19 sites drilled in the Don Creek Valley was used to investigate buried materials. This core was observed for its grain size, matrix content, consolidation, colour, maximum and average clast size, clast lithologies, rounding and sorting. Depths were measured by the drillers and used to infer apparent unit thicknesses. Records of drilling plunges were used to calculate actual unit thicknesses.

3.2 River Sections

Numerous sections are exposed by river erosion in Howard's Pass (Appendix C). These sections reveal a similar stratigraphy with thick sand and gravel underlying a relatively thin diamict. This relationship was observed in many locations across the study area and is exposed in valleys oriented both east-west and north-south (Fig. 3.1). The best stratigraphic exposures in the study area are in an unnamed tributary west of the Pelly River (06DT127, 06DT133). Although the diamict is exposed at the surface, gravel hummocks and terraces lie adjacent to, and stratigraphically above, the exposure. This stratigraphy of a diamict between sand and gravel deposits is similar to the stratigraphy discussed in section 3.5. – Drill Core Stratigraphy.

The same two units are exposed at both 06DT127 and 06DT133. Unit 1 is a 10 to 20 m thick deposit comprised of several packages of coarsening-upward horizontally bedded pebble and cobble gravel with a fine to coarse sand matrix (Fig. 3.2). The bottom five metres of this unit in 06DT133 are consolidated and partly cemented by $CaCO_3$ from the weathering of abundant limestone clasts (Fig. 3.3). Clast orientations and observations of dipping beds in this unit suggest it was deposited down-valley, to the west. Extensive post-depositional normal faulting caused by loading crosscuts bedding in this unit (Fig. 3.3).

Unit 2 is a 1.8 m to 3.5 m thick blocky, consolidated, grey to light brown diamict with a sandy silt matrix. Weathering along sub-horizontal fractures was observed at 06DT139 and 06DT145. Clasts in this unit are striated, keeled, fractured and frequently ploughed (Fig. 3.5). Mean clast measurements of two fabrics taken 50 and 75 cm above the lower contact at 06DT133 suggest paleoice-flow towards the west and only vary by 10^{o} (Fig. 3.2). These fabrics are spread unimodal and have primary eigenvalues equal to 0.68 and 0.80, respectively. Clast orientations measured at 06DT127 have a lower eiganvalue, but also indicate valley-parallel flow to the southwest (S_1 = 0.64, n=49, spread unimodal). An erosive contact separates unit 2 from the underlying unit 1.

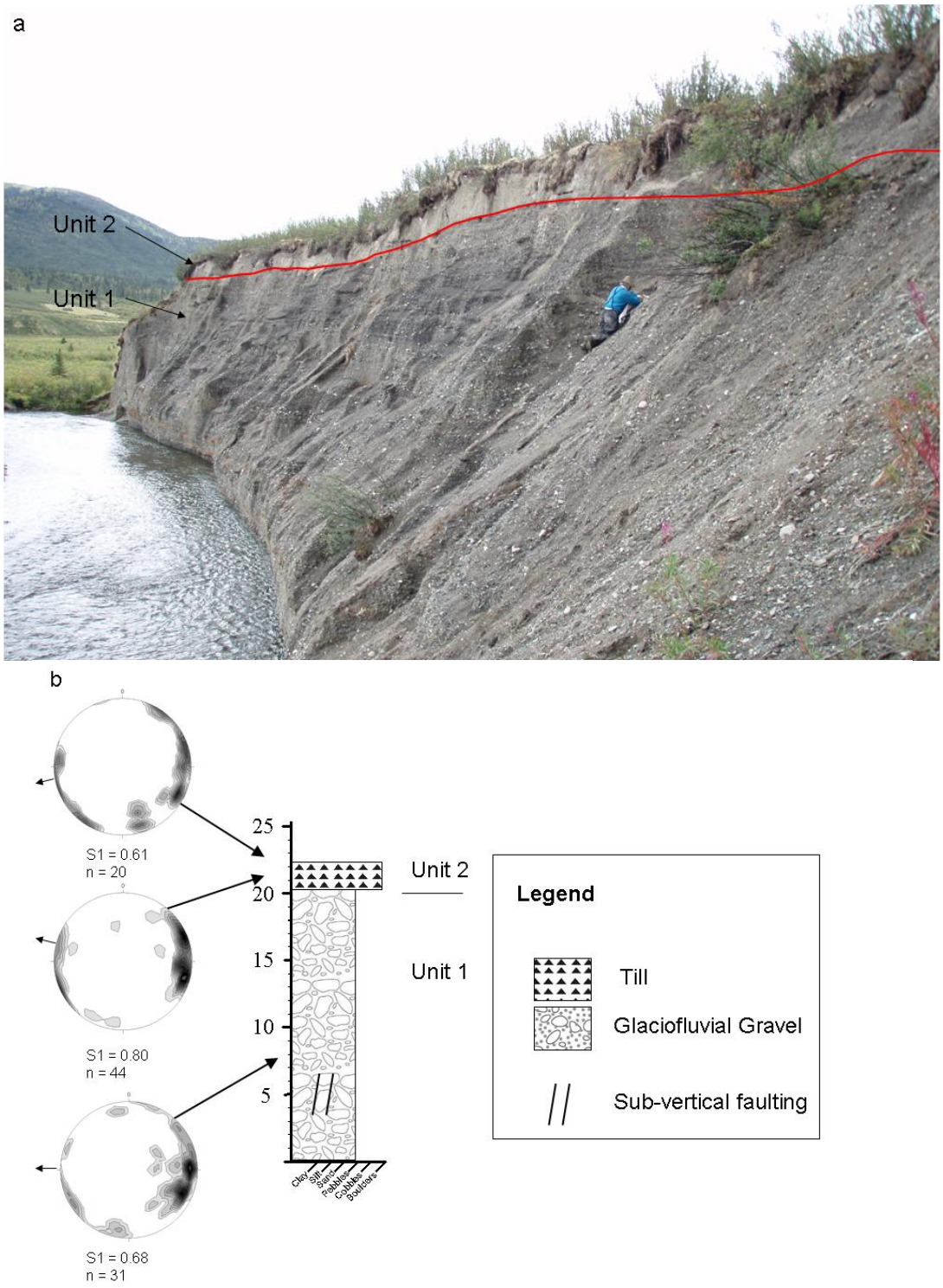

Figure 3.2 (a) Section 06DT133 exposed by a river west of the Pelly River. (b) Stratigraphic log of the exposure. Unit 1 is a pebble-cobble glaciofluvial gravel. Unit 2 is a basal lodgement till. Little arrows in the till fabric and paleoflow indicate the interpreted westward ice-flow and meltwater flow directions, respectively.

Figure 3.3 Glaciofluvial gravel, here exposed at 06DT133, typically form unit 1 across the study area. The sub-angular to well-rounded clasts are cemented in a sand matrix. Post-depositional normal faulting caused by loading has entrained the larger clasts. Pen is 14 cm.

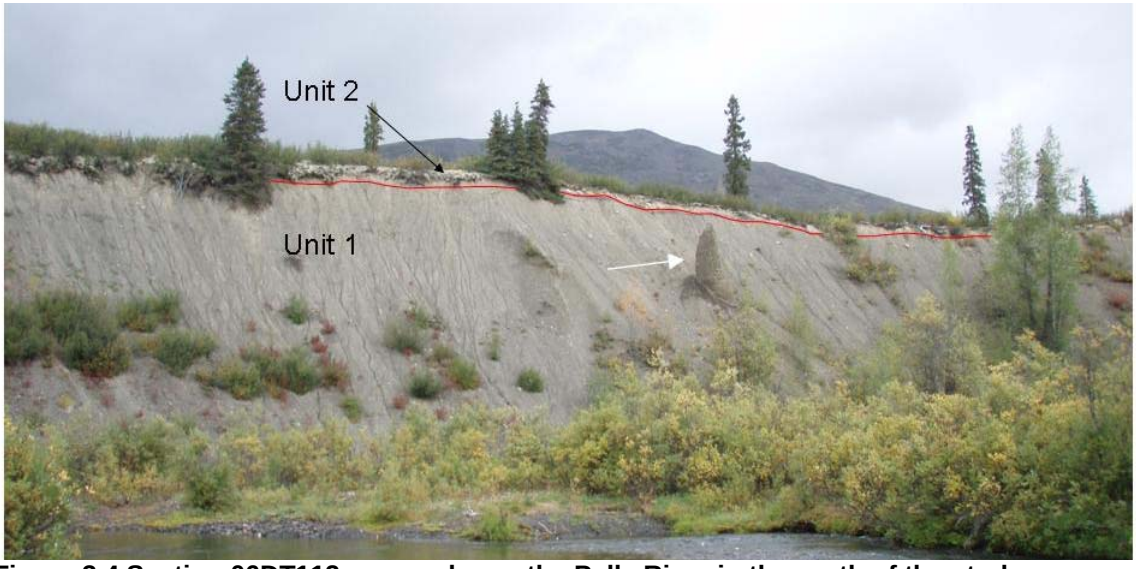

Figure 3.4 Section 06DT112 exposed near the Pelly River in the north of the study area. Unit 1 is glaciofluvial sand and gravel. Unit 2 is a unconsolidated, light grey till. A 4.5 m pillar of gravel (white arrow) illustrates the cohesion of unit 1.

Unit 1 varies across the study area. At a section near the Pelly River (06DT112), it is poorly sorted and is sufficiently consolidated to preserve a large, 4.5 m pillar (Fig. 3.4). At 06DT142, this unit is composed of interbedded cobble to boulder gravel and fine to coarse-grained sand with areas of convoluted bedding. Some of the material in unit 1 was likely sourced from sediment several kilometres from its present location. However, some deposits (e.g. 07DT056) observed in cirques reflect local lithologies, indicating short transport distances.

The same two units are also observed in larger valleys in the south of the study area. At 07DT039, a thin diamict overlies thick sand and gravel for over 300 m. Clast orientations in the diamict suggest flow was up-valley to the west-northwest (S_1 = 0.68, n = 51, spread unimodal). At the far western end of the section, the diamict pinches out and is replaced by 40 cm of light brown, clayey silt with rare clasts. The silt bed is cryoturbated, possibly incorporating some of the underlying

Figure 3.5 Top view of a striated clast in till observed at 07DT009. This clast is also keeled and is fractured on its lee (left) end. These features form from ploughing during subglacial deposition and are indicative of lodgement till.

gravel. Below the lower contact, a 25 cm wide ice wedge pseudomorph descends into the gravel (Fig. 3.6). This feature does not extend up to the contact with the silt and was likely formed synchronous to the gravel deposition.

Approximately 10 km south-southwest of the Don Creek Valley, two sections one kilometre apart contain different materials (Fig. 3.7). The up-valley section (07DT007) is composed of five to ten metres of unconsolidated, weakly stratified light brown, silty diamict with a wide variety of local lithologies. The clasts in this diamict are heavily striated and faceted, and have fractured ends on both their down and up-plunge ends. Further down-valley at 07DT008, eight metres of unconsolidated, weakly stratified pebble gravel is exposed. This unit appears to be imbricated to the south in the opposite direction as modern drainage. This interpretation of flow direction is somewhat supported by a weak alignment of clast orientations that suggest this unit was deposited up-valley toward 185^{o} (Fig. 3.7b).

Unit 1 is likely glaciofluvial based on the grain size, horizontal stratification and coarsening-upward cycles. In addition, the extensive faulting observed in this unit at multiple sections was likely caused by post-depositional loading by the glacial ice. This indicates that unit 1 pre-dates the most recent glacial episode. The stratigraphic relationship between units 1 and 2, and the presence of striated, keeled and ploughed clasts suggest that unit 2 is a till lying unconformably over unit 1. Fabrics measured at 06DT133 and 07DT039 are spread unimodal and have strong eigenvalues indicating valley-parallel deposition. Unit 2 is therefore likely a basal till deposited during valley-parallel ice-flow. The diamict observed at 07DT007 is likely a melt-out till, based on its lack of consolidation and weak stratification. The lack of consolidation in the gravel at 07DT008 suggests it post-dates glaciation. The silt unit observed at 07DT039 above unit 1 is interpreted as either loess or glaciolacustrine sediment.

Figure 3.6 Ice wedge pseudomorph in glaciofluvial gravel at 07DT039.

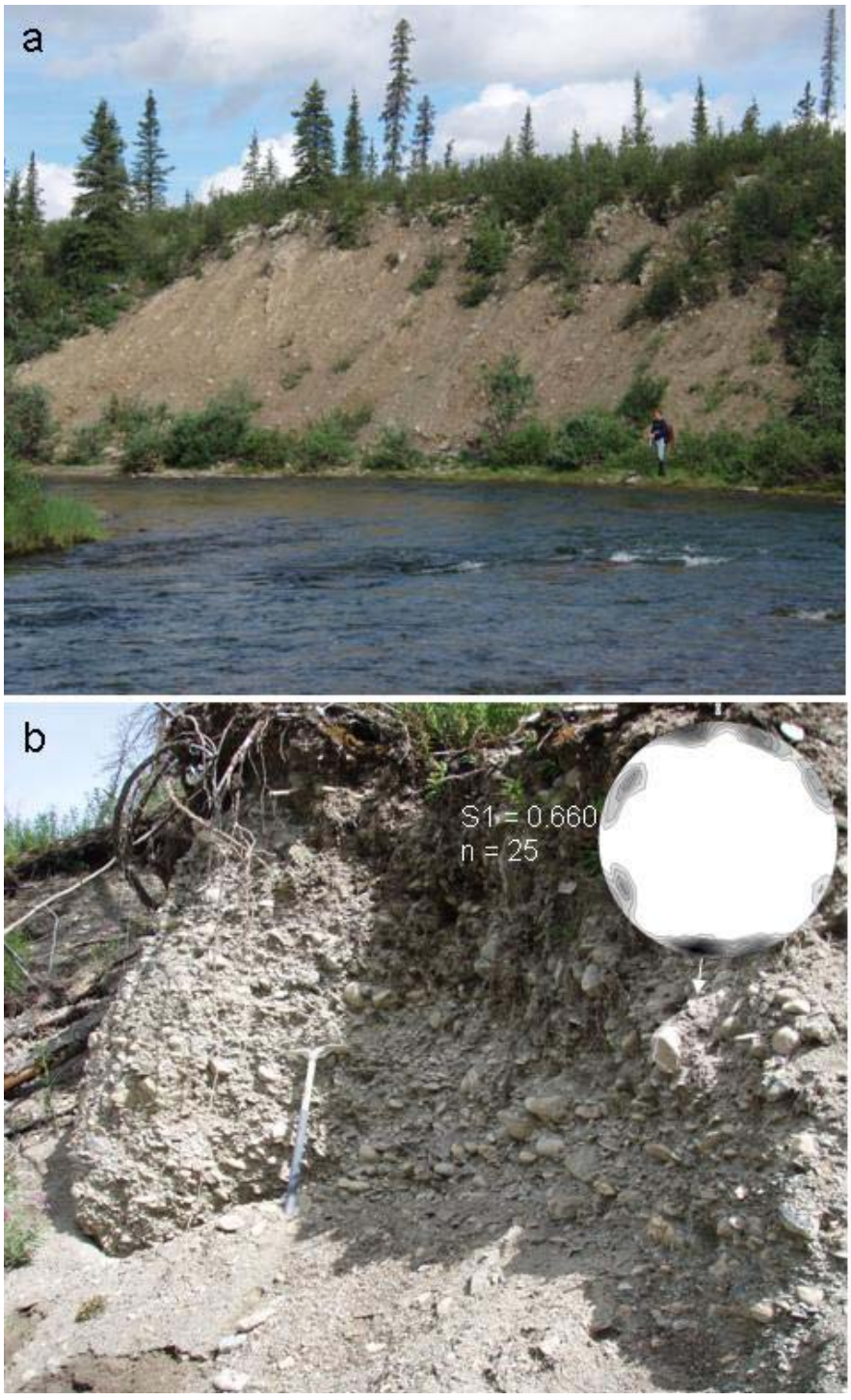

Figure 3.7 Two exposures located approximately 2 km apart in the south of the study area (07DT008). (a) 5-10 m of unconsolidated, silty diamict. (b) 8 m of weakly stratified, pebble gravel with paleoflow measurements indicating up-valley deposition.

3.3 Esker Sedimentology

Eskers are a common form of glaciofluvial deposit in Howard's Pass. They are concentrated in wide valleys oriented east-west and on the western flank of the Nahanni Valley, but are also found in narrow valleys and at differing elevations. A few of these eskers are in contact with meltwater channels at their up-slope end. The longest esker complex extends for roughly 16 km in the Don Creek Valley. This continuous series of eskers and hummocky terrain is approximately 100 m wide and has several hills along its longitudinal axis that are up to 20 m above the adjacent portion of the esker.

Recent road construction in the Don Creek Valley exposed numerous sections through the esker complex. During the 2007 field season, 23 of these sections were visited by ATV (Fig. 3.8). At each section, detailed sedimentological descriptions were made and, where possible, paleoflow measurements of bedding planes or clast orientations were taken (Appendix C). The three best exposures (07DT009, 07DT063 and 07DT016; Figs. 3.9, 3.10 and 3.11) were used to define seven facies of esker sedimentation. These facies were then correlated across the remaining 20 exposures in the Don Creek Valley. In this section, these facies are described and interpreted in approximate stratigraphic order (Table 3.1). The implications of the paleoflow measurements and interpretations of the depositional environments and flow conditions in the conduits during esker aggradation are also discussed.

3.3.1 Facies Descriptions and Interpretations

Facies I is an unconsolidated light brown to black diamict (unit 2 in Fig. 3.9). It has a clayey silt matrix with some fine-grained sand, 15-20% clasts with a maximum size of 40 cm, is mostly massive and has a wide variety of lithologies. The diamict also has a weak fabric and abundant internally interlaminated silt and sand rip-ups (Fig. 3.12a). It is only exposed at 07DT009 and overlies a consolidated, grey diamict with a strong fabric that is interpreted as a till

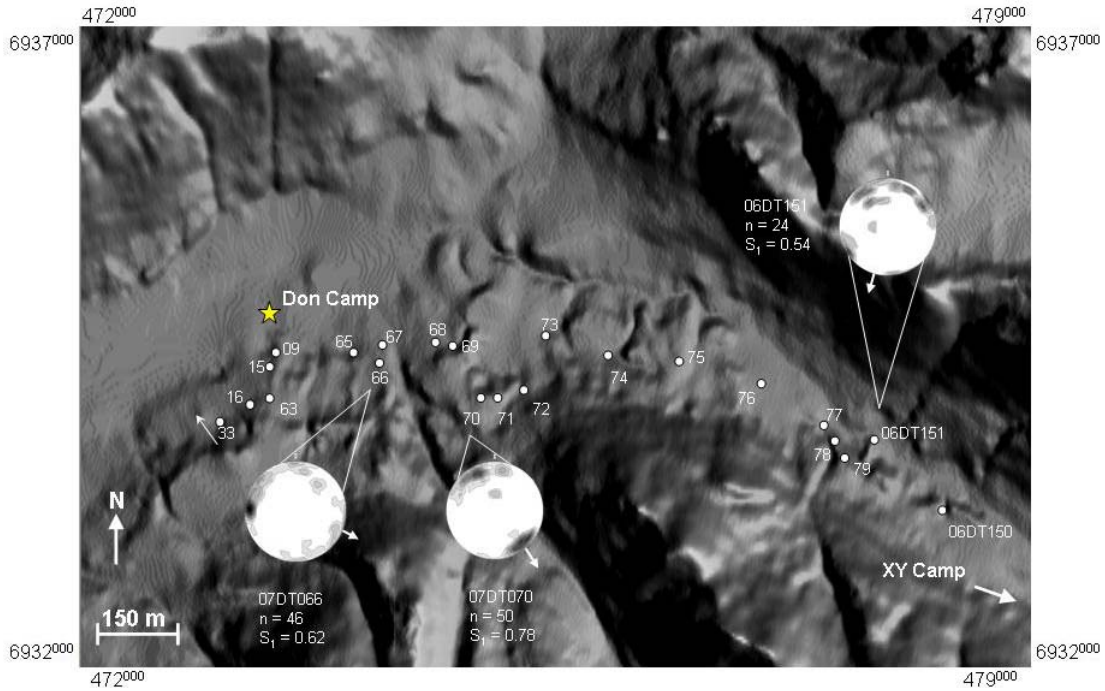

Figure 3.8 Locations and paleoflow measurements of esker exposures in the Don Creek Valley. All two-digit locations are prefixed with 07DT. The small white arrow at 07DT033 denotes measurements of ripple crests and bedding planes interpreted as representing the lateral margins of the esker ridge.

correlating to the regional till in the area (section 3.2). Facies I is interbedded at its upper contact with medium-grained sand beds (Facies IV, see description below; Fig. 3.12b). The rip-ups and interbedding at the upper contact indicate that this diamict was deposited in multiple events that eroded the underlying material, with sand and silt beds deposited between events. This diamict is somewhat enigmatic, but is interpreted as resulting either from mass movement events in a subglacial conduit, with the original source of sediment possibly being either melt-out or basal till, or from recurring episodes of meltout from debris-rich. The former explanation is favoured because of the interpretation of erosion of the underlying material.

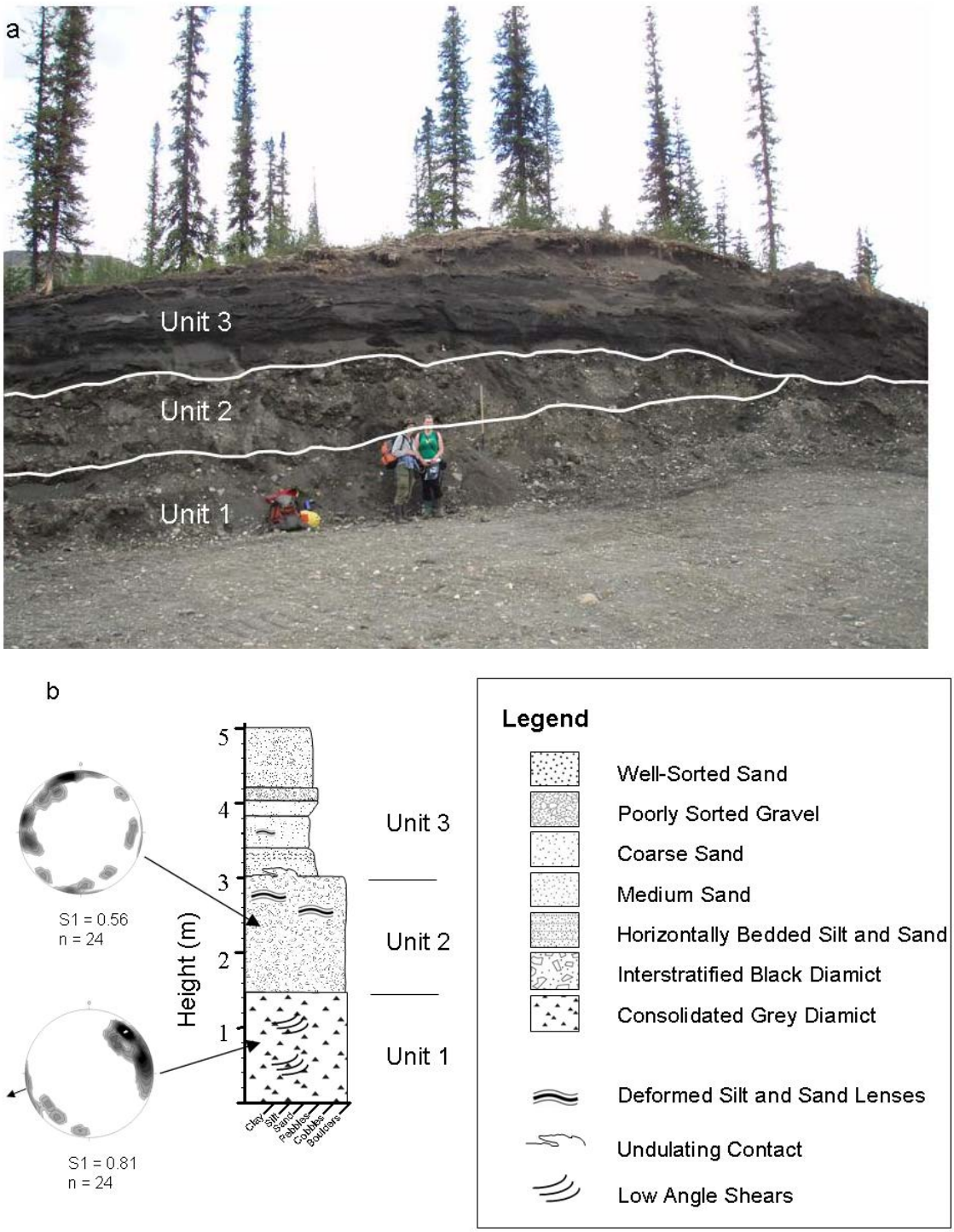

Figure 3.9 (a) Road cut through an esker at 07DT009 near Don camp. (b) Stratigraphic log of the section. Unit 1 is interpreted as a basal till, unit 2 is a meltout or basal till that was subsequently remobilized in the esker conduit, and unit 3 is the base of the esker. The difference between the S_1 of units 1 and 2 supports their formation through different processes. Unit 2 is comprised of Facies I.

Figure 3.10 Road cut through an esker at 07DT063. Two facies are exposed in lateral contact with each other. At this section, Facies IV consists of well-sorted sand and Facies II is composed of poorly-sorted, massive gravel. Facies IV was deposited first, with Facies II depositing laterally following erosion of Facies IV. Both facies were subsequently folded and faulted. Facies VI was observed directly to the left of the photograph.

Figure 3.11 A section through an esker at the Don camp airstrip (07DT016). Interbedded sand and gravel are exposed for 300 m. Multiple structures were observed, including diapers (Fig. 3.16), scour-and-fills (Fig. 3.15), and cross bedding.

Table 3.1 Esker facies descriptions, interpretations and locations in the Don Creek Valley. Each exposure is prefixed with 07DT.

Facies	Description	Interpretation	Exposures
I	Unconsolidated black diamict with a weak fabric and fine-grained rip-ups.	Re-worked lodgement or melt-out till.	09
II	Massive, poorly-sorted, graded gravel supported by a sand matrix.	Rapid deposition in a hyper-concentrated flow.	09, 15, 16, 63, 65, 66, 67, 69, 71, 72, 74, 75, 77, 78
III	Clast-supported, well-sorted, graded pebble gravel.	Sustained high-energy deposition with dominantly bed-load transport.	16, 34, 71, 72
IV	Graded, massive or interbedded fine to coarse sand.	Low-energy grain flow deposition.	09, 33, 63, 64, 66, 67, 68, 69, 73, 74, 75, 76, 78
V	Interbedded poorly-sorted sand and moderate to poorly-sorted, matrix-supported, massive or imbricate gravel.	Recurrent sheet flow on the esker flanks.	15, 16, 34, 63, 66, 70, 77, 79
VI	Rippled interbedded fine to medium-grained sand, silt and clay.	Low-energy deposition on the esker margins or in subglacial pools.	33, 63, 79
VII	Discontinuous, weathered, massive fine sand to silt.	Loess.	33, 63, 64, 66, 76

Facies II is a poorly-sorted, generally massive, matrix-supported gravel. The clasts in this facies range from granules to boulders and the matrix is poorly-sorted sand, with sand also occurring as large, well-sorted lenses in the gravel. This facies typically grades into granule gravel, silt and clay and is laterally discontinuous. It is exposed in 14 of the observed road cuts and is commonly found above and below a different facies. At 07DT063, boulders are observed in this facies surrounded on one side by fine-grained sediment and on the other by pebbles and cobbles (Fig. 3.13).

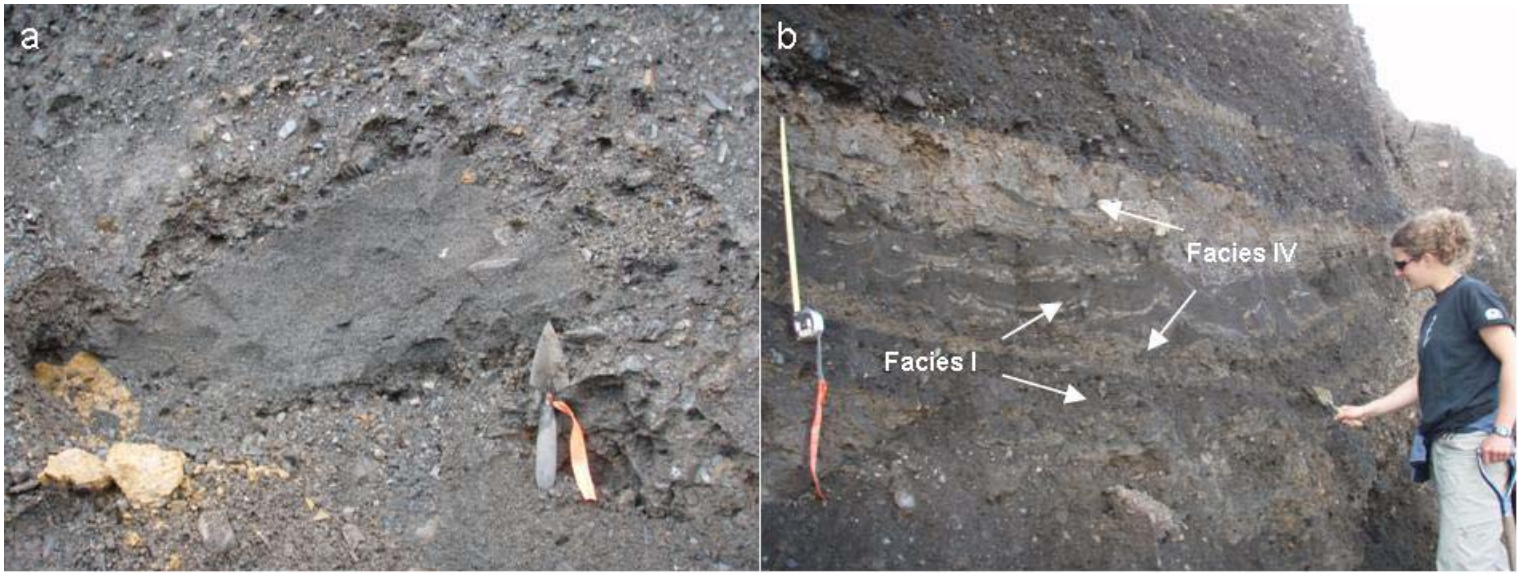

Figure 3.12 (a) Sand rip-ups observed in a clast-rich part of Facies I. This suggests sand deposition preceded Facies I. (b) Interbedded Facies I diamict and sand, silt and clay indicating Facies I deposited in multiple events separated by periods of lower energy.

Figure 3.13 The difference in grain sizes on either side of this boulder in Facies II suggests flow separated around it, depositing pebbles in cobbles on the stoss side and silts and sand on the lee side. It also indicates Facies II was deposited in a more fluidized flow in some locations. The red arrow indicates inferred flow direction.

The massive, poorly-sorted Facies II is interpreted as being a hyperconcentrated flow deposit. The lateral discontinuity of Facies II observed at 07DT063 may have been caused by highly variable conduit hydrodynamics. Variations in discharge in a conduit can cause a change from erosion of the underlying material to deposition of a new facies beside it (Fard and Gruszka, 2007). Changes in flow due to the cessation and re-establishment of subglacial meltwater likely resulted in the lateral discontinuities observed at 07DT063. Facies II was therefore likely deposited quickly, possibly en masse, in a hyperconcentrated flow during high discharge conditions (cf. Brennand, 1994).

The differentiation of grain sizes around boulders observed in Facies II is possibly due to flow separation around larger clasts and subsequent lee-side deposition. These features have been observed elsewhere, commonly near esker cores (Brennand, 1994). The presence of these features in Facies II suggests that portions of this facies were deposited in a more fluidized flow, allowing the separation of grain sizes. These features provide a rough approximation for flow direction with fines deposited down-flow of the boulder. At 07DT063, this relationship suggests flow was to the northeast, corroborating the interpreted esker morphology that also suggests they formed in this direction.

Facies III consists of clast-supported, open-framework, well-sorted gravel dominantly composed of pebbles four to six centimetres in diametre. It can be interbedded with poorly-sorted, coarse-grained sand and is in sharp lateral contact with Facies II. It typically grades up to a matrix-supported gravel with smaller clasts. Open framework gravel is typical of deposition before and during the initial waning stages of flood flow in an esker conduit (Shulmeister, 1989). The lack of finer-grained sediment is a result of mostly bed-load, rather than suspension, transport in a fluid flow during the major flow event (Brennand, 1994). The observed normal grading indicates decreasing discharge conditions in the conduit. Facies III was deposited under a more sustained high-energy flow than Facies II, causing the removal of the finer-grained sediment.

Facies IV was observed above and below both Facies II and III at 13 exposures in the Don Creek Valley. It consists of massive or interbedded and interlaminated fine to coarse-grained sand. At some locations, it contains pebble, silt and clay beds and laminations, and rip-ups of underlying material. The beds and laminations have inverse grading internally, but overall Facies IV is normally graded. Facies IV was observed at the core of the exposure at 07DT063 surrounded by, and intercalated with, Facies II (Fig. 3.10). Both of these facies were extensively folded and then faulted (Fig. 3.14).

Figure 3.14 Folding and subsequent faulting at the contact between Facies IV and Facies II at 07DT063. These structures likely formed from melting of the supporting ice walls or de-coupling and re-coupling of the overlying ice.

At 07DT069, this facies occurs in a 105-cm-long, 40-cm-wide lens that intrudes into the underlying Facies II.

Facies IV accumulated during sustained low-energy deposition. The normal grading indicates decreasing energy associated with progressively lower-discharge deposition. The internal coarsening-upwards within the beds suggests they were deposited as grain flows or other processes with high dispersive pressures. The extensive folding and faulting possibly resulted from either re-coupling of the ice to the sediment bed during lowering discharge (cf. Willis *et al.*, 1990; Brennand, 1994), or from subsequent melting of the lateral supporting ice walls while the sediment was still water saturated.

Facies V consists of rhythmically interbedded sand and matrix-supported, massive or imbricated gravel. The gravel is moderately to poorly-sorted and has a sand matrix. The sand beds are typically poorly-sorted, but are sporadically moderately to well-sorted. These beds exhibit both normal and inverse grading, but the facies as a whole coarsens up, with the gravel beds thickening and the sand beds thinning. This facies also contains rip-ups of underlying material and inversely graded scour-and-fill structures (Fig. 3.15).

Similar interbedded facies to Facies V have been attributed to sheet flow on the flanks of an esker (cf. Blair and McPherson, 1994; Fard and Gruszka, 2007). The rhythmicity of the beds indicates recurrent fluctuating flow conditions, with the overall coarsening-up suggesting increasing discharge during deposition. This energy increase could have resulted from higher discharge associated with less cross-sectional area as the conduit filled with sediment (Brennand, 1994).

Abundant sediment diapers were observed in Facies V at 07DT016 (Fig. 3.16), suggesting a possible sediment source for the esker complex in the Don Creek

Figure 3.15 Inversely graded scour-and-fill structures at 07DT016 indicating channelized flow with increasing energy. The black lines denote the top of inversely graded beds. The silt exposed on either side of the shovel (black arrows) illustrates the bedding morphology.

Valley. Diapers are formed when the pressure in the conduit is less than that from the overriding ice (Brennand, 1994). Under these conditions, sediment is squeezed into the conduit from the underlying sediment bed (Rothlisberger, 1972; Alley, 1991), possibly providing material into the conduit. The low pressure conditions in which this occurs are typically found either during winter (Alley, 1991) or during a drop in conduit discharge (Rothlisberger, 1972; Brennand, 1994).

Facies VI is fine-grained, normally graded and dominated by rhythmically bedded and laminated fine to medium-grained sand, silt and clay. This facies is mostly restricted to small pockets. The one exception to this is at 06DT143, where a 5

Figure 3.16 Diaper structures at 07DT016 suggesting a difference in pressure between the esker conduit and the overriding ice. The dips of the diaper limbs decrease with height. The bottom beds include silt and clay, making the structure more visible. The shovel is 1 m tall.

to 8 m high section was exposed in the side of an isolated hummock following a slump in the summer of 2006 (section 2.5.4; Fig. 2.7). Climbing ripples (B-type) observed in Facies VI grade from low angles of climb to high angles of climb, to symmetrical ripples (S-type) (Fig. 3.17). Many exposures with silt and clay laminations have soft sediment deformation structures.

Facies VI was deposited in low energy environments, likely on the margin of an esker or in small pools or lakes. The rhythmic transition from medium and fine-grained sand with gently climbing ripples, to fine sand, silt and clay with symmetrical ripples indicates multiple fluctuations from hyperpycnal flow to hypopycnal flow and interflows with increased suspended load relative to bed-load. Some of these sediments were probably deposited in supraglacial lakes or lakes adjacent to eskers during the final stages of deglaciation (e.g. 06DT143), similar to deposition in modern lakes in the Don Creek Valley. However, the presence of ripples and undeformed bedding in most of the exposures, and the

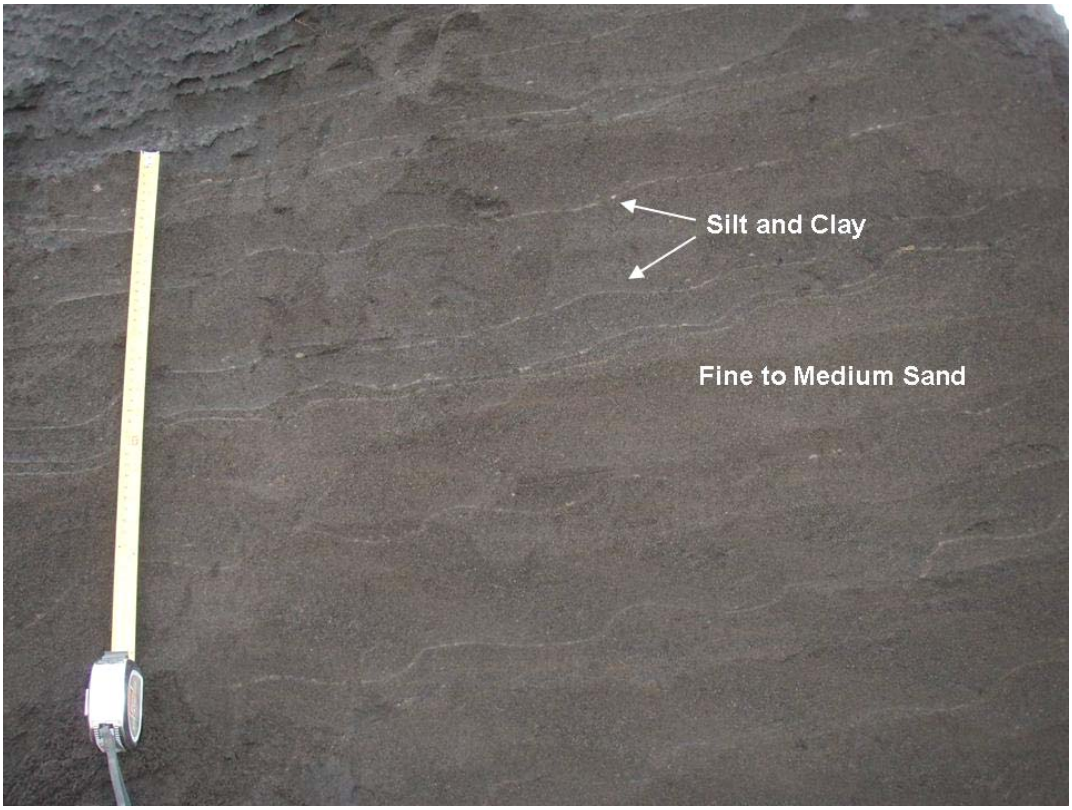

Figure 3.17 Ripples observed in Facies VI at 07DT033. The change from climbing to symmetrical ripples indicates a transition to increased suspension settling compared to bed-load and is indicative of a decreasing energy environment.

proximity of Facies VI to other subglacial facies, indicate that many of these lakes were deposited subglacially, with some deformation possibly resulting from dewatering and sediment movement following melting of supporting ice walls. Facies VI could also have been deposited in isolated channels and cavities that were sealed off from the main R-channels following high discharge events (Brennand, 1994).

Facies VII is exposed at five sections as a discontinuous, 10-15 cm fine sand to silt layer lying stratigraphically above the other six facies described above (Fig. 3.18). This facies is typically weathered orange to light brown and is massive. It is interpreted as loess deposited after deglaciation, when the Don Creek Valley was mostly unvegetated and sediment availability was high. This facies likely correlates to the upper silt unit observed at 07DT039 and described in section 3.3.

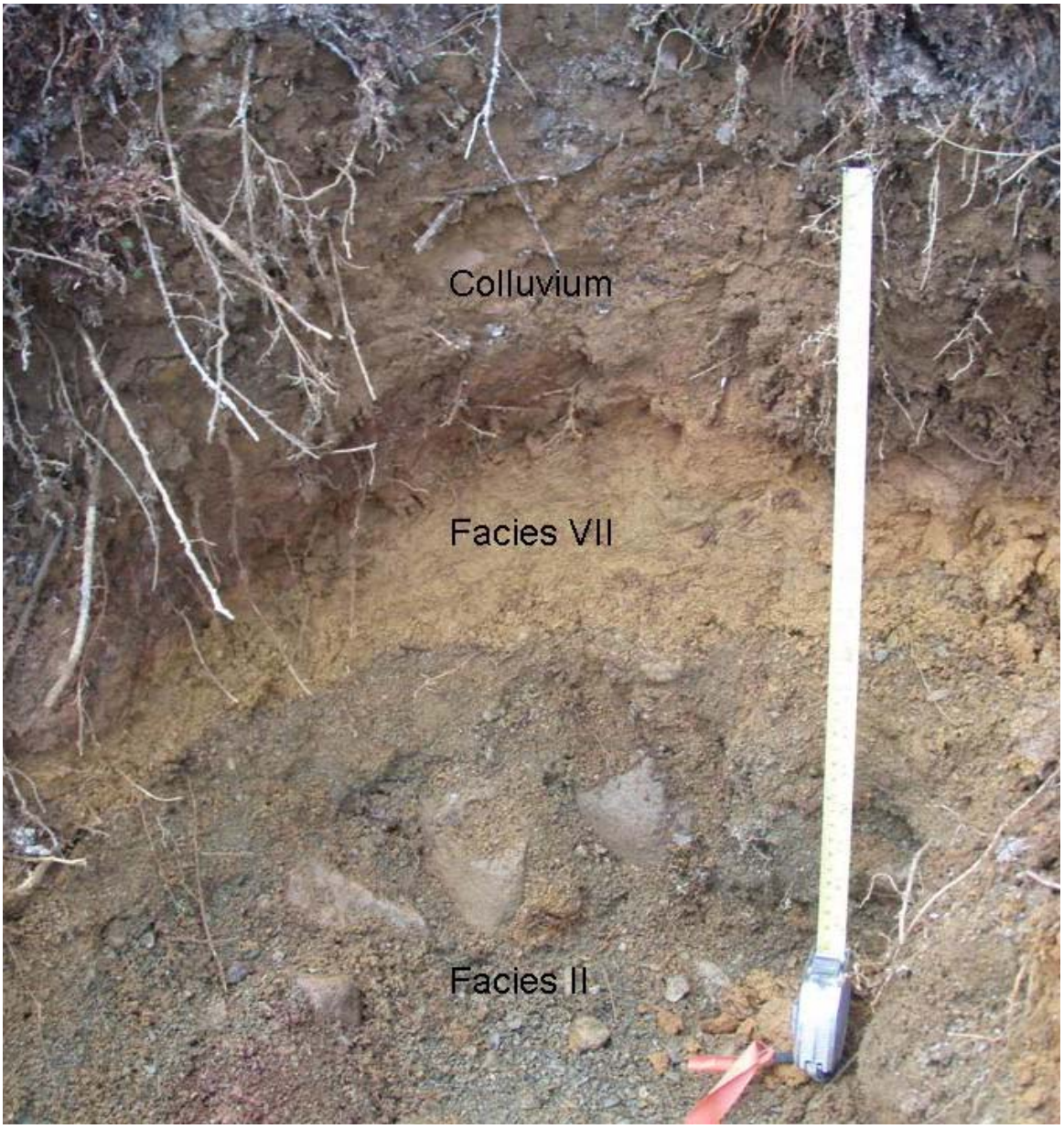

Figure 3.18 Facies VII consisting of 10-15 cm of silt and fine sand. This facies is interpreted as loess and is observed lying stratigraphically above the other facies across the study area. Tape is 50 cm long.

3.3.2 Paleoflow Measurements

Clast orientations, bedding planes and ripple crests were measured at multiple exposures along the recent road construction between Don and XY camps (Fig. 3.8). These measurements were compared to esker morphologies to estimate

flow orientations in the esker conduits and to provide insight into the glacial dynamics during formation.

On the western end of the esker complex, near Don camp at 07DT066 and 07DT070, paleoflow measurements correlate with esker morphology suggesting deposition to the east (Fig. 3.8). The interpretations of esker morphology are based on the down-slope direction of the eskers, and the presence of large meltwater channels acting as potential water sources on their western end. Measurements of bedding planes and ripple crests in fine-grained sediment oriented perpendicular to the inferred esker direction at 07DT033 (Fig. 3.8, 3.17) are likely from low energy deposition on the esker margin. Similar results for bedding planes in coarser grained sediment may be from secondary vortices forming in the esker conduit (Brennand, 1994).

Paleoflow measurements are more inconclusive on the eastern side of the esker complex, even though this area is more topographically restricted. Esker morphology in this area suggests flow was to the west-northwest, based on the dendritic pattern of eskers merging down-slope in this direction (Fig. 2.14). The one paleoflow measurement on this side of the esker complex is weakly oriented to the south (06DT151; Fig. 3.8). Measurements of ripple crests in the glaciolacustrine sediment at 06DT143 (located up-valley toward XY camp on Figure 3.8), show sediment input to the east. However, the sediment exposed at this section were likely deposited after the eskers.

The centre of the esker complex, east of Don camp at the bend in Don Creek, is more complex than either side. The topography here is hummocky, with eskers oriented in multiple directions with parallel channels emanating from a glaciofluvial terrace south of 07DT066 to 07DT069. Measurements of bedding planes in the eskers here indicate no preferential direction. The interpretations of eskers flowing from both the west and the east suggest that the centre of the esker complex was a confluence, with further drainage likely oriented to the north

toward the Nahanni Valley. Abundant meltwater channels on the walls of valleys to the north support this explanation. The association of these interpretations with ice-flow directions and deglaciation are discussed in chapter 4.

3.4 Drill Core Stratigraphy

Drill core from 19 sites in the Don Creek Valley (Fig. 3.19) provided otherwise inaccessible stratigraphic information. Eight of these holes in the southeastern portion of the valley (Fig. 3.20) contain multiple units that were used to create a cross-section of the valley (Fig. 3.21). These holes reveal both advance- and retreat-phase glacial deposition. Holes Don-87, 104, 111 and 112 contain thick glaciofluvial deposits overlying a diamict, interpreted as a till. Don-104 and 111 also have a thin glaciofluvial unit lying stratigraphically below the till. This sequence suggests advance glaciofluvial accumulation, followed by till deposition during glaciation, and subsequent deglacial glaciofluvial deposition. The pre-glacial floodplain in the valley bottom illustrated in Figure 3.21 is inferred from the position of the lower glaciofluvial sand and gravel exposed below till in the river exposures described in section 3.3.

Drill-hole data in the northwestern portion of the Don Creek Valley reveal a similar stratigraphy (Fig. 3.22, 3.23). All of these holes contain thick glaciofluvial materials above bedrock. Don-79 correlates well with holes in the southeast of the valley, with 10 m of glaciofluvial sediments overlying a 2 m thick diamict, interpreted as a till. However, Don-72 has 12 m of fine-grained material with rare pebbles and cobbles. This unit is likely either a clast-poor diamict or ice-proximal glaciolacustrine material. Its isolation, location beside an esker and lack of clasts suggests the latter and indicates that this unit formed in a small lake adjacent to the eskers in the valley during deglaciation.

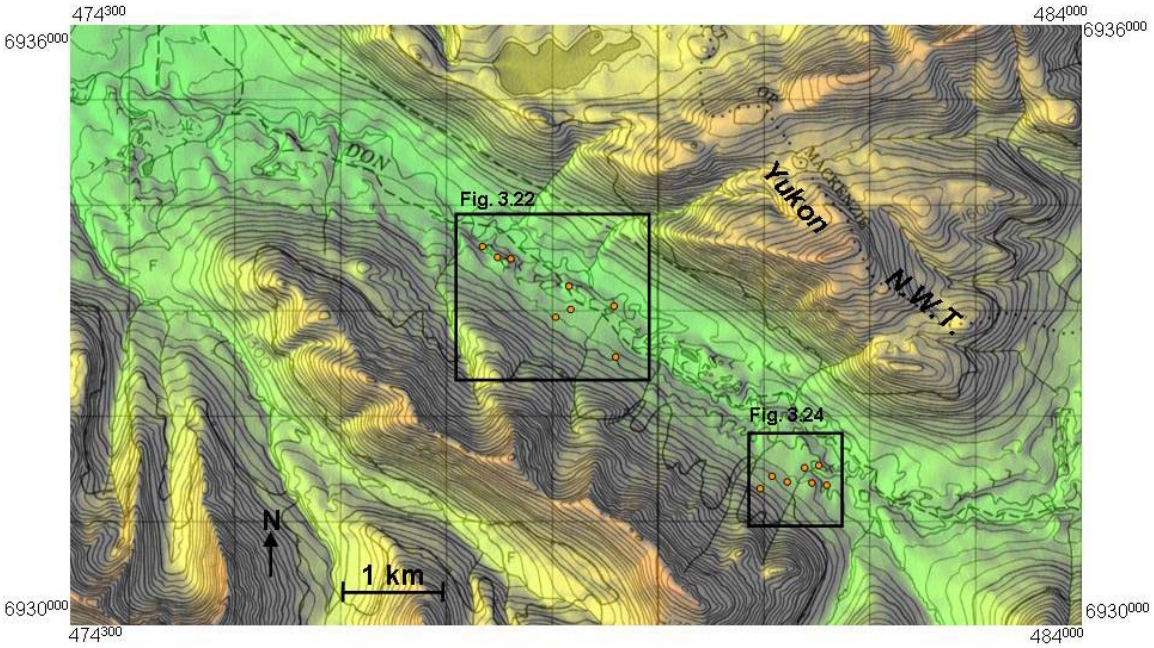

Figure 3.19 Location of drill holes in the Don Creek Valley. Black boxes indicate locations of 3-D figures showing detailed topography and site information.

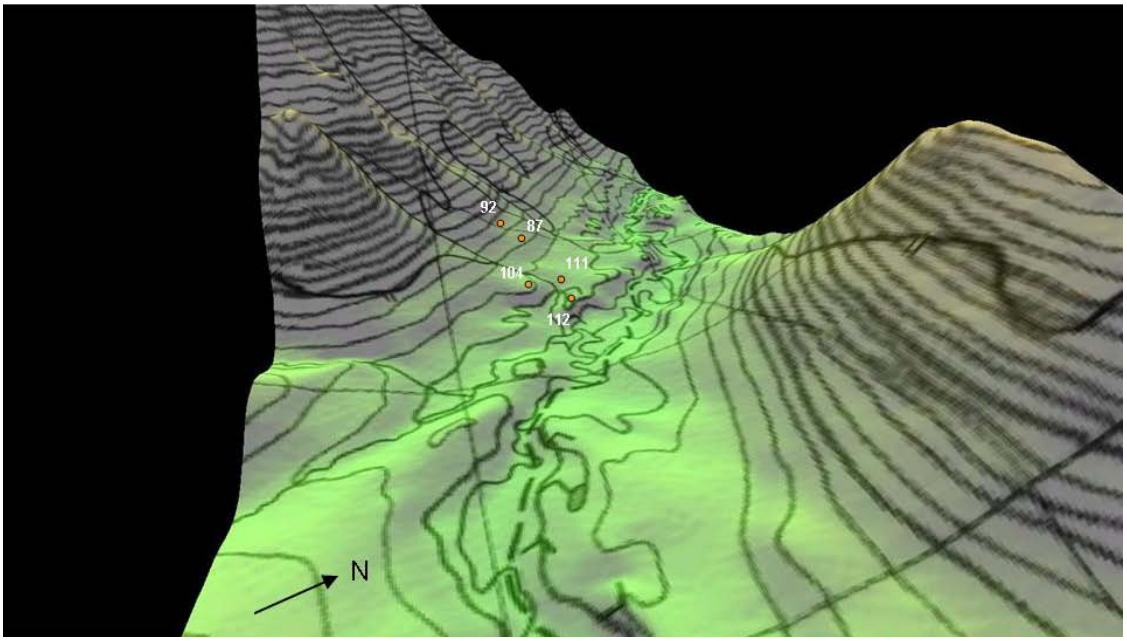

Figure 3.20 3-D view of the locations of drill holes used to create the cross-section in Figure 3.21 for the southeast end of the Don Creek Valley. The topography has two times vertical exageration.

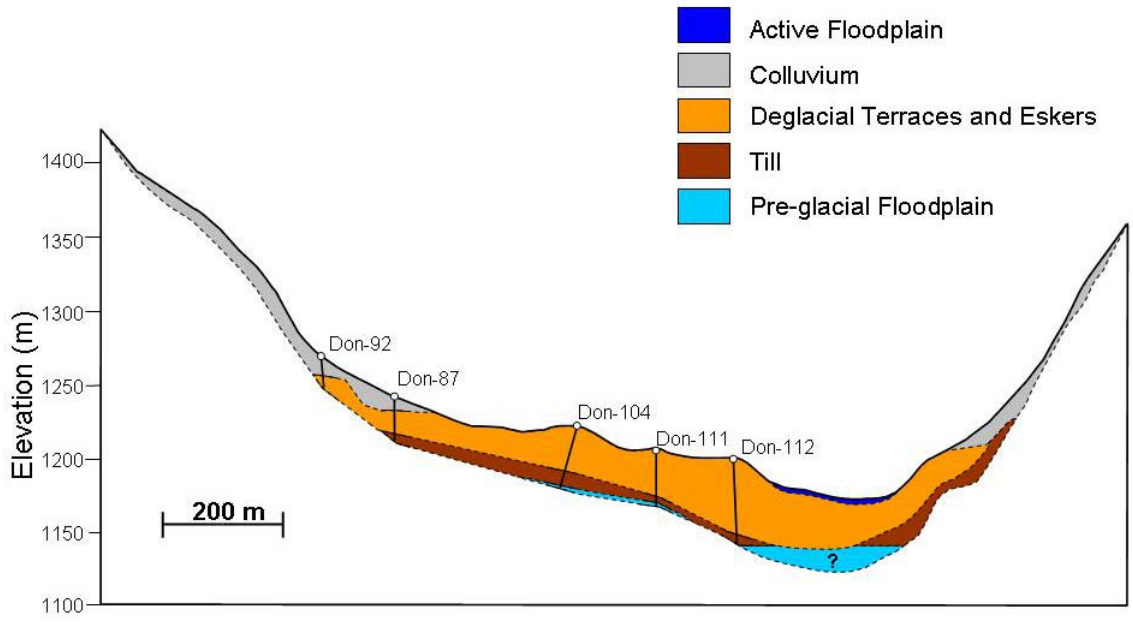

Figure 3.21 Cross-section of the surficial materials in the southeast end of the Don Creek Valley. Depths of the materials are inferred from Quaternary sediments in five drill holes.

Don-93 has a unique stratigraphy compared to the other holes in the Don Creek Valley. In this hole, 15 m of gravel underlie 42 m of an upper and lower clast-poor diamict surrounding a clast-rich diamict. There are numerous possible interpretations for this stratigraphy. The diamicts may represent a re-advance through the Don Creek Valley. However, if the glaciofluvial materials below the diamicts correlate to the eskers running throughout the valley it is unlikely that these eskers would be preserved if there were a subsequent re-advance. Alternatively, the layered diamicts could signify multiple colluvial events entraining till following deglaciation. Another possibility is that the diamicts are an isolated hummock composed of flow till or meltout till deposited during stagnant deglaciation, with possible colluvial additions from the valley side. Although there is no direct evidence to preclude any of these interpretations, the latter two are preferred based on the regional stratigraphy.

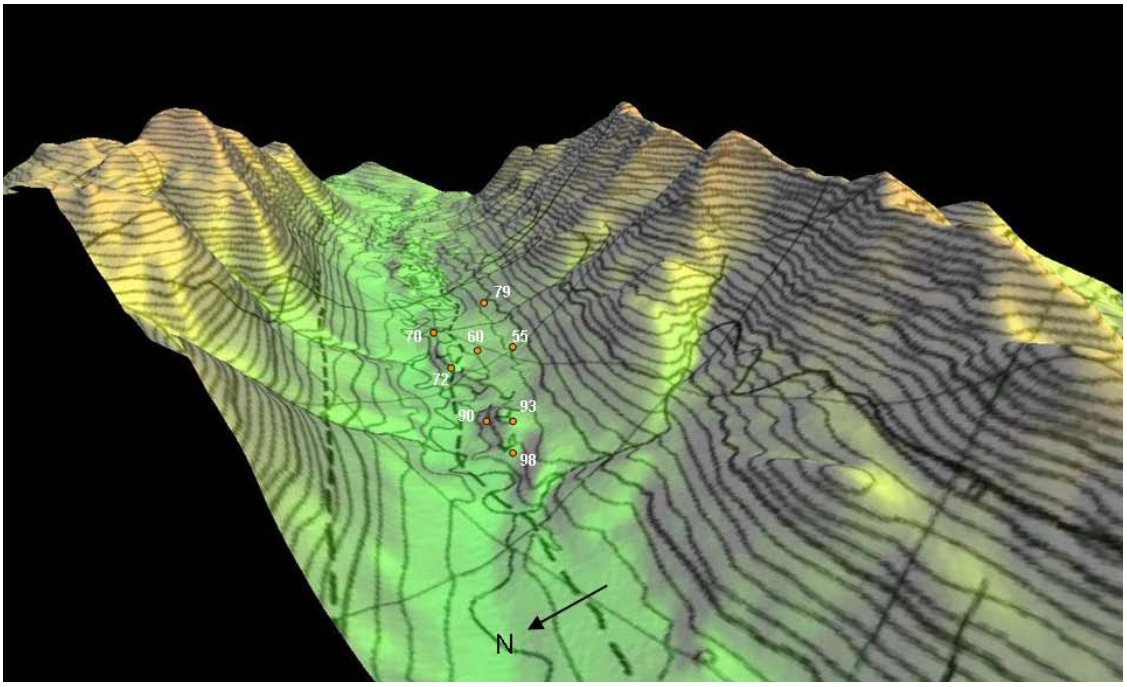

Figure 2.22 3-d view of the locations of drill holes in the northwest end of the Don Creek Valley. Five of the holes were used to create the cross-section in Figure 3.23. The topography has two times vertical exageration.

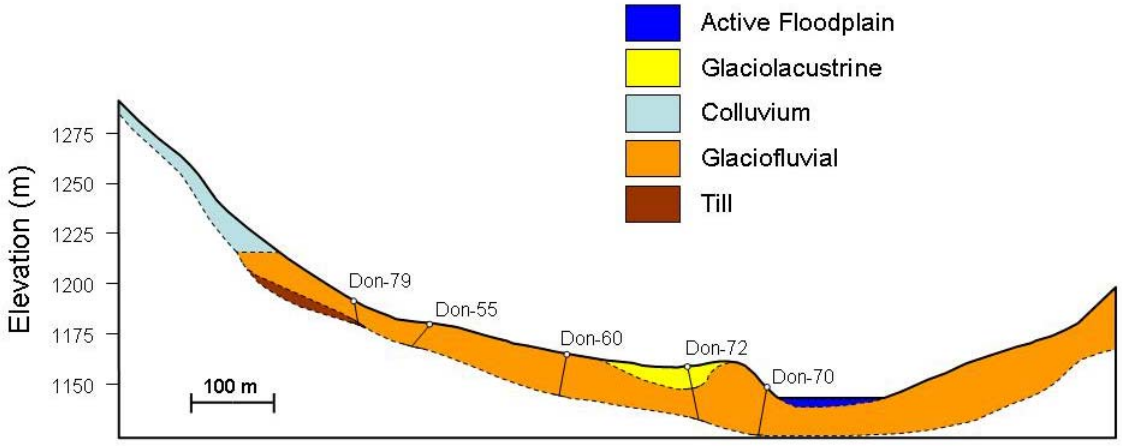

Figure 2.23 Cross-section of the surficial materials in the northwest of the Don Creek Valley. Depths of the materials are inferred from Quaternary sediments in five drill holes.

3.5 Summary

The Quaternary stratigraphy of Howard's Pass was investigated by studying river sections, esker exposures and drill core. A complete glacial sequence is interpreted, with advance and retreat glaciofluvial sand and gravel separated by a thin till, followed by Holocene mass wasting, organic development and fluvial deposition.

The oldest unit in the study area is consolidated, cemented and faulted glaciofluvial sand and gravel. This unit is observed in river sections across the study area and in drill core in the Don Creek Valley. Directly above this unit in both locations is a thin till. These two units are interpreted to represent glaciofluvial deposition during glacial advance, followed by full glacial conditions. The thinness of the till is attributed to erosion during deglaciation.

Stratigraphically above the till is another thick glaciofluvial unit that was likely deposited during deglaciation. This glaciofluvial material is less consolidated than the lower glaciofluvial unit and correlates to eskers and glaciofluvial terraces observed in the Don Creek Valley. Interpretations of seven esker facies provide evidence for the depositional environment of these features. The eskers were formed in a network of continuous conduits beneath a warm-based glacier. Their morphology suggests they formed in multiple directions according to local subglacial hydraulics. In the south of the study area, up-valley paleoflow measurements in this unit suggest that these sediments followed a different drainage pattern than presently exists.

Significant surficial materials were accumulated during and after deglaciation. Glaciolacustrine sediments were deposited in ice-marginal lakes and lakes constrained by hummocky glaciofluvial materials. Lastly, Holocene deposition of colluvium, organics and fluvial sediments lie at the top of the Quaternary stratigraphy in Howard's Pass.

4 ICE-FLOW HISTORY

Growth of the Cordilleran Ice Sheet (CIS) in the late Wisconsinan occurred in four phases (Kerr, 1934; Davis and Matthews, 1944), with local alpine ice coalescing and forming ice sheets with multiple ice caps and ice domes (Fulton, 1991). The northern CIS was not thick enough to reach the final, topographically independent phase of this model across its entire extent (Jackson *et al.*, 1991), although recent evidence suggests it flowed independently over at least some of the ranges in central Yukon (Bond, 2007).

The northern CIS during the late Wisconsinan consisted of multiple ice lobes emanating from different source regions (Jackson *et al.*, 1991; Fig. 1.5). Howard's Pass is located in the inferred source region for the Selwyn lobe. Understanding its ice-flow history is therefore significant for elucidating the dynamics of this lobe. Previous work in the study area affected by the Selwyn lobe (e.g. Dyke, 1990a) has identified recessional moraines, indicating deglaciation by frontal retreat with some areas displaying re-advances (Bond, 2007). However, other studies near the ice divide and in the western portion of the lobe (e.g. Jackson, 1982; Ward and Jackson, 2000) have proposed that deglaciation occurred through a sudden rise in the firn line causing widespread stagnation, similar to the model proposed by Fulton (1991) for the southern CIS.

This chapter discusses the formation and decay of the ice sheet over Howard's Pass, with emphasis on the ice-flow history. The ice-flow history of the area is useful for interpreting geochemical data used to find new mineralized zones in Howard's Pass.

4.1 Methodology

The late Wisconsinan ice-flow history of Howard's Pass was investigated during pre-typing and fieldwork for the creation of a 1:50 000-scale terrain inventory map. Reconnaissance aerial photo interpretation identified large-scale ice-flow indicators such as crag and tails, streamlined bedrock, eskers, moraines and meltwater channels. Subsequent field observations of multiple sets of striations, rat tails, grooves, till fabric measurements and erratics further enhanced ice-flow direction interpretations. Striations, grooves and rat tails were measured, averaged and rounded to the nearest 5^{o}. These measurements are shown in Appendices A and B and are listed in Appendix D. Till fabric data were obtained by measuring clast orientations and by calculating eigenvalues and eigenvectors (refer to chapter 3 for full till fabric methodology). A five-stage ice-flow model is proposed based on these observations (Fig. 4.1). Some of the main sites used to interpret this model and a summary of ice-flow indicator orientations are shown in Figure 4.2.

Terrestrial Cosmogenic Nuclide dating utilizing Be^{10} was used to determine the age of deglaciation in the study area. Samples were collected from six boulders on a moraine in the north of the study area (Fig. 4.2). Four of these boulders were selected for analysis based on criteria detailed by Gosse and Phillips (2001), including height, geometry, quartz content, weathering, and the amount of shielding from both other boulders and from the surrounding topography. The samples were collected at a uniform 2.5 cm depth, using a gas-powered cutout saw. Be^{10} was extracted in the Dalhousie Cosmogenic Nuclide Exposure Dating Facility at the University of Dalhousie by Guang Yang, under the supervision of Dr. John Gosse. Analysis by accelerator mass spectrometry was conducted at Lawrence Livermore National Laboratory at the University of California.

4.2 Ice-Growth Stages

4.2.1 Stage One – Alpine Stage

The first stage of ice-flow in Howard's Pass is logically inferred from previous models of ice sheet growth in the Canadian Cordillera (e.g. Kerr, 1934; Davis and Matthews, 1944, Fulton, 1991). In these models, glaciation is initiated by alpine ice emanating from cirques (Fig. 4.1a). Evidence supporting these interpretations in the northern CIS has been found in numerous areas in Yukon (e.g. Plouffe, 1989; Bond and Kennedy, 2005; Bond, 2007). These valley glaciers subsequently coalesced and formed an ice sheet. In Howard's Pass, this inferred first stage of ice-flow is supported by striations and grooves at three sites.

On a ridge west of Anniv camp at 07DT049 (Fig. 4.2), a 50-cm-wide, 5-cm-deep groove is exposed for 1.5 m (Fig. 4.3). This bidirectional groove oriented 135^{o} or 315^{o} is cross-cut by rat tails and abundant fine and coarse striations oriented southwest. The groove and other indicators are sheltered from any subsequent ice-flow from the south by a five-metre ridge. The presence of the later striations and rat tails suggests this groove represents the earlier, more valley-parallel Alpine stage.

Striations that potentially correlate with this groove were observed at two sites. On a cirque floor oriented north, located east of Anniv camp (07DT114), cirque-parallel striations are cross-cut by perpendicular striations interpreted as representing a subsequent topographically independent ice-flow stage. Similarly, valley-parallel striations preserved preferentially on the west side of outcrops on the side of a shallow valley south of XY camp (07DT140) are cross-cut by multiple sets of striations and rat tails that illustrate both a later, valley-perpendicular ice-flow and a later, valley-parallel ice-flow.

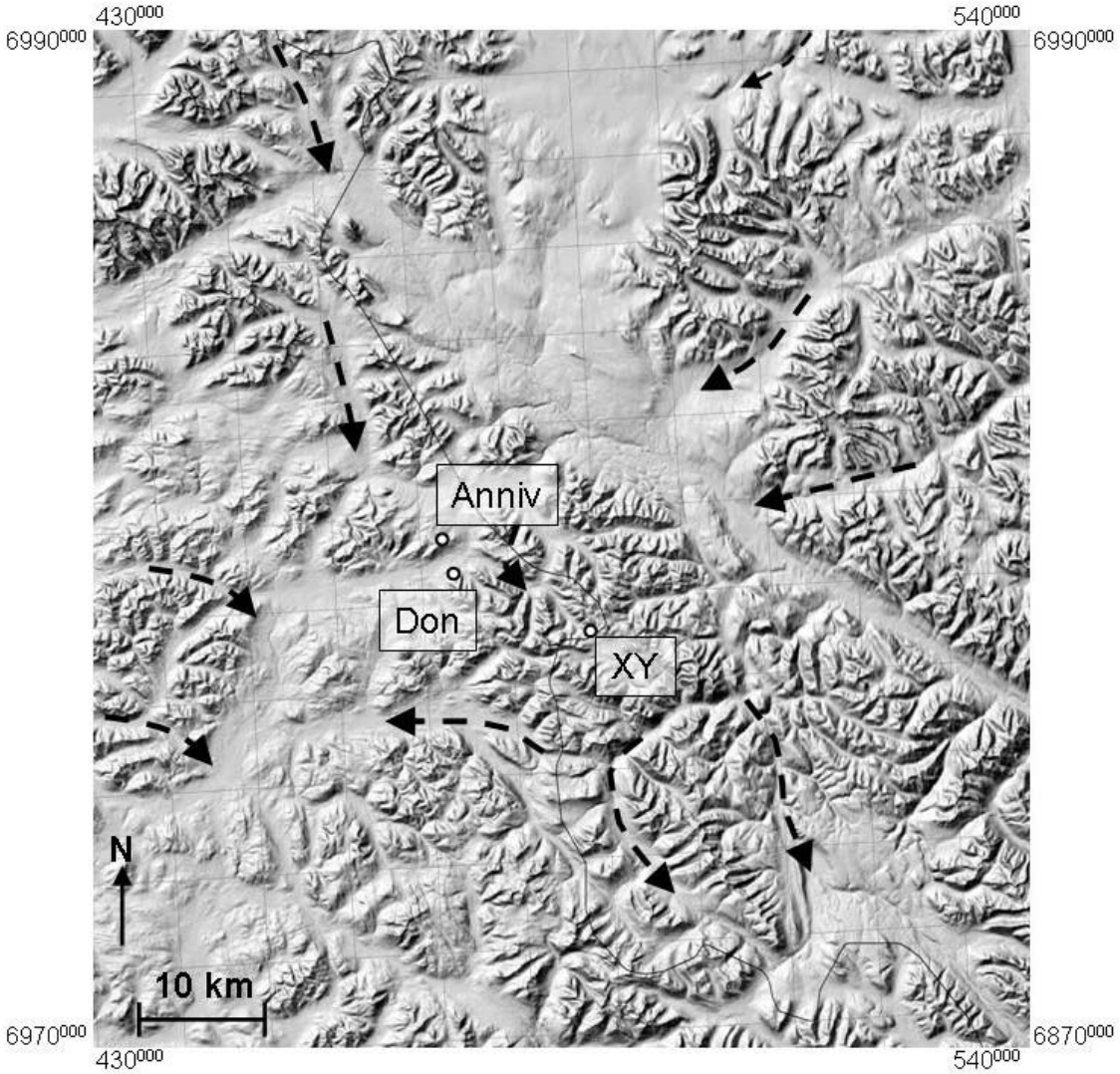

Figure 4.1a Alpine Stage

4.2.2 Stage Two – Nahanni Stage

When the Selwyn lobe initially formed, the ice divide was likely positioned east of the Nahanni River where elevation exceeds 2000 m.a.s.l. and current glaciers exist (Jackson, 1982). Ice flowed from this divide southwest across the study area (Nahanni Stage, Fig. 4.1b). Evidence for the Nahanni Stage includes streamlined bedrock, erratics, striations and rat tails.

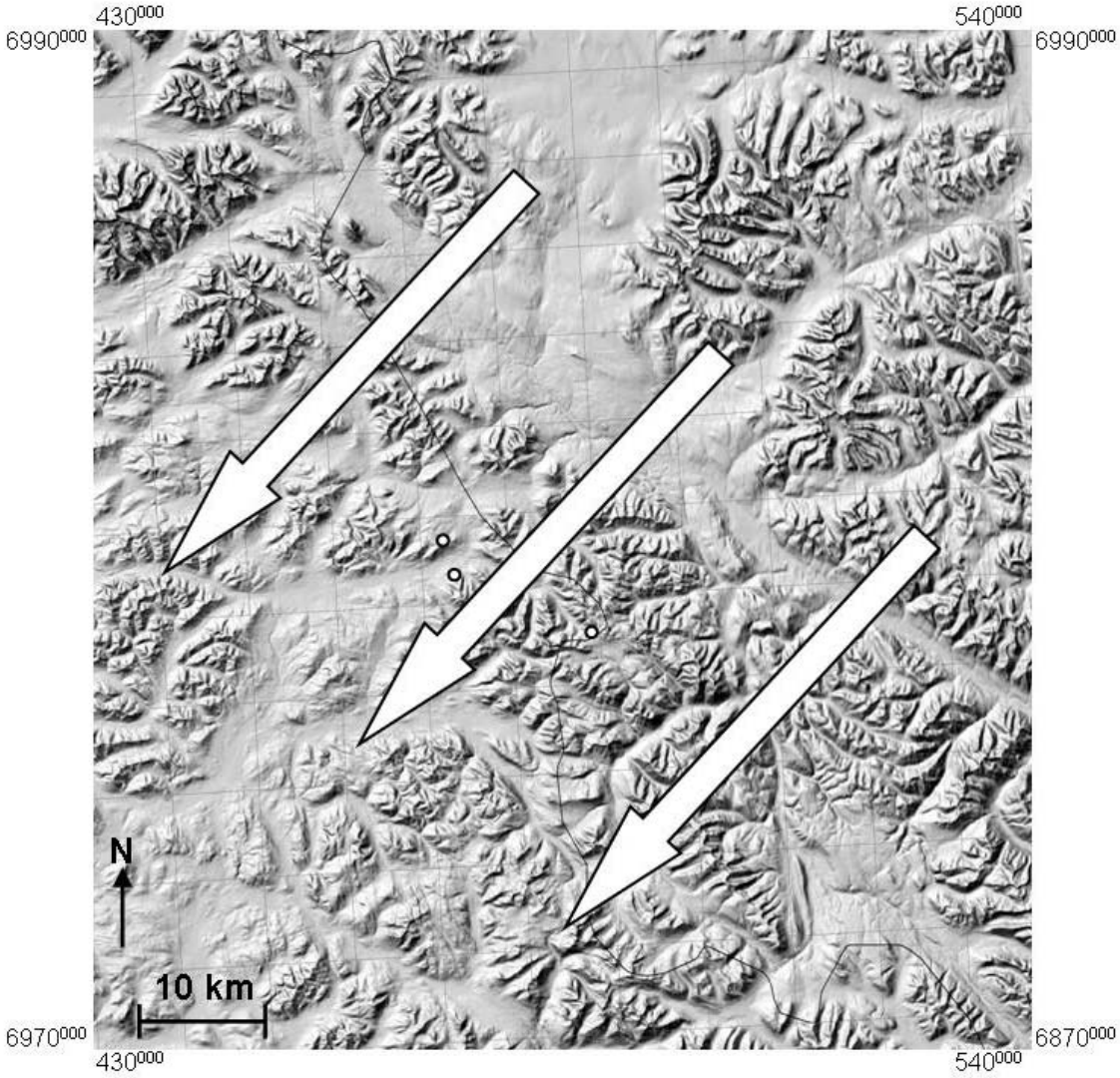

Figure 4.1b Nahanni Stage

Streamlined bedrock ridges were recognized during aerial photo interpretation. Several large ridges in the northern drainage of the Pelly River are oriented approximately 250^{o} (Fig. 4.2). These features were likely created from subglacial erosion by water or ice and suggest that ice flowed over this area towards the southwest.

Sixty granodiorite, diorite and monzonite boulders of differing texture were observed at various elevations throughout Howard's Pass, indicating wide-spread dispersal. Many of these erratics contained feldspar phenocrysts up to seven centimetres long (Fig. 4.4). The presence of erratics at high elevations

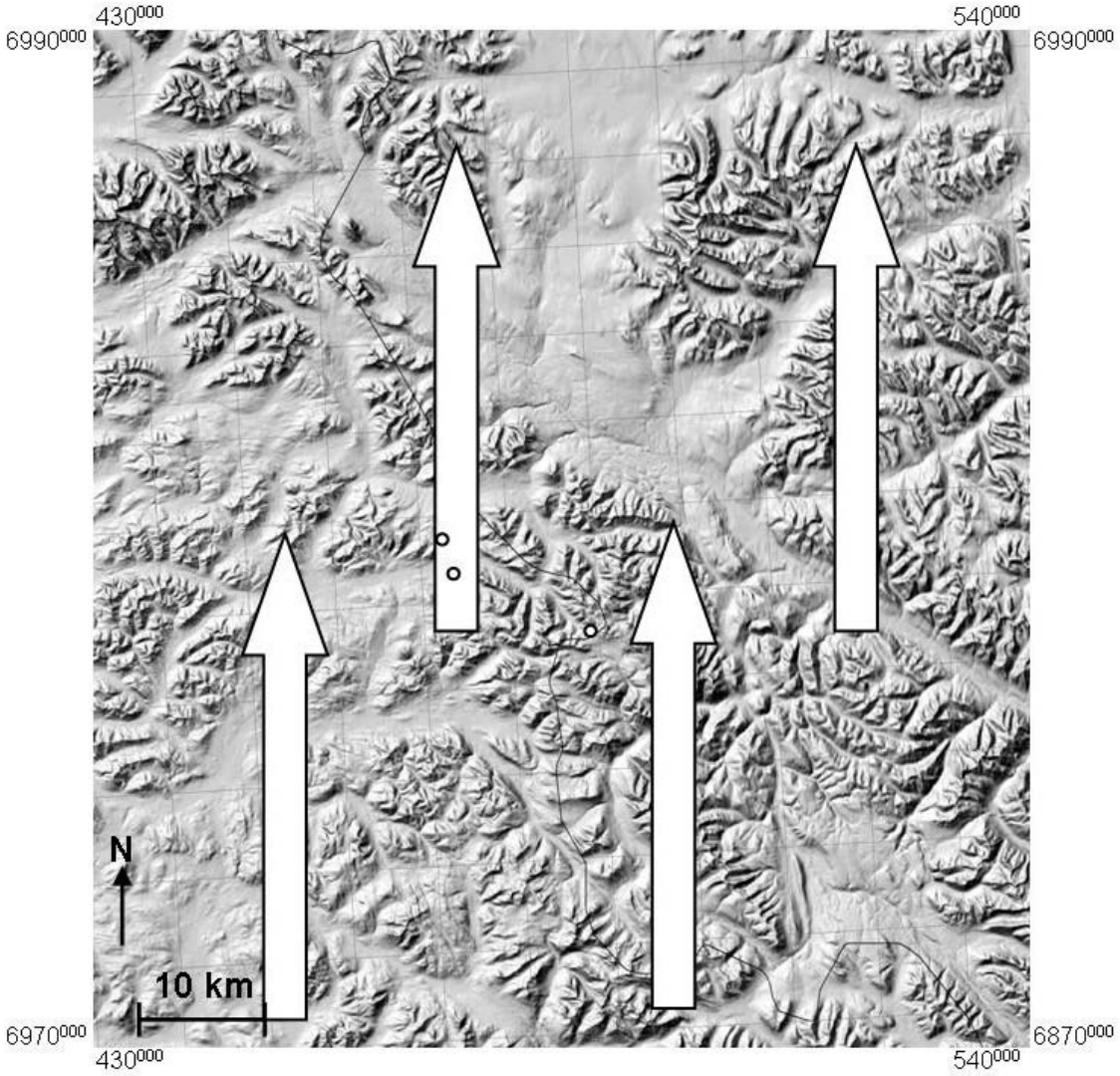

Figure 4.1c Logan Stage

(Fig. 4.5) suggests the Nahanni Stage covered most of the topography within the study area. The erratics were sourced to the northeast from either the O'Grady batholith or the Central Nahanni Pluton (Fig. 1.5), or in one of numerous intrusive bodies to the west. Although a western source cannot be precluded, they are over three times as far from the study area as the intrusives to the northeast and are considerably smaller. The interpretation of a northeastern source area for the Nahanni Stage correlates with directional ice-flow indicators at three sites. At the previously described site west of Anniv camp (07DT049), parallel fine and coarse striations and rat tails cross-cut a well-preserved groove (Fig. 4.3). The rat tails are oriented 245^{o} (Fig. 4.6) and are shielded from any subsequent ice-flow from

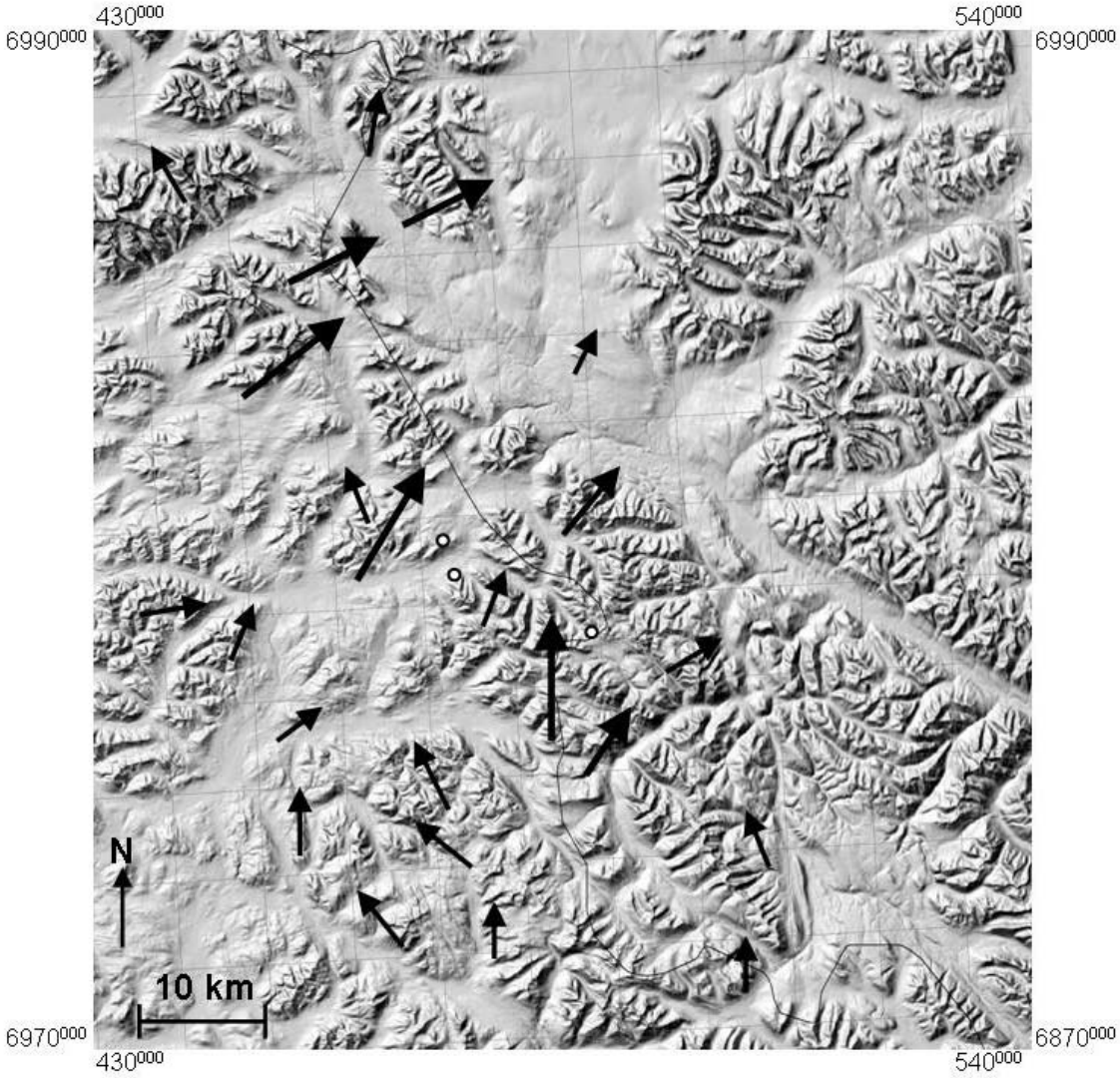

Figure 4.1d Don Stage I

the south by a 5-m-high ridge. On a ridge-top near the Pelly River, at 07DT104, deep, highly weathered striations and fine striations oriented 080°/260° are either cross-cut by another set of striations oriented 145°/325°, or are preserved on outcrops that were in the lee of ice-flow from the south. At 07DT114, nail-head striations and preferential abrasion on one side of the outcrop indicate ice-flow towards 240° (Fig. 4.2). These sites suggest that ice flowed to the southwest during the Nahanni Stage.

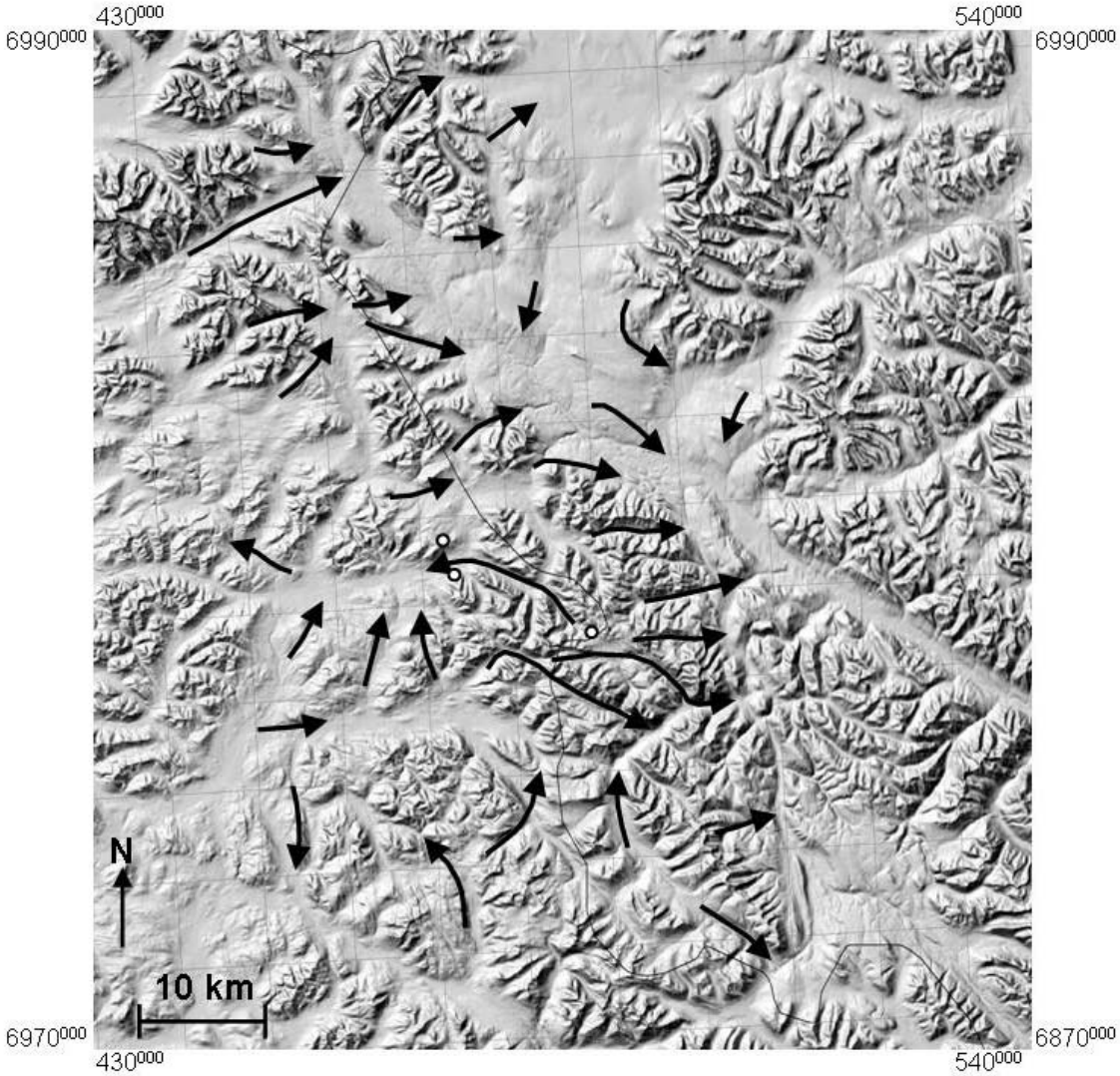

Figure 4.1e Ice-flow model for Howard's Pass. a) Alpine Stage - Ice emanated from local cirques, b) Nahanni Stage - Ice-flowed from an ice divide to the northeast of the study area, c) Logan Stage - Following the development of an ice divide to the south and southwest of Howard's Pass, ice flowed from the south, d) Don Stage I – With thinning of the ice sheet, ice was directed by topography around high elevation ridges, e) Don Stage II – As ice thinned further, ice-flow became valley-parallel and had no dominant regional direction.

4.2.3 Stage Three – Logan Stage

During the Logan Stage, ice-flow changed direction and flowed to the north. This represents a shift in the ice divide to the south. Dyke (1990a) proposed an ice dome in the Logan Mountains to explain ice-flow in the Francis Lake area, which

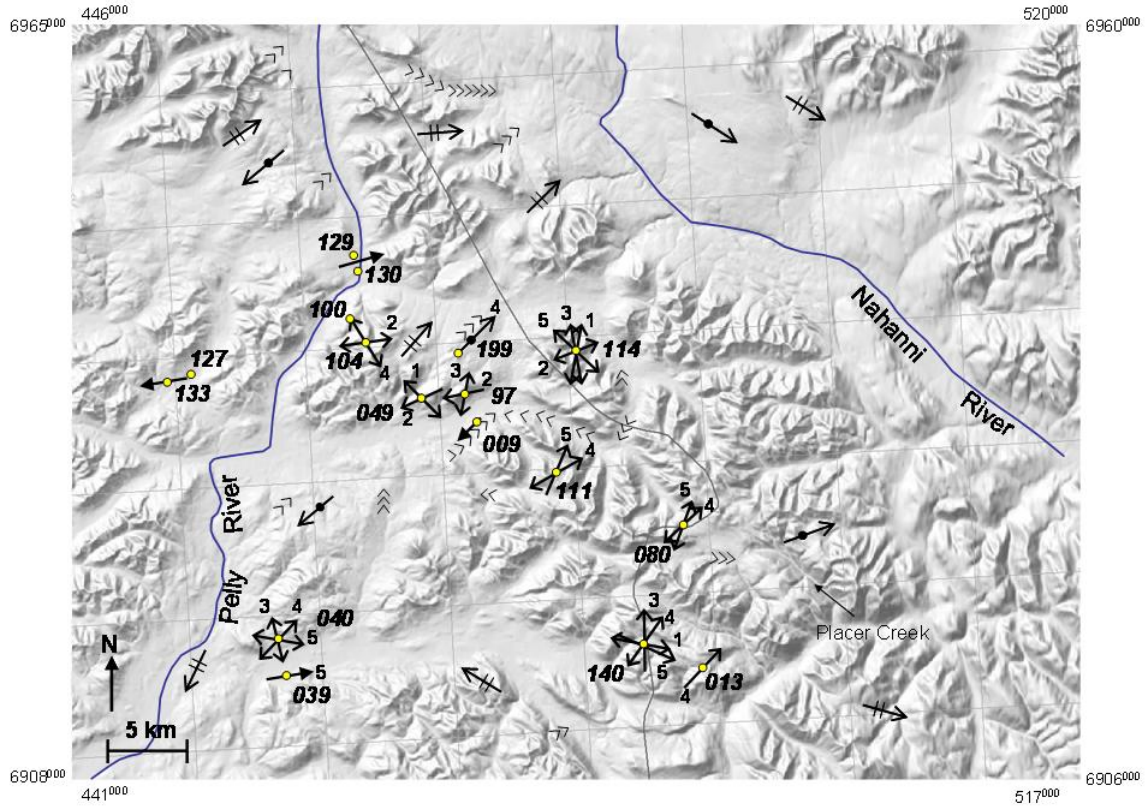

Figure 4.1 Locations of important ice-flow indicator sites discussed in the text. Station numbers are italicized and are prefixed with either 06 or 07 in the text. Each location may represent multiple indicators. Ice-flow indicators are assigned an interpreted ice-flow stage number: Alpine Stage (1), Nahanni Stage (2), Logan Stage (3), Don Stage I (4), Don Stage II (5).

is south of Howard's Pass (Fig. 1.6). Although Dyke proposed an ice dome, a more linear ice divide would also fit his interpretations. Evidence for the Logan Stage includes seven sites with striations, rat tails and grooves (Appendix D). Striations oriented 170°/350° were observed in the far southwest corner of the study area (07DT040). Grooves and striations oriented 010°/190° were also

Figure 4.2 Groove and cross-cutting striations and rat tails at 07DT049. The striations and rat tails (Fig. 4.6) are oriented perpendicular to the groove and indicate a later ice-flow event to the southwest. This site is shielded from any subsequent ice-flow from the south by a 5 m ridge.

observed on a ridge-top near Anniv Camp at 07DT097. At 07DT140, rat tails were observed oriented 010^{o} (Fig. 4.7). All of these striations are cross-cut by other striations formed by subsequent, valley-parallel ice-flow. There are also multiple meltwater channels at high elevations interpreted to indicate drainage to the north also support the Logan Stage. In addition, the abundant data supporting subsequent ice-flow to the northeast during Don Stage I indicate that ice-flow changed direction between the Nahanni and Don Stages.

Figure 4.3 An example of the typical feldspar phenocryst-rich intrusive erratics spread across Howard's Pass at various elevations. These erratics were likely sourced northeast of the study area across the Nahanni River. Some erratics have phenocrysts that reach up to seven centimetres.

Figure 4.4 Granodiorite erratic on top of the ridge directly west of Anniv camp at approximately 1600 m.a.s.l. These erratics indicate ice-flow from the northeast covered peaks up to this elevation across the study area. Shovel is 1.5 m long.

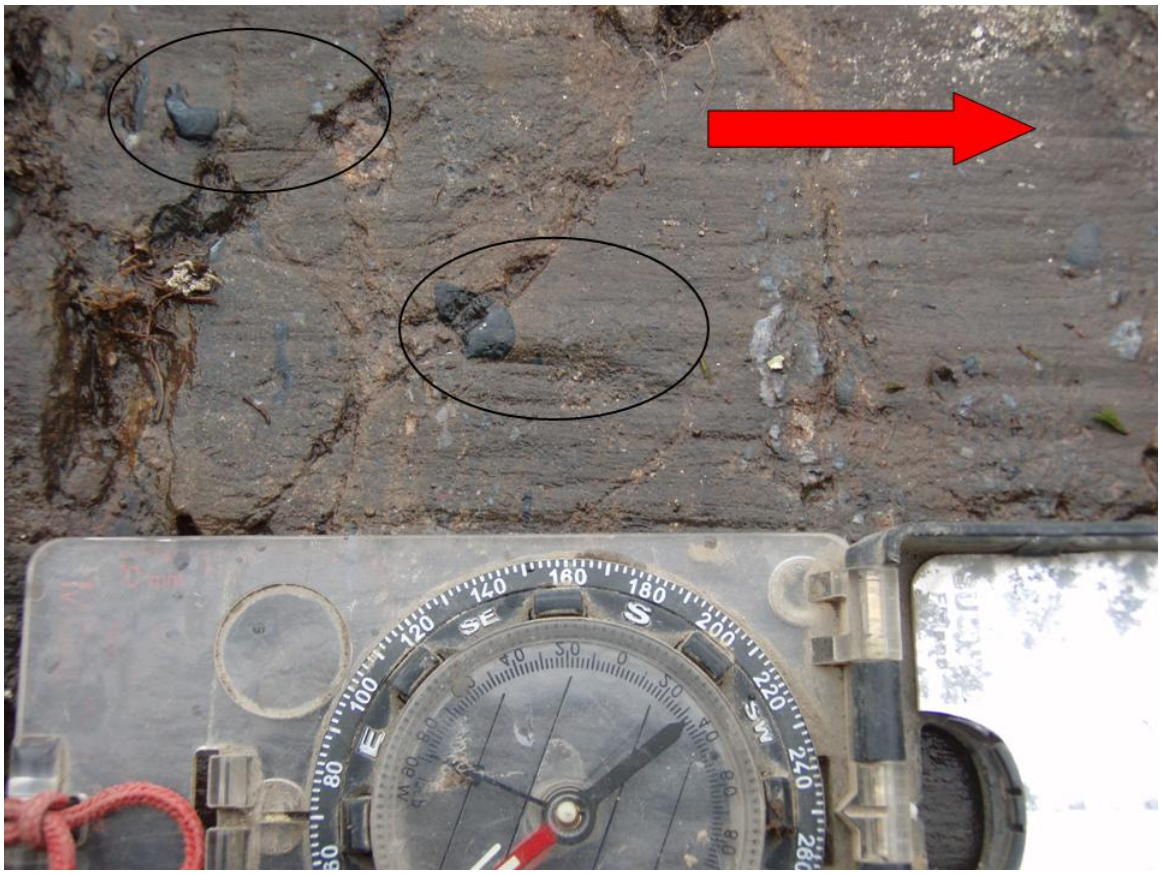

Figure 4.5 Rat tails formed around chert clasts indicate ice-flow to the west-southwest at 07DT049 near Anniv camp. These rat tails cross-cut a deep groove shown in Figure 4.3.

4.2.4 Stage Four and Five – Don Stages I and II

The final phase of ice-flow is split into two stages, Don Stages I and II, which occurred during initial deglaciation as the ice sheet over Howard's Pass thinned and became increasingly topographically influenced. These stages are separated because local ice-flow in many valleys changed once ice thinned below the elevation of the surrounding topography. This resulted in different drift prospecting implications for Don Stages I and II, which will be explored in more detail at the end of the chapter.

Evidence for the transition from Logan Stage to Don Stages I and II ice-flow was observed in an east-west oriented valley at 07DT040. At this location, cross-cutting striations were measured oriented $170^{o}/350^{o}$, $040^{o}/220^{o}$, $060^{o}/240^{o}$ and $100^{o}/280^{o}$ (Fig. 4.2). If the earliest of these striations represents the Logan Stage ice-flow to the north, then the other three sets indicate a progressively more valley-oriented flow to the east during the transition from Logan Stage to Don Stage I to Don Stage II.. The last of these orientations correlate to a nearby till fabric at 07DT039 oriented 075^{o} (n = 51, S_1 = 0.68, spread unimodal) that supports the interpretation of the last phase of ice-flow being valley-parallel (Don Stage II).

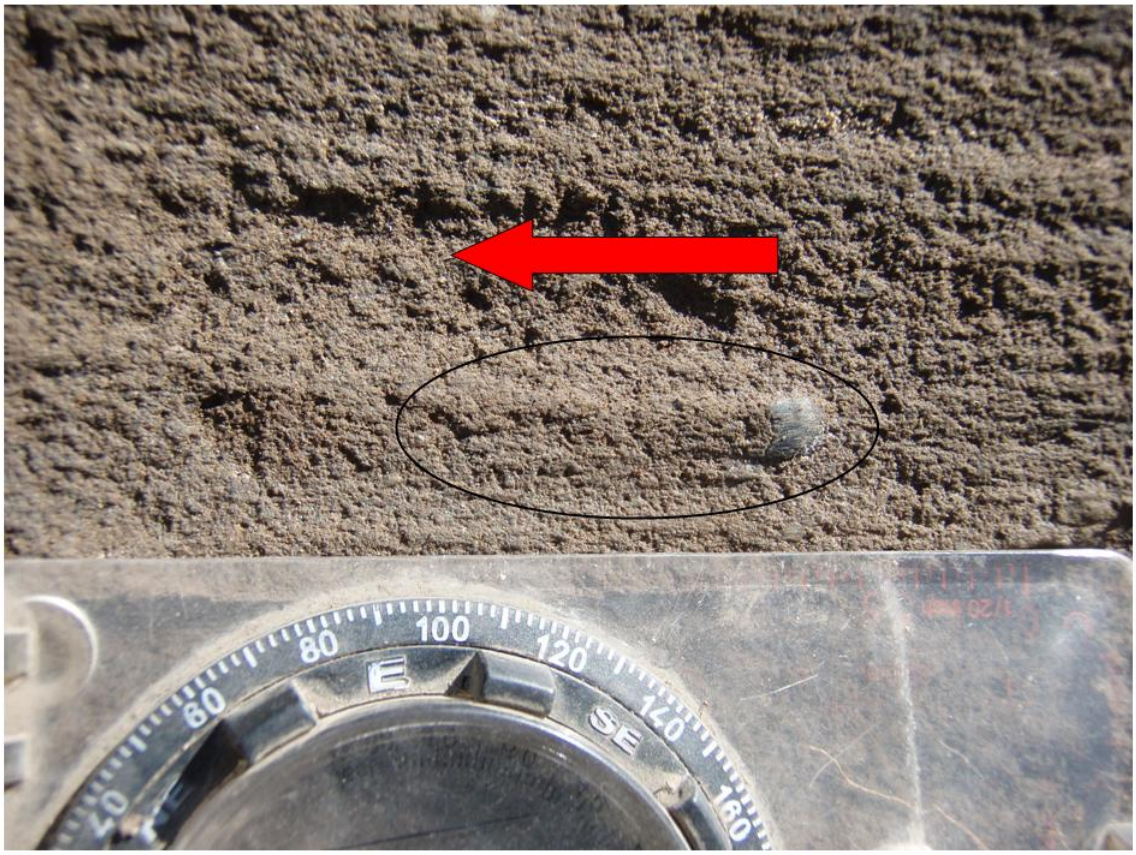

Figure 4.7 An example of the rat tails observed at 07DT140 suggesting ice-flow to the north after and prior to final deglaciation. These feature formed during Logan Stage ice-flow.

Other evidence for Don Stage I ice-flow includes striation data in the southeast of the study area. In a shallow, high elevation saddle in the southeast (07DT013), the dominant striations were oriented 045^{o}/225^{o}, but ranged to 060^{o}/240^{o}, with local plucking and lee surfaces indicating ice-flow to the northeast and east-northeast.

Numerous meltwater channels provide compelling evidence for Don Stages I and II ice-flow. These channels take two forms, proglacial and lateral. Proglacial meltwater channels are restricted to valley bottoms and provide an indication of the position of the former ice margin (Fig. 4.8a). In the study area, they frequently incise large glaciofluvial features. Lateral meltwater channels are more common than proglacial channels. These features form on the side of the ice surface and indicate the former ice surface slope and the position of the ice margin (Fig. 4.8b). These channels are also a proxy for ice-flow direction.

Lateral meltwater channels at high elevations were observed flowing mostly northeast across Howard's Pass, suggesting flow in this direction in the early stages of ice thinning (Don Stage I). However, at lower elevations, lateral meltwater channels are valley-parallel. In addition, large ice-marginal glaciofluvial deposits north of Howard's Pass observed on aerial photos indicate valley-parallel late-stage ice-flow. The change in alignment of meltwater channels with elevation (Appendices A and B) reflects the increasing influence of topography on ice-flow from Don Stage I to Don Stage II.

The change in ice-flow directions associated with the transition from Don Stage I to II is documented by striations at three sites. On a ridge east of the Pelly River (07DT100), striations vary from a cross-cutting, valley-perpendicular pair oriented 030^{o}/210^{o} and 040^{o}/220^{o}, to a more valley-parallel 060^{o}/240^{o} (Appendices D). At a second site, in a cirque immediately south of XY camp (07DT080), grooves and deeply abraded striations oriented 020^{o}/220^{o} are cross-cut by finer striations at 045^{o}/225^{o}. A similar pattern of northeast oriented ice-flow followed by

Figure 4.8 a) Proglacial meltwater channel incised through hummocky topography. These channels form as meltwater exits the front of a glacier. b) Lateral meltwater channels formed on a valley wall indicating former glacier surface slope.

approximately cirque-parallel ice-flow was observed in cross-cutting striations measured in a large cirque located between the Don and XY camps (07DT111). Here, older striations oriented 065°/245° cross-cut by others oriented 025°/205°. At each of these three sites, the earlier abrasions are transverse to the valley and the later abrasions are more valley-parallel, suggesting progressively more topographically influenced ice-flow.

Fabric measurements can also be correlated to the valley-parallel Don Stage II. Measurements of clast orientations at 07DT127 and 07DT133 suggest valley-parallel ice-flow to the southwest. Both of these fabrics were measured 50 cm above the contact with the lower gravel, with the fabric at 07DT127 oriented 235° (n = 49; S_1 = 0.64, spread unimodal) and the fabric at 07DT133 indicating ice-flow toward 265° (Fig. 3.2; n = 44, S_1 = 0.80, spread unimodal). Another fabric measurement taken 75 cm above the contact at 07DT133 had a lower eigenvalue, but a similar orientation of 275° (n = 31, S_1 = 0.68, spread unimodal). It is assumed that these represent Don Stage II, but they could represent earlier valley-parallel ice-flow.

Clast fabric measurements also provide useful information on the ice-flow in the Don Creek Valley during Don Stage II. At 07DT009 (Fig. 3.9), fabric measurements in a basal till layer (Unit 1) suggest ice-flow to 240° (n = 24, S_1 = 0.81, spread unimodal). The lower contact of the till was not observed so the interpretation of this till being deposited during Don Stage II is not conclusive and could represent an earlier valley-parallel ice-flow. However, these measurements correlate to striations and rat tails oriented 220° on a roughly three-metre-wide boulder partially excavated from the same unit (Fig. 4.9). Although this boulder may have been rotated after the creation of the rat tails, the alignment between the rat tails and the fabric orientations suggest the rat tails are indicative of late stage ice-flow and likely formed during lodgement. These data are approximately parallel to the orientation of the valley (070°/250°), but contrast with the

interpreted orientation of eskers running northwest through the western limb of the Don Creek Valley. This dichotomy will be addressed in section 4.5.

An alternative explanation for Don Stage II ice-flow is that a re-advance followed regional deglaciation, as observed in more distal areas of the Selwyn lobe (e.g. Bond, 2007). This re-advance would have likely emanated from cirques similar to the Alpine Stage proposed above. If this occurred, it would significantly affect

Figure 4.9 Rat tails on a 3-m-diameter boulder exhumed from the lower diamict unit at 07DT009 (Fig. 3.9). These rat tails correlate with till fabric measurements and indicate ice-flow to the southwest.

some of the interpretations made in this and previous chapters. For example, if the till interpreted at 06DT127 and 06DT133 resulted from a re-advance, the thick glaciofluvial sand and gravel under it would have been deposited from regional deglaciation instead of proglacial advance. While there is insufficient evidence to preclude a regional re-advance, the simpler interpretation is that continuous thinning caused increasing topographic control on ice-flow during initial deglaciation. This was then followed by stagnation and down-wasting of the ice sheet.

4.3 Deglaciation and Deglacial Chronology

Deglaciation in Howard's Pass likely occurred through initial thinning during Don Stages I and II, followed by stagnation and rapid downwasting of the remaining ice sheet (Fig. 4.10). Regional stagnation was invoked by Jackson (1982, 1987) to explain the presence of stagnation deposits in cirques in the study area. This is evident in many cirques throughout Howard's Pass, including south of XY camp. Regional stagnation is also supported by: the interpretation of an ice-proximal lake formed at XY camp that was dammed by ice at lower elevations (see below); frequent ice-marginal glaciofluvial terraces in tributaries that were blocked by ice in the lower valleys (Fig. 2.7); a lack of recessional moraines in valley bottoms; and the abundance of kame and kettle terrain throughout the study area. Kame and kettle deposits imply an uneven ice surface during melt, causing pockets of coarser sediments to collect and form local topographic highs. These landforms are more likely to form with stagnant ice rather than actively flowing ice.

Another glacial landform common in the study area is eskers. Although the abundant eskers in tributaries to the Nahanni River mimicking modern draining are likely good proxies for Don Stage II ice-flow (Fig. 4.2), the eskers in the Don Creek Valley are complex and difficult to resolve. On their eastern margin, their

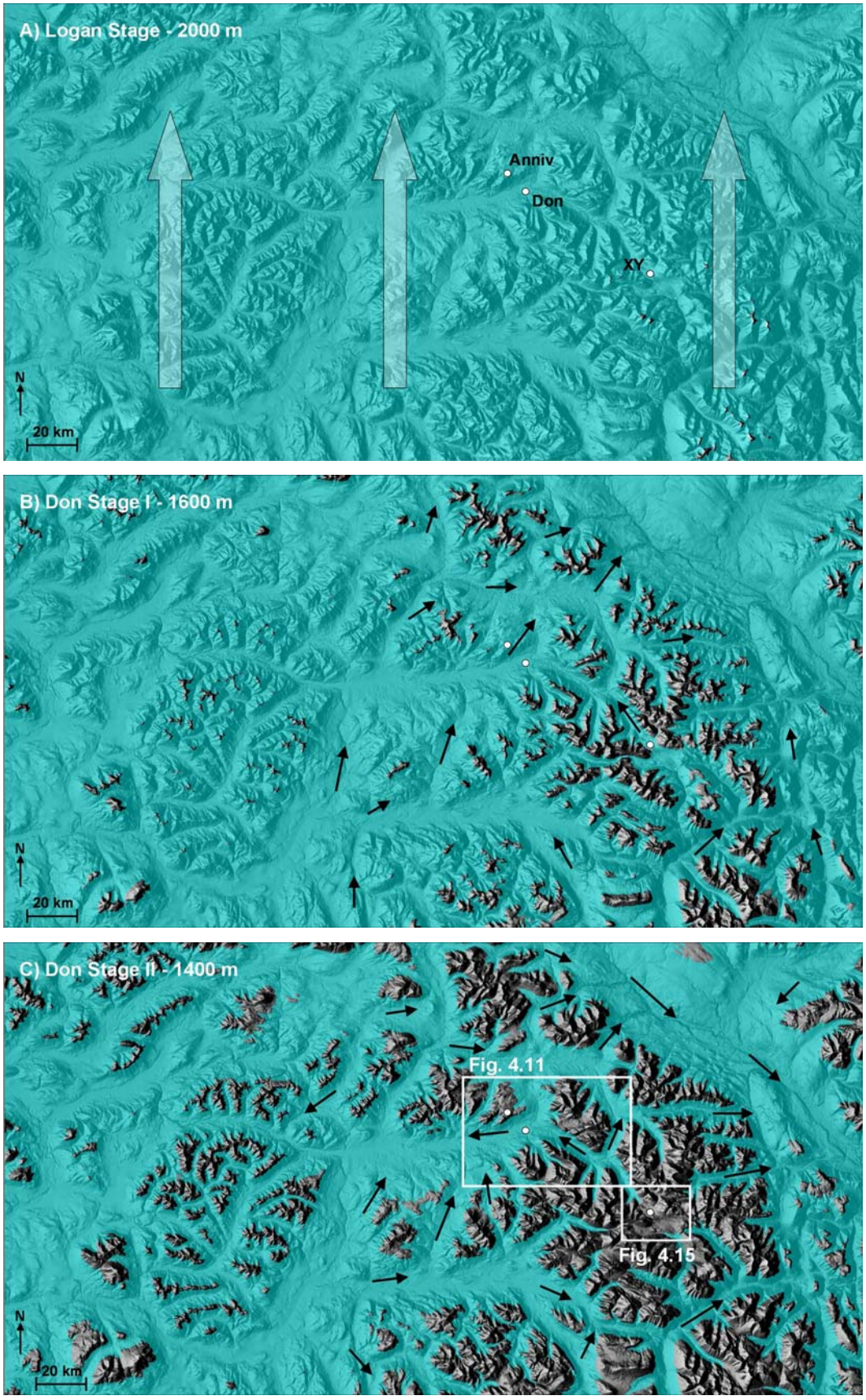
A) Logan Stage - 2000 m
Anniv
Don
XY
N
20 km
B) Don Stage I - 1600 m
N
20 km
C) Don Stage II - 1400 m
Fig. 4.11
Fig. 4.15
N
20 km

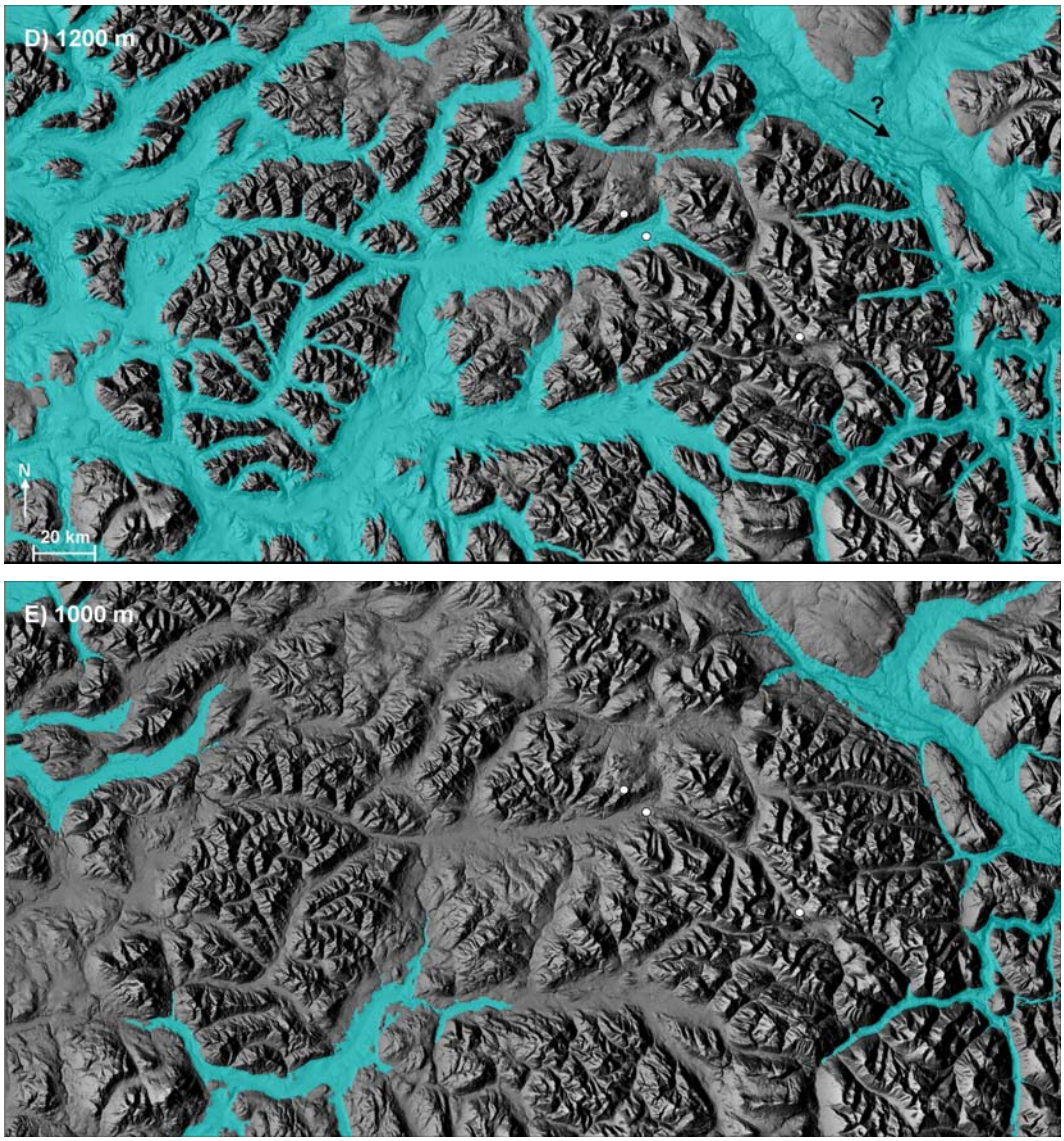

Figure 4.10 Proposed model of deglaciation with initial ice thinning starting at an elevation of 2000 m.a.s.l. progressing to approximately 1200 m.a.s.l., followed by stagnation and downwasting to 1000 m.a.s.l. The black arrows indicate ice-flow indicator sites discussed in the text and illustrated on the terrain inventory map (Appendices A and B). Some of these arrows represent numerous ice-flow indicators in the same area.

morphology indicates flow to the west (Fig. 4.11). Conversely, on their western margin, the esker morphology and deeply incised meltwater channels that likely acted as input channels for subglacial meltwater suggest flow to the east. A plausible explanation for this dichotomy is that these eskers formed under a stagnant ice sheet, with local topography controlling subglacial hydraulics. A problem with this interpretation is the lack of an outlet for the meltwater once it

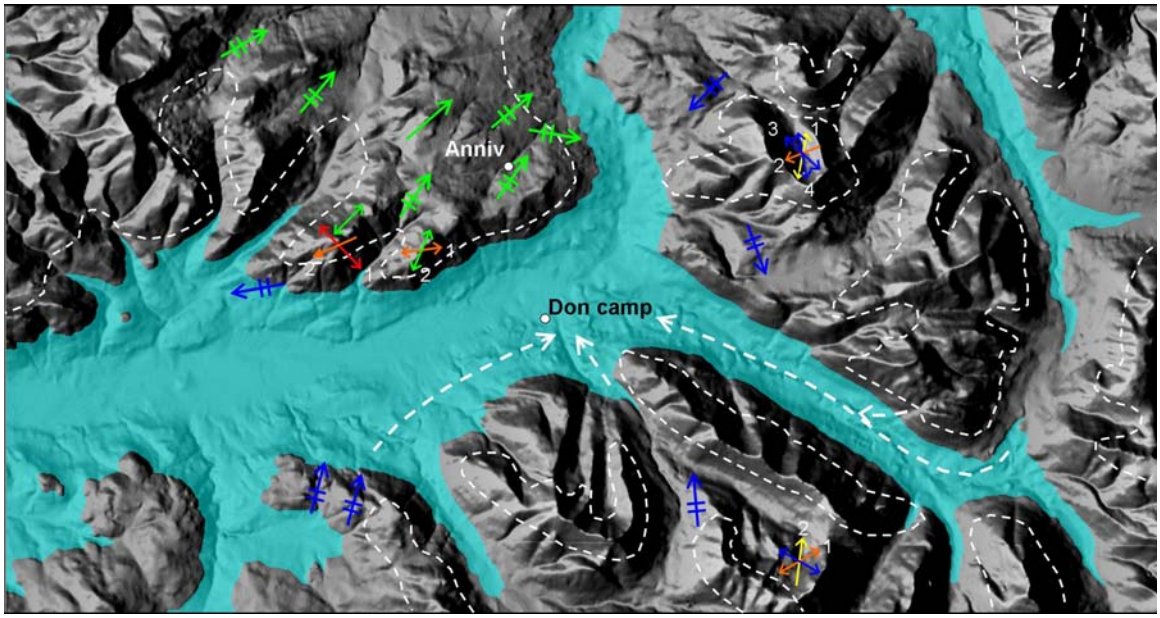

Figure 4.11 Ice flow directions near Don Camp. Red arrows indicate Alpine Stage ice-flow, orange arrows indicate Nahanni Stage ice-flow, yellow arrows indicate Logan Stage ice-flow, green arrows indicate Don Stage I ice-flow and blue arrows indicate Don Stage II ice-flow. White dashed arrows denote esker directions interpreted from morphology. The white dashed areas approximately separate drift controlled by Nahanni and Logan Stage ice-flows (high elevations) from those affected by Don Stage I and II ice-flow (low elevations). The light blue shading represents a stagnant ice surface at 1250 metres above sea level.

converged in the centre of the esker complex. One possibility is that it was diverted to the west, towards the modern Pelly River. Another option is that drainage was to the north, towards the Nahanni River. However, there is no evidence of drainage in this direction, although the channels may have been in-filled by glaciofluvial and glaciolacustrine sediment.

Terrestrial cosmogenic nuclide dating utilizing Be^{10} in four boulders in the north of the study area (Fig. 4.12) returned minimum dates for deglaciation between 9.2 ± 0.4 ka to 29 ± 2.6 ka (Table 4.1). Corrections were made for snow cover, shielding, erosion and boulder dip (Appendix G). There are multiple possible interpretations for this range in dates. The most likely is that the two older dates (06YUK-3, 06YUK-5) reflect inherited ^{10}Be from before deglaciation. If this is true, the sampled surfaces of these two boulders must have been exposed before being covered by ice. The two younger dates (06YUK-1, 06YUK-4) likely more

closely approximate deglaciation. The difference between these two younger dates is possibly from the down-slope movement of 06YUK-1 following initial deposition by the ice sheet. Thus, the age of 12 ± 0.6 ka is thought to most closely approximate deglaciation. This interpretation allows MacDonald's (1983) minimum date of approximately 9 ka BP (~10 200 cal y) for deglaciation in the source area of the Selwyn lobe. Alternatively, 06YUK-4 may also have some inheritance and 06YUK-1 reflects the age of deglaciation. Without further data to support one of these possibilities, interpretations should proceed with caution.

The four boulders sampled were all located on the same landform, interpreted as a late Wisconsinan lateral moraine (Fig. 4.13). The position of this moraine and its distance from any nearby cirques suggests it was not created during a post-glacial re-advance. If this moraine was deposited during a regional re-advance, then one possibly interpretation is that deglaciation occurred at 12 ± 0.6 ka and the re-advance occurred at 9.2 ± 0.4 ka. While this is possible, it is more likely that this moraine formed during valley-parallel Don Stage II during the first phase of deglaciation.

Table 4.1 Sample locations and terrestrial cosmogenic nuclide data from four boulders sampled in the north of the study area.

06YUK-#		1	3	4	5
Latitude	(deg)	62.76	62.77	62.77	62.77
Longitude	(deg)	129.70	129.65	129.65	129.65
Elevation	(m.a.s.l.)	1436	1496	1506	1508
^{10}Be Concentration	(atom/g x 10^5)	2.01	4.27	1.90	5.22
^{10}Be/^{9}Be	(x 10^5)	4.900	12.45	5.549	15.37
Corrected Production Rate	(atoms/g/yr)	18.06	18.89	19.04	19.15
Age without erosion correction	**(kyr)**	**9.0**	**18**	**12**	**27**
2σ precision	(ka)	0.4	0.8	0.6	2.2
Age with erosion correction	**(kyr)**	**9.2**	**19**	**13**	**29**
2σ precision	(ka)	0.4	1.0	0.6	2.6


A


B

Figure 4.12 Four boulders sampled for analysis of Be^{10}. The criteria for the selection of these samples included height, geometry, quartz content, weathering and shielding. This analysis is used to study the timing of regional deglaciation. a) 06YUK-01 (9.5 ka), b) 06YUK-03 (19 ka), c) 06YUK-04 (13 ka), d) 06YUK-05 (28 ka).

Figure 4.13 The lateral moraine where the four boulders were sampled for analysis of Be^{10} content. This moraine is located at approximately 1400 m.a.s.l. and is interpreted to have formed before regional deglaciation.

4.4 Implications of Ice-Flow History for Drift Prospecting

Proper evaluation of surficial geochemical data requires a complete understanding of the number and intensity of glacial transport directions. The last stage of ice-flow is usually the most significant for drift prospecting (Plouffe and Bond, 2004; Bond, 2007). At lower elevations in the study area, Don Stage II was the last phase of ice-flow. This stage was topographically dependent and likely remobilized material that had been previously transported by earlier ice-flows. Anomalies at low elevations are therefore likely to be valley-parallel, but are probably complicated by inherited material from previous transport directions. Conversely, the ice-flow history at higher elevations is simpler with the Logan Stage likely controlling drift transport, with possible contributions from the earlier

Nahanni Stage. These earlier stages of ice-flow possibly created fan, ribbon or amoeba-shaped anomalies (Shilts, 1976; DiLabio, 1990), although amoeba-shaped anomalies are more likely given the proximity of the ice divide (e.g. Shilts, 1976; Parent *et al.*, 1996). Unfortunately, the elevation at which the ice-flow history changes from simple to complex differs across Howard's Pass.

Local variations in ice-flow can greatly affect drift prospecting (Klassen, 1997). Near Don camp, the morphology of the eskers to the south and east, as well as meltwater channel orientations and the fabric in the till unit exposed at 07DT009 suggest late-stage, valley-parallel ice-flow to the west (Fig. 4.11). This is in contrast to the interpreted esker morphology that suggests ice-flow to the east, and ice-flow indicators at higher elevations to the north that suggest ice-flow to the northeast. This dichotomy in ice-flow directions resulted from the change from Don Stage I to Don Stage II ice-flow. During Don Stage I, ice likely flowed northeast across the Don Creek Valley. However, with more thinning, ice was unable to flow over the ridge adjacent to Anniv camp. Instead, ice sourced near XY camp flowed west down the Don Creek Valley. As this ice thinned further and began to stagnate, eskers formed according to localized controls on subglacial hydraulics, possibly reversing the flow in the western portion of the Don Creek Valley.

Ice-flow during Don Stage I and II was simpler at XY camp than at Don camp. Ice flowed from cirques to the south and southwest and was directed by topography to the northwest across XY camp, and east down Placer Creek (Fig. 4.14). As this ice melted, a small lake developed on the level area around XY camp, evidenced by a 100-m-long, 50-m-wide subaqueous cone (07DT010; Fig. 4.15) with steeply interbedded inversely graded gravel, massive pebbly sand and massive clast-supported gravel. In addition, a blanket of at least 50 cm of clayey-silt with fewer than 5% clasts, interpreted to be glaciolacustrine material, covers the plateau at XY camp. The dip of the beds in the subaqueous cone indicates it was fed by meltwater from ice to the southeast. Because of the local topography,

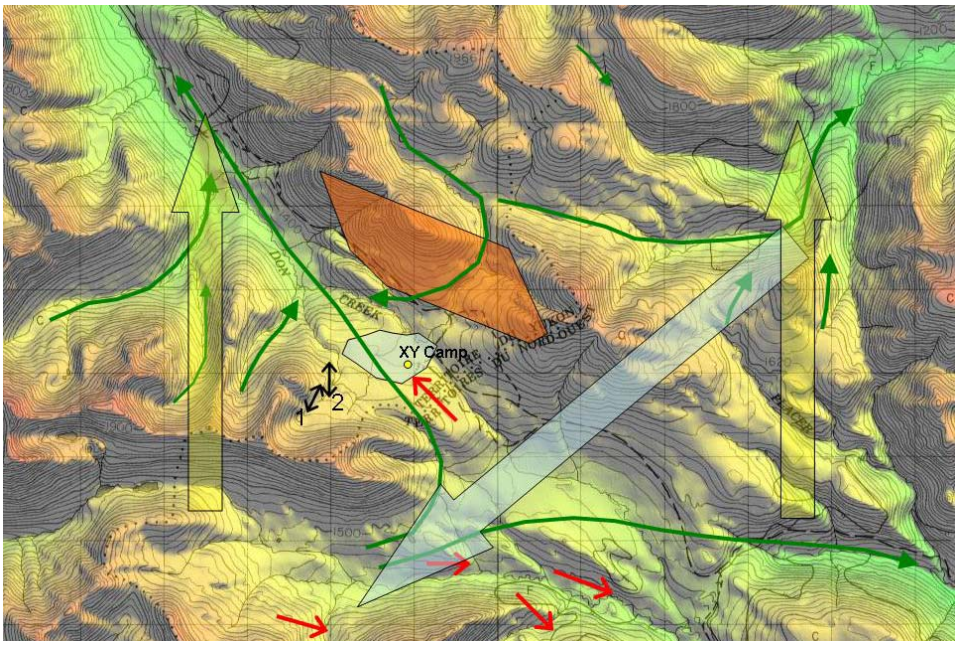

Figure 4.14 Ice-flow at XY Camp. The blue arrow indicates Nahanni Stage ice-flow. Large yellow arrows indicate Logan Stage ice-flow. Small green and red arrows illustrate Don Stage ice-flow as evidenced by meltwater channels and glaciofluvial deposits, respectively. Black arrows represent striations (with the one labelled 2 cross-cutting the one labelled 1) showing ice deflecting out of cirques down-valley. The blue area near XY camp is the interpreted outline of a late-glacial lake fed from the east. The orange area is the inferred XY ore zone.

Figure 4.15: Steeply-bedded stratified gravels interpreted as a subaqueous cone deposited near XY camp (in background). The position and bedding of this cone suggests deposition into an ice-proximal lake with meltwater flow to the northwest.

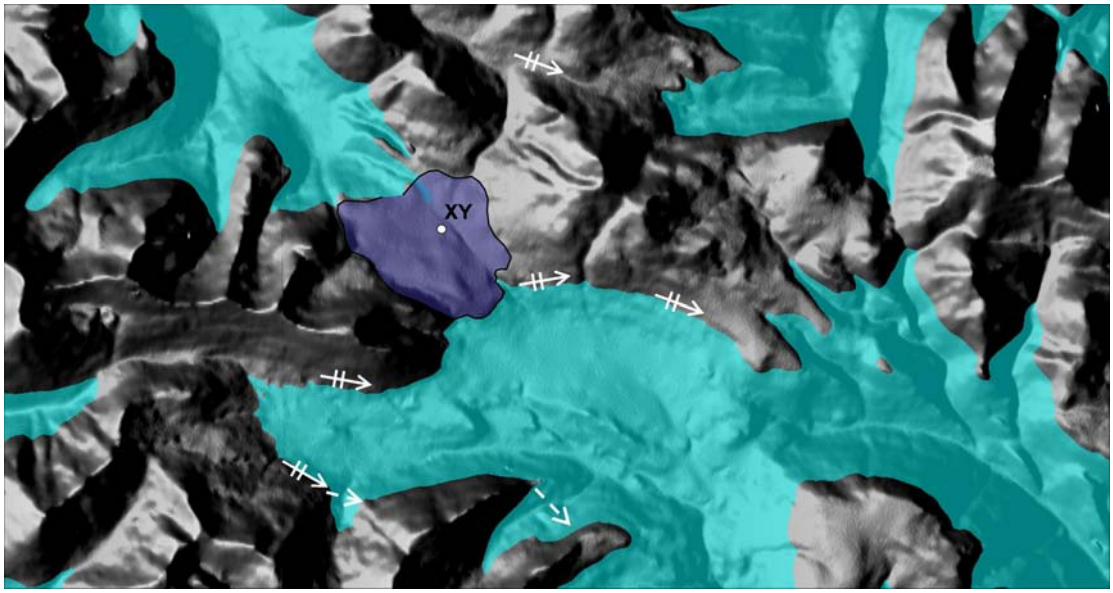

Figure 4.16 Proposed ice surface (light blue shading) during the last phase of deglaciation near XY camp at 1550 m.a.s.l. The formation of an ice marginal lake at XY camp (dark blue shading) indicates ice melted at high elevations before low elevations, supporting downwasting as a mode of deglaciation. Meltwater channels at low elevations and subglacial eskers are noted with solid and dashed arrows, respectively.

the lake was likely ponded against ice in the valley to the northwest (Fig. 4.16). The presence of an ice-marginal lake on the plateau near XY camp and the persistence of ice in the lower valley suggest that the last phase of deglaciation occurred through downwasting rather than frontal retreat into the cirques in this area.

4.5 Discussion and Summary

Howard's Pass was a major accumulation zone for the Selwyn lobe during the late Wisconsinan glaciation. This lobe spread west for more than 200 km and was possibly over 2000 m thick at its maximum over the study area (Jackson *et al.*, 1991), 200 m above the highest mountains in the study area. Previous work in the area has suggested the location of an ice divide near the study area. Jackson (1982, 1994) positioned the divide to the east, in the Nahanni Valley, and Dyke (1990a) interpreted a major ice dome to the southwest of the study

area. Ice-flow indicators such as striations, meltwater channels, eskers, moraines and streamlined bedrock were used to infer the ice-flow history of Howard's Pass.

The earliest Alpine Stage of ice-flow involved valley glaciers originating in local cirques. As these glaciers coalesced and developed into an ice sheet, the ice divide was centred east of the Nahanni River. The ice-flow during this Nahanni Stage was southwest across the study area and completely covered the landscape.

Following the Nahanni Stage, ice flowed dominantly north. This suggests that either the ice divide migrated across the study area, or that a second ice divide developed to the south and southwest of Howard's Pass and caused an ice-flow reversal. This stage of ice-flow is termed the Logan Stage. Ice divide migrations have been observed in the southern CIS (e.g. Stumpf *et al.*, 2000), but have not been described in the northern CIS. The Selwyn lobe ice divide likely changed locations due to changes in the locus of maximum precipitation and subsequent ice thicknesses. As the ice sheet grew in both thickness and extent, the change in topography and associated cooling may have caused a westward shift in moisture accumulation from Pacific air masses.

It is unclear whether the Nahanni or Logan Stage represents glacial maximum in the area. The presence of boulders deposited during the Nahanni Stage that were not significantly transported by the Logan Stage suggests that the Nahanni Stage was maximal. However, the proximity of the Selwyn lobe ice divide suggests that cold-based ice conditions and/or limited horizontal ice-flow vectors could have preserved these boulders during glacial maximum ice-flow. Thus, the timing of glacial maximum ice-flow is enigmatic.

Deglaciation occurred as two phases. As the ice sheet thinned, increased topographic control channelled ice-flow parallel to the major valleys.

Subsequently, deglaciation continued through stagnation and downwasting of the ice sheet, similar to other areas in the Cordillera (Fulton, 1991). This resulted in the deposition of kame and kettle topography, ice-marginal glaciofluvial terraces and eskers in the Don Creek Valley. Terrestrial cosmogenic nuclide dating of ^{10}Be in four boulders on a late-glacial moraine in the north of the study area suggests deglaciation occurred between 9.2 to 12 ka.

The last stage of ice-flow is usually the most significant for drift prospecting. At high elevations, drift transport was controlled by the Nahanni Stage ice-flow from the northeast and Logan Stage ice-flow from the south. Conversely, at lower elevations, valley-parallel ice-flow re-deposited drift, causing more complex and locally variable drift transport histories.

5 GEOCHEMISTRY

Previous analysis of glacially dispersed geochemical anomalies by multiple companies in Howard's Pass has been impeded by a lack of documented ice-flow history and sampling conducted regardless of surficial material. These sampling methods do not allow for the detection of new geochemical anomalies. For example, a survey that samples weathered ore and till would have background values too high to detect subtle anomalies in the till. As a result, these surveys confirm the location of outcropping ore bodies, and are less successful in locating buried mineralized zones. Recent stream sampling is also unreliable as weathering of carbonate-rich bedrock increases the water pH and inhibits the dispersal of mobile elements (Lett, 2001). In order to provide an alternative to traditional till geochemistry, a Mobile Metal Ion geochemistry (MMI) case study was conducted over the known Anniv Central deposit in Howard's Pass, directly east of Anniv camp (Fig. 1.3).

The exact processes that result in MMI anomalies are still not fully understood. MMI utilizes the loose attachment of mobile ions to soil particles as they migrate from oxidizing mineral deposits to the surface (Fig. 5.1). Oxidation of mineralized bedrock is exothermic, causing elements to migrate upward through the soil profile along a temperature and density gradient (Mann *et al.*, 2005). Convection, electrochemistry, diffusion and seismic pumping have all been suggested as possible mechanisms of upward transport (Mann *et al.*, 1998). In addition, ions above the water table may also be brought to the surface by capillary rise. Mobile ions are converted at the surface to insoluble compounds or particles occluded to, or adsorbed onto, soil materials (Mann *et al.*, 1998). This conversion likely occurs during pedogenic development. Because MMI only analyzes unbound ions, those ions that become bound in the soil and may be subject to down-slope

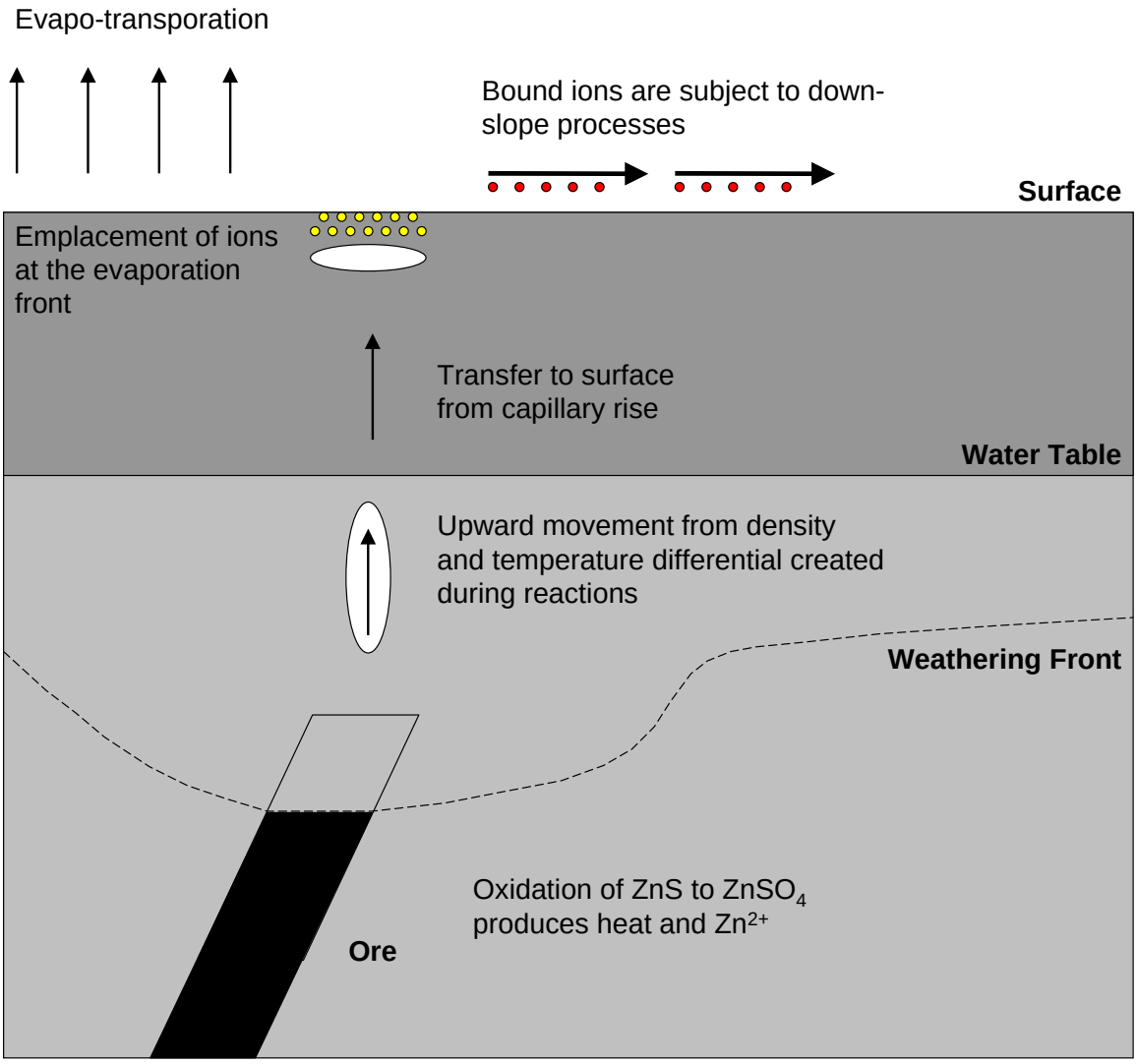

Figure 5.1 Possible processes contributing to the creation of Mobile Metal Ion geochemistry (MMI) anomalies. Initial oxidation of buried mineralized bedrock is followed by migration of metal ions to the surface. These ions become bound to soil particles (red) and are subject to lateral transport. However, because MMI analyses only recently surfaced, unbound ions (yellow), MMI anomalies are detected directly above the mineralized bedrock. Modified from Mann *et al.* (2005).

processes are neglected. MMI anomalies should therefore be found directly above mineralized bedrock (Harris *et al.*, 1988).

The purported benefits of using MMI in mountainous terrain include sharp and precise anomalies, minimal nugget effects and the potential to detect deeply buried mineralization (Mann *et al.*, 1998). In addition, because the mobile ions

migrate upwards to the same depth regardless of material type, samples are taken at a fixed depth, simplifying the sampling process.

Deposits in the study area have similar geochemistry as other deposits in the Selwyn Basin. Besides anomalous Pb and Zn bound in galena and sphalerite, the area is enriched in pyrite, resulting in anomalous values of As, Co, Cu, Ni and Sb (Goodfellow, 2007). Other commonly anomalous elements in the Selwyn Basin are Ba, Cd, Hg and Se (Goodfellow, 2007).

The Anniv Central deposit was selected for this case study based on the presence of near-surface mineralized bedrock, the number of drill holes nearby and the good road access. Unfortunately, the bedrock geology in the area is more complex than initially thought, with multiple sub-vertical faults crossing the ore zone. An outline of the bedrock stratigraphy is given in section 1.2. For detailed descriptions, refer to Morganti (1979).

Other than the complex bedrock geology, the survey area was well-suited for MMI and till geochemistry. The relief across the survey was less than five metres and it only had one small stream dissecting it (Fig. 5.2). The last stage of ice-flow in this area was likely Don Stage I (near Anniv camp on Figure 4.11) and was to the northeast. The surficial material sampled was a light brown to light grey till with a silt matrix between one to three metres thick. The till contains 10-30% clasts reflecting local lithologies of mostly shale with some limestone and conglomerate. Poor drainage in the till prevented sample collection of the lower two intervals at four locations, and precluded analysis of an additional three samples. This poor drainage may have caused capillary rise to be a more prominent ion transporting processes than it would in a dry area.

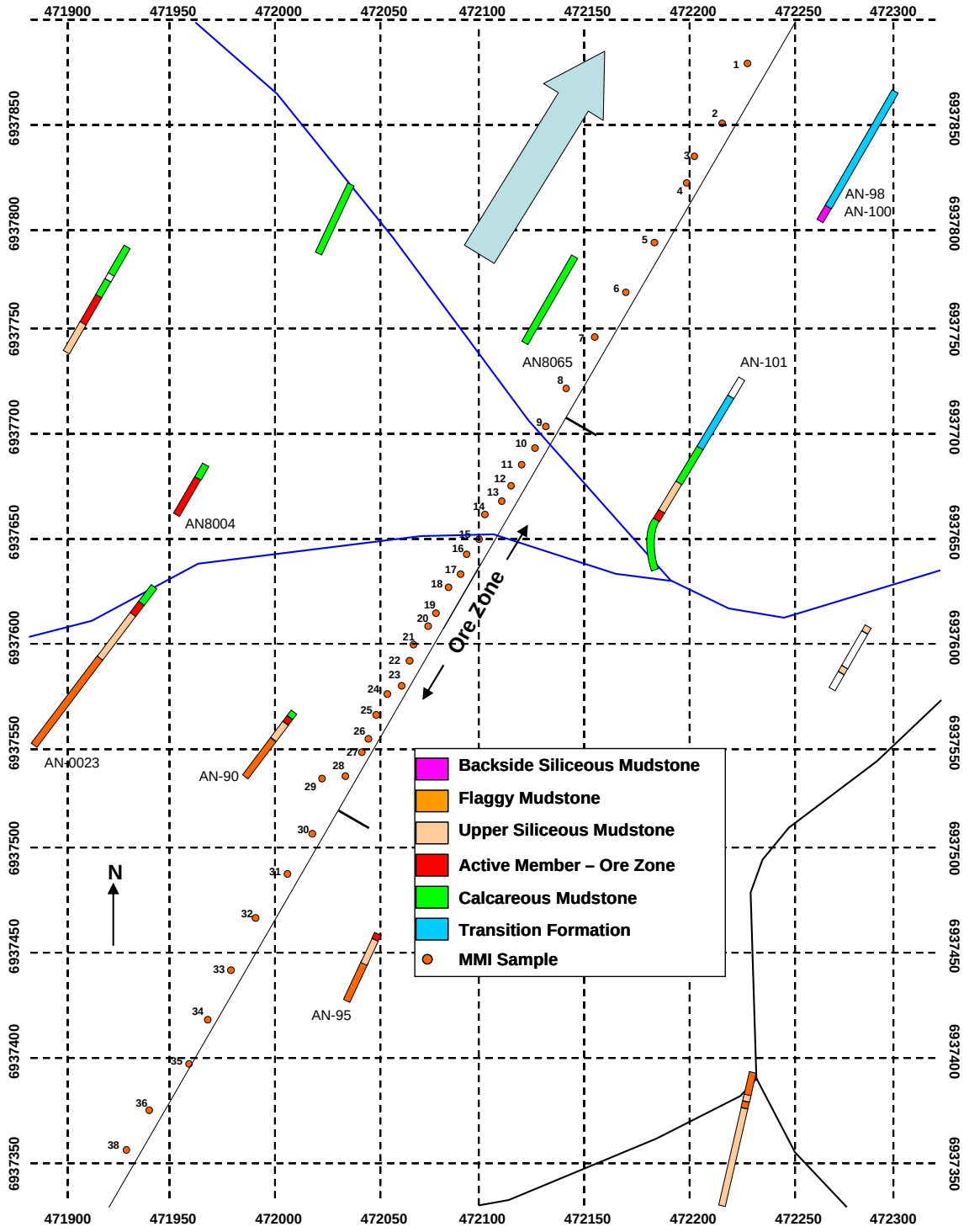

Figure 5.2 Location of Mobile Metal Ion geochemistry (MMI) samples collected over the Anniv Central deposit ore zone, inferred using nearby drill core. Thirty-nine samples were collected over 600 m, two of which were duplicates. Samples had 10-m-spacing directly over the ore zone, inferred ore zone, and 25-m-spacing on either side. Nearby drill holes shown as coloured bars correlate to those shown on Figure 5.6. Blue lines are streams and black lines are roads. The blue arrow is the inferred direction of the last phase of ice-flow over the survey area.

5.1 Methodology

In the summer of 2006, MMI samples were collected at 37 locations in a 600 m survey over the known Anniv Central deposit in Howard's Pass (Fig. 5.2). Because sampling was completed before the detailed deglacial ice-flow history was determined, samples were collected parallel to the inferred ice-flow. Samples were collected at 25-m-spacing for the first and last 200 m, and 10-m-spacing directly over the ore zone inferred from nearby drill core, between 200 and 400 m. MMI samples were collected at four, 10-cm-intervals below the lowest organic horizon to evaluate which interval contained the highest element concentrations. Because MMI is highly sensitive to sampling contamination, all jewellery was removed before sampling and plastic trowels and shovels were used to collect the samples. The samples were then sealed in two or three plastic bags.

MMI samples were analysed by the MMI Multi-Element Leach (MMI-M5) complimentary of SGS Minerals. This extraction analyzes over 40 elements, including base metals, precious metals and rare earth elements (REEs). In order to successfully analyze MMI samples, extractants containing strong ligands detach weakly attached metal ions from soil particles (Mann *et al.*, 1998). These ligands "complex with and change the salvation energy status of the metal ions" (Mann *et al.*, 1998), instead of extracting the ions from a solid particle. The concentrations of mobile metals released from this extraction are well within the range of inductively coupled plasma mass spectrometers.

For comparison, 37 conventional till geochemistry samples were collected at the same locations as the MMI samples. The till samples were collected 30 to 50 cm below the lowest organic horizon to avoid possible enrichment in plant tissue. These samples were analyzed for 28 elements at ALS Chemex Ltd. using aqua-regia digestion of the silt and clay fraction of the till samples, with sieving down to the 180 micron (120 mesh) size. The samples were then analyzed using either

inductively coupled plasma with atomic emission spectroscopy or with mass spectroscopy, depending on the precision level required (http://www.alsglobal.com/ Mineral/DivisionServices.aspx).

In order to make the data comparable to future MMI transects that will have different background values, response ratios were calculated for Pb and Zn in each sample. The response ratio is a ratio of the elemental concentration to the calculated background concentration for each element. Background values were taken as the average of the concentrations below the 20^{th} percentile and anomalous values were taken as the top 90^{th} percentile. However, the close proximity of the ore body likely resulted in elevated metal concentrations for all of the samples. Response ratios are also an effective tool for isolating anomalies and evaluating the level of contrast for each element over the ore body. A low contrast anomaly has a response ratio < 20, while moderate and high contrast anomalies have response ratios between 20 and 50, and > 50, respectively (Fedikow, 2006).

One sample taken in the middle of the survey, directly over the inferred ore zone (06DTMMI-20), had concentrations that were an order of magnitude higher than the surrounding samples. This sample was likely either contaminated during sampling or was subject to a nugget effect, with small amounts of ore included in the sample. It is therefore not included in the analyses in this chapter.

Fourteen lab and two field duplicates were collected from both the MMI and till surveys to test the precision of these samples. Both the MMI and till geochemistry results had a high level of precision based on comparisons between the sample data and the lab and field duplicates. Lab duplicates were compared between 14 samples for Pb, Zn, Al, Ag, Co and Cu (Fig. 5.3). This comparison resulted in R^2 values greater than 0.94 for all of these elements except Co (R_{Cu}^2 = 0.813), indicating an overall high level of precision. More mixed results were found with the field duplicates (Fig. 5.4). Although one

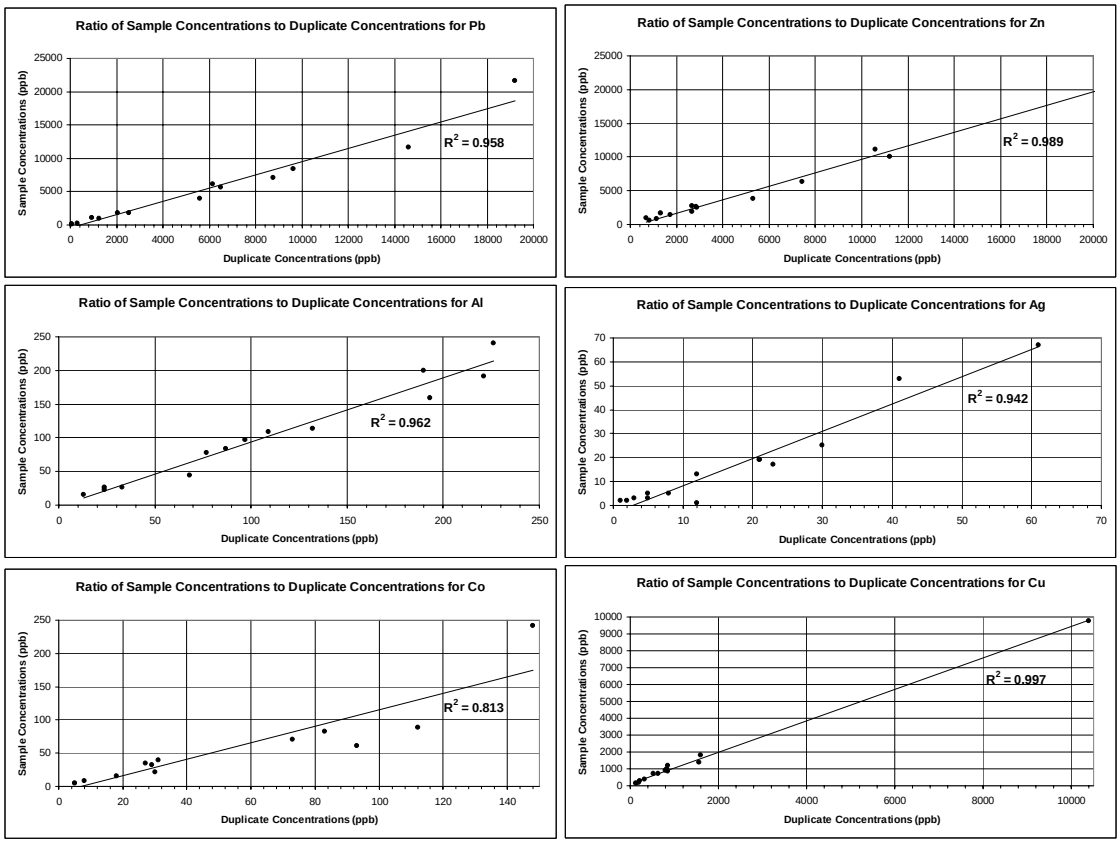

Figure 5.3 Laboratory duplicate results for six elements from MMI samples showing a general high level of repeatability.

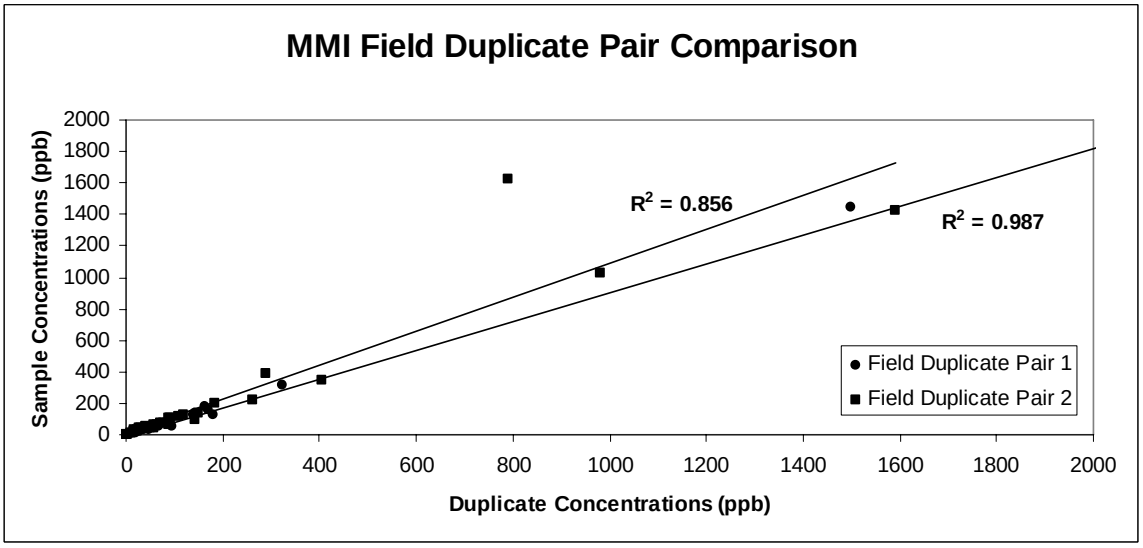

Figure 5.4 Two field duplicate pairs for all elements analyzed from the MMI survey. Each data point is a different element. One pair shows a high level of high repeatability, while the other is significantly worse.

sample-duplicate pair had an R^2 value of 0.987, the other had an R^2 value of 0.856. It is not surprising that the field duplicates yielded less precision than the lab duplicates, as there are more possible sources of error in the field than in the lab, such as the potential heterogeneity of the two field samples.

5.2 Results of MMI and Till Geochemistry

Because MMI surveys require sampling at the same depth regardless of material type, the case study was designed to test what interval would be best for future surveys. For most elements, including all of the rare earth elements, the most reactive interval was 30-40 cm. This is shown graphically for four elements on Figure 5.5 and is supported by the average concentrations of the four intervals for 13 elements and the REEs (Table 5.1). The exception was the results for Pb that had higher concentrations in the 0-10 cm interval. All data are shown in more detail in Appendices E and F.

Table 5.1 Average interval concentrations for 14 elements from the MMI survey.

Element	**Ag**	**Au**	**Ca**	**Cd**	**Co**	**Cu**	**REE**
Units	ppb	ppb	ppb	ppb	ppb	ppb	ppb
Detection Limit	1	0.1	10	10	5	10	0.5
0-10 cm	35	0.1	119	217	136	1281	24.5
10-20 cm	31	0.1	124	206	149	1261	34.2
20-30 cm	40	0.1	144	219	181	1717	42.2
30-40 cm	50	0.2	153	237	89	1637	41.2

Element	**Fe**	**Mg**	**Ni**	**Pb**	**Sr**	**U**	**Zn**
Units	ppm	ppm	ppb	ppb	ppb	ppb	ppb
Detection Limit	1	1	5	10	10	1	20
0-10 cm	100	9	930	10476	178	203	9512
10-20 cm	79	10	903	10895	202	226	9533
20-30 cm	69	10	1095	11533	195	248	10831
30-40 cm	62	12	1092	11984	211	203	14313

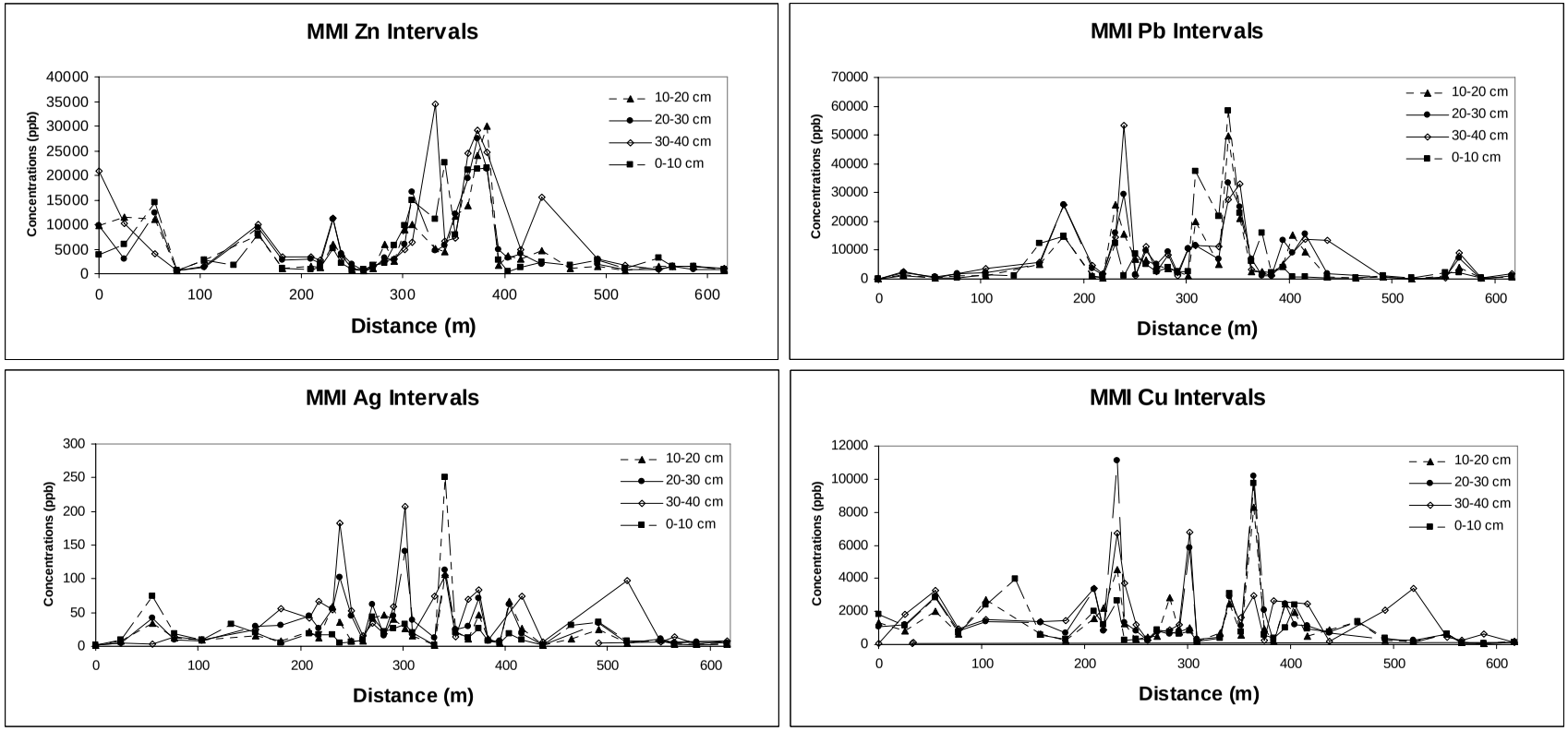

Figure 5.5 MMI samples were collected from 10-cm-intervals below the lowest organic horizon to test what depth recovered the best results. Both Zn and Pb were generally most reactive in the lowest (30-40 cm) interval.

Both Zn and Pb show significant peaks in concentrations and response ratios in the MMI results approximately 50 m from the sub-cropping ore observed in drill holes in the area (Figs. 5.6, Fig. 5.7). The average concentration of Pb over the ore zone was 11.71 ppm, compared to 5.29 ppm outside the ore zone. Zn ranged from an average of 9.9 ppm over the ore zone to 5.4 ppm outside the ore zone (Fig. 5.6). Other transition metals such as Ni, Ag, Co, Cd and Au showed various-sized anomalies over the ore zone (Fig. 5.8, Appendix F). The calculated background MMI concentrations for Pb and Zn were 0.37 ppm and 1.1 ppm, respectively.

The till geochemistry trends for Zn and Pb are similar to those from the MMI survey, with anomalies dispersed approximately 50 m down-ice from the sub-cropping ore (Fig. 5.6). Elements such as Cu, Ag and Ni (Fig. 5.8) have smaller anomalies than Pb and Zn, and elements such as Ba, As and the rare earth elements show no anomalous values (Appendix F). Anomalous values of Co and Mg were only found using MMI digestion. These differences in size and dispersion of various elements may simply reflect the mineralogy of the ore zone, but are also controlled by properties such as the till thickness and the difference between the elemental concentrations between the mineralized and country rock (Klassen, 1999, Plouffe and Bond, 2004). The presence of limited down-ice anomaly in an area of thin till thickness supports the position of the inferred ore zone and indicates that other anomalies in thin drift across the study area likely reflect nearby sub-cropping ore zones.

The background values for Pb and Zn in the till geochemistry survey were 41.6 ppm and 251.1 ppm. The concentrations of the till samples were significantly higher than the MMI samples, likely due to the different digestion techniques used. The similarity between the anomalies found for Ag, Cu, Ni, Co and Cd, and the anomalies found for Pb and Zn indicates that these elements are potential pathfinders for Pb and Zn in Howard’s Pass.

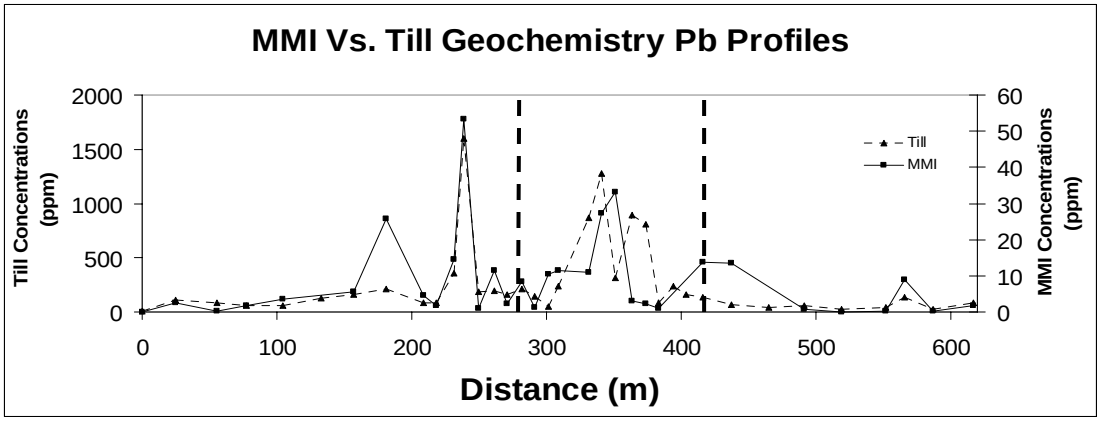

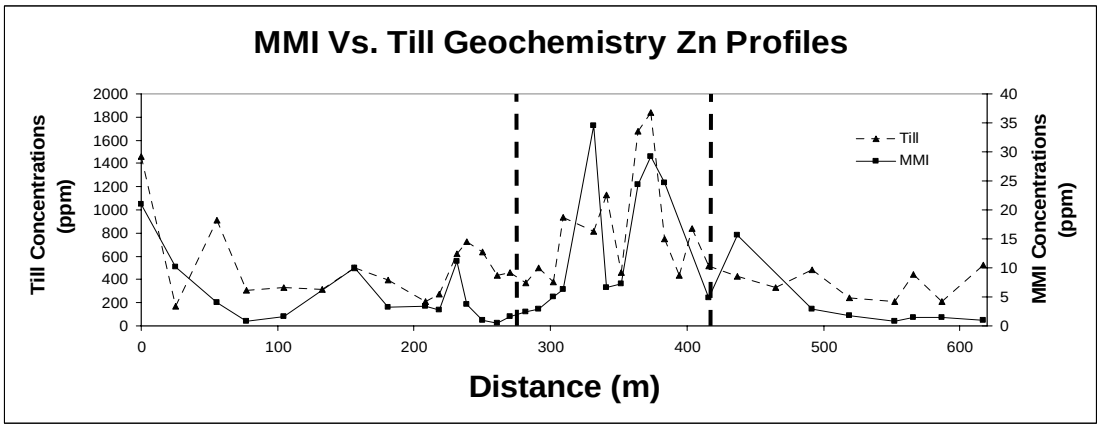

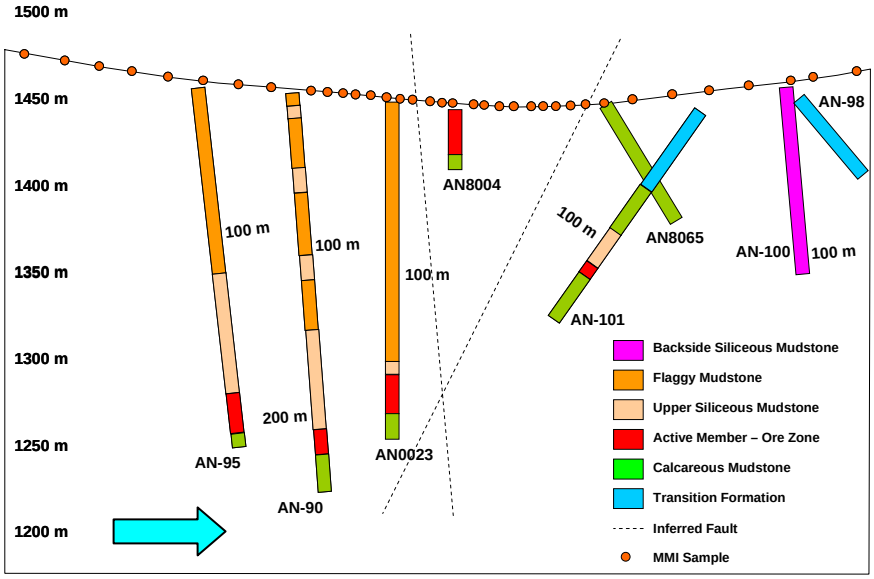

Figure 5.6 MMI and till geochemistry profiles for Pb and Zn compared with drill hole logs. In general, the MMI anomalies have lower backgrounds than the till samples. Till metal concentrations are significantly higher than MMI concentrations due to the difference in digestion methods. The ore zone is bounded by two inferred faults (approximated by the dashed lines). Ice-flow is illustrated by the blue arrow.

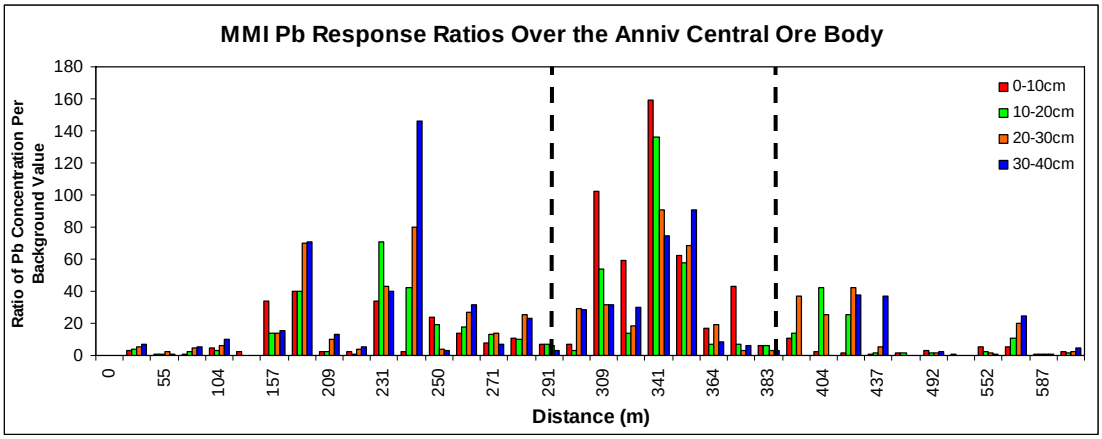

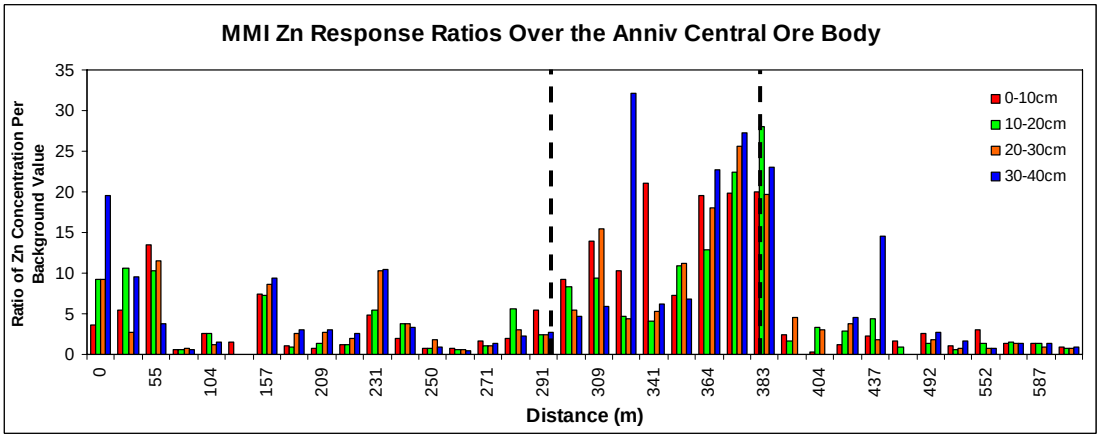

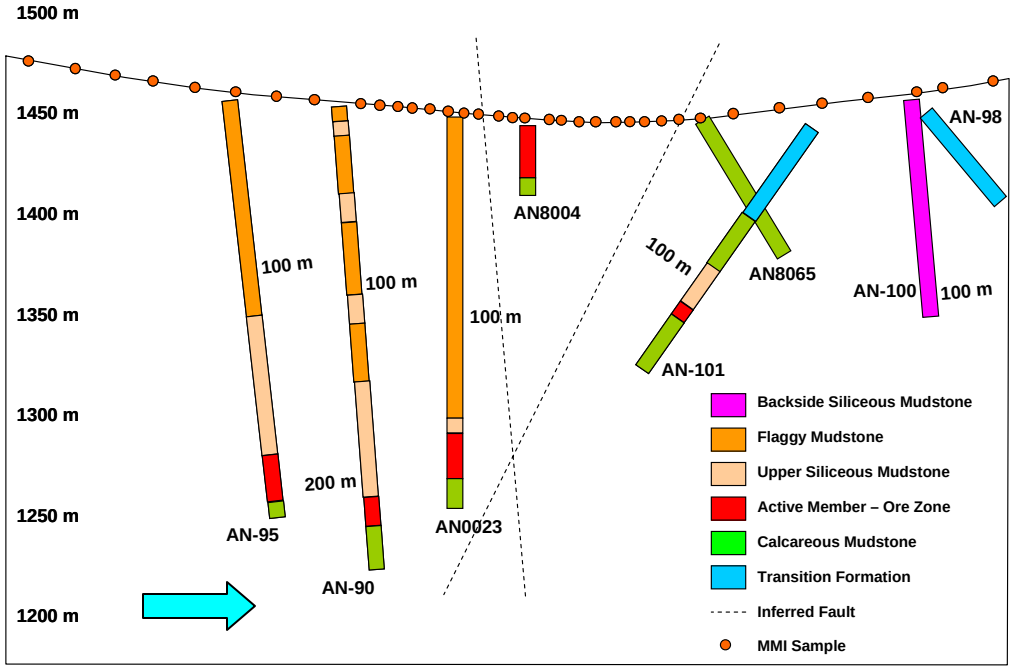

Figure 5.7 Response ratios of Pb and Zn over the Anniv Central ore body. Response Ratios are ratios between the elemental concentration and the background value. Background values are the average of the concentrations below the 20th percentile for each element. Blue arrow indicates the ice-flow direction.

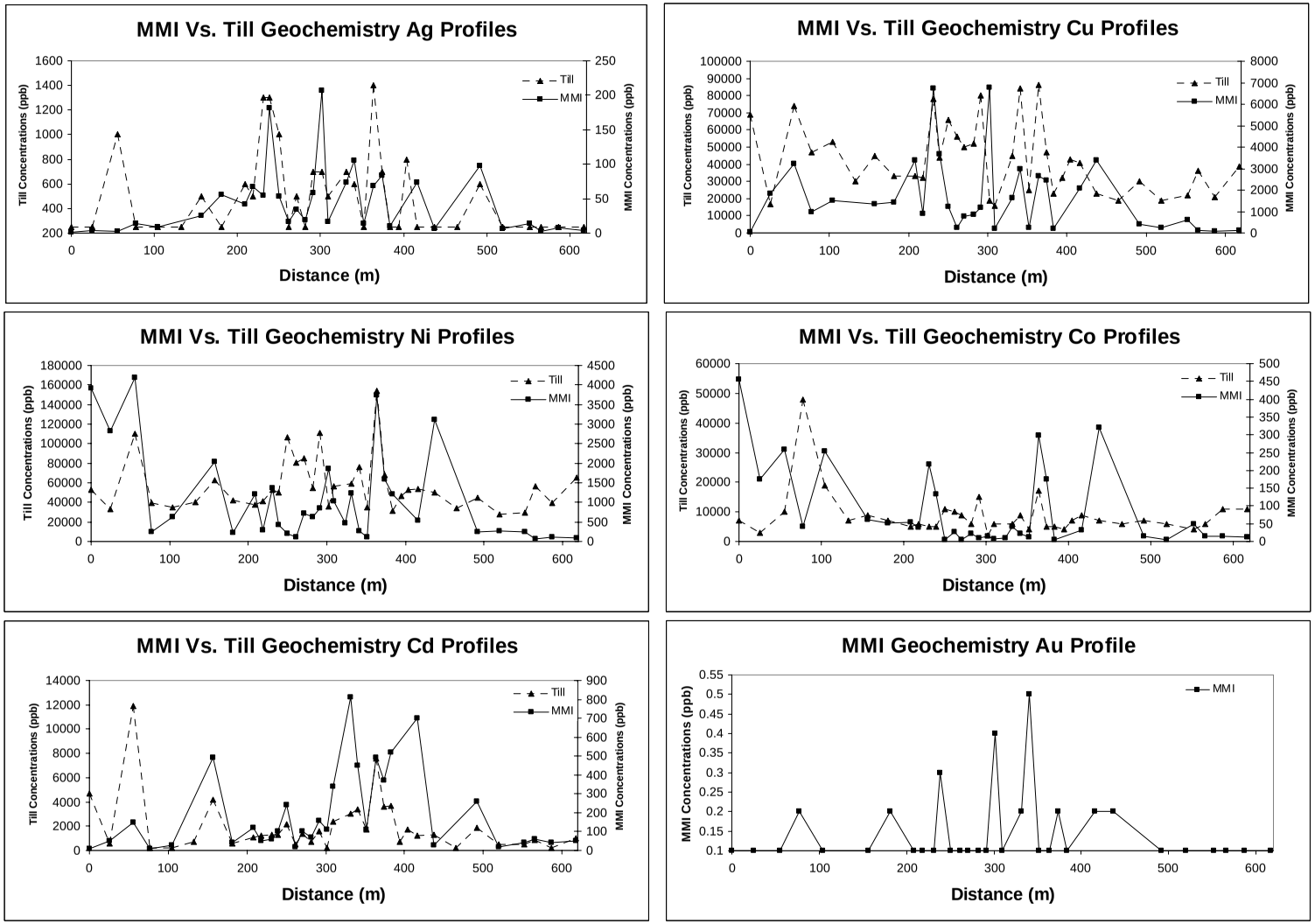

Figure 5.8 MMI and till geochemistry profiles for five elements, and MMI concentrations for Au. All of these elements show anomalous values over the ore zone.

There is a significant difference in the contrast of the anomalies found using the MMI and till geochemistry surveys. For Pb, four MMI samples had high contrast anomalies and four more had moderate contrast anomalies (Fig. 5.9). Comparatively, the Pb till geochemistry samples only had three moderate contrast anomalies and no high contrast anomalies. The Zn samples showed similar results, with the MMI samples having four moderate contrast anomalies and the till geochemistry samples showing no high or moderate contrast anomalies (Fig. 5.9).

One explanation for the difference in contrasts between the MMI and till geochemistry is that the till survey did not extend far enough down-ice to include the centre of the dispersal plume. However, the similarity of the anomalous concentration patterns of the two surveys suggests that the plume was included in the survey. Thus, the differences are more likely cause by the different digestion methods causing relatively higher background values in the till geochemistry results. The background concentrations in the till survey results may also reflect elevated values inherited from previous ice-flow stages (cf. Klassen, 1999).

Although the contrasts differ, the similarity of the patterns of the MMI and till geochemistry surveys has important implications. If the anomalous MMI values reflect the presence of ore directly below, then the correspondence of anomalous till geochemistry signatures imply extremely rapid upward mobility of ore through the till column. It would also indicate that the ore zone is as extensive as interpreted in figures 5.2, 5.6 and 5.7. Alternatively, if the ore zone is narrower than inferred and is located 50 m up-ice from the anomalies, the MMI anomalies do not directly overlie mineralized bedrock.

One possible scenario to explain the presence of MMI anomalies without underlying ore is that the MMI survey detected oxidized detrital ore transported in

the till. This suggests that MMI geochemistry was not effective at detecting the inferred ore zone and instead only identified changes in amount of ore transported in the dispersed till. A potential reason for the lack of an isolated MMI signature above the inferred ore zone is the typically downward net movement of ions in till profiles in areas with shallow water tables such as the surveyed area. This is in contrast to more arid regions where the technique has been tested that would have upward groundwater movement. This downward movement could potentially prevent rapid upward movement of mobile ions from buried sub-cropping mineralized ore.

5.3 Summary and Implications for Drift Prospecting

The complicated glacial history of Howard's Pass (Fig. 4.1) makes tracing subtle geochemical anomalies difficult. To provide a more effective method of detecting anomalies, an MMI case study was conducted directly over a known deposit. This survey resulted in anomalous values of Pb and Zn, indicating abundant galena and sphalerite in the ore zone. Additional anomalous results for Ni, Ag, Co, Cd and Au suggest that these elements are potential pathfinders in the study area where Pb and Zn are not anomalous. Some of these elements likely reflect weathering cherts and shales, while others probably reflect pyrite in the ore zone.

The MMI survey detected anomalous values of Pb and Zn, with a peak roughly 50 m down-ice of the sub-cropping ore observed in drill core, and a decrease in concentrations on either side (Fig. 5.6). However, concentrations of samples taken at the edge of the survey, that likely overlie more deeply buried mineralization, are unusually high for background concentrations (W. Grondin, pers. comm., 2007). These high background values possibly suggest that the MMI technique can recognize mineralization through approximately 200 m of non-mineralized bedrock and drift. However, a more plausible explanation is that the presence of abundant black shales in the area is affecting the background levels. If the survey edges are detecting deeply buried mineralization, then this geochemical cross-section provides important data on the change in MMI

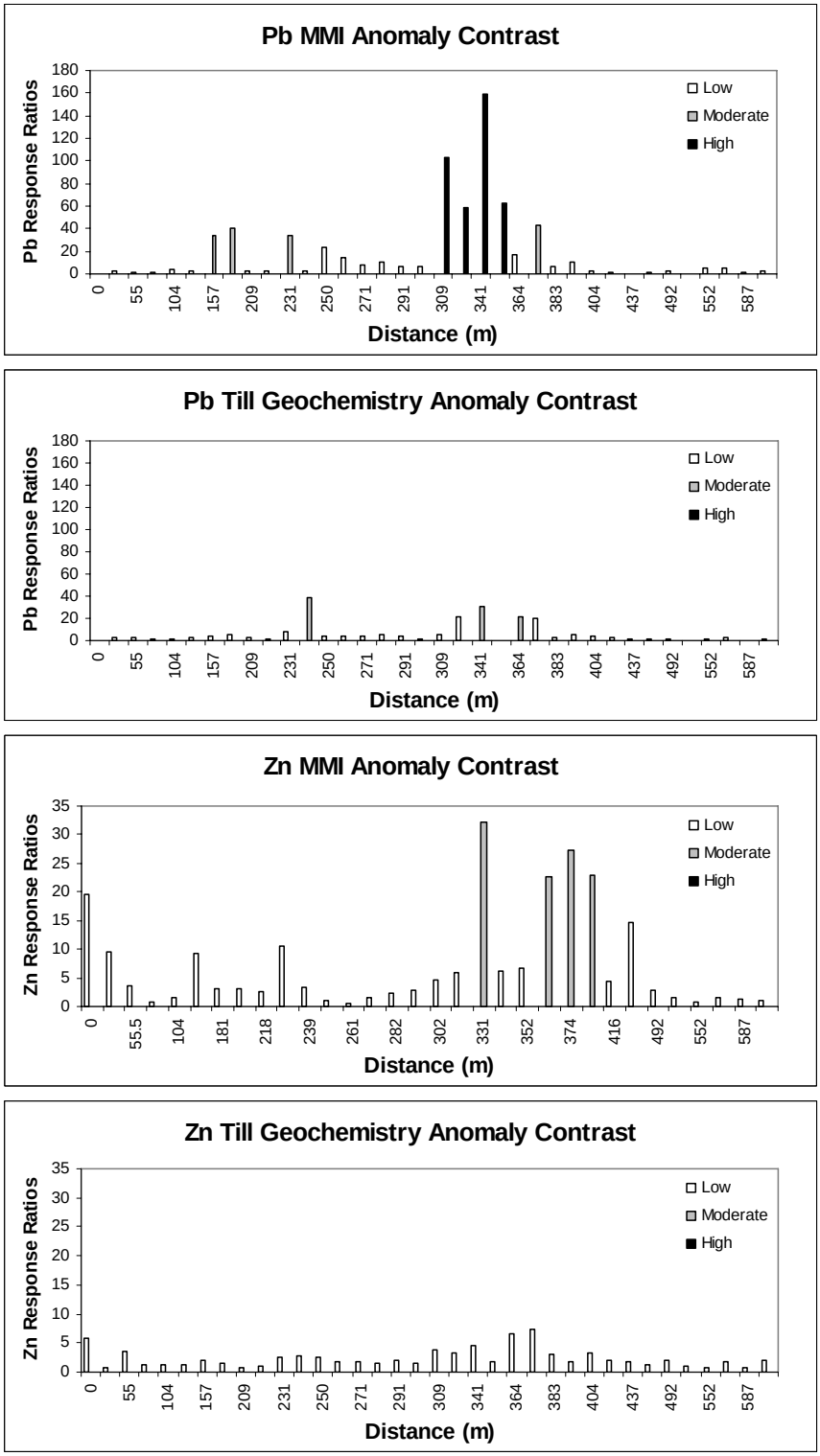

Figure 5.9 Anomaly contrasts from response ratios of Pb and Zn for both MMI and till geochemistry. Low contrast anomalies have response ratios < 20, moderate contrast anomalies are from 20 to 50, and high contrast anomalies have ratios > 50.

concentrations with ore depth. The central Pb and Zn anomalies would therefore reflect the near-surface mineralization, with the inferred faults possibly acting as conduits for ion transmission. Another MMI survey further from an ore zone is necessary to reveal the true background concentrations in the area and to test the penetration depth of MMI geochemistry through bedrock.

Although the 30-40 cm interval resulted in the highest concentrations (except for Pb), all four intervals sampled had similar patterns. This is especially true directly above the inferred sub-cropping ore zone. This suggests that using the 30-40 cm interval is not vital. Instead, shallower intervals will likely yield similar results, and will allow sampling where the water table is close to the surface. Whatever interval is used, samples must still be taken at a consistent depth.

The till geochemistry survey conducted at the same locations as the MMI survey also produced anomalies in Pb and Zn approximately 50 m down-ice of the sub-cropping ore. These results suggest that either a rapid mobilization of ions occurred through the till over this deposit, or that the last stage of ice-flow at Anniv Central was short-lived. The results support the interpreted ice-flow direction to the northeast. Other elements such as Ag and Cu show more poorly-defined anomalies over the ore zone, Many properties may control this difference such as the till thickness and the contrast between the mineralogy of the host and country rock (Plouffe, 1998; Plouffe and Bond, 2004).

A possible interpretation of the similarity of the pattern of the MMI and till geochemistry anomalies is that the MMI was not effective at detecting the inferred ore zone. Instead, the MMI anomalies may have resulted from oxidation of detrital ore in the till, producing elevated concentrations down-ice of the inferred ore zone. The absence of more data on the position of the ore zone makes this interpretation unsubstantiated. However, further use of MMI

geochemistry should be preceded with more detailed work around a more well-defined ore zone.

The various directions of sediment transport and the thickness of the drift covering lower elevations in Howard's Pass makes interpretation of traditional soil survey data difficult. A comparison of MMI and till geochemistry suggests that MMI anomalies are easier to identify, but are similar to till geochemistry anomalies. An analysis of the response ratios for Pb and Zn indicates that MMI anomalies have a higher contrast and provide a more precise estimate of the location of mineralized ore zones than till geochemistry anomalies. In addition, till geochemistry is poorly suited for areas where till overlies thick glaciofluvial deposits, such as in the Don Creek Valley. However, areas of thin till cover are well-suited to till geochemistry surveys.

Future geochemical surveys in the study area should utilize till geochemistry in areas of shallow till cover, whereas MMI geochemistry may be more useful in areas where ore zones are buried beneath thick drift. If MMI were employed further in Howard's Pass, another orientation survey over a more geologically understood area such as the XY deposit is required.

6 SUMMARY AND CONCLUSIONS

Howard's Pass is significant as a source area for the Selwyn lobe of the northern Cordilleran Ice Sheet (CIS) and as a target for mineral exploration. In order to investigate the glacial history of the area and to aid drift prospecting and infrastructure development, a joint M.Sc. project between Simon Fraser University, the Yukon Geological Survey and Selwyn Resources Ltd. was designed. Objectives for this study included the creation of a terrain inventory map, the reconstruction of ice-flow and the pattern of deglaciation, and the completion of a Mobile Metal ion geochemistry (MMI) orientation survey over a known deposit.

6.1 Terrain Inventory Map

A 1: 50 000-scale terrain inventory map was completed for Howard's Pass. This map includes information on the texture, surficial materials, surface expressions and geomorphological processes in the map area. Several geomorphological processes that are ubiquitous across the study area were only included where they are especially prevalent or hazardous. This includes avalanche tracks and slow mass movements such as creep and solifluction.

The terrain inventory map is useful for mine development as it highlights the location of certain surficial materials and expressions that are important for infrastructure development. For example, the paucity of glaciolacustrine sediments, useful as a tailing pond liner, makes the small deposits located between esker ridges and valley sides significant. An example of utilizing certain surface expressions is the use of the continuous, well-drained eskers running through the Don Creek Valley for roads connecting the multiple ore zones in the

area. The map is also useful for identifying significant hazards associated with certain geomorphological processes, such as potential debris flow and avalanche tracks.

Another use for the terrain inventory map is for tracing geochemical anomalies across the study area. Previously, geochemical data collected from soil samples was interpreted regardless of surficial material. In this way, soil samples collected from polygons consisting predominantly of till can by analyzed separately, allowing for the detection of new anomalies.

6.2 Ice-Flow History

Five stages of ice-flow were reconstructed in Howard's Pass during the late Wisconsinan. These stages are similar to Fulton's (1991) model of growth and decay for the southern CIS. The earliest stage of ice-flow (Alpine Stage) involved valley glaciers originating from nearby cirques. As these glaciers coalesced and developed into an ice sheet, an ice divide was centred northeast of the study area. The ice-flow during this stage (Nahanni Stage) was southwest across Howard's Pass, completely covering the landscape.

Following glacial maximum, either the ice divide migrated across the study area, or another ice divide developed to the south and southwest of Howard's Pass. Ice-flow during this stage (Logan Stage) was to the north. This change was possibly due to increased precipitation accumulation to the west of the initial divide as the Selwyn lobe extended prior to deglaciation.

Deglaciation occurred in two phases. Initially, the ice sheet began to thin and was deflected by topography mostly to the northeast (Don Stage I). With increased topographic control, ice-flow was channelled parallel to the valleys (Don Stage II). During Don Stage II, ice from near XY camp flowed along the Don Creek Valley to the northwest, reaching Don camp and continuing west to the modern

Pelly River. With extensive ice thinning, ice-flow stagnated, forming kame and kettle topography in some of the major valleys. Some eskers formed according to localized controls on subglacial hydraulics and appear to be out of sync with Don Stage II ice-flow direction.

The second phase of deglaciation in Howard's Pass was by stagnation and downwasting. This is supported by a lack of moraines, extensive stagnation terrain and the presence of an ice marginal lake at near XY camp. The only end moraines observed in the study area are located in cirques and are likely due to small re-advances following regional deglaciation. The lack of recessional moraines in the valley bottoms suggests frontal retreat did not occur in these valleys. Instead, thick kame and kettle deposits in many valley bottoms indicate that ice was stagnant during the last phase of deglaciation. In addition, an ice marginal lake that formed at XY camp during deglaciation was blocked by ice in the valley bottom, indicating that ice melted first at higher elevations.

Howard's Pass was likely ice free between 9.2 to 12 ka. Evidence for these dates was provided by terrestrial cosmogenic nuclide dating using the amount of Be^{10} in four erratics. Although these boulders produced a wide range of dates, the two older dates likely reflect inheritance from before glaciation. These four boulders were deposited on a lateral moraine that formed during Don Stage II ice-flow. These dates allow for MacDonald's (1983) minimum age of 9 ka B.P., also taken in a source area for the Selwyn lobe.

Understanding the ice-flow history of Howard's Pass is useful for continued mineral exploration in the area. Tracing geochemical anomalies requires an understanding of the distance and direction surficial materials have been transported. This is vital in Howard's Pass, where the direction of the last ice-flow to affect an area depends on its elevation. In low elevation areas, the last ice-flow was valley-parallel, whereas materials at high elevations were last exposed to either Logan Stage or Don Stage I ice-flow. Subsequently, anomalies found at

higher elevations reflect regional transportation trends, while anomalies traced at lower elevations are dominantly valley-oriented.

6.3 Mobile Metal Ion and Till Geochemistry

An MMI orientation survey and a till geochemistry survey were completed over the known Anniv Central deposit in Howard's Pass. This survey detected anomalous values of Pb and Zn approximately 50 m down-ice of sub-cropping ore observed in drill core. The detection of high background values of Pb and Zn at the edges of the survey possibly suggests that MMI is able to penetrate through up to 200 m of bedrock. In addition, anomalous values of Ni, Ag, Co, Cd and Au indicate that these may be potential pathfinders for Pb and Zn in the study area. Compared to the till geochemistry survey over the same area, the MMI survey provided more precise, higher contrast anomalies for approximately the same cost.

The results of the MMI and till geochemistry surveys are significant for drift exploration in Howard's Pass. MMI should detect mineralized bedrock through thick drift and should be unaffected by glacial transport. It is therefore a potential tool for drift prospecting in Howard's Pass because drift thicknesses can exceed 50 m in the valley bottoms, and because the area was exposed to multiple directions of ice-flow. Till geochemistry is better suited to areas of thinner till cover.

However, the similarity of MMI and till geochemistry patterns and the down-ice dispersal of the anomalies from the observed sub-cropping ore suggests that the MMI results are reflecting detrital ore in the till rather than underlying mineralized bedrock. Further drilling in the area may provide better control over the extent of the ore zone and identify large sub-cropping mineralized bedrock directly beneath the anomalies. If MMI or till geochemistry were employed further in the

study area, another orientation survey over a more geologically understood area such as the XY deposit is required.

6.4 Future Studies

Further academic studies in Howard's Pass should focus on obtaining a better glacial chronology. Further dating using terrestrial cosmogenic dating of the granitic erratics throughout the study area would provide a better date of deglaciation in the study area. Dating the lower glaciofluvial material observed in the drill core and at 06DT127 and 06DT133 may provide the timing of the onset of McConnell glaciation in the area.

To help obtain these dates, stratigraphic sections immediately outside the study area should be visited. Sections along the Nahanni River, in an unnamed valley west of the Pelly River and those exposed by further infrastructure development in the Don Creek Valley may be useful to future studies. The latter may also provide new information on the dynamics of the eskers in the Don Creek Valley. Ongoing drilling will continue to offer the possibility of observing buried stratigraphic relations.

If more terrain mapping is required near Howard's Pass, the planned transportation corridors linking the area to major highway or railway networks should be targeted. In addition, sampling and analyzing the engineering properties of the surficial materials would provide valuable information for future development.

This study has shown that MMI and till geochemistry are potentially useful for detecting subtle geochemical anomalies in Howard's Pass. However, if either is to be used extensively, a longer orientation survey extending well beyond an ore zone is required. A survey stretching northwest down the Don Creek Valley from the XY deposit is recommended as it has excellent access and is more

geologically understood than Anniv Central. To further investigate till geochemistry dispersal plumes near ore zones in Howard's Pass, a two-dimensional till survey that investigates the change in concentrations parallel and perpendicular to ice-flow over a well-defined deposit is recommended.

REFERENCE LIST

Alley, R.B., 1991. Deforming-bed origin for southern Laurentide till sheets? Journal of Glaciology, 37, 67-76.

Andrews, J.T., Shimizu, K., 1966. Three-dimensional vector technique for analyzing till fabrics: discussion and Fortran program. Geographical Bulletin, 8, 151-165.

Blair, T.C. and McPherson, J.G., 1994. Alluvial fans processes and forms. *In*: Geomorphology of Desert Environments, A.D. Abrahams, A.J. Parsons (eds.), Chapman and Hall, London, 354-402.

Bond, J. D., 2004. Late Wisconsinan McConnell glaciation of the Whitehorse map area (105D), Yukon. *In*: Yukon Exploration and Geology 2003, *edited by*: D.S. Emond, L.L. Lewis, Yukon Geological Survey, 73-88.

Bond, J.D., 2007. Late Wisconsinan McConnell glaciation of the Big Salmon Range, Yukon. *In*: Yukon Exploration and Geology 2006, *edited by*: D.S. Emond, L.L. Lewis, L.H. Weston, Yukon Geological Survey, 105-122.

Bond, J.D., Kennedy, K.E., 2005. Late Wisconsinan McConnell ice-flow and sediment distribution patterns in the Pelly Mountains, Yukon. *In*: Yukon Exploration and Geology 2004, *edited by*: D.S. Emond, L.L. Lewis, G.D. Bradshaw, Yukon Geological Survey, 67-82.

Bostock, H.S., 1966. Notes on glaciation in central Yukon Territory. Geological Survey of Canada Paper 65-36, 18 p.

Boulton, G.S., 1987. Subglacial sediment deformation and the origin of drumlins during the coarse of a glacial period. Congress of the International Union for Quaternary Research, 12, p. 135.

Brennand, T.A., 1994. Macroforms, large bedforms and rhythmic sedimentary sequences in subglacial eskers, south-central Ontario: implications for esker genesis and meltwater regime. Sedimentary Geology, 91, 9-55.

Davis, N.F.G., Mathews, W.H., 1944. Four phases of glaciation with illustrations from southwestern British Columbia. Journal of Geology, 52, 403-413.

DiLabio, R.N.W., 1990. Glacial dispersal trains. *In*: Glacial Indicator Tracing, R. Kujansuu and M. Saarnisto (eds.), A.A. Balkema, Rotterdam, 109-122.

Dreimanis, A., 1989. Tills: Their genetic terminology and classification. *In*: Genetic classification of glacigenic deposits, Goldthwait, R.P., Matsch, C.L. (eds.). Rotterdam, Balkema, 17-83.

Duk-Rodkin, A., 1999. Glacial limits map of Yukon Territory; Geological Survey of Canada, Open File 3694, Indian and Northern Affairs Canada Geoscience Map 1999-2, scale 1:1 000 000.

Duk-Rodkin, A., 2001a. Glacial limits, Niddery Lake – Sekwi Mountain, west of sixth meridian, Yukon Territory. Geological Survey of Canada, Open File, 3803.

Duk-Rodkin, A., 2001b. Glacial limits, Flat River, west of sixth meridian, Yukon Territory. Geological Survey of Canada, Open File, 3808.

Duk-Rodkin, A., Jackson, L.E., Jr., Rodkin, O., 1986. A composite profile of the Cordilleran ice sheet during McConnell Glaciation, Glenlyon and Tay River map areas, Yukon Territories. *In*: Current Research, part B, Geological Survey of Canada, Paper 86-1B, 257-262.

Duk-Rodkin, A., Huntley, D., 2006. Quaternary geology and glacial limits of southern Mackenzie Mountains and foothills. Abstract Volume (Geological Association of Canada), 31, 43 p.

Dyke, A.S., 1990a. Quaternary geology of the Frances Lake map area, Yukon and Northwest Territories. Geological Survey of Canada, Memoir 426, 39p., Maps 1674A, 1675A, 1676A, 1677A, scale 1:100 000.

Dyke, A.S., 1990b. Surficial Materials and Landforms, Dolly Varden Creek, Yukon Territory. Geological Survey of Canada, “A” Series Map, 1674A.

Dyke, A.S., 1990c. Surficial Materials and Landforms, Frances River, Yukon Territory. Geological Survey of Canada, “A” Series Map, 1675A.

Dyke, A.S., 1990d. Surficial Materials and Landforms, Yusezyu River, Yukon Territory. Geological Survey of Canada, “A” Series Map, 1676A.

Dyke, A.S., 1990e. Surficial Materials and Landforms, Little Hyland River, Yukon Territory. Geological Survey of Canada, “A” Series Map, 1677A.

Fard, A.M. and Gruszka, B., 2007. Subglacial conditions in a branching Saalian esker in north-central Poland. Sedimentary Geology, 193, 33-46.

Fedikow, M.A., 2006. Aqua regia mobile metal ions and enzyme leach (super SM) soil geochemistry study results from the Timmins area: Discover Abitibi Initiative. Open File Report – Ontario Geological Survey, Report: 6179, 22 p.

Ford, D.C., 1976. Evidences of multiple glaciations in Southern Nahanni National Park, Northwest Territories. Canadian Journal of Earth Science, 13, 1433-1445.

Froese, D.G., Barendregt, R.W., Enkin, R.J., Baker, J., 2000. Paleomagnetic evidence of multiple Late Pliocene Early Pleistocene glaciations in the Klondike area, Yukon Territory. Canadian Journal of Earth Sciences, 37, 863-877.

Fulton, R.J., 1991. A conceptual model for growth and decay of the Cordilleran Ice Sheet. Geographie Physique et Quaternaire, 45, 281-286.

Goodfellow, W.D., 1989. Interpretation of stream geochemistry leading to the discovery of a secondary zinc deposit, Pelly River, Nahanni map area, Yukon. *In*: Current Research 98-1 E. Geological Survey of Canada, 31-50.

Goodfellow, W.D., 2007. Base metal metallogeny of the Selwyn Basin, Canada. *In:* Mineral Deposits of Canada: A Synthesis of Major Deposit Types, District Metallogeny, the Evolution of Geological Provinces, and Exploration Methods: Geological Association of Canada, Mineral Deposits Division, Special Publication No. 5, W.D. Goodfellow (eds.), p. 553-579.

Goodfellow, W.D. and Lydon, J.W., 2007. Sedimentary exhalative (SEDEX) deposits. *In:* Mineral Deposits of Canada: A Synthesis of Major Deposit Types, District Metallogeny, the Evolution of Geological Provinces, and Exploration Methods: Geological Association of Canada, Mineral Deposits Division, Special Publication No. 5, W.D. Goodfellow (eds.), p. 163-183.

Goodfellow, W.D., Jonasson, I.R., Morin, J.A., 1986. Environment of formation of the Howard's Pass (XY) deposit, Selwyn Basin, Yukon. Canadian Institute of Mining and Metallurgy, Special Volume, 37, 19-50.

Gordey, S.P., 1981. Geology of the Nahanni map-area, Yukon Territory and District of Mackenzie. Geological Survey of Canada, Open File, 780.

Gosse, J.C., Phillips, F.M., 2001. Terrestrial in situ cosmogenic nuclides: theory and application. Quaternary Science Reviews, 20, 1475-1560.

Haldorsen, S. 1983. Mineralogy and geochemistry of basal till and its relationship to till-forming processes. Norsk Geologisk Tidsskrift, 63, 15-25.

Harris, M., Widnall, M.A., Jones, E.M., Steele, G.B., 1988. Application of top-of-bedrock geochemical sampling techniques at the Lagalochan intrusive complex,

western Argyll, Scotland. Institution of Mining and Metallurgy, Transactions, Section B: Applied Earth Science, 97, B22-B28.

Hicock, S.R., 1990. Genetic till prism. Geology, 18, 517-519.

Hicock, S.R., Goff, J.R., Lian, O.B., Little, E.C., 1996. On the interpretation of subglacial till fabric. Journal of Sedimentary Research, 66, 928-934.

Howes, D.E. and E. Kenk (ed.). 1997. Terrain Classification System for British Columbia. Version 2. MOE Manual 10. BC Updated by Resources Inventory Branch, BC Ministry of Environment, Lands and Parks. Victoria, BC.

Hughes, O.L., Campbell, R.B., Muller, J.E., Wheeler, J.O., 1969. Glacial limits and flow patterns, Yukon Territory, south of 65 degrees north latitude. Geological Survey of Canada, Paper 68-32, 9 p.

Jackson, L.E. Jr., 1982. Terrain conditions, Nahanni, Yukon and District of Mackenzie, map and notes. Geological Survey of Canada, Open File 886.

Jackson, L.E., Jr., 1986a. Terrain Inventory, Finlayson Lake, Yukon Territory. Geological Survey of Canada, Open File, 1379.

Jackson, L.E. Jr., 1986b. Terrain Inventory, Kananaskis Lakes, Alberta, 82-J. Geological Survey of Canada, Preliminary Map, 2-1984, 1:25 000-scale.

Jackson, L.E., Jr., 1987. Terrain inventory and Quaternary history of Nahanni map area, Yukon Territory and Northwest Territories. Geological Survey of Canada, Paper 86-18, 23 p.

Jackson, L.E., Jr., 1989. Paleoglaciology of the Selwyn lobe of the Cordilleran Ice Sheet and Quaternary stratigraphy of east-central Yukon, p. 60-65. *In*: Late Cenozoic history of the interior basins of Alaska and Yukon, *edited by*: L.D. Carter, T.D. Hamilton, J.P. Galloway, U.S. Geological Survey, Circular 1026, 114 p.

Jackson, L.E., Jr., 1993a. Surficial Geology, Big Timber Creek, Yukon Territory. Geological Survey of Canada, “A” Series Map, 1834A.

Jackson, L.E., Jr., 1993b. Surficial Geology, Hoole River, Yukon Territory. Geological Survey of Canada, “A” Series Map, 1794A.

Jackson, L.E., Jr., 1993c. Surficial Geology, Fortin Lake, Yukon Territory. Geological Survey of Canada, “A” Series Map, 1795A.

Jackson, L.E., Jr., 1993d. Surficial Geology, Lonely Creek, Yukon Territory. Geological Survey of Canada, “A” Series Map, 1796A.

Jackson, L.E., Jr., 1993e. Surficial Geology, Rainbow Creek, Yukon Territory. Geological Survey of Canada, “A” Series Map, 1797A.

Jackson, L.E., Jr., 1994. Terrain inventory and Quaternary history of the Pelly River area, Yukon Territory. Geological Survey of Canada, Memoir, 437, 41 p,

Jackson, L.E., Jr., Morison, S.E., 1984. Terrain Inventory, Sheldon Lake. Geological Survey of Canada, Open File, 1033.

Jackson, L.E., Jr., Ward, B.C., Duk-Rodkin, A., Hughes, O. L., 1991. The latest Cordilleran ice sheet in Yukon Territory. Géographie Physique et Quaternaire 45, 341-354.

Jackson, L.E., Jr., Morison, S.R., McKenna, K., 1993a. Surficial Geology, Dragon Lake, Yukon Territory. Geological Survey of Canada, “A” Series Map, 1832A.

Jackson, L.E., Jr., Morison, S.R., McKenna, K., 1993b. Surficial Geology, Prevost River, Yukon Territory. Geological Survey of Canada, “A” Series Map, 1833A.

Jackson, L.E., Jr., Morison, S.R., McKenna, K., 1993c. Surficial Geology, Radar Lake, Yukon Territory. Geological Survey of Canada, “A” Series Map, 1835A.

Jonasson, I.R., Jackson, L.E., Jr., Sangster, D.F., 1983. A Holocene zinc orebody formed by the supergene replacement of mosses. Journal of Geochemical Exploration, 18, 189-194.

Kerr, F.A., 1934. Glaciation in northern British Columbia. Royal Society of Canada Transactions, Series 3, 28, 4, 17-31.

Klassen, R.W., 1987. The Tertiary-Pleistocene stratigraphy of the Liard Plain, southeastern Yukon; Geological Survey of Canada, Paper 86-17, 16 p.

Klassen, R.A., 1997. Glacial history and ice flow dynamics applied to drift prospecting and geochemical exploration. *In*: Proceedings of Exploration 97; fourth decennial international conference on Mineral exploration, Toronto, Canada, Sept. 14-18, 1997, Geological Survey of Canada, 221-232.

Lee, J., Jonasson, I.R., Goodfellow, W.D., 1984. Metal accumulation by byrophytes in some zinc-rich blanket bogs, Selwyn Mountains, Yukon. Canadian Journal of Botany, v. 62, 4, 722-728.

Lett, R.E., 2001. Geochemical signatures around massive sulphide deposits in southern British Columbia, Canada. *In*: Drift Exploration in Glaciated Terrain. McClenaghan, M.B., Bobrowsky, P.T., Hall, G.E.M., Cook, S.J. (eds.), Geological Society, London, Special Publications, 185, 301-321.

Levson, V., 1992. The sedimentology of Pleistocene deposits associated with placer gold bearing gravels in the Livingston Creek area, Yukon Territory. *In*: Yukon Geology, Vol. 2; Exploration and Geological Services Division, Yukon Region, Indian and Northern Affairs Canada, 99-132.

MacDonald, G.M., 1983. Holocene vegetational history of the upper Natla River area, Northwest Territories, Canada. Arctic and Alpine Research, 15, 169-180

Mann, A.W., Birrell, R.D., Mann, A.T., Humphreys, D.B., Perdrix, J.L., 1998. Application of the mobile metal ion technique to routine geochemical exploration. Journal of Geochemical Exploration, 61, 87-102.

Mann, A.W., Birrell, R.D., Fedikow, M.A.F., de Souza, H.A.F., 2005. Vertical ionic migration: mechanisms, soil anomalies, and sampling depth for mineral exploration. Geochemistry: Exploration, Environment, Analysis, 5, 201-210.

Morganti, J.M., 1979. The geology and ore deposits of the Howard's Pass area, Yukon and Northwest Territories: The origin of basinal sedimentary stratiform sulfide deposits. PhD Thesis, University of British Columbia, Vancouver, B.C., 317 p.

Nelson, J., Paradis, S., Christensen, J., Gabites, J., 2002. Canadian Cordilleran Mississippi Valley-type deposits; a case for Devonian-Mississippi back-arc hydrothermal origin. Economic Geology, 97, 1013-1036.

Parent, M., Paradis, S.J., Doiron, A., 1996. Palimpsest glacial dispersal trains and their significance for drift prospecting, Journal of Exploration Geochemistry, 56, 123-140.

Pearson, C., Plouffe, A., Bond, J.D., 2004. Drift prospecting in the region of the Yukon-Tanana Terrane, southern Yukon. *In*: Yukon Exploration and Geology 2003, D.S. Emond, L.L. Lewis (eds.), Yukon Geological Survey, 221-257.

Plouffe, A., 1989. Drift prospecting and till geochemistry in Tintina Trench, Southeastern Yukon. M.Sc. thesis, Carleton University and Ottawa-Carleton Geoscience Centre, Ottawa, 111 p.

Plouffe, A., Jackson, L.E., Jr., 1992. Drift prospecting for gold in the Tintina Trench. *In* Yukon Geology, Vol. 3. Exploration and Geological Services Division, Yukon, Indian and Northern Affairs Canada, 196-213.

Plouffe, A., 1998. Detrital transport of metals by glaciers, an example from the Pinchi Mine, central British Columbia. Environmental Geology, 33, 183-196.

Plouffe, A., Bond, J.D., 2004. Drift prospecting in the region of the Yukon-Tanana Terrane, southern Yukon. *In*: Yukon Exploration and Geology 2003, *edited* by: D.S. Emond L.L. Lewis, Yukon Geological Survey, 221-257.

Rothlisberger, H., 1972. Water pressure in intra- and sub-glacial channels. Journal of Glaciology, 11, 177-203.

Shaw, L., Kvill, D., Rains, B., 1989. Drumlins and catastrophic subglacial floods. Sedimentary Geology, 62, 177-202.

Shilts, W.W., 1976. Glacial till and mineral exploration. Special Publications – Royal Society of Canada, no. 12, Glacial till; an inter-disciplinary study, 205-224.

Shulmeister, J., 1989. Flood deposits in the Tweed esker (southern Ontario, Canada). Sedimentary Geology, 65, 153-163

Singer, D.A., 1995. World class base and precious metal deposits – A quantitative analysis. Economic Geology, 90, 88-104.

Stumpf, A.J., Broster, B.E., Levson, V.M., 2000. Multiphase flow of the late Wisconsinan Cordilleran ice sheet in Western Canada. GSA Bulletin, 112-12, 1850-1863.

Ward, B.C., Jackson, L.E., Jr., 1992. Late Wisconsinan glaciation of the Glenlyon Range, Pelly Mountains, Yukon Territory, Canada. Canadian Journal of Earth Science, 29, 2007-2012.

Ward, B.C., Jackson, L.E., Jr., 2000. Surficial geologyy of Glenlyon map area (105L), Yukon Territory. Geological Survey of Canada Bulletin 559, 61 p.

Ward, B.C., Bond, J.D., Gosse, J.C., 2007. Evidence for a 55-50 ka (early Wisconsin) glaciation of the Cordilleran ice sheet, Yukon Territory, Canada. Quaternary Research, 68, 141-150.

Willis, I.C., Sharp, M.J., Richards, K.S., 1990. Configuration of the drainage system of Midtdalsbreen, Norway, as indicated by bye-tracing experiments. Journal of Glaciology, 36, 89-101.

APPENDICES

Appendix A: Terrain Inventory Maps

The paper maps attached in the back pocket forms a part of this work.

Open File 2008-19. Terrain Inventory of the Howard's Pass area (NTS 105I/12 and parts of 105I/11, 6 and 5 and 105J/9 and 8), Yukon and Northwest Territories (1:50 000 scale).

Open File 2008-20. Terrain Inventory of the Howard's Pass area (NTS 105I/11 and parts of 105I/10, 6 and 7), Yukon and Northwest Territories (1:50 000 scale).

Appendices B - G: CD-ROM Data

The CD-ROM attached forms a part of this work.

Appendix B data files can be opened with ArcGIS or other GIS programs. The PDF files were created with Adobe Acrobat, but may be opened in any PDF program.

Appendix	Type of File	Description	File Size
B	ArcGIS	Polygons	15 MB
	ArcGIS	On-Site Symbols	1.5 MB
	ArcGIS	Eskers and Moraines	84 KB
	PDF	Western Portion of Terrain Inventory Map	14 MB
	PDF	Eastern Portion of Terrain Inventory Map	15 MB
C	PDF	River Sections	765 KB
	PDF	Esker Sedimentology Sections	1.74 MB
	PDF	Drill Core Sections	700 KB
D	PDF	Ice-flow Indicator Data	14 KB
E	PDF	MMI Geochemistry Data	99.7 KB
F	PDF	Till Geochemistry Data	21.7 KB
G	PDF	Terrestrial Cosmogenic Nuclide Data	14.1 KB

Appendix C: Section Descriptions

River Sections

06DT112

466247 N
6944974 E

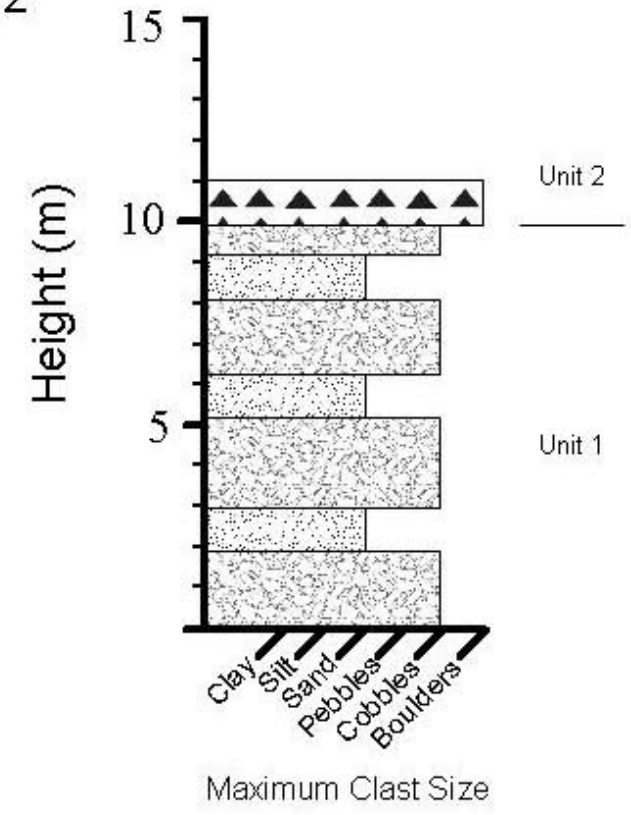

Unit 2: Till with a silty, fine-grained sand matrix. It has 10% clasts with a maximum clast size of 3 cm, and the average size is granule. The clasts are rounded to sub-angular, with an average of sub-rounded. It is consolidated and light brown.

Unit 1: Interbedded gravel and sand. Gravel has a maximum clast size of 10 cm and a sand matrix. It has small sand lenses and is imbricated down-stream. The sand beds are moderately-sorted and have a maximum thickness of one metre.

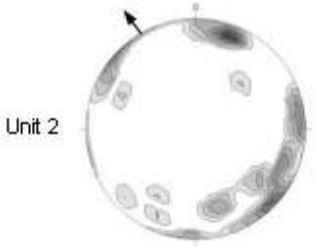

06DT127

451178 N
6938378 E

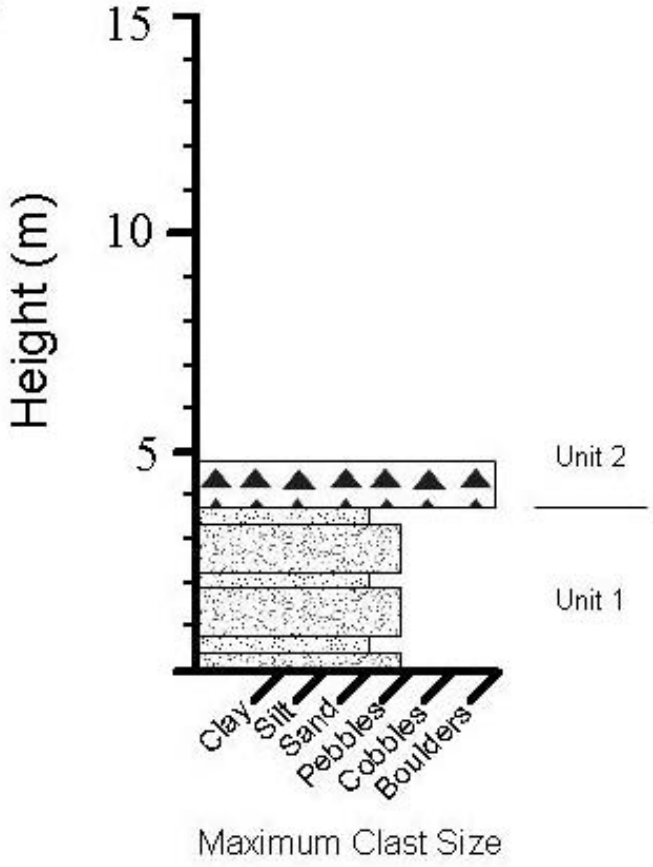

Unit 2: Till with 25-30% ranging from granule to boulder with an average size of cobble. Silty clay matrix, blocky texture, brown, cemented at the bottom near the contact. Clasts have varied lithology with many striated clasts. Average roundness is sub-rounded.

Unit 1: Interbedded sand and gravel. Gravel is clast supported and imbricated downstream. It has rounded to angular clasts, average sub-rounded. Clast lithology is mostly shale with a maximum clast size of 10 cm, average pebble. Fine to medium-grained sand matrix. The gravel coarsens upward and is well-sorted. The sand beds are fine to medium grained with some well-rounded to angular granule beds. The granules have a maximum clast size of 1 cm.

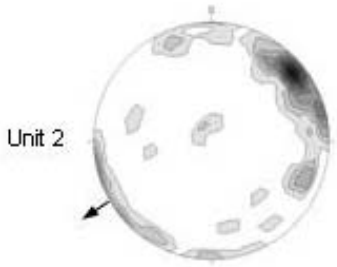

S1 = 0.64
n = 49

06DT129

464471 N
6946747 E

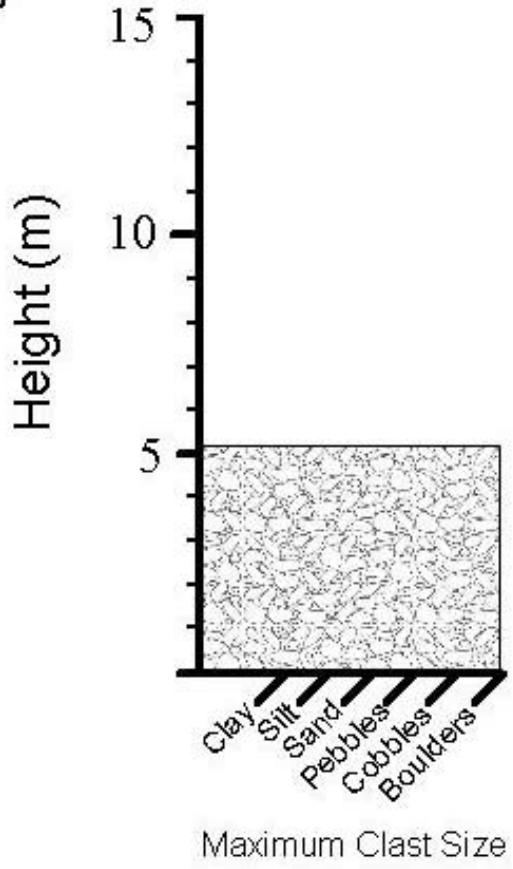

Unit 1

Unit 1: Unconsolidated gravel with silty sand matrix. Clasts are sub-angular to well-rounded with a maximum clast size of boulder.

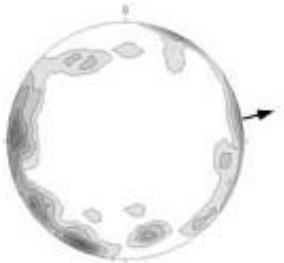

S1 = 0.57
n = 49

06DT130

464650 N
6946262 E

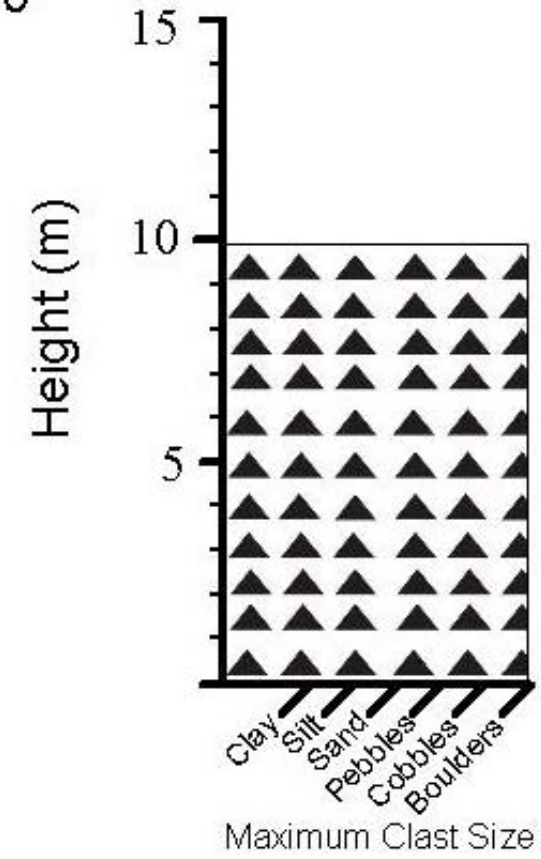

Unit 1

Unit 1: Diamict with a silty matrix and 25% clasts that are well-rounded to sub-angular, average sub-rounded. Some silty sand lenses.

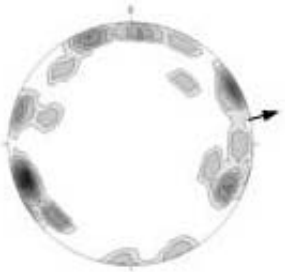

S1 = 0.56
n = 25

06DT133

449745 N
6937840 E

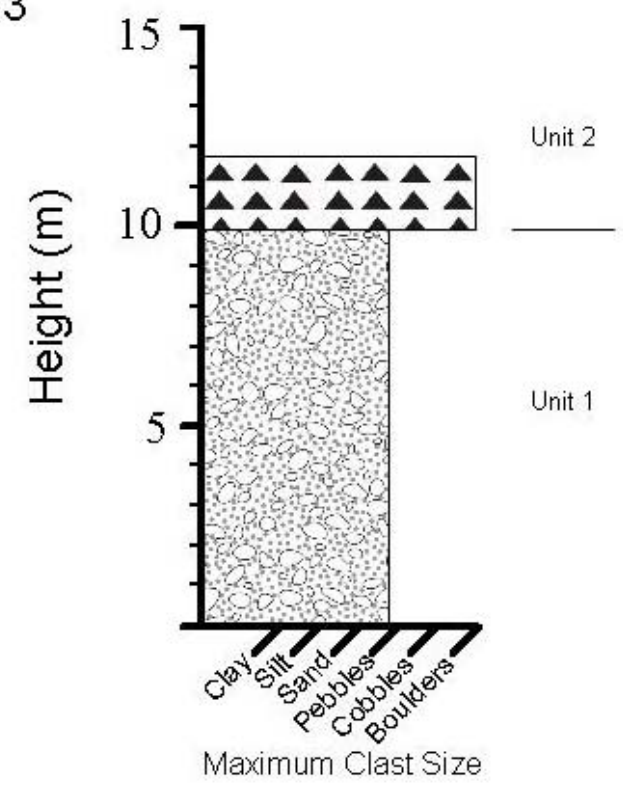

Unit 2: Diamict with a clay silt matrix. Clasts are sub-angular to well-rounded, average sub-rounded. The maximum clast size is 20 cm. The diamict is weathered light grey, and is dark grey on a fresh surface.

Unit 1: Coarse gravel with a fine to coarse sand matrix. Clasts are angular to well-rounded, average sub-rounded. The maximum clast size in 10 cm, average pebble. Clast lithology dominantly shale, but contains some granodiorite, quartz and conglomerate clasts. Imbrication varies through the unit by 180°. Iron staining and vertical faults that cross-cut bedding are observed. The upper contact is sharp and horizontal.

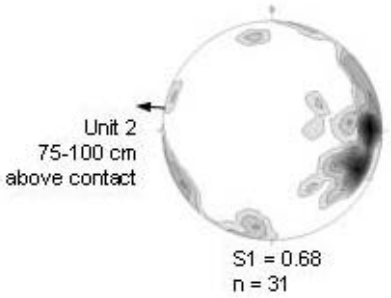

S1 = 0.68
n = 31

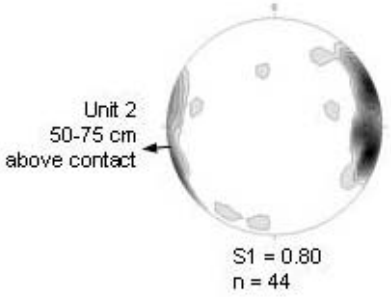

S1 = 0.80
n = 44

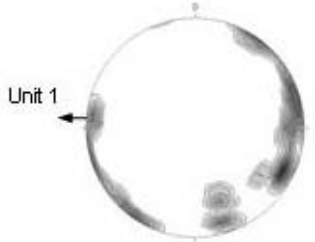

S1 = 0.61
n = 20

06DT139

459906 N
6940296 E

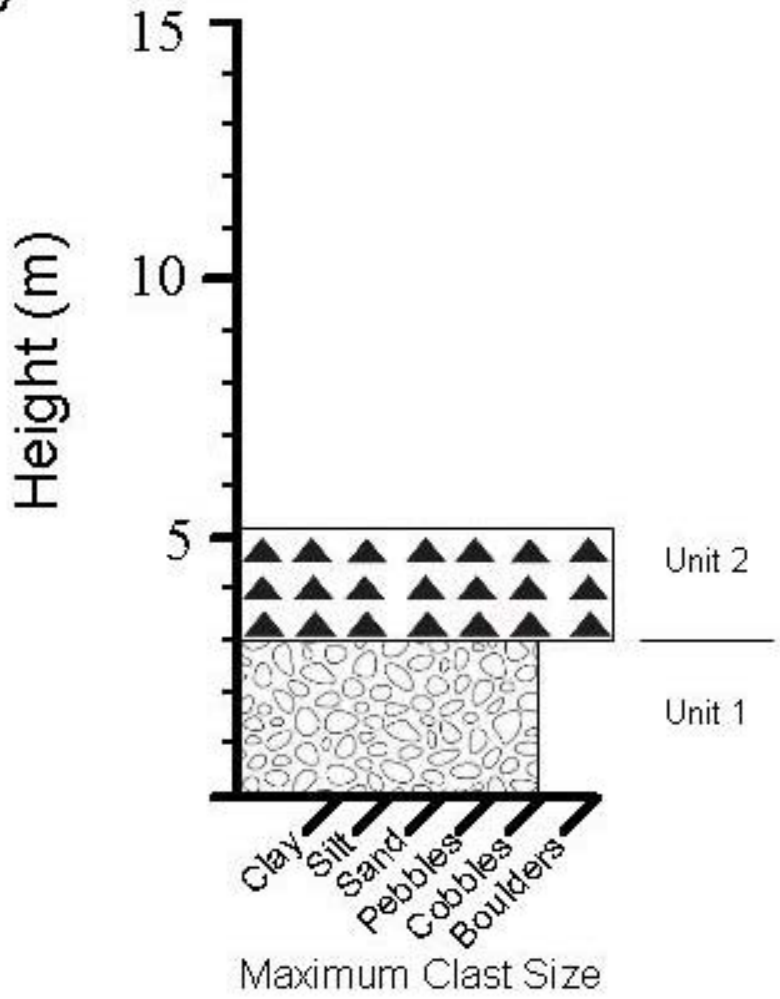

Unit 2: Diamict with a silt matrix. Clasts have a maximum size of boulder that are sub-rounded to angular and striated. Average clast size is cobble.

Unit 1: Massive gravel with a silty sand matrix. It is well-sorted in the bottom metre and becomes poorly-sorted and finer at the top. Clasts are sub-rounded to sub-angular, average sub-angular. Clasts have a maximum size of 45 cm, with an average size of cobble. The upper contact is gradual.

06DT142

474387 N
6921030 E

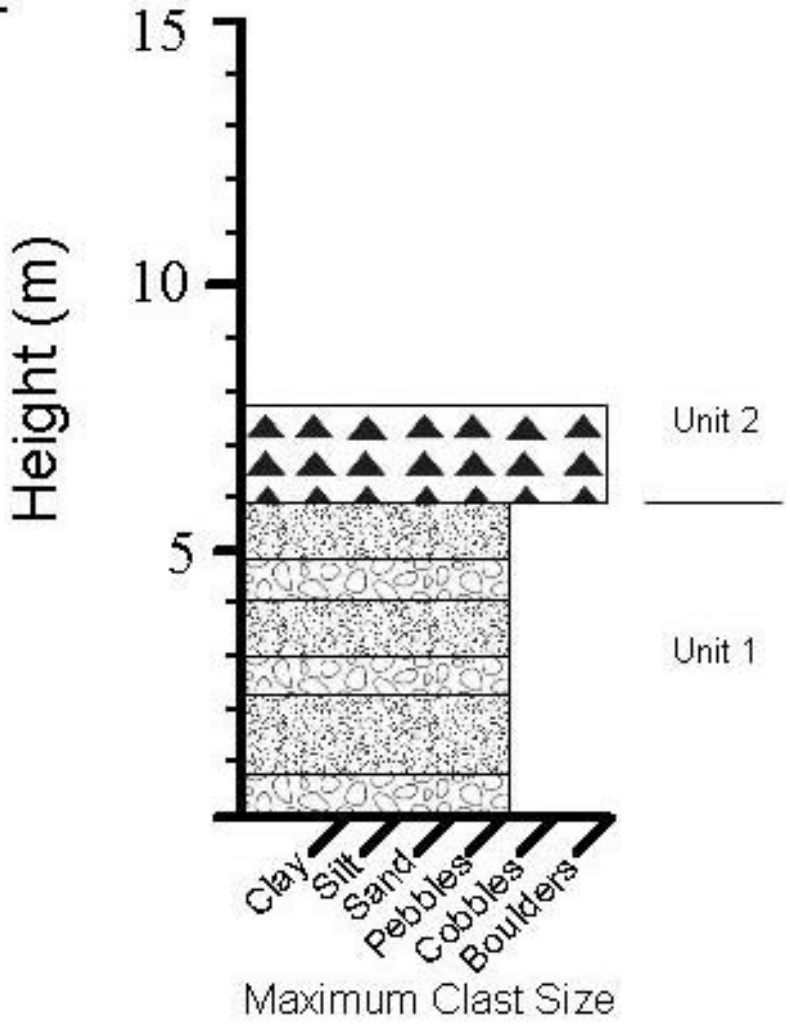

Unit 2: Dark grey diamict with a silty clay matrix. There are 20-25% clasts that are sub-rounded to sub-angular and have a maximum clast size of 11 cm, average pebble. This unit is overconsolidated.

Unit 1: Interbedded coarse and fine gravel. The coarse beds are less than 50 cm thick and are clast supported. The maximum clasts size is 15 cm, average pebble. Clasts are well-rounded to angular, average rounded. The fine gravel beds are matrix supported with some 10 cm sand beds. The sand beds are dipping down-stream to the west.

06DT143

483808 N
6931582 E

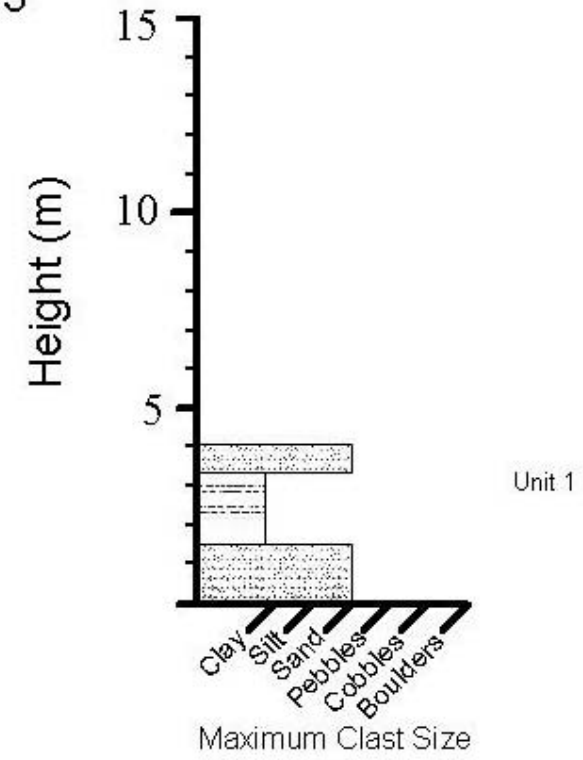

Unit 1

Unit 1: Inter-bedded silt, sand and clay. Drunken trees are on top and on the sides of the section.

350-385 cm: Undulating rippled sand and clay beds. Paleo-current measurements of ripple crests in the sand beds indicate flow towards 067o.

340-350 cm: Bedded sand with climbing ripples. The wavelength and angle of climb indicate increasing discharge deposition upwards. The ripple amplitude is 1.5 cm.

315-340 cm: Interbedded light brown silty clay and silty fine-grained sand. The clay beds are 3 cm thick, the sand beds are 1 cm thick.

260-315 cm: Couplets of sand and clay. The sand beds dip at low angles to the east. The clay beds are laminated and coarsens up to sand.

160-260 cm: Laminated clayey silt with soft sediment deformation overlain by massive sand.

90-160 cm: Interbedded medium to coarse sand and clayey silt. The silt beds are 3 cm thick and the sand beds are 10 cm thick. The sand beds fine up into silt.

0-90 cm: Interbedded coarse sand and clayey silt. The sand bed are 7 cm thick and the silt beds are 1-2 cm thick.

06DT145

459723 N
6940097 E

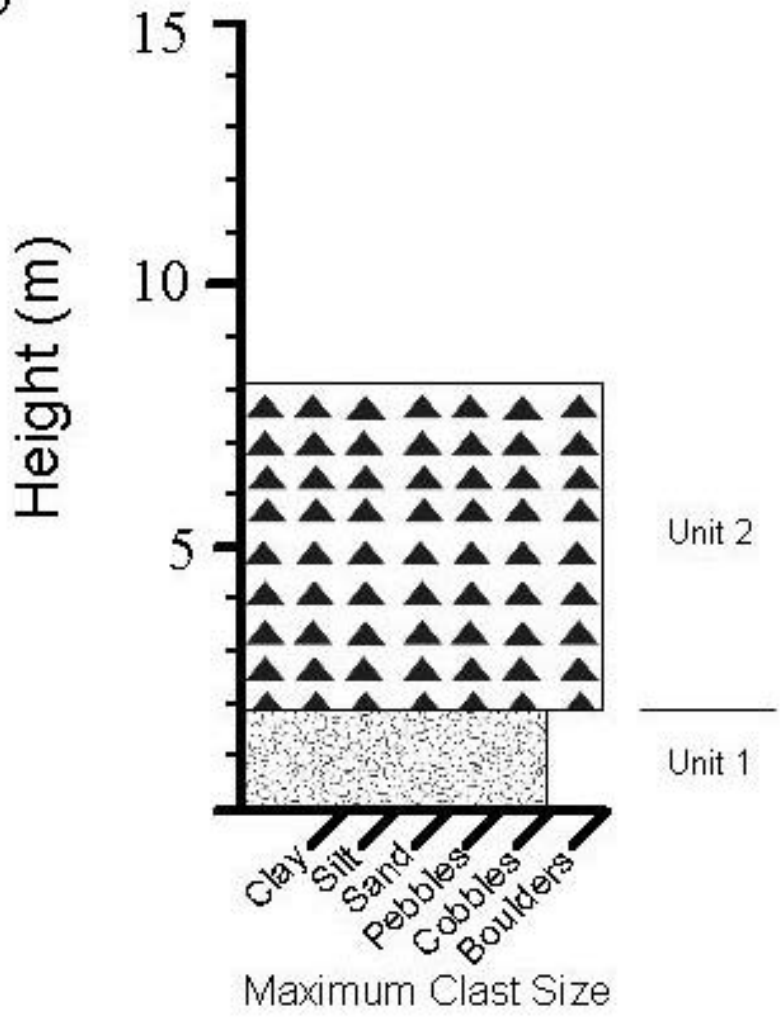

Unit 2: Dark grey diamict with a sandy silt matrix. There are 30-35% clasts with abundant striations. The maximum clast size is boulder, average cobble. Some vertical fractures were observed.

Unit 1: Cemented gravel with abundant striated limestone clasts. The clasts are well-rounded to sub-angular, average rounded. The maximum clast size is 10 cm.

06DT148

464844 N
6946818 E

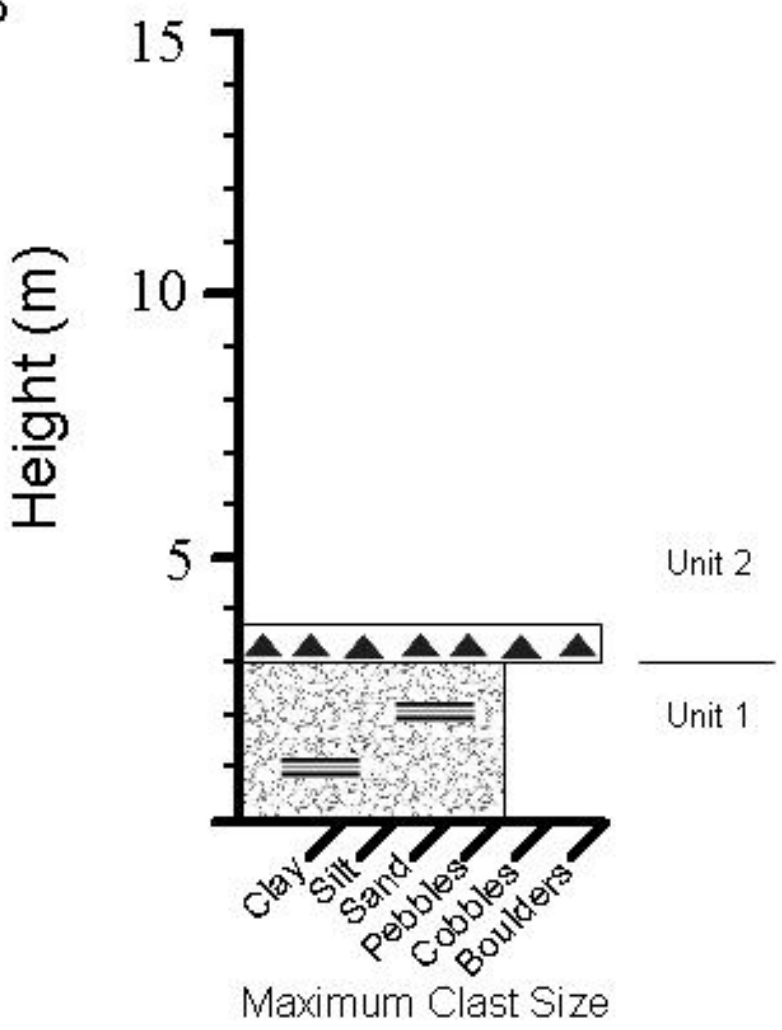

Unit 2: Diamict with a clayey silt matrix. The maximum clast size is 20 cm, average pebble.

Unit 1: Loose, moderately-sorted gravel with a medium- to coarse-grained sand matrix. The maximum clast size is 30 cm, average pebble. Lenses of silty fine-grained sand were observed in the gravel.

07DT007

478173 N
6911194 E

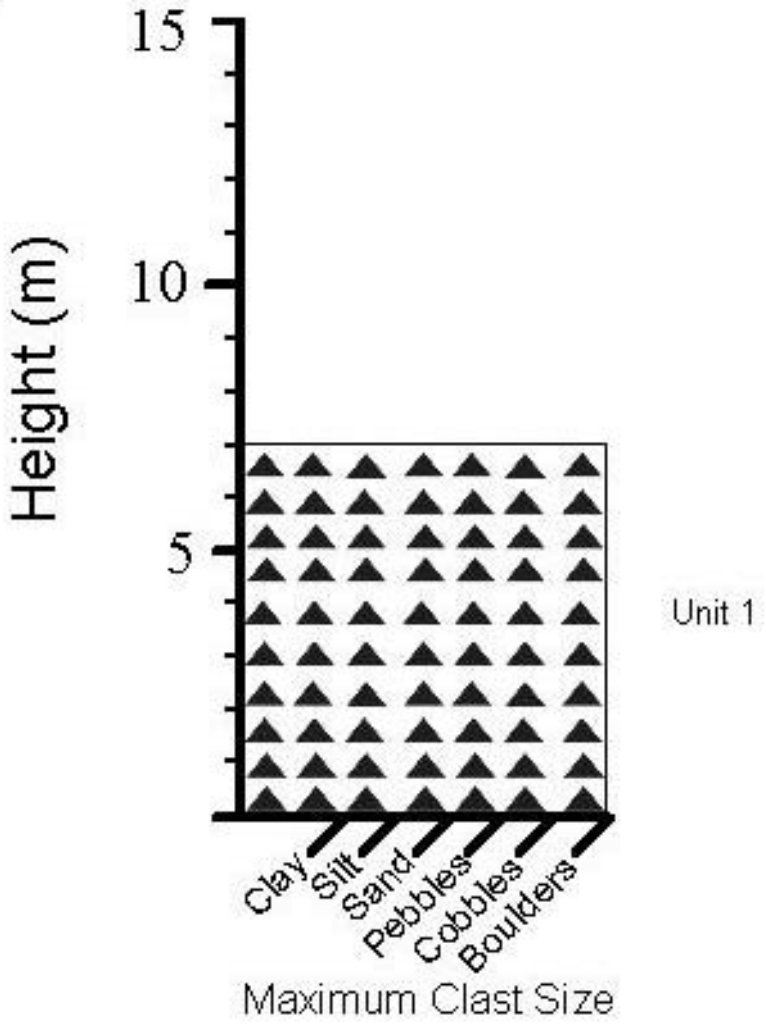

Unit 1: Light brown diamict with a silt matrix. The unit is well-drained and has 15% clasts of various lithologies that are striated and have lee-end fractures.

07DT008

477339 N
6912009 E

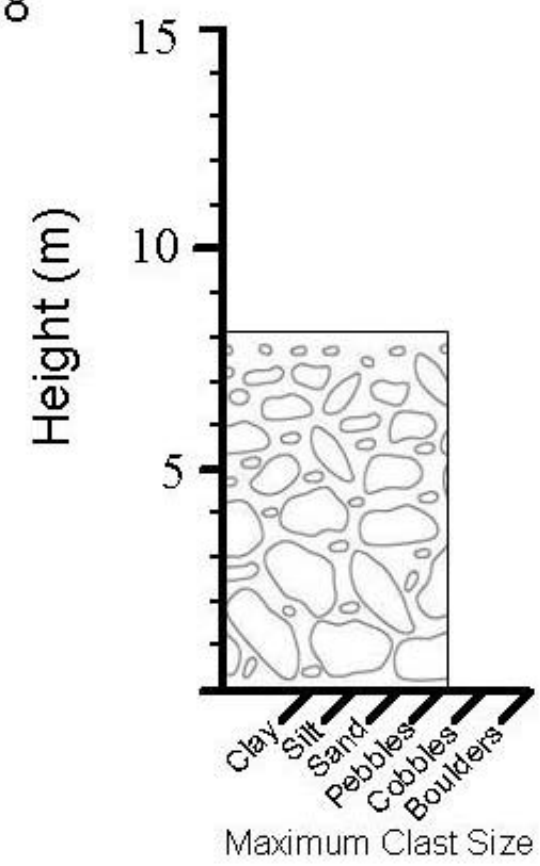

Unit 1

Unit 1: Massive, clast-supported gravel containing various lithologies including granodiorite clasts. It has a medium to coarse sand matrix. The maximum clast size is 10 cm. The clasts are sub-rounded to well-rounded. The unit becomes matrix-supported upward with more sand and a maximum clast size of 20 cm.

S1 = 0.66
n = 25

07DT009

473241 N
6934529 E

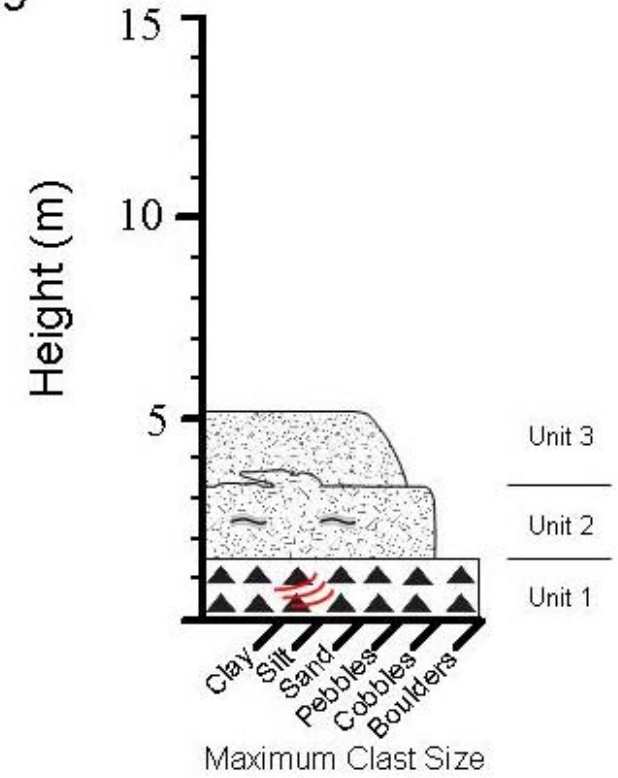

Unit 3: 65-cm-thick gravel consisting of well-rounded to rounded pebbles and a coarse-grained sand matrix fines up into interbedded coarse- and medium-grained sand beds. The sand beds are 40-cm-thick and are well-sorted.

Unit 2: Grey, unconsolidated diamict with a clayey silt matrix. The maximum clast size is 40 cm. This unit contains multiple sand beds.

Unit 1: Light brown, consolidated, massive diamict with a clay matrix. It is composed of 20% clasts with a maximum size of 3 m. Low angle faults were observed in this unit.

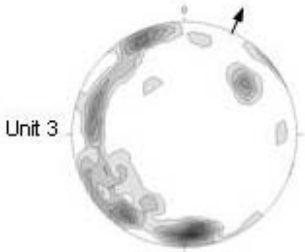

S1 = 0.52
n = 49

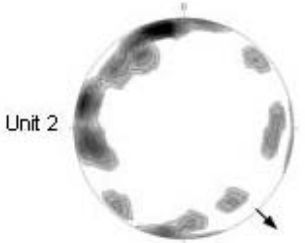

S1 = 0.56
n = 24

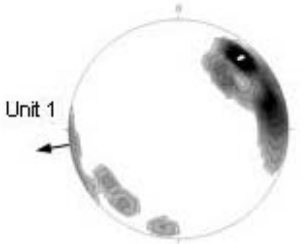

S1 = 0.81
n = 24

07DT010

488914 N
6925292 E

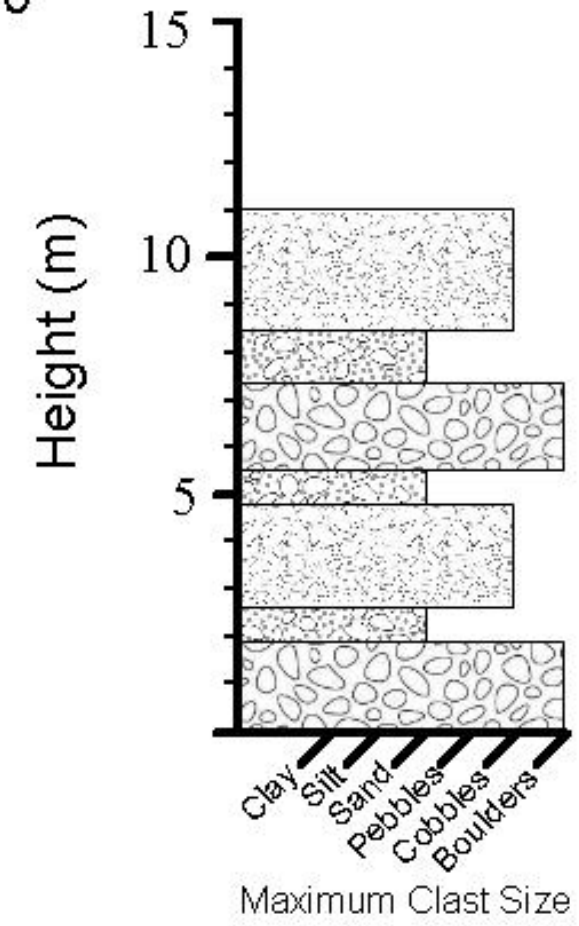

Unit 1: Steeply inclined interbedded gravel and sand. Some gravel beds are clast-supported and poorly-sorted, with clasts ranging from pebbles to boulders and a coarse-grained sand matrix. Other gravel beds are inversely graded from poorly-sorted pebbly sand to a moderately-sorted gravel. The sand beds are approximately 50 cm thick and contain 10-25% pebbles and granules. The beds are inclined 10-20°.

07DT016

473004 N
6934168 E

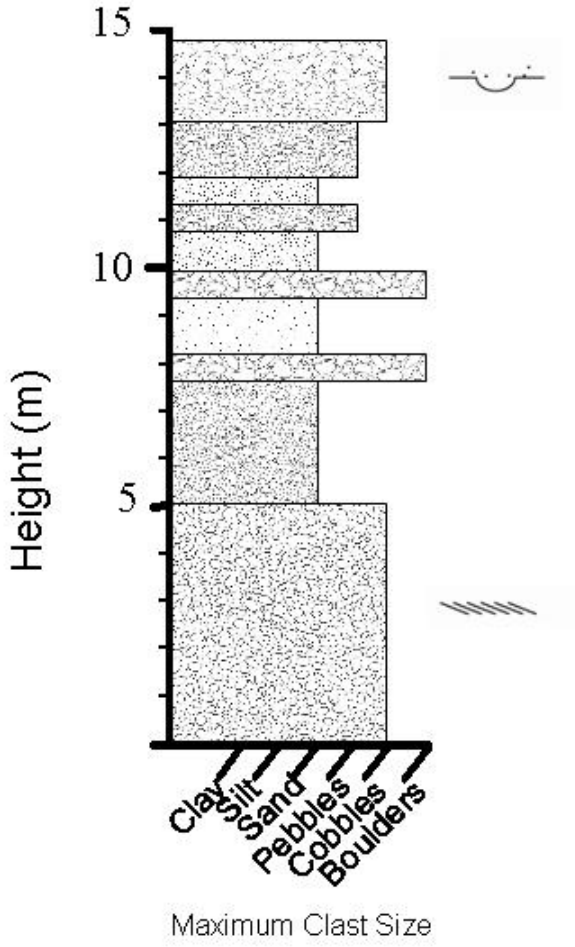

Unit 1:

13-15m: Scours filled by interbedded silt, sand and gravel. The gravel beds are moderately to well-sorted with pebble to cobble, rounded to well rounded clasts. The beds are inversely graded from silt to gravel.

10-13 m: Rhythmically-bedded sand and matrix-supported massive or imbricated gravel. The gravel is moderately to poorly-sorted gravel with a sand matrix. The sand beds are poorly-sorted. The gravel beds thicken with height and the sand beds thin. Multiple rip-ups of likely underlying material were observed in the gravel beds.

7.5-10 m: Interbedded gravel and sand. The gravel is poorly to moderately-sorted with pebble and cobble-sized clasts and a well-sorted coarse-grained sand matrix. The sand beds are poorly to well-sorted. The gravel beds are ~1 m thick and the sand beds are ~50 cm thick. There are also a few beds of 20-50 cm thick well-sorted, pebble to cobble-sized gravel. All of the beds are inclined ~5-10°. Some small faults cross-cut bedding.

5-7.5 m: Massive, poorly-sorted sand with granules to cobble-sized rounded to sub-rounded clasts.

0-5 m: Cross-bedded sand and gravel. The gravel is moderately to well-sorted and clast-supported. The grain sizes range from pebbles to cobbles and are well-rounded to sub-rounded. The sand beds are medium-grained and well-sorted with a few pebbles.

07DT039

458610 N
6916999 E

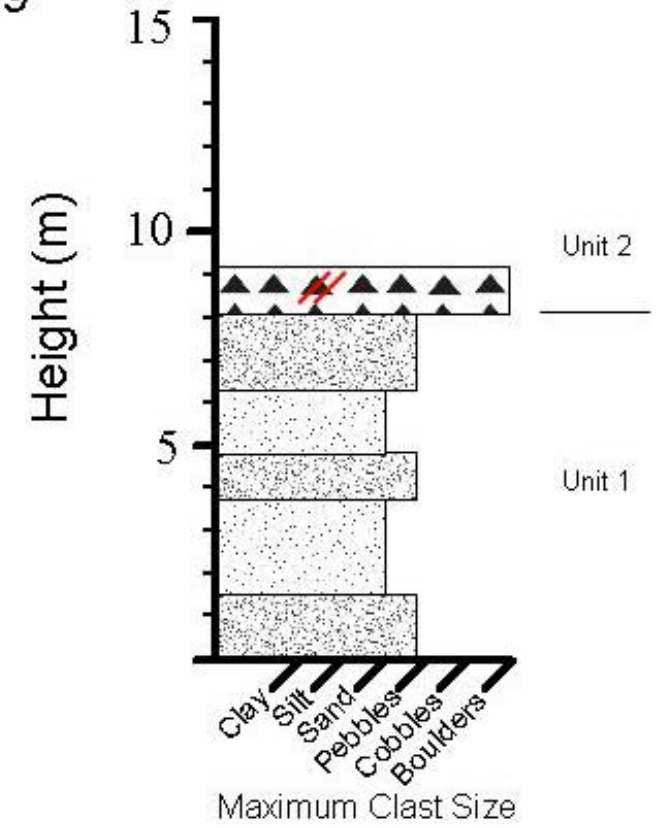

Unit 2: Light grey diamict with 35-40% clasts of various lithology. The clasts are well-rounded to sub-angular, average sub-angular. The maximum clasts size is 10 cm. Sub-vertical faults were observed in this unit.

Unit 1: Horizontally interbedded coarse sand and cobble gravel. The gravel is clast-supported with a coarse sand matrix. The sand beds are mostly massive with some weak stratification.

07DT056

481723 N
6925667 E

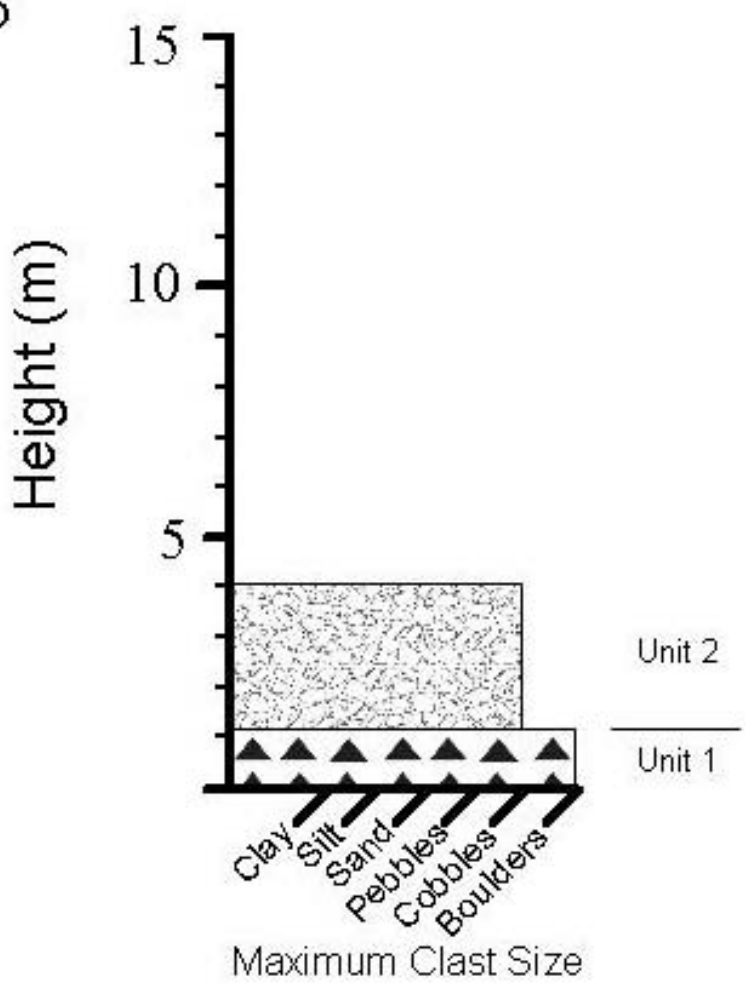

Unit 2: Poorly- to moderately-sorted massive clast-supported gravel. The clasts are angular to sub-rounded with a maximum size of 45 cm. The unit is cemented by an unknown material.

Unit 1: Light brown diamict with a silty clay matrix. It is unconsolidated and is comprised of 30-35%angular black shale clasts.

07DT063

473190 N
6934207 E

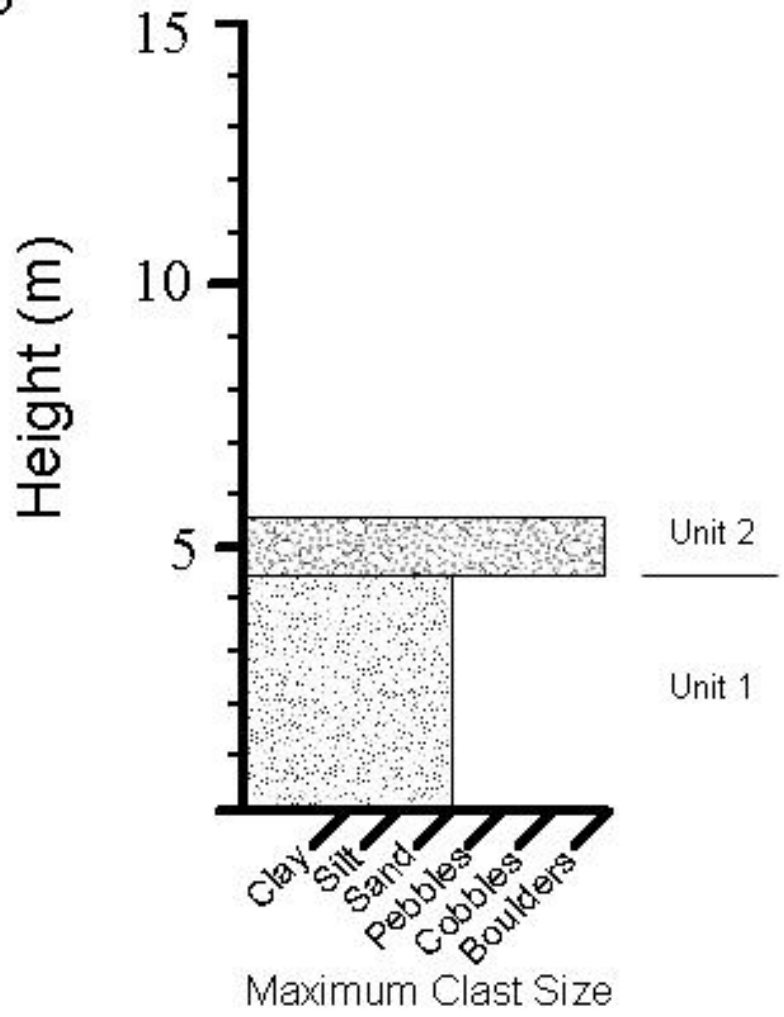

Unit 2: Poorly-sorted, massive, matrix-supported gravel with a poorly-sorted sand matrix. Unit 2 both overlies, and is lateral contact with, unit 1 where the two units are intercalated. The contact between units 1 and 2 are folded and subsequently faulted.

Unit 1: Massive to interbedded and interlaminated, moderately to well-sorted sand. Rare pebbles. Some beds are inversely graded. Extensive faulting cross-cuts bedding.

07DT134

491097 N
6922494 E

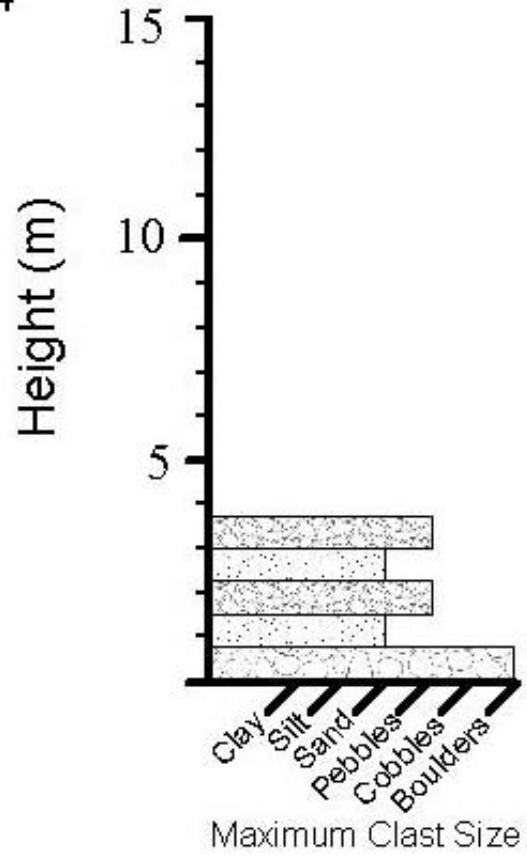

Unit 1

Unit 1: Interbedded sand, pebble gravel and boulder gravel. The sand beds are coarse-grained and massive. The finer gravel beds are well-rounded to sub-angular and are weakly stratified. The coarse gravel beds are clast-supported with well-rounded to sub-angular clasts of various lithologies.

S1 = 0.60
n = 36

Esker Sedimentology Sections

07DT033

472799 N
6934080 E

Elevation: 1139 masl

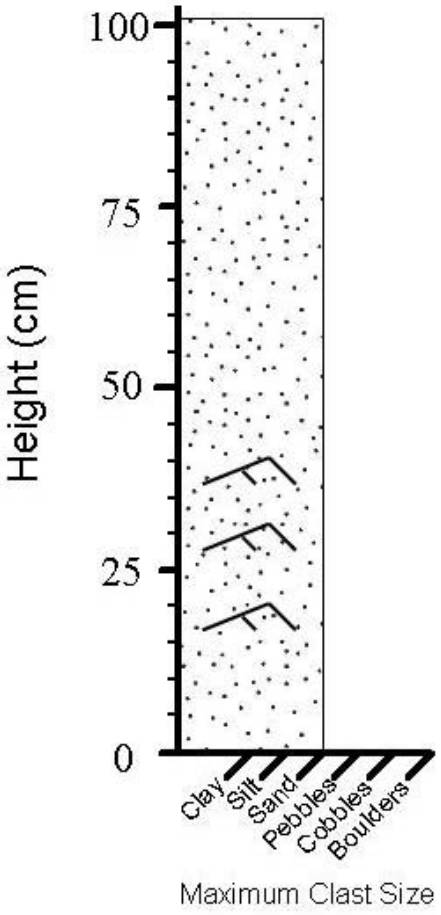

0-100: Light brown to grey bedded and laminated medium-grained sand. Well-sorted. Rippled silt laminations throughout with possible coarsening-upwards. Angle of climb increases upwards from 55° until the ripples are symmetrical. Some sand beds are deformed.

07DT065

473914 N
6934537 E

Elevation: 1423 masl

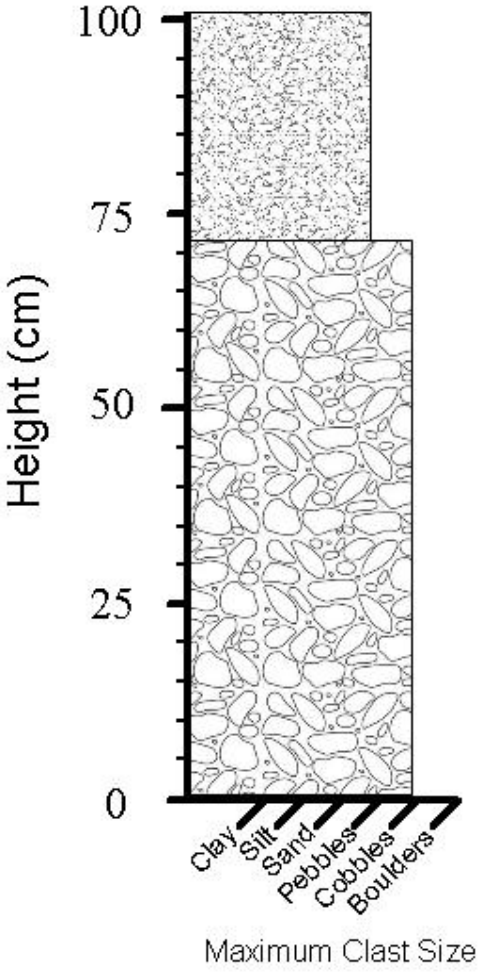

70-100: Light brown gravel. Silty sand matrix. Maximum clast size is pebble. Some cryoturbation in the top 10 cm.

0-70: Grey gravel. Angular to sub-rounded clasts, average sub-rounded. Well-sorted. Medium to coarse-grained sand matrix. Pebble to cobble sized clasts, average cobble. Maximum clast size is 15 cm. Possibly fines upwards, but not by much.

07DT066

474122 N
6934442 E

Elevation: 1127 masl

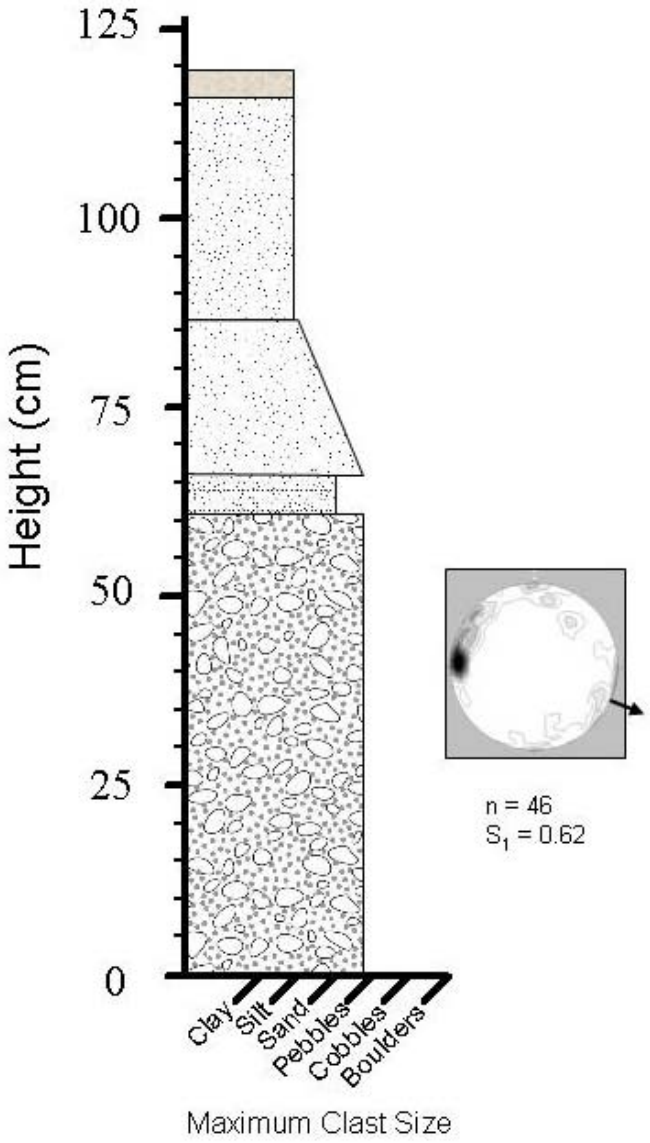

115-120: Volcanic ash.

85-115: Well-sorted medium-grained sand. Rare granules and pebbles (~1-2%), only in the bottom 10 cm.

65-85: Fining-upwards sequence. Bottom 10 cm is granule-rich, moderately sorted coarse-grained sand. The top 10 cm is well-sorted medium-grained sand. The top 2-3 cm fines to well-sorted fine-grained sand.

60-65: Planer bedded fine to medium-grained sand. A few 2-3 cm thick silt beds at the bottom. Not laterally continuous. One small cobble at the top.

0-60: Massive to weakly stratified gravel. Medium to coarse-grained sand matrix. Well-rounded to sub-angular clasts, average well-rounded. All matrix-supported, but the top 30 cm are more clast-rich.

07DT067

474160 N
6934565 E

Elevation: 1118 masl

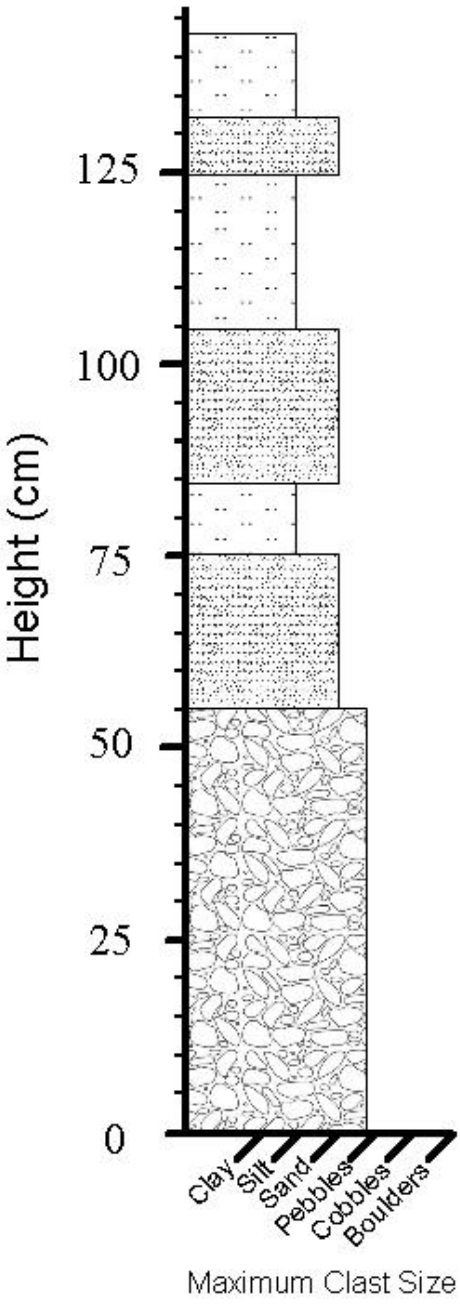

115-120: Interbedded silt and sand beds. Silt beds are well-sorted with few pebbles (<5%). Sand beds are stratified and medium-grained. The silt beds thicken up and the sand beds thin.

0-115: Massive, dark grey gravel. Moderately-sorted. Medium to coarse-grained sand matrix. Clasts are angular to rounded, average rounded and range in size from granule to pebble with an average size of 1 cm.

07DT068

474601 N
6934603 E

Elevation: 1138 masl

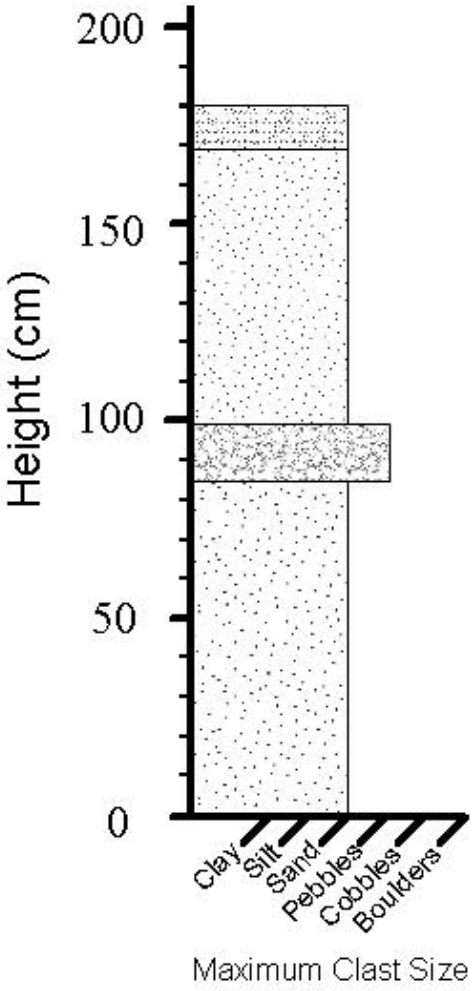

170-180: Light brown massive medium to coarse-grained sand with laterally variable silt beds near the lower contact. Silt beds have a maximum thickness of 8 cm.

100-170: Moderately-sorted medium to coarse-grained sand. Massive.

85-100: Moderately-sorted gravel. Average clast size is pebble. The clasts are strongly imbricated towards 108°. Well-sorted medium to coarse-grained sand matrix. Matrix-supported. Well-rounded to sub-angular clasts, average well-rounded.

0-85: Well to moderately-sorted medium to coarse-grained sand with rare granules and pebbles (<5%). Frequency of pebbles increases upwards and sorting decreases

07DT069

474762 N
6934562 E

Elevation: 1169 masl

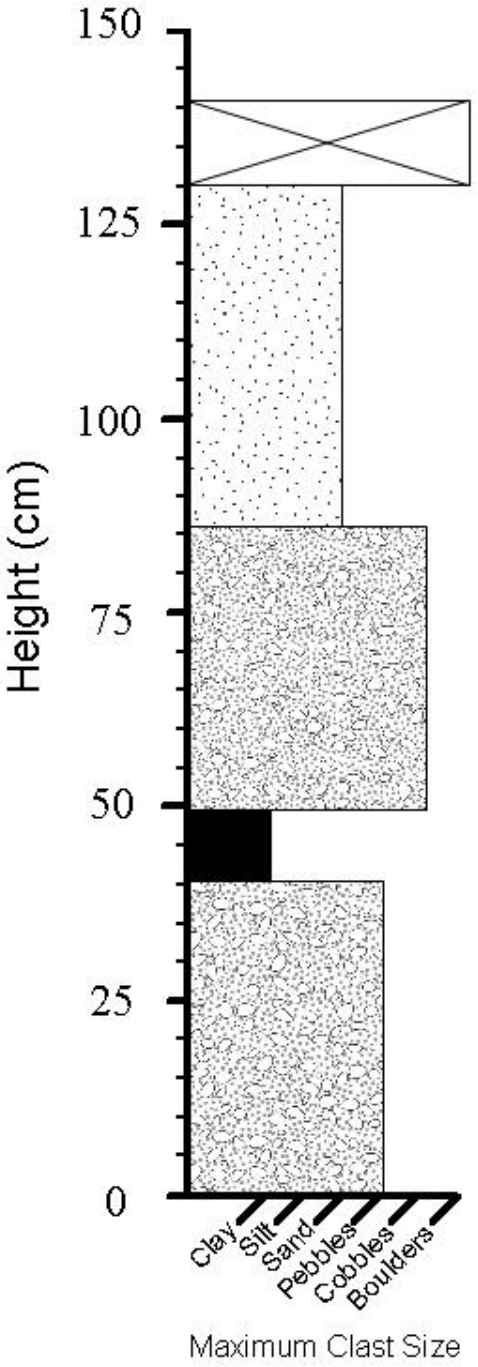

130-140: Covered

85-130: Massive well-sorted medium-grained sand. Coarsens to coarse-grained sand in the top 25 cm.

50-85: Poorly-sorted gravel. Clasts range from granule to cobble. Matrix-supported. Fine to medium-grained sand matrix. Well-rounded to sub-angular clasts, average rounded. Some clasts penetrate into the underlying clay.

40-50: Silty clay with a few 1-2 cm beds of fine-grained sand. Well-stratified beds and laminations undulate.

0-40: Poorly-sorted gravel. Matrix-supported by fine to coarse-grained sand. Clasts range from granule to pebble. Maximum clast size is 15 cm. Well-rounded to angular, average sub-rounded.

07DT070

474999 N
6934201 E

Elevation: 1189 masl

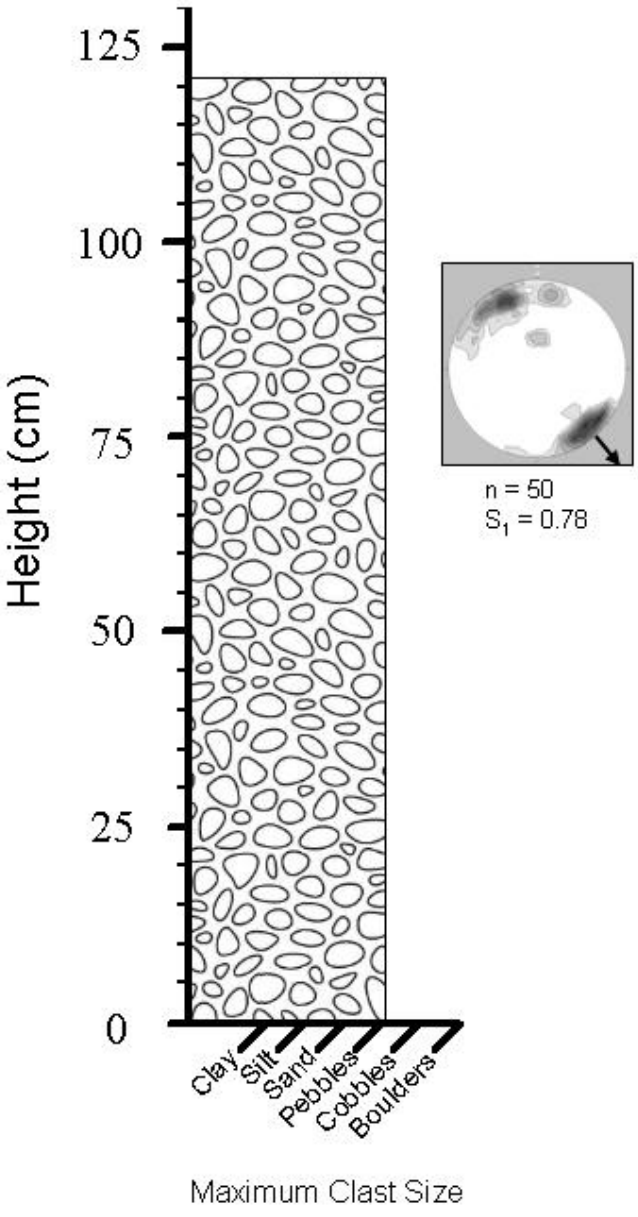

n = 50
S_1 = 0.78

0-120: Stratified moderately to well-sorted gravel. Clasts are granules and pebbles. Maximum clast size is 6 cm. Clasts are well-rounded to sub-angular, average sub-rounded. Matrix-supported by medium to coarse-grained sand.

07DT071

475366 N
6934251 E

Elevation: 1190 masl

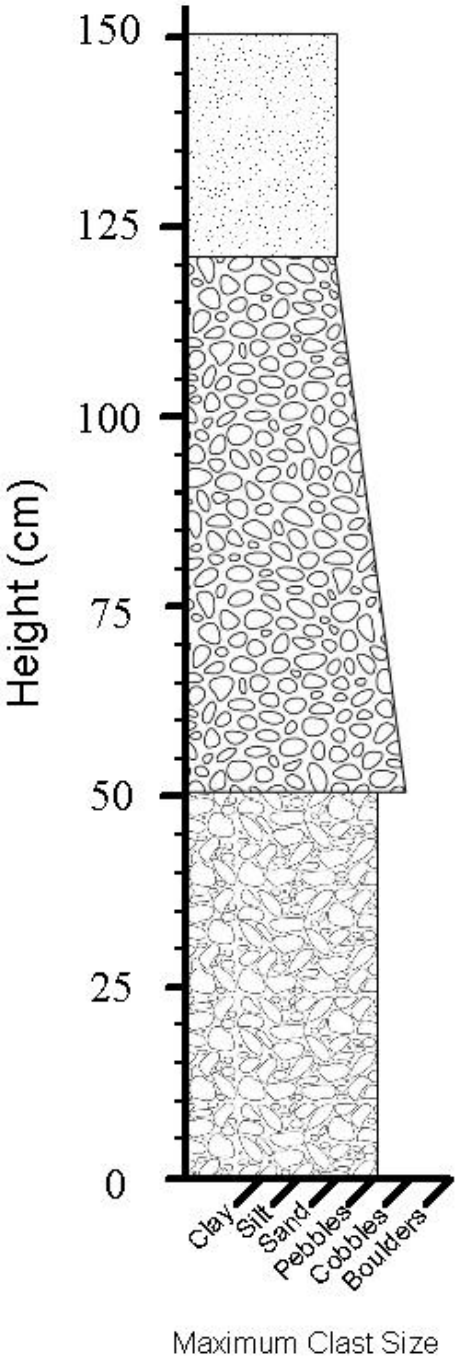

120-150: Light brown well-sorted fine sand with rare (~1-2%) granules.

35-120: Fining-upwards gravel. Clast content and size decreases upwards from pebble and cobble to granule and pebble. The clasts are imbricated towards ~345°. Matrix is medium-grained sand.

0-35: Weakly imbricated gravel. Clasts are dominantly pebbles. Well-sorted medium-grained sand matrix. Clasts are sub-rounded.

07DT072

475366 N
6934251 E

Elevation: 1163 masl

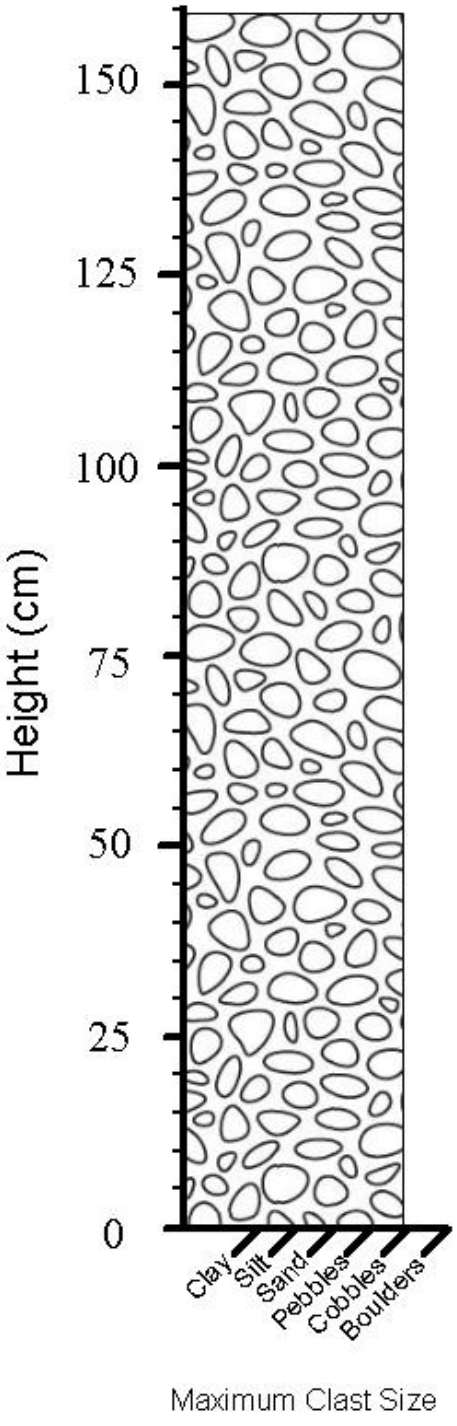

0-160: Weakly stratified gravel. Clasts range from granule to cobble. Well-sorted coarse-grained sand matrix. Well-rounded to sub-angular clasts, average rounded. Maximum clast size is 25 cm. A few 2-5 cm beds of fine to medium-grained sand. Clast lithologies vary, but include granites and granodiorites.

07DT073

475550 N
6934629 E

Elevation: 1135 masl

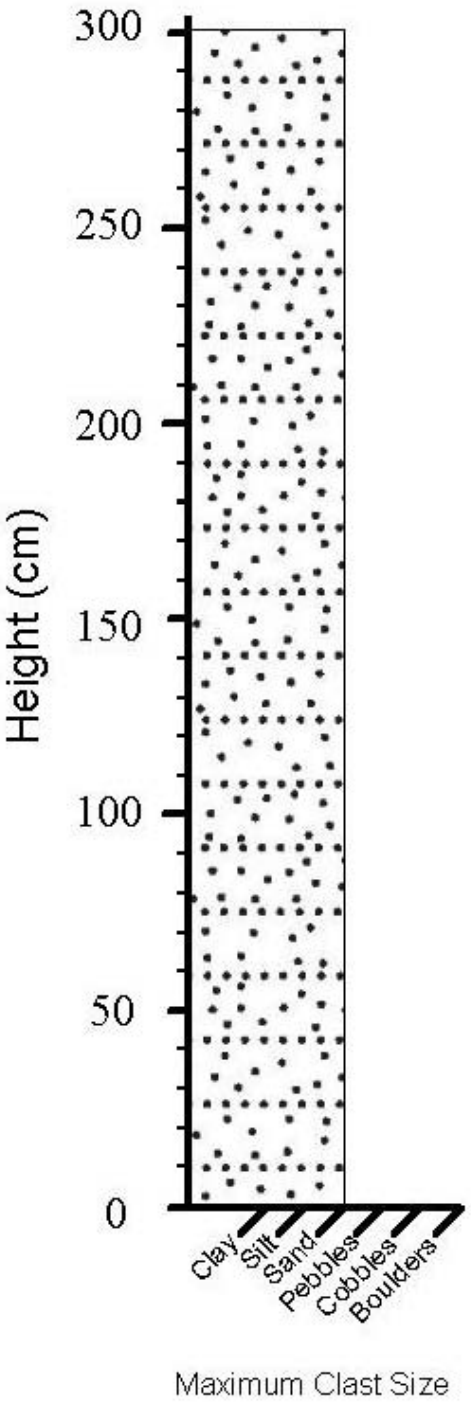

0-300: Fine to medium-grained sand. Well-sorted. Well-stratified. Large pieces of shales are incorporated into some of the lower sand beds. Bedrock pieces are deformed, but bedding is still recognizable.

07DT074

476085 N
6934510 E

Elevation: 1154 masl

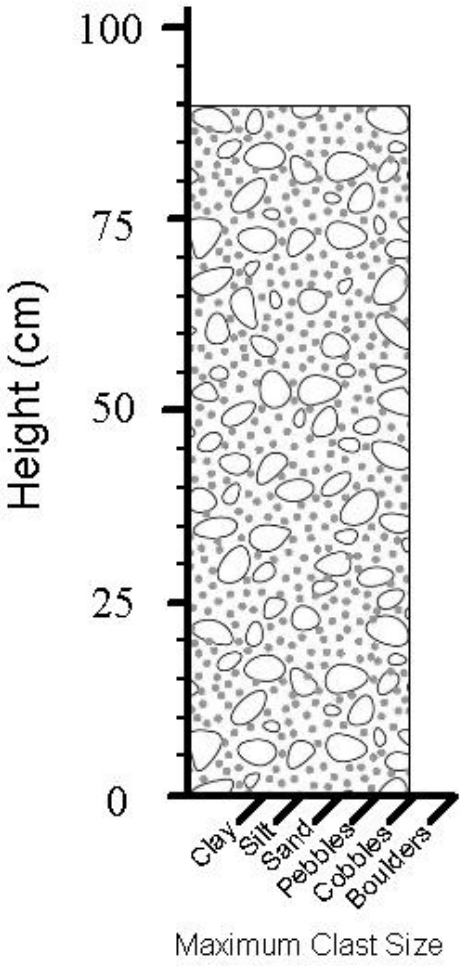

0-90: Massive matrix-supported gravel. Clast sizes range from pebble to cobble, with a maximum size of 11 cm. Clasts are well-rounded to angular, average rounded. Matrix is fine to coarse-grained sand. Laterally discontinuous with well-sorted medium to coarse-grained sand.

07DT075

476692 N
6934465 E

Elevation: 1183 masl

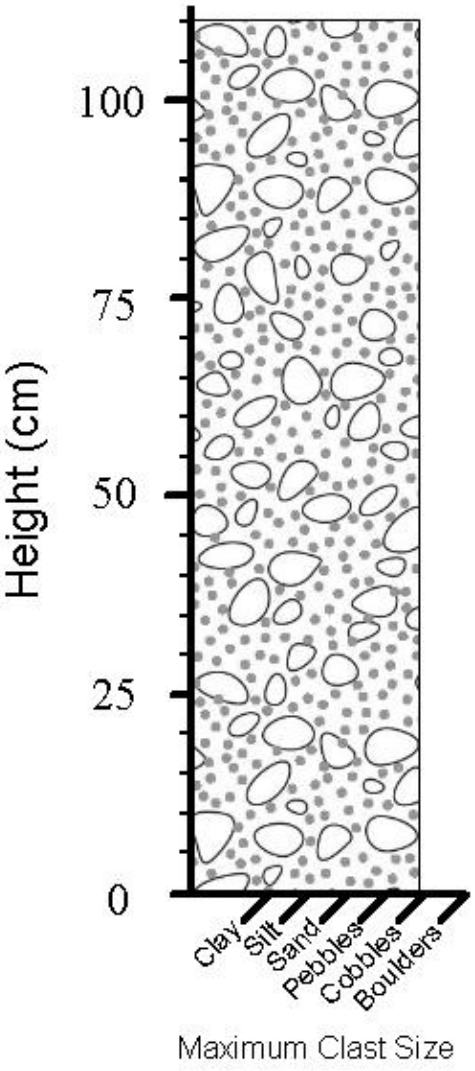

0-90: Massive matrix-supported gravel. Clasts are well-rounded to angular and have a maximum size of 15 cm. Matrix is medium to coarse-grained sand. The top 10 cm fines into a light brown sand with abundant granules and pebbles. A few ~2 cm thick well-sorted medium to coarse-grained sand beds throughout the gravel.

07DT076

477405 N
6934313 E

Elevation: 1163 masl

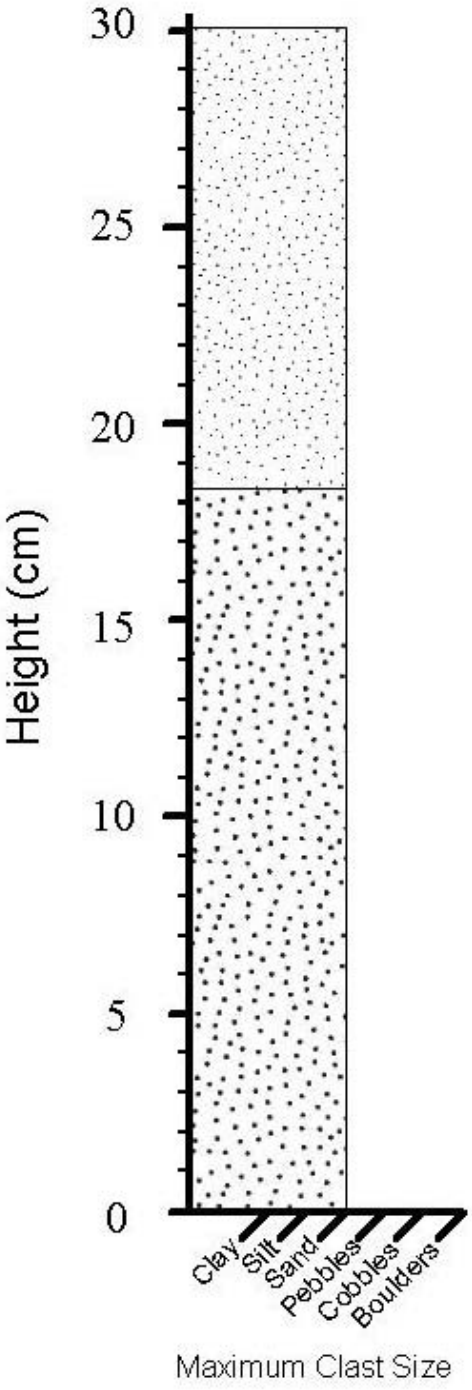

18-30: Light brown, massive silty fine to medium-grained sand. Rare pebbles (<5%)

0-18: Moderately-sorted, coarse-grained, massive sand with some well-rounded pebbles.

07DT077

477923 N
6934006 E

Elevation: 1139 masl

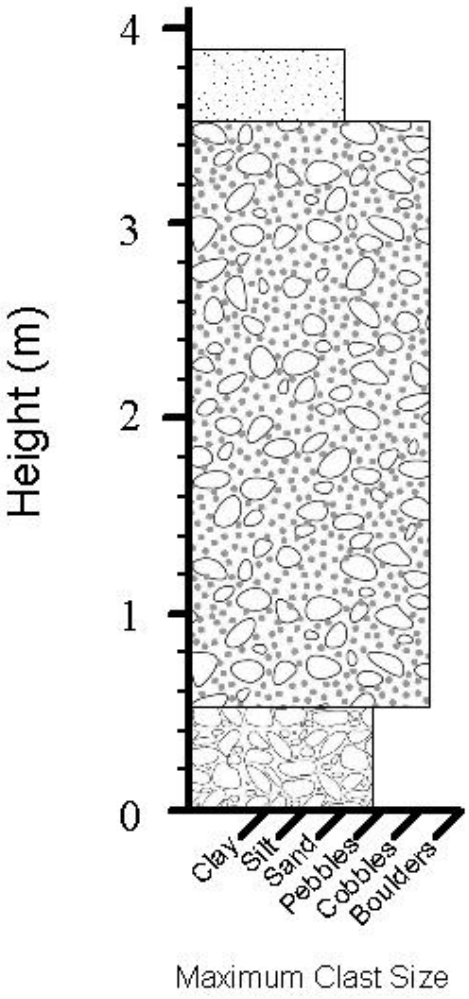

350-385: Fine to medium-grained sand. Cryoturbated in the top 10 cm.

50-350: Poorly-sorted gravel. Clasts range from granule to cobble with an maximum size of 40 cm. Clasts are well-rounded to angular. Fine to coarse-grained sand matrix.

0-50: Moderately-sorted gravel. Coarse-grained sand matrix. Average clast size is pebble. At the bottom are a few beds 2-5 cm thick of clast-supported gravel with an average size of granule.

07DT078

478023 N
6933891 E

Elevation: 1161 masl

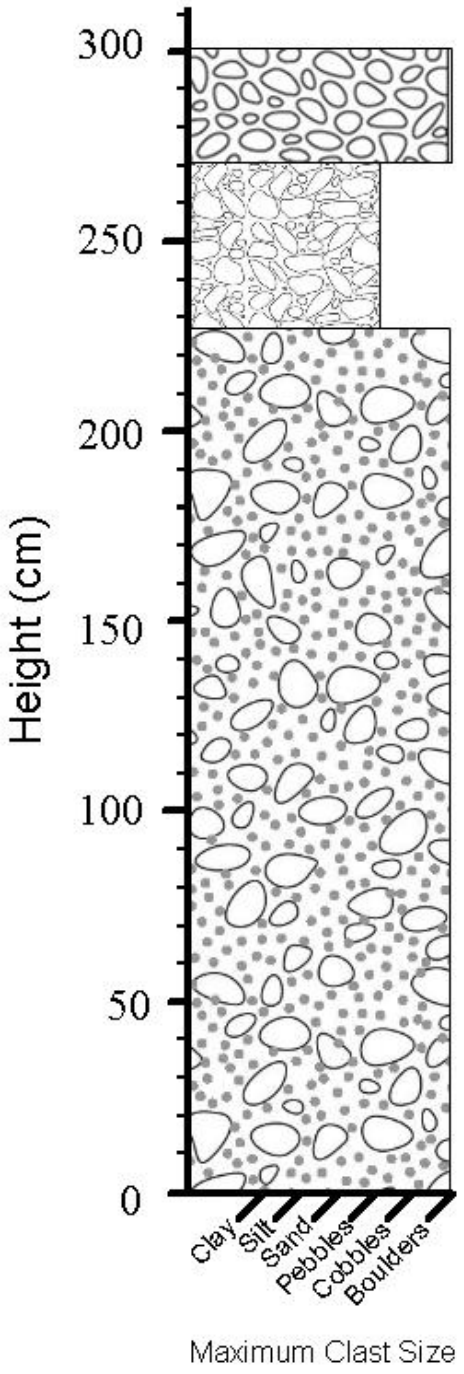

225-270: Gravel with a fine-grained sand matrix. Maximum clast size is granule.

0-225: Matrix-supported, poorly-sorted gravel. Clasts range from pebble to boulder and are well-rounded to sub-angular, average well-rounded. Maximum clast size is 35 cm. Medium to coarse-grained sand matrix. There are 220 cm x 22 cm well-sorted, medium-grained sand lenses throughout the unit.

07DT079

478099 N
6933781 E

Elevation: 1189 masl

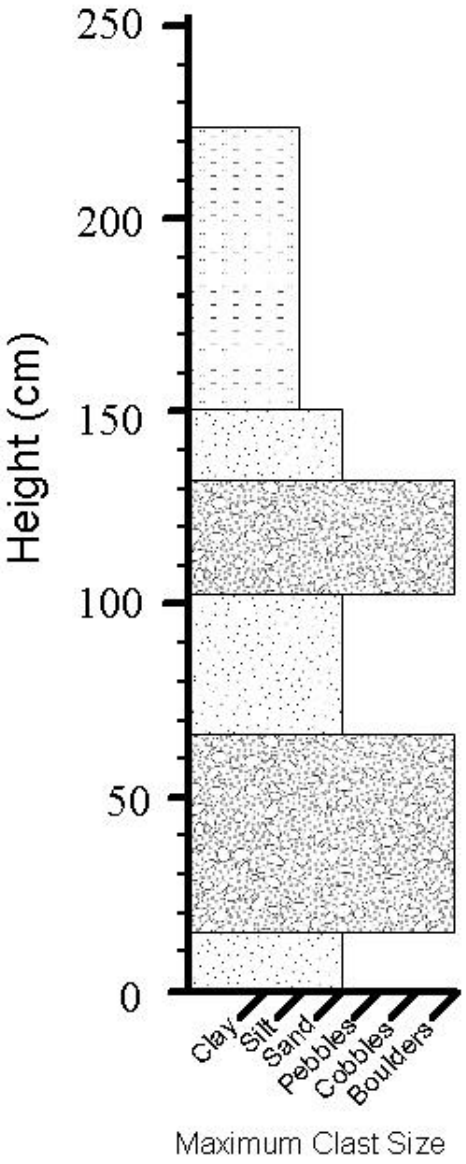

150-225: Interbedded and interlaminated silt, clay and fine-grained sand. A few pebbles with a maximum size of 7 cm. The clay beds are deformed.

0-250: Interbedded sand and gravel. The sand is well-sorted and medium-grained with a few thin (<5 cm) pebble beds. The gravel is poorly-sorted with clasts ranging from pebble to boulder and a medium to coarse-grained, well-sorted sand matrix. The sand beds thicken upwards.

06DT151

478354 N
6935911 E

Elevation: 1147 masl

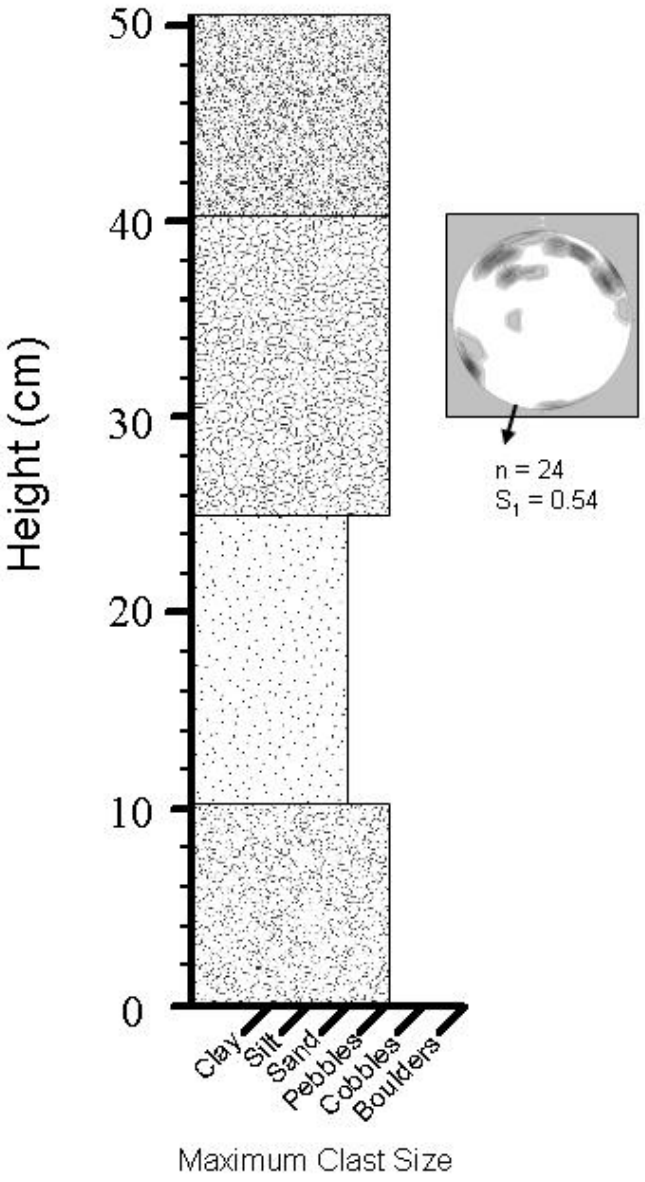

40-50: Well-sorted gravel with a medium-grained sand matrix. Clast size is granule to small pebble.

25-35: Well-sorted massive gravel with a medium-grained sand matrix. Clasts are rounded. Average clast size is pebble.

10-25: Silty fine-grained brown sand. Massive. The bottom half is mottled light brown and brown.

0-10: Well-sorted, massive gravel. Maximum clast size is 5 cm, average pebble. Clasts are sub-rounded to rounded, average sub-rounded. Fine-grained sand matrix.

Drill Core Sections

Don-55

478283 N
6934703 E

Dip: 50°

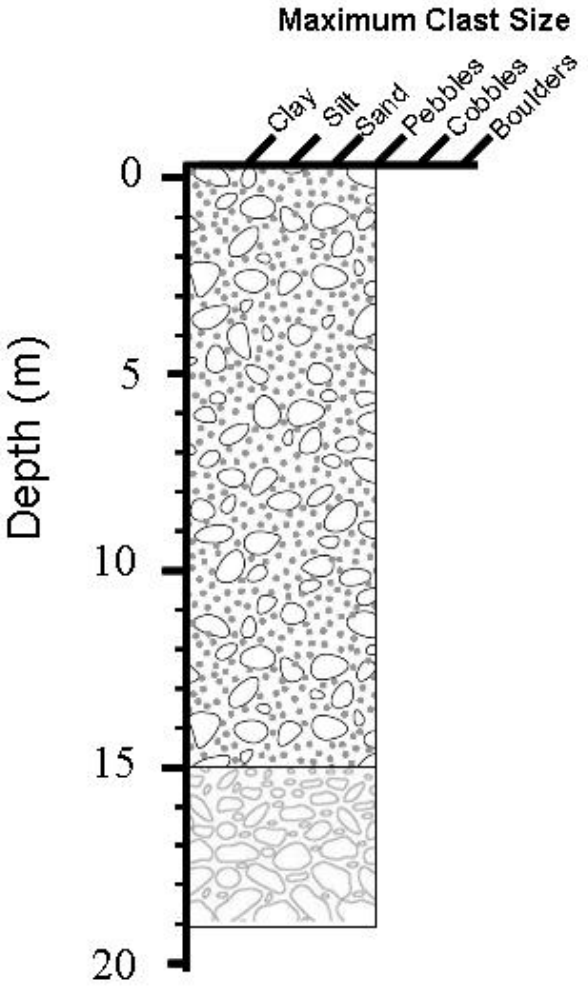

Unit 2: Gravel with a silty, medium to coarse-grained sand matrix. Angular to sub-round clasts. The unit appears to coarsen with depth. Clasts are mostly pebbles.

Unit 1: Fining-upward moderately sorted gravel with a medium to fine-grained sand matrix. Clasts are sub-angular to well-rounded. The unit bottoms on bedrock at 19 m.

Don-60

478317 N
6934526 E

Dip: 80°

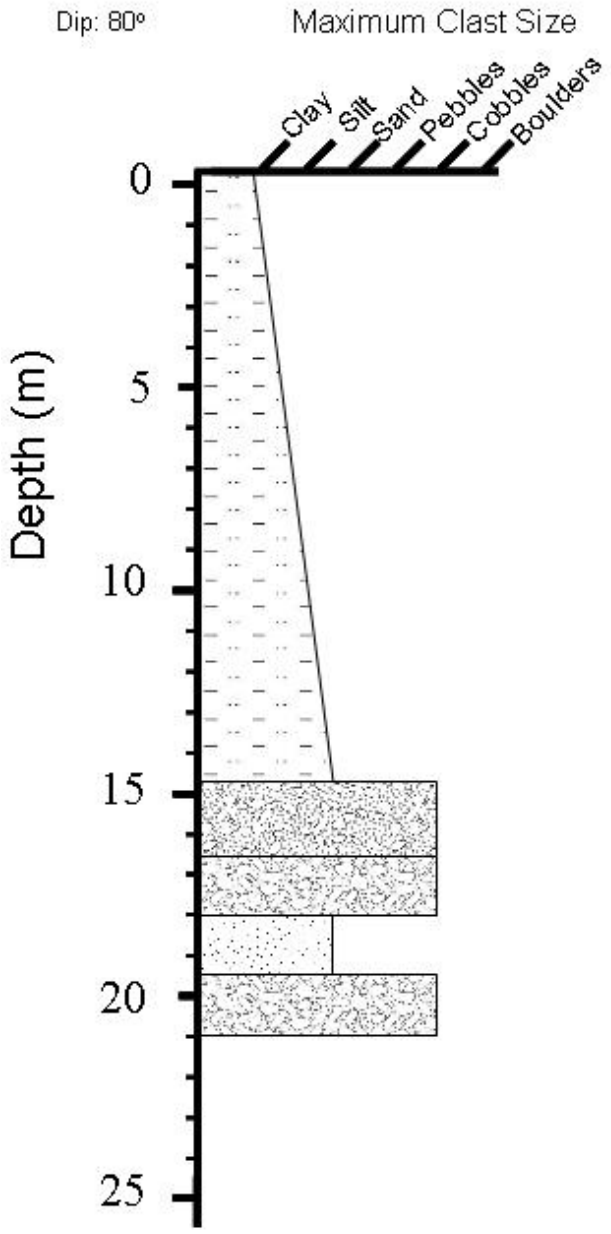

Unit 3: Silty fine-grained sand fines upwards into clayey silt. Very few pebbles.

Unit 2: Matrix-supported gravel or diamict. Clast-poor (~5-10%). Angular to well-rounded clasts. Silty fine-grained sand matrix.

Unit 1: Interbedded sand and gravel. Sand coarsens with depth from fine and medium-grained sand, to coarse-grained sand.

Don-70

478317 N
6934526 E

Dip: 80°

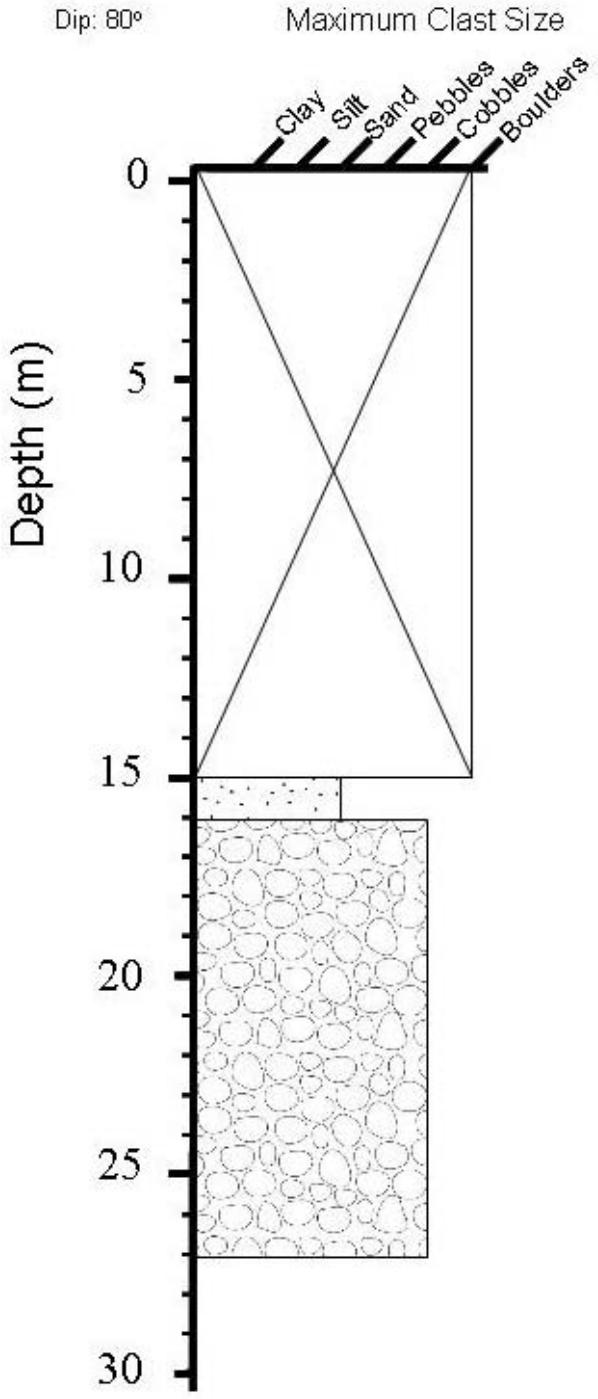

Top 15 m missing from drill core

Unit 2: Fine to coarse sand. Rare (<5%) sub-angular carbonate and mudstone clasts.

Unit 1: Coarse very well-sorted pebble to cobble gravel with a few boulders. Likely matrix supported, but dominantly clasts remain in drill core. Medium to coarse-grained sand matrix. Wide range in clast lithologies. Maximum clast size is 45 cm.

Don-72

480671 N
6931979 E

Dip: 80°

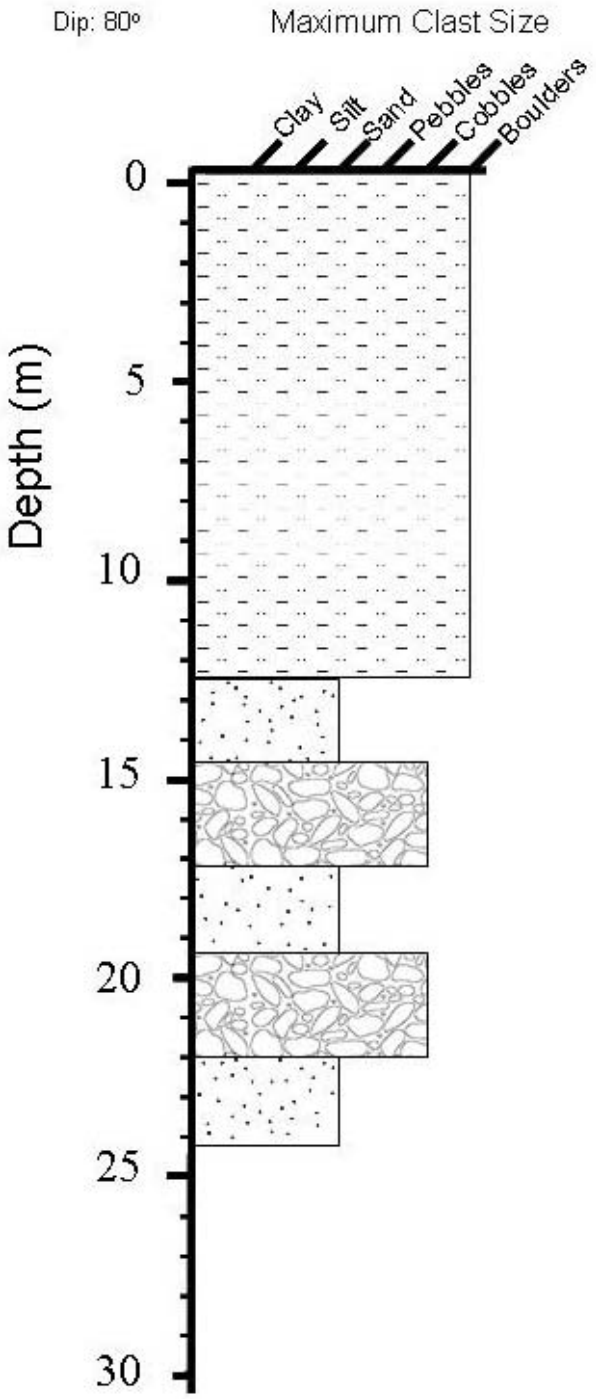

Unit 2: Clayey-silt. Rare (<5%) angular to sub-rounded clasts of varying lithology.

Unit 1: Interbedded coarse sand with some pebbles, and pebble-cobble gravel with a medium to coarse-sand matrix.

Don-79

481095 N
6931753 E

Dip: 80°

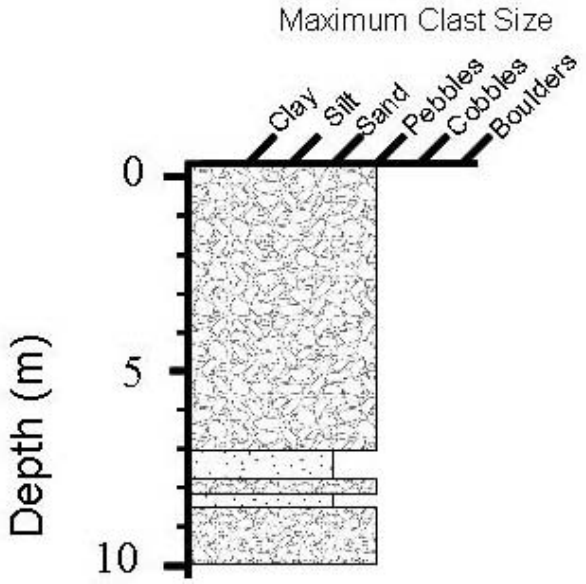

Unit 2: Moderately-sorted gravel with a medium to coarse-grained sand matrix. Clasts are granule to pebble sized.

Unit 1: Interbedded moderately-sorted gravel with an average clast size of pebble and a medium-grained sand matrix, and medium-grained sand. Sand beds thicken upwards from 10 cm to approximately 1 m.

Don-87

481483 N
6931542 E

Dip: 80°

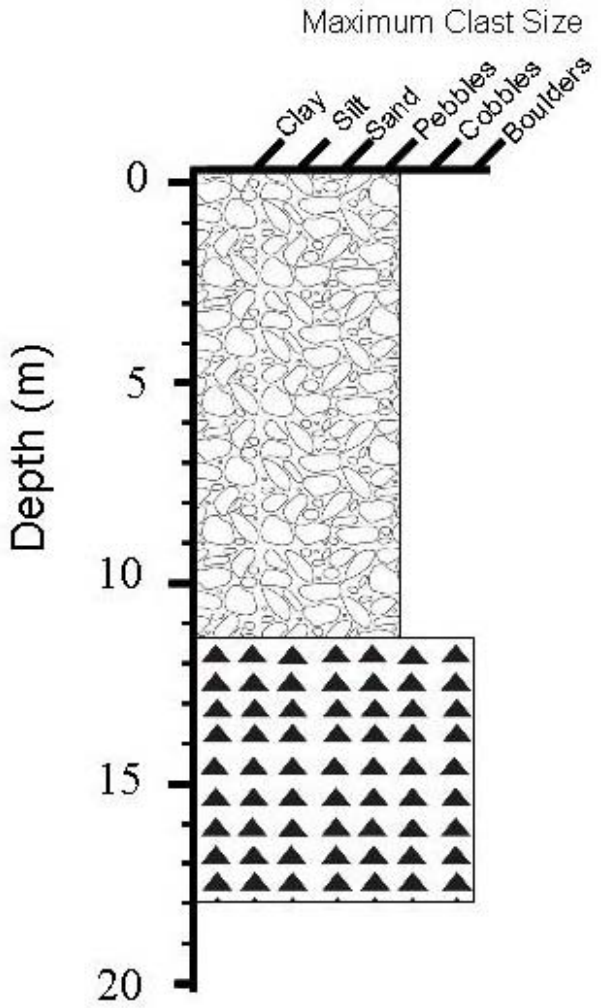

Unit 2: Moderately to well-sorted gravel with a silty, medium to coarse-grained sand matrix. Angular to well-round, average rounded, pebble and cobble clasts. Maximum clasts size is 7 cm. Clast lithologies includes sandstone, mudstone and conglomerate. No observed granitics. The unit appears to coarsen with depth. Clasts are mostly pebbles.

Unit 1: Consolidated light grey diamict. Sandy silt matrix. >30% Angular to sub-rounded, mostly angular, clasts with a maximum size of 8 cm. Some clasts are granitic, but there are also abundant shale, limestone, conglomerate and mudstone. Average clast size is pebble.

Don-92

481370 N
6931395 E

Dip: 80°

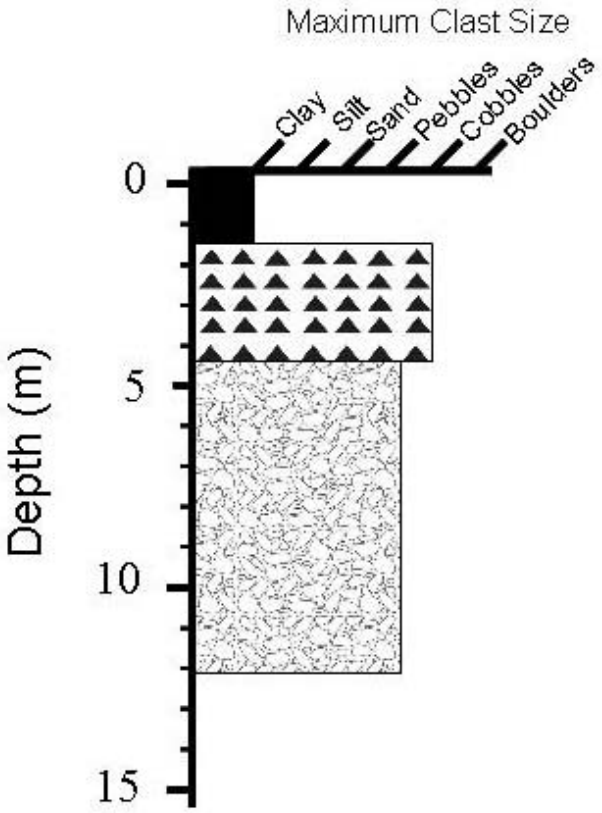

Unit 3: Undescribed organics

Unit 2: Light brown diamict. Clay matrix. ~15% clasts of mostly limestone and Shale lithology

Unit 1: Moderately-sorted gravel with angular to sub-rounded clasts, average angular. Sand matrix. Dominantly limestone clasts.

Don-93

480855 N
6931487 E

Dip: 80°

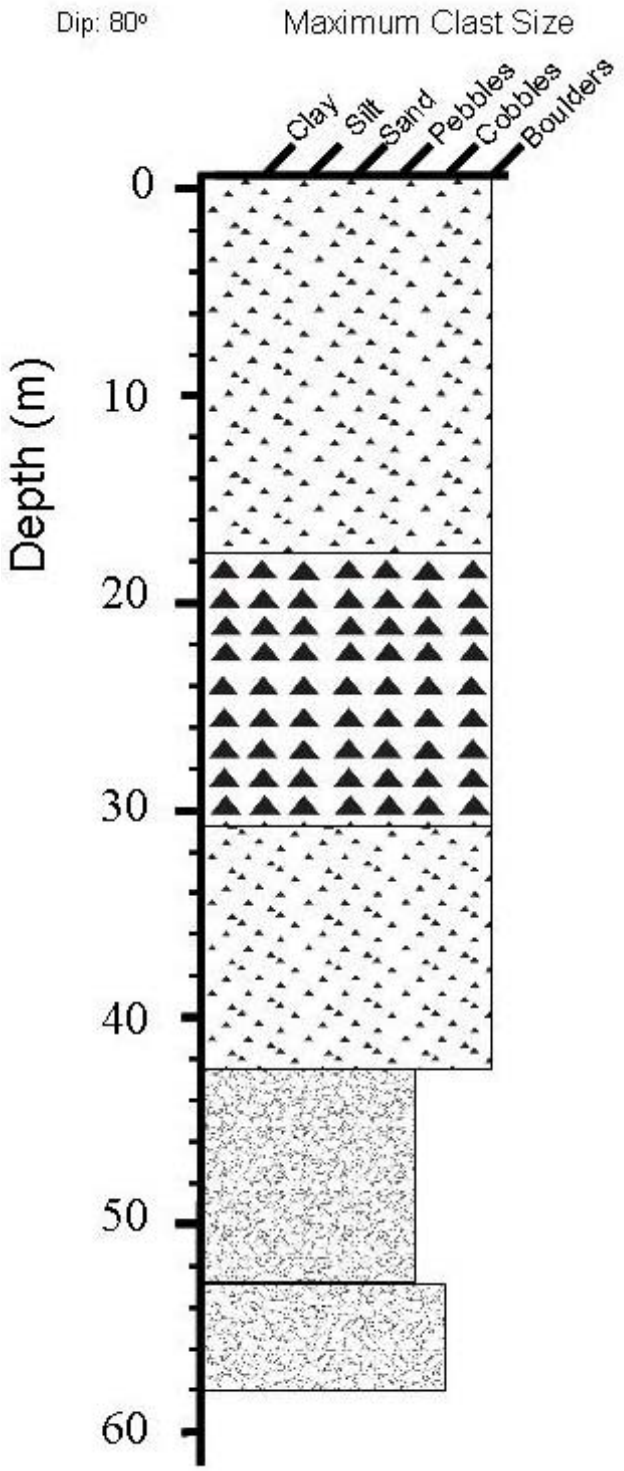

Unit 5: Silty-clay diamict. 10-15% clasts with a maximum size of 10 cm. Well-rounded to sub-angular.

Unit 4: Clast-rich diamict (~40%). Maximum observed clasts size is 20 cm. Clasts are rounded to sub-rounded with a fine to medium-grained sand matrix. Poorly sorted. Some clay and silt in the matrix.

Unit 3: Diamict with a clay matrix. Some well-rounded granitic clasts, but mostly angular shale. ~15% clasts.

Unit 2: Moderately-sorted gravel. Maximum clasts size is 20 cm. Well-rounded to sub-angular clasts with an average size of large pebble. Matrix likely silty fine-grained sand, but most of it is missing.

Unit 1: Moderately-sorted gravel. Coarse-grained sand matrix. Average clast size is cobble. Lacks granitic clasts

Don-104

481334 N
6931554 E

Dip: 80°

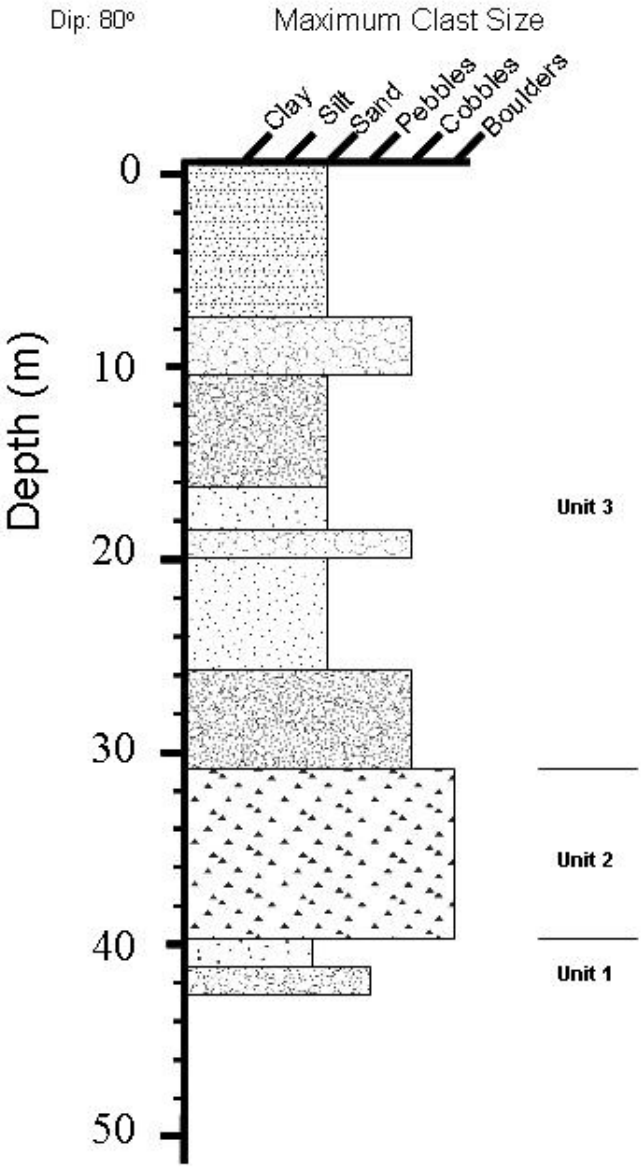

0-7.5 m: Interbedded well-sorted fine-grained sand with rare clasts <5 cm, poorly-sorted fine to medium-grained sand with 5-15% pebbles and moderately-sorted, fine to coarse-grained sand with ~5% pebbles.

7.5-10.5 m: Interbedded clast-supported pebble gravel and matrix-supported gravel.

10.5-16.5 m: Poorly-sorted coarse-grained sand with abundant granules and pebbles.

16.5-20 m: Interbedded well-sorted medium-grained sand and clast-supported gravel with a medium-grained sand matrix and mixed lithologies. The sand beds are less than 10 cm thick.

20-26 m: Poorly-sorted sand with <5 cm beds of pebble-rich sand.

26-30.5 m: Matrix-supported, poorly-sorted gravel with pebble to cobble sized clasts. Maximum clast size is 10 cm. Matrix is fine to coarse-grained sand. The bottom 20 cm consists of clast-supported gravel with an average clast size of 2-3 cm.

30.5-39.5 m: Diamict. Clay matrix with 10-15% clasts. Clasts are all >5 cm. Clasts are angular with mixed lithologies. It is consolidated, but becomes looser with depth. Lower contact sharp.

39.5-41 m: Moderately to well-sorted coarse-grained sand.

41-42.5 m: Interbedded poorly-sorted coarse-grained sand and clast-supported gravel. Gravel clasts have mixed lithologies and range from granule to large pebbles. Unit bottoms on bedrock.

Don-111

481267 N
6931704 E

Dip: 80°

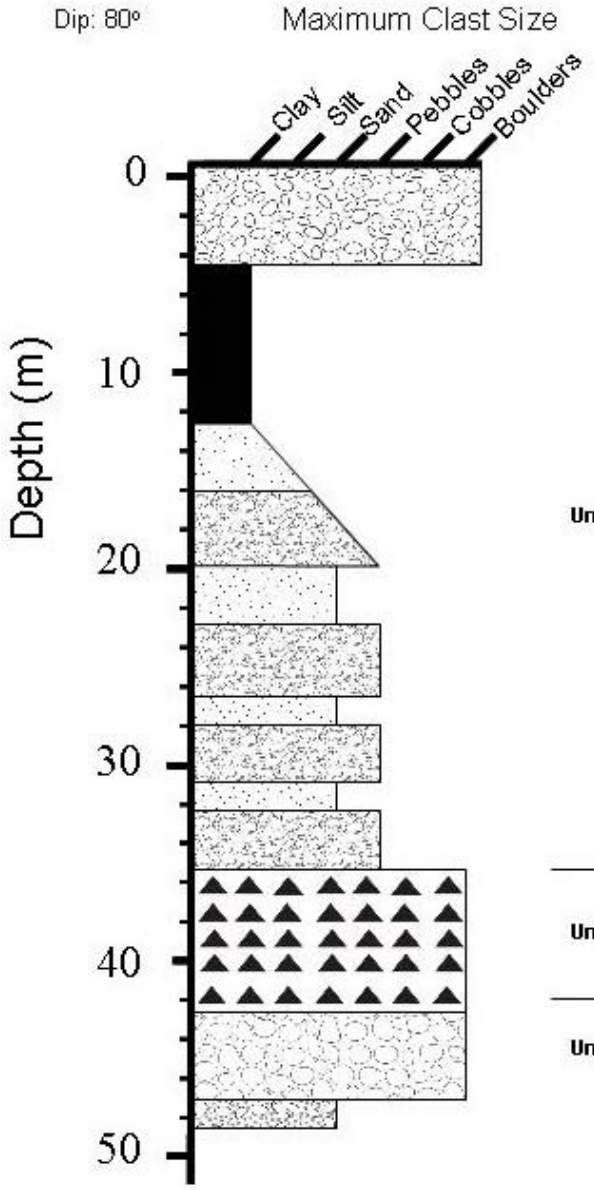

0-4.5 m: Almost entirely Earn Group clasts of varying size. Likely colluvium.

4.5-13 m: Silty clay. Very few clasts (<5%).

13-17 m: Fining-upwards well-sorted sand.

17-20 m: Fining-upwards from moderately-sorted gravel with a sand matrix, to fine-grained sand

20-36.5 m: Interbedded sand and gravel. The sand is well-sorted and coarse-grained. The gravel is moderately-sorted and sand matrix-supported, with granule and pebble clasts.

36.5-43 m: Grey diamict. Sandy-silt matrix. The maximum clast size is 15 cm. The clasts are dominantly angular and consist of Earn Group conglomerate.

43-47m: Clast-supported, poorly-sorted gravel. Clasts range from pebble to boulder with a maximum clast size of >30 cm.

47-48m: Poorly-sorted gravel with a sand matrix. Clasts are well-rounded to sub-angular, average sub-angular. Matrix-supported.

Don-112

481409 N
6931716 E

Dip: 80°

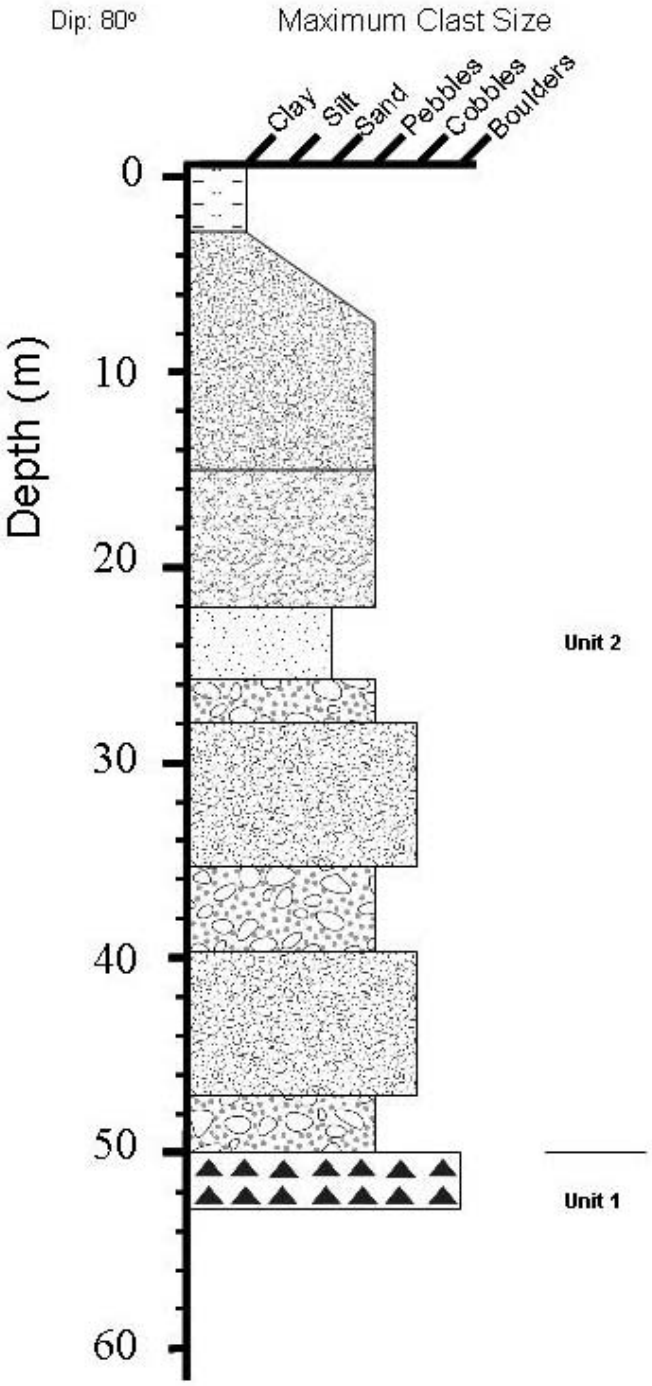

0-3 m: Clayey silt. No observed clasts.

3-15 m: Poorly-sorted gravel. Silty-sand matrix with pebble-sized clasts. Matrix-supported. Top 4.5 m fines-upwards into silt.

15-22 m: Moderately-sorted gravel with a silty-sand matrix. Maximum clast size is >15 cm.

22-26 m: Well-sorted brown sand. Few clasts (<5%).

26-50 m: Interbedded matrix-supported gravel with pebble-sized clasts, and a well-sorted, clast-supported gravel with a sand matrix.

50-53 m: Grey consolidated diamict. Silt matrix. Angular clasts at approximately 15%.

Appendix D: Ice-flow Indicator Data

The following are all summarizations of complex outcrops. The listed orientations are either averages or the most representative direction(s).

Bold indicates sites shown on Figure 4.2

Alpine Stage	1
Nahanni Stage	2
Logan Stage	3
Don Stage I	4
Don Stage II	5

Station #	Easting	Northing	Elevation asl	GPS error (+/-)	Type	Orientation	Unidirectional (U) or Bi (B)	Ice-flow Stage
07DT013	489145	6914503		8	**Lee side striations**	043/223	B	**4**
					Striations	062/242	B	4
07DT023	499650	6922028		8	Striations	062/242	B	4
07DT024	498660	6922218		8	Striations	078/258	B	4
07DT026	498517	6921976		6	Groove	070/250	B	4
07DT040	458658	6917545	1037	8	Striations	093/183	B	5
					Striations	172/352	B	**3**
					Lee side striations	042/222	B	**4**
					Lee side striations	058/238	B	4
					Striations	100/280	B	**5**

Station #	Easting	Northing	Elevation asl	GPS error (+/-)	Type	Orientation	Unidirectional (U) or Bi (B)	Ice-flow Stage
07DT047	469644	6936260	1668	7	Striations	044/224	B	4
07DT048	469646	6936301	1664	8	Striations	042/222	B	4
07DT049	469579	6936118	1579	5	**Groove**	136/316	B	**1**
					Rat tail	246	U	**2**
07DT050	469454	6936260	1563	8	Striations	080/260	B	4
					Striations	074/254	B	4
07DT052	469287	6936237	1565	6	Striations	041/221	B	4
07DT053	468837	6935997	1552	7	Possible erratic train	185	U	5
07DT054	468354	6935520	1300	9	Striations	064/244	B	4
07DT080	487645	6924943	1686	10	**Striations and grooves**	020/200	B	**5**
					Striations	047/227	B	**4**
07DT081	487675	6924972		8	Striations	066/246	B	5
07DT082	487677	6925035		7	Groove	020/220	B	4
					Striations	026/206	B	4
					Striations	012/192	B	5
					Striations	031/211	B	5
07DT083	471682	6936416	1564	10	Striations	094/274	B	5
					Striations	060/240	B	4
07DT084	471570	6936354	1598	6	Striations	075/255	B	5
07DT092	471507	6936248	1619	6	Striations	020/200	B	3
07DT094	471371	6936008	1608	7	Striations	078/258	B	5
					Rat tail	258	U	**2**
07DT096	471364	6935987	1547	7	Striations	069/249	B	5
					Striations	047/227	B	4
07DT097	471328	6935995	1556		**Striations**	011/191	B	**3**
					Striations	038/218	B	4
07DT098	470944	6935783	1465	6	Striations	087/267	B	5

Station #	Easting	Northing	Elevation asl	GPS error (+/-)	Type	Orientation	Unidirectional (U) or Bi (B)	Ice-flow Stage
07DT099	463735	6941569	1544		Striations	055/235	B	5
07DT100	463760	6941537	1488	10	Striations	029/209	B	4
					Striations	039/217	B	5
07DT101-1	463905	6941371	1469	7	Striations	040/220	B	4
07DT101-2	463938	6941361	1486	10	Striations	062/242	B	5
07DT102	464075	6941340	1499	8	Striations	042/222	B	4
07DT103	464151	6941414	1492	6	Striations	052/232	B	5
07DT104	464723	6940685	1641	7	**Striations and grooves**	145/325	B	**4**
					Striations	081/261	B	**2**
					Striations	107/287	B	5
07DT107	479030	6929148	1686	10	Grooves	130/310	B	5
07DT109	478941	6929240	1681	8	Striations	042/222	B	5
07DT110	478998	6929223	1683	8	Striations	065/245	B	4
					Lee side striations	20	U	5
07DT111	479069	6929264	1676	10	**Striations**	065/245	B	**4**
					Striations	044/224	B	4
					Lee side striations	024	U	**5**
07DT114	479346	6938335	1599	10	**Striations**	010/190	B	**1**
					Lee side and nailhead striations	60/240	U	**2**
					Lee side and nailhead striations	140/320	B	**3**
					Striations	160/340	B	**5**
07DT115	47981	6938134	1610	10	Striations	151/331	B	5

Station #	Easting	Northing	Elevation asl	GPS error (+/-)	Type	Orientation	Unidirectional (U) or Bi (B)	Ice-flow Stage
07DT139	484354	6919271	1679	6	Lee side striations	019	U	4
07DT140	484468	6916293	1643	6	**Striations**	**100/280**	B	**1**
					Rat tails	**008**	U	**3**
07DT141	484701	6919351	1628	8	**Striations**	**034/214**	B	**3**
					Rat tails	**120**	U	**5**
07DT142	484735	6919303	1639	8	Striations	100/280	B	5
					Striations	012/192	B	3
07DT143	484335	6919570	1589	12	Striations	155/335	B	5
					Striations	120/300	B	5
					Striations	015/195	B	3

Appendix E: Mobile Metal Ion Geochemistry Data

Interval A (0-10 cm)

ANALYTE	Ag	Al	As	Au	Ba	Bi	Ca	Cd
DETECTION	1	1	10	0.1	10	1	10	10
UNITS	PPB	PPM	PPB	PPB	PPB	PPB	PPM	PPB
06DTMMI-01A	2	240	30	<0.1	170	<1	<10	<10
06DTMMI-02A	10	127	20	<0.1	190	3	20	50
06DTMMI-03A	75	63	30	0.1	1110	<1	140	1800
06DTMMI-04A	19	15	<10	<0.1	50	<1	<10	10
06DTMMI-05A	9	96	20	<0.1	210	<1	<10	40
06DTMMI-06A	33	116	140	0.4	540	1	<10	60
06DTMMI-07A	20	100	30	<0.1	24100	<1	40	1160
06DTMMI-08A	5	292	60	<0.1	4180	<1	<10	10
06DTMMI-09A	18	51	<10	<0.1	2600	<1	180	50
06DTMMI-10A	17	91	<10	<0.1	2350	<1	200	110
06DTMMI-11A	17	20	40	<0.1	750	2	260	30
06DTMMI-12A	4	76	<10	<0.1	1760	<1	240	20
06DTMMI-13A	6	233	10	<0.1	2760	<1	10	30
06DTMMI-14A	10	255	20	<0.1	2630	<1	<10	30
06DTMMI-15A	43	69	<10	<0.1	1880	<1	230	140
06DTMMI-16A	22	215	10	<0.1	1770	<1	60	100
06DTMMI-17A	27	150	10	<0.1	2010	<1	100	180
06DTMMI-18A	32	109	<10	<0.1	4270	<1	190	250
06DTMMI-19A	20	122	<10	<0.1	4860	<1	240	470
06DTMMI-20A	465	25	10	<0.1	1240	<1	100	990
06DTMMI-21A	<1	84	50	0.2	2720	<1	110	140
06DTMMI-22A	251	19	10	0.3	7790	<1	200	580
06DTMMI-23A	21	204	80	0.1	7830	2	90	210
06DTMMI-24A	13	26	20	0.4	2340	<1	130	280
06DTMMI-25A	26	83	30	<0.1	3390	<1	210	340
06DTMMI-26A	8	155	<10	<0.1	2010	<1	140	240
06DTMMI-27A	5	114	20	<0.1	4850	<1	10	30
06DTMMI-28A	18	144	20	0.2	5130	<1	10	10
06DTMMI-29A	10	210	60	<0.1	4810	1	<10	10
06DTMMI-30A	1	55	20	<0.1	8050	<1	160	40
06DTMMI-31A	31	13	40	0.1	2610	<1	340	80
06DTMMI-32A	35	76	10	<0.1	2190	<1	300	240
06DTMMI-33A	7	12	<10	<0.1	2600	<1	310	20
06DTMMI-34A	7	125	<10	<0.1	8520	<1	200	100
06DTMMI-35A	3	173	<10	<0.1	4180	<1	60	70
06DTMMI-37A	2	159	<10	<0.1	1390	<1	30	60
06DTMMI-38A	3	205	<10	<0.1	1500	<1	20	50
06DTMMI-36A	3	180	<10	<0.1	2680	<1	20	120
06DTMMI-39A	3	193	<10	<0.1	1280	<1	10	50

ANALYTE	Gd	La	Li	Mg	Mo	Nb	Nd	Ni
DETECTION	1	1	5	1	5	0.5	1	5
UNITS	PPB	PPB	PPB	PPM	PPB	PPB	PPB	PPB
06DTMMI-01A	4	9	8	<1	53	3.4	11	2340
06DTMMI-02A	38	83	21	<1	207	3.8	135	2160
06DTMMI-03A	85	60	<5	15	21	<0.5	194	3200
06DTMMI-04A	36	5	<5	<1	<5	<0.5	67	261
06DTMMI-05A	113	32	<5	<1	16	0.8	214	1070
06DTMMI-06A	91	32	<5	<1	32	0.6	191	671
06DTMMI-07A	167	301	<5	1	11	<0.5	453	1760
06DTMMI-08A	19	27	5	<1	19	1.7	43	125
06DTMMI-09A	14	18	<5	35	18	<0.5	40	722
06DTMMI-10A	9	11	<5	28	14	<0.5	26	473
06DTMMI-11A	27	44	6	37	40	<0.5	69	486
06DTMMI-12A	2	7	<5	33	8	0.8	9	171
06DTMMI-13A	31	33	<5	<1	6	2.4	80	315
06DTMMI-14A	24	27	<5	<1	7	3.3	57	143
06DTMMI-15A	51	82	<5	<1	6	<0.5	132	914
06DTMMI-16A	72	130	<5	<1	10	3	214	368
06DTMMI-17A	126	187	<5	3	7	0.8	354	397
06DTMMI-18A	55	61	<5	9	6	<0.5	133	2840
06DTMMI-19A	8	21	<5	9	7	<0.5	27	1300
06DTMMI-20A	22	88	<5	5	6	0.6	83	271
06DTMMI-21A	80	166	<5	8	19	1.7	226	332
06DTMMI-22A	55	67	<5	9	41	<0.5	145	235
06DTMMI-23A	109	200	<5	<1	24	2.6	333	264
06DTMMI-24A	59	78	<5	15	80	<0.5	155	8490
06DTMMI-25A	104	155	<5	15	18	<0.5	288	691
06DTMMI-26A	10	12	<5	10	12	2.4	23	1020
06DTMMI-27A	3	4	<5	2	20	2.1	16	442
06DTMMI-28A	7	10	<5	<1	10	0.7	18	295
06DTMMI-29A	15	50	<5	<1	22	8.3	53	458
06DTMMI-30A	11	15	<5	6	88	<0.5	26	334
06DTMMI-31A	51	64	<5	26	53	<0.5	137	519
06DTMMI-32A	107	104	<5	18	8	<0.5	274	394
06DTMMI-33A	11	10	<5	19	7	0.7	25	73
06DTMMI-34A	19	12	<5	7	7	0.8	32	752
06DTMMI-35A	25	44	<5	2	6	2	89	48
06DTMMI-37A	86	93	<5	1	<5	<0.5	261	34
06DTMMI-38A	30	44	<5	1	<5	1.6	91	53
06DTMMI-36A	14	11	<5	3	<5	1.8	33	45
06DTMMI-39A	28	33	<5	<1	<5	1.5	75	54

ANALYTE	Pb	Pd	Pr	Rb	Sb	Sc	Sm	Sn
DETECTION	10	1	1	5	1	5	1	1
UNITS	PPB	PPB	PPB	PPB	PPB	PPB	PPB	PPB
06DTMMI-01A	70	<1	4	12	11	11	3	<1
06DTMMI-02A	1000	1	37	186	15	37	33	<1
06DTMMI-03A	300	<1	42	312	8	29	65	<1
06DTMMI-04A	250	<1	10	49	2	61	25	<1
06DTMMI-05A	1580	<1	39	121	11	108	82	<1
06DTMMI-06A	940	1	35	188	30	76	71	<1
06DTMMI-07A	12500	<1	117	115	8	54	129	<1
06DTMMI-08A	14700	<1	11	116	13	32	14	<1
06DTMMI-09A	890	<1	9	75	4	<5	12	<1
06DTMMI-10A	730	<1	6	156	2	<5	8	<1
06DTMMI-11A	12500	<1	18	46	10	53	21	<1
06DTMMI-12A	920	<1	3	24	1	<5	2	<1
06DTMMI-13A	8610	<1	18	68	3	24	24	<1
06DTMMI-14A	5130	<1	13	51	4	33	17	<1
06DTMMI-15A	2700	<1	31	95	2	6	37	<1
06DTMMI-16A	3850	<1	52	43	3	38	55	<1
06DTMMI-17A	2500	<1	83	71	1	54	92	<1
06DTMMI-18A	2600	<1	30	62	2	18	45	<1
06DTMMI-19A	37500	<1	8	22	1	11	7	<1
06DTMMI-20A	138763	<1	23	36	2	7	18	<1
06DTMMI-21A	21600	<1	57	119	9	39	65	<1
06DTMMI-22A	58300	<1	28	73	3	25	43	<1
06DTMMI-23A	22700	<1	75	135	13	85	91	1
06DTMMI-24A	6130	<1	31	38	8	52	45	<1
06DTMMI-25A	15800	<1	62	152	4	40	81	<1
06DTMMI-26A	2350	<1	6	71	3	21	8	<1
06DTMMI-27A	4020	<1	4	52	6	26	5	<1
06DTMMI-28A	870	<1	4	103	4	36	6	<1
06DTMMI-29A	670	<1	13	55	7	26	13	1
06DTMMI-30A	220	<1	6	<5	16	41	8	<1
06DTMMI-31A	450	<1	27	20	3	13	41	<1
06DTMMI-32A	1010	<1	52	113	1	8	84	<1
06DTMMI-33A	230	<1	5	38	<1	<5	9	<1
06DTMMI-34A	2000	<1	7	20	2	30	12	<1
06DTMMI-35A	2060	<1	20	8	1	14	23	<1
06DTMMI-37A	370	<1	52	49	<1	79	68	<1
06DTMMI-38A	810	<1	20	42	<1	23	24	<1
06DTMMI-36A	1660	<1	7	9	<1	13	11	<1
06DTMMI-39A	1030	<1	16	71	<1	26	22	<1

ANALYTE	Sr	Ta	Tb	Te	Th	Ti	Tl	U
DETECTION	10	1	1	10	0.5	3	0.5	1
UNITS	PPB	PPB	PPB	PPB	PPB	PPB	PPB	PPB
06DTMMI-01A	30	1	<1	<10	9.1	709	1.2	49
06DTMMI-02A	<10	<1	7	<10	71.6	939	20.8	78
06DTMMI-03A	120	<1	15	<10	23.4	57	6.6	213
06DTMMI-04A	<10	<1	6	<10	11.9	12	12.6	45
06DTMMI-05A	<10	<1	20	<10	58.8	140	8.2	203
06DTMMI-06A	<10	<1	17	<10	77.1	178	5.8	206
06DTMMI-07A	140	<1	31	<10	47.1	63	3.9	136
06DTMMI-08A	10	<1	4	<10	65.9	332	2.7	53
06DTMMI-09A	210	<1	2	<10	4.2	16	1.3	266
06DTMMI-10A	200	<1	1	<10	4.4	26	1.9	531
06DTMMI-11A	250	<1	5	<10	25.8	42	<0.5	1240
06DTMMI-12A	300	<1	<1	<10	2.5	46	0.5	313
06DTMMI-13A	60	<1	6	<10	42.4	284	1.6	40
06DTMMI-14A	20	<1	5	<10	36.2	508	1.7	61
06DTMMI-15A	230	<1	9	<10	6	14	1.2	124
06DTMMI-16A	80	<1	13	<10	33.7	492	1	194
06DTMMI-17A	80	<1	23	<10	23.3	152	1.1	395
06DTMMI-18A	200	<1	9	<10	11.5	41	1.7	298
06DTMMI-19A	410	<1	1	<10	5.6	34	1	492
06DTMMI-20A	120	<1	3	<10	5.2	91	2.2	35
06DTMMI-21A	100	3	14	<10	56.7	147	1.8	122
06DTMMI-22A	250	1	8	<10	27.4	11	2.9	153
06DTMMI-23A	120	1	18	<10	105	519	3.1	230
06DTMMI-24A	130	<1	9	<10	18.2	49	3.1	371
06DTMMI-25A	230	<1	15	<10	37.8	63	4	157
06DTMMI-26A	190	<1	2	<10	19.5	373	2.5	86
06DTMMI-27A	100	<1	<1	<10	36.6	362	1.4	45
06DTMMI-28A	80	<1	1	<10	26.6	131	2.3	152
06DTMMI-29A	70	<1	2	<10	45.1	1640	1.3	29
06DTMMI-30A	390	<1	2	<10	6.5	42	<0.5	630
06DTMMI-31A	620	<1	7	<10	18.7	23	<0.5	255
06DTMMI-32A	440	<1	16	<10	16.9	42	0.8	123
06DTMMI-33A	560	1	2	<10	15.2	24	<0.5	19
06DTMMI-34A	520	<1	4	<10	20.4	65	<0.5	70
06DTMMI-35A	110	<1	4	<10	29.1	300	<0.5	16
06DTMMI-37A	100	<1	15	<10	52.9	55	<0.5	47
06DTMMI-38A	80	<1	5	<10	32.8	227	0.6	17
06DTMMI-36A	100	<1	3	<10	21.5	248	<0.5	14
06DTMMI-39A	70	<1	5	<10	31.1	223	0.8	19

ANALYTE	W	Y	Yb	Zn	Zr
DETECTION	1	5	1	20	5
UNITS	PPB	PPB	PPB	PPB	PPB
06DTMMI-01A	2	62	6	3830	78
06DTMMI-02A	2	223	12	5900	213
06DTMMI-03A	1	550	37	14400	72
06DTMMI-04A	<1	328	26	610	28
06DTMMI-05A	<1	646	57	2810	86
06DTMMI-06A	4	531	44	1660	196
06DTMMI-07A	1	910	47	8030	77
06DTMMI-08A	1	120	7	1130	168
06DTMMI-09A	<1	80	4	880	21
06DTMMI-10A	<1	42	2	1270	44
06DTMMI-11A	1	199	13	5210	55
06DTMMI-12A	<1	12	<1	2090	18
06DTMMI-13A	<1	260	17	800	117
06DTMMI-14A	<1	221	14	790	127
06DTMMI-15A	<1	394	20	1760	29
06DTMMI-16A	<1	614	37	2160	210
06DTMMI-17A	<1	1100	79	5810	91
06DTMMI-18A	<1	299	16	9870	74
06DTMMI-19A	<1	57	4	15000	34
06DTMMI-20A	<1	184	9	143467	57
06DTMMI-21A	2	433	19	11100	97
06DTMMI-22A	2	327	22	22600	37
06DTMMI-23A	2	589	31	7800	248
06DTMMI-24A	1	472	36	21000	89
06DTMMI-25A	1	709	37	21300	125
06DTMMI-26A	<1	64	6	21400	139
06DTMMI-27A	<1	31	6	2660	97
06DTMMI-28A	<1	62	11	330	79
06DTMMI-29A	1	84	6	1320	269
06DTMMI-30A	1	110	11	2420	38
06DTMMI-31A	<1	227	13	1710	55
06DTMMI-32A	<1	512	25	2720	52
06DTMMI-33A	3	42	2	1070	29
06DTMMI-34A	<1	145	11	3170	83
06DTMMI-35A	<1	109	6	1480	101
06DTMMI-37A	<1	409	25	1460	73
06DTMMI-38A	<1	141	9	940	100
06DTMMI-36A	<1	86	6	2110	79
06DTMMI-39A	<1	159	10	1130	101

Interval B (10-20 cm)

ANALYTE	Ag	Al	As	Au	Ba	Bi	Ca	Cd
DETECTION	1	1	10	0.1	10	1	10	10
UNITS	PPB	PPM	PPB	PPB	PPB	PPB	PPM	PPB
06DTMMI-01A	2	231	30	<0.1	5	<1	<10	10
06DTMMI-02A	7	95	30	<0.1	510	5	40	50
06DTMMI-03A	34	59	40	<0.1	950	<1	110	1300
06DTMMI-04A	12	65	<10	<0.1	50	<1	<10	<10
06DTMMI-05A	9	57	<10	<0.1	5	<1	<10	50
06DTMMI-06A					0			
06DTMMI-07A	16	71	30	<0.1	31000	<1	40	580
06DTMMI-08A	7	224	50	<0.1	2290	<1	<10	<10
06DTMMI-09A	21	13	<10	<0.1	3160	<1	160	90
06DTMMI-10A	13	74	<10	<0.1	1310	<1	220	150
06DTMMI-11A	59	17	40	<0.1	2820	2	210	10
06DTMMI-12A	35	24	<10	<0.1	5090	<1	360	180
06DTMMI-13A	8	223	30	<0.1	2170	<1	40	30
06DTMMI-14A	8	240	20	<0.1	2520	<1	<10	40
06DTMMI-15A	42	114	10	<0.1	1980	<1	210	130
06DTMMI-16A	47	207	20	0.1	1550	<1	40	260
06DTMMI-17A	40	184	10	<0.1	2280	<1	90	170
06DTMMI-18A	26	61	<10	<0.1	9870	<1	260	150
06DTMMI-19A	16	98	<10	<0.1	1710	<1	200	420
06DTMMI-20A	344	27	10	<0.1	800	<1	90	1150
06DTMMI-21A	<1	83	50	0.2	3090	<1	160	130
06DTMMI-22A	107	57	30	0.5	10900	<1	130	270
06DTMMI-23A	22	234	40	0.1	5220	1	50	180
06DTMMI-24A	11	21	30	0.3	1710	<1	140	170
06DTMMI-25A	47	54	20	0.1	3580	<1	240	390
06DTMMI-26A	11	179	<10	<0.1	3430	<1	200	530
06DTMMI-27A	4	153	100	0.2	7540	2	10	<10
06DTMMI-28A	66	238	20	0.3	4700	<1	<10	130
06DTMMI-29A	26	249	60	<0.1	6330	<1	20	150
06DTMMI-30A	2	57	20	<0.1	2360	<1	190	60
06DTMMI-31A	11	34	30	0.1	1560	<1	300	60
06DTMMI-32A	24	56	20	<0.1	1830	<1	190	110
06DTMMI-33A	5	51	<10	<0.1	1900	<1	360	20
06DTMMI-34A	9	99	10	<0.1	7380	<1	230	50
06DTMMI-35A	3	185	<10	<0.1	3920	<1	30	80
06DTMMI-37A	3	165	<10	<0.1	1160	<1	40	60
06DTMMI-38A	3	195	<10	<0.1	1630	<1	30	40
06DTMMI-36A	2	142	<10	<0.1	3170	<1	60	60
06DTMMI-39A	3	195	<10	<0.1	1330	<1	40	30

ANALYTE	Ce	Co	Cr	Cu	Dy	Er	Eu	Fe
DETECTION	5	5	100	10	1	0.5	0.5	1
UNITS	PPB	PPB	PPB	PPB	PPB	PPB	PPB	PPM
06DTMMI-01A	18	86	<100	1340	3	3	0.7	51
06DTMMI-02A	190	273	<100	830	39	18.2	9.1	63
06DTMMI-03A	179	22	<100	2040	75	40.2	17.3	36
06DTMMI-04A	431	42	<100	650	105	62.4	24.4	45
06DTMMI-05A	108	89	<100	2730	54	40.6	13.9	61
06DTMMI-06A				0				
06DTMMI-07A	543	28	<100	620	131	64.7	32.1	31
06DTMMI-08A	230	29	<100	270	36	11.8	8.4	87
06DTMMI-09A	58	48	<100	1550	19	8.5	4.9	22
06DTMMI-10A	26	99	<100	2200	3	1.4	1.2	9
06DTMMI-11A	277	15	<100	4550	50	26.3	14.6	69
06DTMMI-12A	67	52	<100	1270	11	5.2	3.2	53
06DTMMI-13A	136	122	<100	300	40	20.3	8.8	118
06DTMMI-14A	34	58	<100	440	41	29.2	5	120
06DTMMI-15A	136	<5	<100	530	68	37.5	14.4	28
06DTMMI-16A	473	27	<100	2800	212	150	41.6	69
06DTMMI-17A	237	51	<100	740	114	80.2	19.7	124
06DTMMI-18A	26	<5	<100	1000	20	8.4	6.8	15
06DTMMI-19A	48	<5	<100	180	3	1.6	1.3	20
06DTMMI-20A	77	10	<100	910	17	10.1	5.3	17
06DTMMI-21A	332	296	<100	660	87	33.5	17.5	115
06DTMMI-22A	283	24	<100	2430	143	76.8	36.5	10
06DTMMI-23A	259	76	<100	550	75	36.3	17.2	165
06DTMMI-24A	155	2210	<100	8310	47	32	11.4	214
06DTMMI-25A	162	10	<100	920	65	35.5	15.9	52
06DTMMI-26A	45	6	<100	200	19	11.5	3.5	37
06DTMMI-27A	58	192	<100	2440	16	10.8	3.4	412
06DTMMI-28A	168	80	<100	1940	235	144	32.9	118
06DTMMI-29A	1190	588	100	490	182	80.5	53.8	156
06DTMMI-30A	69	31	<100	860	30	23.4	5.5	136
06DTMMI-31A	103	51	<100	1410	16	8.3	5.5	70
06DTMMI-32A	157	10	<100	270	54	24.6	16	20
06DTMMI-33A	21	<5	<100	210	7	3	2.1	18
06DTMMI-34A	33	79	<100	640	12	6.3	2.2	134
06DTMMI-35A	33	33	<100	140	29	14.6	4.4	88
06DTMMI-37A	444	13	<100	70	106	48.8	25	29
06DTMMI-38A	219	15	<100	160	46	20.6	11.3	31
06DTMMI-36A	96	19	<100	80	19	8.5	4.7	49
06DTMMI-39A	376	16	<100	180	36	16.5	11.5	23

ANALYTE	Gd	La	Li	Mg	Mo	Nb	Nd	Ni
DETECTION	1	1	5	1	5	0.5	1	5
UNITS	PPB	PPB	PPB	PPM	PPB	PPB	PPB	PPB
06DTMMI-01A	2	6	9	<1	56	2.2	7	2520
06DTMMI-02A	42	66	36	4	173	2	128	3910
06DTMMI-03A	82	61	<5	10	18	<0.5	173	2390
06DTMMI-04A	124	69	<5	<1	<5	<0.5	326	231
06DTMMI-05A	70	21	<5	<1	7	<0.5	138	922
06DTMMI-06A								
06DTMMI-07A	148	246	<5	1	10	<0.5	391	1570
06DTMMI-08A	37	87	5	<1	15	1.1	114	87
06DTMMI-09A	23	18	5	33	20	<0.5	55	571
06DTMMI-10A	4	8	<5	37	16	<0.5	15	1240
06DTMMI-11A	59	96	8	33	41	<0.5	167	258
06DTMMI-12A	14	19	<5	63	11	<0.5	36	821
06DTMMI-13A	40	49	<5	<1	7	2.4	108	231
06DTMMI-14A	25	13	<5	<1	6	2.1	39	148
06DTMMI-15A	72	127	<5	<1	5	<0.5	188	407
06DTMMI-16A	203	274	<5	<1	7	1	555	1280
06DTMMI-17A	102	122	<5	3	6	2.1	260	424
06DTMMI-18A	30	27	<5	21	7	<0.5	70	2520
06DTMMI-19A	4	21	<5	5	8	1.4	20	1480
06DTMMI-20A	22	87	<5	5	7	0.6	86	332
06DTMMI-21A	83	128	<5	9	24	1.4	217	484
06DTMMI-22A	174	138	<5	7	46	<0.5	390	130
06DTMMI-23A	79	111	<5	<1	14	3.6	219	213
06DTMMI-24A	53	60	<5	15	105	<0.5	136	4750
06DTMMI-25A	74	102	<5	18	16	<0.5	199	833
06DTMMI-26A	16	19	<5	15	8	0.6	35	1530
06DTMMI-27A	15	29	<5	1	64	2.4	42	609
06DTMMI-28A	165	63	<5	<1	13	0.8	247	325
06DTMMI-29A	223	498	<5	<1	21	2.4	783	274
06DTMMI-30A	24	32	<5	6	97	<0.5	55	277
06DTMMI-31A	23	51	<5	19	41	0.6	78	516
06DTMMI-32A	70	87	<5	11	8	<0.5	193	222
06DTMMI-33A	9	10	<5	22	8	0.6	21	171
06DTMMI-34A	11	12	<5	6	15	1.4	26	604
06DTMMI-35A	22	10	<5	3	5	0.8	40	65
06DTMMI-37A	110	142	<5	1	<5	<0.5	361	52
06DTMMI-38A	53	61	<5	<1	<5	0.6	165	97
06DTMMI-36A	22	35	<5	4	<5	1.2	71	41
06DTMMI-39A	49	126	<5	<1	<5	1.4	210	75

ANALYTE	Pb	Pd	Pr	Rb	Sb	Sc	Sm	Sn
DETECTION	10	1	1	5	1	5	1	1
UNITS	PPB	PPB	PPB	PPB	PPB	PPB	PPB	PPB
06DTMMI-01A	20	<1	3	15	27	8	2	<1
06DTMMI-02A	1280	<1	34	260	45	50	34	<1
06DTMMI-03A	380	<1	38	207	7	40	60	<1
06DTMMI-04A	960	<1	68	176	2	167	93	<1
06DTMMI-05A	1200	<1	24	86	7	35	50	<1
06DTMMI-06A								
06DTMMI-07A	5110	<1	99	103	7	47	115	<1
06DTMMI-08A	14700	<1	32	148	10	34	31	<1
06DTMMI-09A	910	<1	12	87	3	5	18	<1
06DTMMI-10A	310	<1	4	51	4	<5	4	<1
06DTMMI-11A	25800	<1	41	82	13	69	50	<1
06DTMMI-12A	15600	<1	9	25	2	12	11	<1
06DTMMI-13A	7030	<1	26	97	5	34	31	<1
06DTMMI-14A	6360	<1	8	53	3	37	15	<1
06DTMMI-15A	4790	<1	46	122	3	15	51	<1
06DTMMI-16A	3710	<1	130	80	3	134	150	<1
06DTMMI-17A	2600	<1	57	80	2	44	73	<1
06DTMMI-18A	990	<1	14	51	2	<5	25	<1
06DTMMI-19A	19800	<1	7	25	2	<5	4	<1
06DTMMI-20A	159876	<1	23	40	2	7	19	<1
06DTMMI-21A	5030	<1	51	143	10	39	63	<1
06DTMMI-22A	49800	<1	73	163	5	67	128	<1
06DTMMI-23A	21100	<1	48	119	7	74	62	<1
06DTMMI-24A	2670	<1	26	32	14	43	39	<1
06DTMMI-25A	2500	<1	42	177	3	22	58	<1
06DTMMI-26A	2210	<1	8	158	1	30	12	<1
06DTMMI-27A	5130	<1	10	95	19	56	12	1
06DTMMI-28A	15400	1	41	149	6	145	99	<1
06DTMMI-29A	9400	<1	184	143	14	105	198	1
06DTMMI-30A	570	<1	12	<5	11	55	18	<1
06DTMMI-31A	480	<1	18	21	3	13	19	<1
06DTMMI-32A	700	<1	39	74	2	10	56	<1
06DTMMI-33A	140	<1	5	24	<1	<5	7	<1
06DTMMI-34A	950	<1	6	25	5	16	8	<1
06DTMMI-35A	3820	<1	7	8	2	13	15	<1
06DTMMI-37A	320	<1	75	69	<1	96	94	<1
06DTMMI-38A	590	<1	33	57	<1	28	44	<1
06DTMMI-36A	2250	<1	16	7	<1	13	19	<1
06DTMMI-39A	380	<1	49	85	<1	24	47	<1

ANALYTE	Sr	Ta	Tb	Te	Th	Ti	Tl	U
DETECTION	10	1	1	10	0.5	3	0.5	1
UNITS	PPB	PPB	PPB	PPB	PPB	PPB	PPB	PPB
06DTMMI-01A	10	<1	<1	<10	5.7	478	2.1	33
06DTMMI-02A	<10	<1	8	<10	119	436	14.8	110
06DTMMI-03A	90	<1	15	<10	22.7	76	5.6	143
06DTMMI-04A	<10	<1	21	<10	99.4	31	11.7	61
06DTMMI-05A	<10	<1	10	<10	21.5	28	5	68
06DTMMI-06A								
06DTMMI-07A	170	<1	27	<10	34.5	41	3.5	118
06DTMMI-08A	10	<1	8	<10	59.7	235	3.3	47
06DTMMI-09A	230	<1	4	<10	8.9	11	1.5	237
06DTMMI-10A	260	<1	<1	<10	1.4	<3	1.1	631
06DTMMI-11A	270	<1	10	<10	61.7	59	0.5	292
06DTMMI-12A	580	<1	2	<10	6.7	9	0.7	855
06DTMMI-13A	70	1	8	<10	55.7	242	1.9	63
06DTMMI-14A	<10	<1	6	<10	34	284	1.4	72
06DTMMI-15A	170	<1	13	<10	12.1	48	1.6	98
06DTMMI-16A	60	<1	37	<10	51.8	168	1.4	279
06DTMMI-17A	70	<1	19	<10	21.4	244	1.3	340
06DTMMI-18A	350	<1	5	<10	3.9	12	1.6	701
06DTMMI-19A	220	<1	<1	<10	4.9	107	1	185
06DTMMI-20A	90	<1	3	<10	6.9	83	2.5	52
06DTMMI-21A	140	2	15	<10	45.4	139	1.8	128
06DTMMI-22A	170	1	25	<10	60.7	19	4.1	155
06DTMMI-23A	100	1	13	<10	96.4	580	2.5	174
06DTMMI-24A	120	<1	8	<10	16.4	44	2	302
06DTMMI-25A	270	<1	11	<10	27.1	35	5.7	377
06DTMMI-26A	360	<1	3	<10	23.2	81	3.4	146
06DTMMI-27A	80	<1	3	<10	62.2	559	2.5	134
06DTMMI-28A	60	<1	33	<10	103	183	2.8	757
06DTMMI-29A	50	<1	35	<10	112	473	2.3	70
06DTMMI-30A	260	<1	4	<10	11.4	46	<0.5	1010
06DTMMI-31A	440	<1	3	<10	10.8	52	<0.5	217
06DTMMI-32A	300	<1	10	<10	27.8	49	1.2	78
06DTMMI-33A	580	<1	1	<10	6.9	24	<0.5	47
06DTMMI-34A	480	<1	2	<10	12.6	103	<0.5	47
06DTMMI-35A	150	<1	4	<10	25	133	<0.5	20
06DTMMI-37A	120	<1	18	<10	54.5	45	<0.5	57
06DTMMI-38A	130	<1	8	<10	32.4	94	0.8	22
06DTMMI-36A	140	<1	3	<10	25.3	177	<0.5	17
06DTMMI-39A	70	<1	7	<10	28.3	199	0.7	15

ANALYTE	W	Y	Yb	Zn	Zr
DETECTION	1	5	1	20	5
UNITS	PPB	PPB	PPB	PPB	PPB
06DTMMI-01A	<1	27	3	9860	56
06DTMMI-02A	2	261	14	11400	175
06DTMMI-03A	<1	527	31	11000	58
06DTMMI-04A	<1	652	59	730	79
06DTMMI-05A	<1	467	43	2750	28
06DTMMI-06A				0	
06DTMMI-07A	1	844	46	7810	59
06DTMMI-08A	1	181	6	970	156
06DTMMI-09A	<1	133	6	1420	17
06DTMMI-10A	<1	20	1	1350	13
06DTMMI-11A	<1	338	24	5920	98
06DTMMI-12A	<1	70	4	4060	10
06DTMMI-13A	2	276	14	760	111
06DTMMI-14A	<1	349	27	680	85
06DTMMI-15A	<1	567	27	1110	44
06DTMMI-16A	1	1830	132	6000	120
06DTMMI-17A	<1	976	70	2590	143
06DTMMI-18A	<1	124	6	8860	24
06DTMMI-19A	<1	21	2	10000	50
06DTMMI-20A	<1	182	9	154938	64
06DTMMI-21A	1	451	18	5100	95
06DTMMI-22A	2	1010	59	4440	69
06DTMMI-23A	2	414	26	11700	276
06DTMMI-24A	1	363	30	13800	75
06DTMMI-25A	<1	440	27	24000	108
06DTMMI-26A	<1	136	10	30000	77
06DTMMI-27A	2	97	9	1780	216
06DTMMI-28A	2	1780	110	3530	252
06DTMMI-29A	3	1100	52	3020	273
06DTMMI-30A	2	218	21	4670	47
06DTMMI-31A	<1	110	7	960	55
06DTMMI-32A	<1	335	16	1490	83
06DTMMI-33A	1	37	2	640	34
06DTMMI-34A	<1	67	5	1470	92
06DTMMI-35A	<1	160	10	1590	49
06DTMMI-37A	<1	639	32	1500	71
06DTMMI-38A	<1	217	14	820	45
06DTMMI-36A	<1	103	6	1130	65
06DTMMI-39A	<1	226	12	690	113

Interval C (20-30 cm)

ANALYTE	Ag	Al	As	Au	Ba	Bi	Ca	Cd
DETECTION	1	1	10	0.1	10	1	10	10
UNITS	PPB	PPM	PPB	PPB	PPB	PPB	PPM	PPB
06DTMMI-01A	1	240	30	<0.1	<10	<1	<10	<10
06DTMMI-02A	5	111	70	<0.1	970	5	80	20
06DTMMI-03A	42	89	80	0.1	1260	<1	130	1330
06DTMMI-04A	9	95	10	<0.1	110	<1	<10	10
06DTMMI-05A	8	77	20	<0.1	70	<1	<10	20
06DTMMI-06A								
06DTMMI-07A	30	98	40	<0.1	32100	<1	40	570
06DTMMI-08A	31	250	120	0.2	2250	<1	<10	10
06DTMMI-09A	45	15	<10	<0.1	3330	<1	200	140
06DTMMI-10A	27	25	20	<0.1	2250	<1	170	70
06DTMMI-11A	55	15	80	0.3	1140	<1	160	40
06DTMMI-12A	102	10	70	0.2	4490	<1	200	90
06DTMMI-13A	45	84	<10	<0.1	2360	<1	200	200
06DTMMI-14A	9	255	30	<0.1	1690	<1	<10	30
06DTMMI-15A	62	108	10	0.1	1550	<1	190	170
06DTMMI-16A	15	187	30	<0.1	2330	<1	80	70
06DTMMI-17A	45	172	10	<0.1	2170	<1	140	170
06DTMMI-18A	141	34	<10	0.3	14400	<1	380	180
06DTMMI-19A	38	61	<10	<0.1	2450	<1	330	380
06DTMMI-20A	293	20	<10	<0.1	1010	<1	110	1190
06DTMMI-21A	12	87	60	0.1	2500	<1	120	130
06DTMMI-22A	113	55	30	0.4	15200	<1	90	360
06DTMMI-23A	24	218	70	0.2	5490	1	60	260
06DTMMI-24A	29	38	20	0.3	1850	<1	220	280
06DTMMI-25A	71	62	<10	0.1	3300	<1	240	550
06DTMMI-26A	8	121	<10	<0.1	2690	<1	140	410
06DTMMI-27A	8	182	70	0.3	9660	<1	30	90
06DTMMI-28A	62	188	30	0.1	6510	<1	50	120
06DTMMI-29A	18	98	30	<0.1	19700	<1	70	410
06DTMMI-30A	2	44	160	<0.1	1380	1	240	<10
06DTMMI-31A	N.A.	N.A.	N.A.	N.A.	N.A.	N.A.	N.A.	N.A.
06DTMMI-32A	34	58	10	<0.1	1230	<1	180	140
06DTMMI-33A	5	23	<10	<0.1	2670	<1	380	10
06DTMMI-34A	11	39	10	<0.1	24400	<1	410	40
06DTMMI-35A	4	171	20	<0.1	4830	<1	80	70
06DTMMI-37A	6	95	<10	<0.1	1030	<1	210	40
06DTMMI-38A	4	184	<10	<0.1	1590	<1	50	40
06DTMMI-36A	3	159	<10	<0.1	3680	<1	70	70
06DTMMI-39A	3	200	<10	<0.1	1420	<1	40	50

ANALYTE	Ce	Co	Cr	Cu	Dy	Er	Eu	Fe
DETECTION	5	5	100	10	1	0.5	0.5	1
UNITS	PPB	PPB	PPB	PPB	PPB	PPB	PPB	PPM
06DTMMI-01A	17	93	<100	1070	3	2.6	0.7	52
06DTMMI-02A	199	80	<100	1180	58	29.4	13	89
06DTMMI-03A	237	165	<100	2890	94	51.9	21.8	59
06DTMMI-04A	1040	46	<100	800	275	164	53.7	61
06DTMMI-05A	335	104	<100	1410	71	43.7	17.9	86
06DTMMI-06A								
06DTMMI-07A	604	63	<100	1320	208	108	50.9	44
06DTMMI-08A	503	40	100	720	107	36.5	24	122
06DTMMI-09A	62	50	<100	3330	24	10.7	6.9	14
06DTMMI-10A	27	36	<100	790	8	3.2	2.8	21
06DTMMI-11A	416	253	<100	11100	91	55.7	25.3	84
06DTMMI-12A	158	30	<100	1340	31	14.5	9.8	47
06DTMMI-13A	181	<5	<100	820	104	63.7	21.9	25
06DTMMI-14A	36	31	<100	220	38	18.2	4.2	99
06DTMMI-15A	395	<5	<100	800	155	89.9	33	29
06DTMMI-16A	339	18	<100	640	62	31.7	13.8	74
06DTMMI-17A	329	29	<100	830	103	69.7	20.6	65
06DTMMI-18A	84	<5	<100	5860	41	20	12.5	14
06DTMMI-19A	36	5	<100	290	3	1.8	1.3	20
06DTMMI-20A	88	7	<100	710	16	9.9	5.2	21
06DTMMI-21A	420	40	<100	460	104	40.3	21.8	90
06DTMMI-22A	372	35	<100	2910	177	97.9	46.6	11
06DTMMI-23A	372	228	100	1140	89	44.2	21.7	198
06DTMMI-24A	106	3650	<100	10200	34	25.1	7.8	180
06DTMMI-25A	121	20	<100	2080	38	21.6	10.2	98
06DTMMI-26A	30	<5	<100	140	17	11.1	3.1	28
06DTMMI-27A	126	398	<100	2460	48	29.6	9.5	312
06DTMMI-28A	844	71	<100	1170	206	114	53.2	84
06DTMMI-29A	838	441	<100	1140	220	127	59.2	42
06DTMMI-30A	233	242	<100	710	29	16.2	8.5	149
06DTMMI-31A	N.A.	N.A.	N.A.	N.A.	N.A.	N.A.	N.A.	N.A.
06DTMMI-32A	92	6	<100	330	44	20.4	13	16
06DTMMI-33A	6	<5	<100	270	5	2	1.3	16
06DTMMI-34A	41	69	<100	650	13	6	2.7	61
06DTMMI-35A	163	26	<100	140	60	24.5	12.4	69
06DTMMI-37A	531	8	<100	40	104	46.6	31.6	15
06DTMMI-38A	405	18	<100	150	58	24.5	16.1	26
06DTMMI-36A	176	16	<100	130	57	23.3	12.1	49
06DTMMI-39A	343	35	<100	140	67	29	16.4	45

ANALYTE	Gd	La	Li	Mg	Mo	Nb	Nd	Ni
DETECTION	1	1	5	1	5	0.5	1	5
UNITS	PPB	PPB	PPB	PPM	PPB	PPB	PPB	PPB
06DTMMI-01A	2	5	9	<1	56	2	7	2740
06DTMMI-02A	61	61	9	10	227	1.5	173	1450
06DTMMI-03A	103	78	<5	9	31	0.5	225	2900
06DTMMI-04A	290	256	<5	<1	6	<0.5	782	268
06DTMMI-05A	88	103	<5	<1	11	<0.5	250	581
06DTMMI-06A								
06DTMMI-07A	240	287	<5	2	16	<0.5	575	1790
06DTMMI-08A	106	198	20	2	36	1.6	301	202
06DTMMI-09A	33	20	7	43	28	<0.5	69	1080
06DTMMI-10A	12	8	<5	30	17	<0.5	25	312
06DTMMI-11A	106	156	7	25	47	<0.5	294	1160
06DTMMI-12A	44	51	<5	33	42	<0.5	108	255
06DTMMI-13A	106	144	<5	<1	<5	<0.5	247	315
06DTMMI-14A	22	11	<5	<1	8	1.2	32	142
06DTMMI-15A	163	297	<5	<1	5	<0.5	444	457
06DTMMI-16A	64	199	<5	1	10	1.2	222	864
06DTMMI-17A	102	191	<5	5	6	1.6	306	532
06DTMMI-18A	57	61	<5	38	7	<0.5	135	4090
06DTMMI-19A	5	17	<5	10	11	0.6	19	2220
06DTMMI-20A	22	71	<5	8	6	<0.5	79	331
06DTMMI-21A	104	160	<5	6	19	1.1	269	358
06DTMMI-22A	215	177	<5	6	24	<0.5	490	253
06DTMMI-23A	98	165	<5	1	22	3.8	293	374
06DTMMI-24A	37	44	<5	23	102	<0.5	92	7550
06DTMMI-25A	47	62	<5	17	12	<0.5	129	2770
06DTMMI-26A	14	13	<5	12	7	<0.5	28	1200
06DTMMI-27A	46	53	<5	2	34	1.9	110	510
06DTMMI-28A	238	386	<5	<1	14	0.9	672	287
06DTMMI-29A	266	491	<5	2	12	<0.5	791	425
06DTMMI-30A	33	89	<5	6	295	1.1	119	1850
06DTMMI-31A	N.A.	N.A.	N.A.	N.A.	N.A.	N.A.	N.A.	N.A.
06DTMMI-32A	57	55	<5	10	6	<0.5	145	260
06DTMMI-33A	6	4	<5	23	20	<0.5	12	222
06DTMMI-34A	15	19	<5	14	11	<0.5	39	321
06DTMMI-35A	61	55	<5	4	6	0.5	143	92
06DTMMI-37A	136	236	<5	3	<5	<0.5	479	73
06DTMMI-38A	71	143	<5	<1	<5	0.9	264	90
06DTMMI-36A	57	57	<5	4	<5	<0.5	140	71
06DTMMI-39A	71	94	<5	<1	6	0.7	224	101

ANALYTE	Pb	Pd	Pr	Rb	Sb	Sc	Sm	Sn
DETECTION	10	1	1	5	1	5	1	1
UNITS	PPB	PPB	PPB	PPB	PPB	PPB	PPB	PPB
06DTMMI-01A	20	<1	2	20	20	8	2	<1
06DTMMI-02A	2070	1	41	217	137	71	48	1
06DTMMI-03A	740	<1	49	193	14	66	77	<1
06DTMMI-04A	1650	<1	182	158	3	198	207	<1
06DTMMI-05A	2180	<1	58	134	7	66	68	<1
06DTMMI-06A								
06DTMMI-07A	5080	<1	137	127	10	77	178	<1
06DTMMI-08A	25700	1	84	197	30	98	84	1
06DTMMI-09A	3560	<1	13	95	4	6	25	<1
06DTMMI-10A	1480	<1	5	141	3	<5	9	<1
06DTMMI-11A	15800	1	70	78	20	113	85	<1
06DTMMI-12A	29300	<1	23	18	8	14	34	<1
06DTMMI-13A	1340	<1	56	85	1	27	74	<1
06DTMMI-14A	9790	<1	7	153	4	21	13	<1
06DTMMI-15A	5060	<1	109	101	3	31	118	<1
06DTMMI-16A	9280	<1	63	51	5	43	51	<1
06DTMMI-17A	2170	<1	74	90	2	37	76	<1
06DTMMI-18A	10600	<1	29	15	2	9	46	<1
06DTMMI-19A	11500	<1	6	63	1	<5	5	<1
06DTMMI-20A	142128	<1	20	90	1	6	18	<1
06DTMMI-21A	6870	<1	64	118	10	44	80	<1
06DTMMI-22A	33200	<1	94	161	4	103	161	<1
06DTMMI-23A	24900	<1	67	134	13	92	80	<1
06DTMMI-24A	6970	<1	18	69	8	47	28	<1
06DTMMI-25A	1220	<1	27	110	2	24	38	<1
06DTMMI-26A	1200	<1	6	100	1	20	10	<1
06DTMMI-27A	13600	1	23	108	21	78	34	1
06DTMMI-28A	9220	<1	145	127	7	151	188	<1
06DTMMI-29A	15600	<1	175	63	8	125	215	<1
06DTMMI-30A	1830	<1	29	8	61	38	28	<1
06DTMMI-31A	N.A.	N.A.	N.A.	N.A.	N.A.	N.A.	N.A.	N.A.
06DTMMI-32A	550	<1	27	88	1	7	45	<1
06DTMMI-33A	80	<1	3	19	<1	<5	5	<1
06DTMMI-34A	610	<1	8	21	3	5	12	<1
06DTMMI-35A	7220	<1	29	19	3	16	46	<1
06DTMMI-37A	160	<1	101	49	<1	23	124	<1
06DTMMI-38A	980	<1	58	91	1	30	64	<1
06DTMMI-36A	7060	<1	29	9	2	14	44	<1
06DTMMI-39A	1030	<1	47	105	2	39	61	<1

ANALYTE	Sr	Ta	Tb	Te	Th	Ti	Tl	U
DETECTION	10	1	1	10	0.5	3	0.5	1
UNITS	PPB	PPB	PPB	PPB	PPB	PPB	PPB	PPB
06DTMMI-01A	<10	<1	<1	<10	5.8	410	1.3	31
06DTMMI-02A	10	<1	11	<10	151	341	6.7	195
06DTMMI-03A	80	<1	18	<10	33.3	129	4.8	201
06DTMMI-04A	<10	<1	52	<10	159	72	8.6	71
06DTMMI-05A	<10	<1	14	<10	71.2	104	8.8	63
06DTMMI-06A								
06DTMMI-07A	170	<1	42	<10	42.6	57	3.8	192
06DTMMI-08A	50	<1	22	<10	95.9	531	5.3	72
06DTMMI-09A	270	<1	5	<10	6.4	65	1.7	245
06DTMMI-10A	240	<1	2	<10	6.1	39	1.8	377
06DTMMI-11A	150	<1	18	<10	68.7	44	1.2	483
06DTMMI-12A	330	<1	7	<10	17.4	53	1.6	248
06DTMMI-13A	190	<1	19	<10	7.7	5	1	106
06DTMMI-14A	<10	<1	6	<10	29.3	168	2	60
06DTMMI-15A	160	<1	29	<10	17.5	35	1.3	123
06DTMMI-16A	110	<1	12	<10	49.1	214	1.2	85
06DTMMI-17A	90	<1	18	<10	20.3	226	1.3	337
06DTMMI-18A	570	<1	9	<10	8.1	5	0.8	1620
06DTMMI-19A	370	<1	<1	<10	4.4	48	2.1	380
06DTMMI-20A	140	<1	3	<10	8.2	69	3	70
06DTMMI-21A	110	2	18	<10	56.7	126	1.5	132
06DTMMI-22A	160	1	32	<10	68.1	21	4	144
06DTMMI-23A	90	1	16	<10	110	714	3.3	227
06DTMMI-24A	210	<1	6	<10	10.1	36	5.2	671
06DTMMI-25A	290	<1	7	<10	12.1	43	10.2	998
06DTMMI-26A	250	<1	3	<10	16.1	44	2.8	137
06DTMMI-27A	120	<1	8	<10	70.3	458	3.5	110
06DTMMI-28A	70	<1	36	<10	126	218	2.9	584
06DTMMI-29A	150	<1	39	<10	66.2	82	1.5	87
06DTMMI-30A	170	<1	5	<10	27.6	186	<0.5	321
06DTMMI-31A	N.A.	N.A.	N.A.	N.A.	N.A.	N.A.	N.A.	N.A.
06DTMMI-32A	240	<1	8	<10	11.8	77	1	71
06DTMMI-33A	670	<1	<1	<10	10.4	13	<0.5	60
06DTMMI-34A	760	<1	2	<10	11.1	11	<0.5	57
06DTMMI-35A	180	<1	11	<10	37	97	<0.5	34
06DTMMI-37A	290	<1	20	<10	24.2	33	<0.5	81
06DTMMI-38A	110	<1	11	<10	39.8	118	0.9	24
06DTMMI-36A	130	<1	10	<10	30.3	54	<0.5	28
06DTMMI-39A	110	<1	12	<10	44.8	128	0.7	26

ANALYTE	W	Y	Yb	Zn	Zr
DETECTION	1	5	1	20	5
UNITS	PPB	PPB	PPB	PPB	PPB
06DTMMI-01A	<1	27	3	9880	56
06DTMMI-02A	3	399	21	2880	189
06DTMMI-03A	1	664	42	12400	91
06DTMMI-04A	1	1810	142	740	97
06DTMMI-05A	<1	636	39	1290	44
06DTMMI-06A					
06DTMMI-07A	2	1320	83	9330	77
06DTMMI-08A	3	597	17	2830	303
06DTMMI-09A	<1	159	8	2900	17
06DTMMI-10A	<1	48	2	2050	11
06DTMMI-11A	1	680	54	11100	166
06DTMMI-12A	<1	218	11	4130	42
06DTMMI-13A	1	847	45	1920	20
06DTMMI-14A	<1	240	11	620	68
06DTMMI-15A	<1	1170	68	1160	46
06DTMMI-16A	<1	485	25	3170	111
06DTMMI-17A	<1	881	58	2660	121
06DTMMI-18A	<1	286	16	5880	40
06DTMMI-19A	<1	26	2	16600	28
06DTMMI-20A	<1	172	9	176113	42
06DTMMI-21A	3	589	24	4710	114
06DTMMI-22A	2	1250	80	5750	76
06DTMMI-23A	2	588	31	12100	312
06DTMMI-24A	1	329	24	19400	54
06DTMMI-25A	<1	257	19	27400	79
06DTMMI-26A	<1	111	10	21200	41
06DTMMI-27A	2	306	24	4910	231
06DTMMI-28A	2	1430	91	3200	284
06DTMMI-29A	2	1770	102	4130	120
06DTMMI-30A	2	179	14	1950	101
06DTMMI-31A	N.A.	N.A.	N.A.	N.A.	N.A.
06DTMMI-32A	<1	276	13	1890	64
06DTMMI-33A	<1	27	2	800	34
06DTMMI-34A	<1	72	4	780	33
06DTMMI-35A	<1	324	14	1500	46
06DTMMI-37A	<1	571	31	930	51
06DTMMI-38A	<1	291	16	790	89
06DTMMI-36A	<1	313	13	1450	29
06DTMMI-39A	<1	385	18	1620	63

Interval D (30-40 cm)

ANALYTE	Ag	Al	As	Au	Ba	Bi	Ca	Cd
DETECTION	1	1	10	0.1	10	1	10	10
UNITS	PPB	PPM	PPB	PPB	PPB	PPB	PPM	PPB
06DTMMI-01A	<1	181	<10	<0.1	<10	<1	20	<10
06DTMMI-02A	4	126	170	0.1	620	11	70	50
06DTMMI-03A	3	120	30	0.1	1880	<1	70	150
06DTMMI-04A	14	78	30	0.2	190	<1	<10	10
06DTMMI-05A	9	90	50	<0.1	70	<1	<10	30
06DTMMI-06A								
06DTMMI-07A	25	109	30	<0.1	31600	<1	50	490
06DTMMI-08A	56	211	130	0.2	2380	1	<10	40
06DTMMI-09A	42	12	<10	<0.1	3150	<1	200	120
06DTMMI-10A	67	26	10	<0.1	1880	<1	150	50
06DTMMI-11A	54	9	60	0.1	830	<1	150	60
06DTMMI-12A	182	12	50	0.3	5530	<1	220	100
06DTMMI-13A	53	78	<10	<0.1	2000	<1	230	240
06DTMMI-14A	16	278	40	<0.1	1300	<1	<10	20
06DTMMI-15A	34	104	10	<0.1	1860	<1	180	100
06DTMMI-16A	19	191	20	0.1	1960	<1	40	70
06DTMMI-17A	59	91	10	<0.1	1700	<1	210	160
06DTMMI-18A	207	18	10	0.4	11100	<1	290	110
06DTMMI-19A	17	97	<10	<0.1	5420	<1	310	340
06DTMMI-20A	230	21	<10	<0.1	1690	<1	150	1720
06DTMMI-21A	74	98	30	0.2	6450	<1	230	810
06DTMMI-22A	105	43	20	0.5	22700	<1	120	450
06DTMMI-23A	14	227	10	<0.1	2380	<1	10	110
06DTMMI-24A	69	19	20	<0.1	1430	<1	220	490
06DTMMI-25A	84	32	50	0.2	2510	<1	240	370
06DTMMI-26A	10	102	<10	<0.1	2450	<1	190	520
06DTMMI-27A								
06DTMMI-28A								
06DTMMI-29A	74	45	<10	0.2	47800	<1	190	700
06DTMMI-30A	6	58	630	0.2	2430	3	230	30
06DTMMI-31A	N.A.	N.A.	N.A.	N.A.	N.A.	N.A.	N.A.	N.A.
06DTMMI-32A	98	29	20	<0.1	1760	<1	190	260
06DTMMI-33A	6	14	<10	<0.1	2210	<1	340	20
06DTMMI-34A	14	30	<10	<0.1	25400	<1	420	40
06DTMMI-35A	3	143	10	<0.1	4160	<1	70	60
06DTMMI-37A	8	121	10	<0.1	710	<1	140	40
06DTMMI-38A	4	120	<10	<0.1	1290	<1	80	50
06DTMMI-36A	5	145	30	<0.1	4400	<1	70	70
06DTMMI-39A	7	163	10	<0.1	1420	<1	80	60

ANALYTE	Ce	Co	Cr	Cu	Dy	Er	Eu	Fe
DETECTION	5	5	100	10	1	0.5	0.5	1
UNITS	PPB	PPB	PPB	PPB	PPB	PPB	PPB	PPM
06DTMMI-01A	<5	455	<100	60	<1	0.7	<0.5	47
06DTMMI-02A	260	175	100	1850	108	55.1	23.6	145
06DTMMI-03A	50	259	<100	3240	33	23.6	5.8	236
06DTMMI-04A	1190	42	<100	960	348	203	67.6	89
06DTMMI-05A	395	253	<100	1530	101	58.9	24.5	167
06DTMMI-06A								
06DTMMI-07A	546	61	<100	1360	164	84.7	40.9	56
06DTMMI-08A	673	51	<100	1440	230	110	53.6	125
06DTMMI-09A	57	55	<100	3380	18	8	5.8	13
06DTMMI-10A	35	39	<100	890	16	5.9	5.3	15
06DTMMI-11A	199	216	<100	6720	52	30.7	14.3	52
06DTMMI-12A	200	132	<100	3680	34	20	10.7	40
06DTMMI-13A	205	<5	<100	1210	97	60.2	22.3	22
06DTMMI-14A	70	28	<100	240	36	16.3	4.5	109
06DTMMI-15A	174	5	<100	770	71	43.4	15.5	41
06DTMMI-16A	510	21	<100	850	95	42.2	19.9	58
06DTMMI-17A	161	10	<100	1170	77	52.7	15.8	43
06DTMMI-18A	72	14	<100	6760	69	33.4	18	10
06DTMMI-19A	55	8	<100	190	8	4.4	2.4	34
06DTMMI-20A	78	10	<100	530	15	8.4	4.8	36
06DTMMI-21A	285	41	<100	1620	87	48.5	23.3	48
06DTMMI-22A	222	22	<100	2970	131	70.6	34.5	6
06DTMMI-23A	50	13	<100	230	22	12.6	3.9	83
06DTMMI-24A	56	297	<100	2650	18	11.4	4.5	29
06DTMMI-25A	128	175	<100	2460	44	25.9	11.6	169
06DTMMI-26A	54	<5	<100	200	21	11.9	4.7	25
06DTMMI-27A								
06DTMMI-28A								
06DTMMI-29A	210	32	<100	2100	125	77.2	27.7	13
06DTMMI-30A	1110	319	<100	3390	116	53.8	33.4	175
06DTMMI-31A	N.A.	N.A.	N.A.	N.A.	N.A.	N.A.	N.A.	N.A.
06DTMMI-32A	60	16	<100	420	70	30.8	19.6	20
06DTMMI-33A	6	<5	<100	250	5	2.1	1.2	29
06DTMMI-34A	25	49	<100	600	11	5.2	1.5	30
06DTMMI-35A	245	15	<100	110	59	23.9	13	50
06DTMMI-37A	1080	14	<100	80	179	84	52.2	23
06DTMMI-38A	740	12	<100	110	88	38.6	25.7	22
06DTMMI-36A	244	36	<100	160	71	27.4	14.8	61
06DTMMI-39A	549	21	<100	150	93	41.6	25.4	37

ANALYTE	Gd	La	Li	Mg	Mo	Nb	Nd	Ni
DETECTION	1	1	5	1	5	0.5	1	5
UNITS	PPB	PPB	PPB	PPM	PPB	PPB	PPB	PPB
06DTMMI-01A	<1	<1	9	5	14	<0.5	<1	3920
06DTMMI-02A	109	68	13	10	519	5.2	280	2820
06DTMMI-03A	28	15	<5	10	54	<0.5	45	4190
06DTMMI-04A	351	302	<5	<1	10	1.3	957	247
06DTMMI-05A	115	81	<5	<1	20	0.6	292	637
06DTMMI-06A								
06DTMMI-07A	191	265	<5	1	16	<0.5	484	2040
06DTMMI-08A	239	241	10	<1	42	1.6	617	220
06DTMMI-09A	26	20	6	39	22	<0.5	64	1200
06DTMMI-10A	24	17	<5	20	11	<0.5	50	292
06DTMMI-11A	61	72	5	19	55	<0.5	146	1360
06DTMMI-12A	47	72	<5	39	65	<0.5	135	419
06DTMMI-13A	107	153	<5	<1	<5	<0.5	261	197
06DTMMI-14A	22	27	<5	<1	12	0.5	44	122
06DTMMI-15A	76	174	<5	<1	6	0.5	239	720
06DTMMI-16A	93	292	<5	<1	10	1.3	311	635
06DTMMI-17A	80	114	<5	11	<5	<0.5	212	854
06DTMMI-18A	88	62	<5	28	11	<0.5	173	1850
06DTMMI-19A	10	22	<5	28	13	<0.5	30	1030
06DTMMI-20A	20	45	<5	13	6	<0.5	63	480
06DTMMI-21A	104	143	<5	22	20	0.9	292	1230
06DTMMI-22A	162	106	<5	10	32	<0.5	335	259
06DTMMI-23A	17	21	<5	<1	7	2.6	41	117
06DTMMI-24A	21	21	<5	22	48	<0.5	49	3740
06DTMMI-25A	53	77	<5	14	32	<0.5	155	1590
06DTMMI-26A	21	22	<5	13	11	<0.5	55	1200
06DTMMI-27A								
06DTMMI-28A								
06DTMMI-29A	143	122	<5	3	5	<0.5	302	532
06DTMMI-30A	134	290	<5	6	1020	2.6	465	3120
06DTMMI-31A	N.A.	N.A.	N.A.	N.A.	N.A.	N.A.	N.A.	N.A.
06DTMMI-32A	90	67	<5	13	9	<0.5	188	245
06DTMMI-33A	5	2	<5	21	34	<0.5	8	272
06DTMMI-34A	13	10	<5	21	9	<0.5	26	238
06DTMMI-35A	62	87	<5	4	8	<0.5	178	67
06DTMMI-37A	229	643	<5	2	<5	<0.5	919	107
06DTMMI-38A	106	359	<5	<1	<5	<0.5	439	87
06DTMMI-36A	72	83	<5	3	11	0.5	174	109
06DTMMI-39A	106	229	<5	<1	7	0.6	388	125

ANALYTE	Pb	Pd	Pr	Rb	Sb	Sc	Sm	Sn
DETECTION	10	1	1	5	1	5	1	1
UNITS	PPB	PPB	PPB	PPB	PPB	PPB	PPB	PPB
06DTMMI-01A	<10	<1	<1	8	8	<5	<1	<1
06DTMMI-02A	2660	2	63	179	423	134	87	4
06DTMMI-03A	310	<1	10	122	14	49	18	<1
06DTMMI-04A	1880	<1	221	200	6	195	261	<1
06DTMMI-05A	3530	<1	63	143	14	91	93	<1
06DTMMI-06A								
06DTMMI-07A	5700	<1	118	133	9	77	147	<1
06DTMMI-08A	25800	2	146	160	37	168	182	<1
06DTMMI-09A	4670	<1	13	100	3	<5	21	<1
06DTMMI-10A	1840	<1	11	132	2	6	18	<1
06DTMMI-11A	14600	<1	33	59	26	42	46	6
06DTMMI-12A	53400	<1	31	13	11	21	37	<1
06DTMMI-13A	990	<1	58	104	1	22	76	<1
06DTMMI-14A	11400	<1	11	163	7	24	15	<1
06DTMMI-15A	2420	<1	61	79	2	16	58	<1
06DTMMI-16A	8380	<1	91	116	6	49	75	3
06DTMMI-17A	1260	<1	47	112	1	17	57	<1
06DTMMI-18A	10400	<1	33	19	2	25	65	<1
06DTMMI-19A	11600	<1	8	82	1	9	8	<1
06DTMMI-20A	117108	<1	16	130	2	8	17	<1
06DTMMI-21A	11100	<1	62	86	6	40	85	<1
06DTMMI-22A	27400	<1	59	128	2	48	115	<1
06DTMMI-23A	33100	<1	9	63	2	39	13	<1
06DTMMI-24A	3130	<1	9	60	4	11	16	<1
06DTMMI-25A	2320	<1	32	100	5	29	43	<1
06DTMMI-26A	1020	<1	12	105	1	18	17	<1
06DTMMI-27A								
06DTMMI-28A								
06DTMMI-29A	13700	<1	57	20	2	42	100	<1
06DTMMI-30A	13500	2	110	38	194	118	120	2
06DTMMI-31A	N.A.	N.A.	N.A.	N.A.	N.A.	N.A.	N.A.	N.A.
06DTMMI-32A	790	<1	34	129	2	5	65	<1
06DTMMI-33A	110	<1	2	17	1	<5	4	<1
06DTMMI-34A	340	<1	5	19	2	<5	9	<1
06DTMMI-35A	8940	<1	39	<5	4	15	51	<1
06DTMMI-37A	340	<1	216	64	<1	90	212	<1
06DTMMI-38A	1720	<1	112	102	2	35	97	<1
06DTMMI-36A	8960	<1	38	18	7	19	55	<1
06DTMMI-39A	1820	<1	89	125	3	46	94	<1

ANALYTE	Sr	Ta	Tb	Te	Th	Ti	Tl	U
DETECTION	10	1	1	10	0.5	3	0.5	1
UNITS	PPB	PPB	PPB	PPB	PPB	PPB	PPB	PPB
06DTMMI-01A	40	<1	<1	<10	1.3	14	0.9	11
06DTMMI-02A	<10	<1	21	<10	307	1340	4.1	392
06DTMMI-03A	90	<1	6	<10	19.1	70	2	200
06DTMMI-04A	<10	<1	65	<10	168	182	9.4	86
06DTMMI-05A	<10	<1	20	<10	103	145	9.7	95
06DTMMI-06A								
06DTMMI-07A	170	<1	34	<10	47.3	74	3.2	182
06DTMMI-08A	60	<1	45	<10	121	466	5.3	108
06DTMMI-09A	270	<1	4	<10	6.1	13	1.8	212
06DTMMI-10A	180	<1	4	<10	4	23	0.8	380
06DTMMI-11A	130	<1	10	<10	45.1	37	1.7	535
06DTMMI-12A	360	<1	7	<10	22.2	46	1.4	333
06DTMMI-13A	140	<1	18	<10	9.3	13	1.1	124
06DTMMI-14A	<10	<1	6	<10	40.3	138	1.8	67
06DTMMI-15A	180	<1	13	<10	19.9	78	1.3	112
06DTMMI-16A	60	<1	19	<10	44.7	259	2	89
06DTMMI-17A	210	<1	14	<10	8.2	38	1	457
06DTMMI-18A	460	<1	15	<10	34.6	6	0.9	455
06DTMMI-19A	480	<1	2	<10	3.8	20	1.7	443
06DTMMI-20A	210	<1	3	<10	14.3	49	3.4	125
06DTMMI-21A	260	2	16	<10	34.2	77	2.2	286
06DTMMI-22A	220	1	24	<10	46.4	10	3.7	157
06DTMMI-23A	40	1	3	<10	43.3	457	1.4	89
06DTMMI-24A	210	<1	3	<10	7.7	18	4.9	347
06DTMMI-25A	250	<1	8	<10	20.1	47	7.1	458
06DTMMI-26A	250	<1	3	<10	11.2	35	2.4	133
06DTMMI-27A								
06DTMMI-28A								
06DTMMI-29A	390	<1	21	<10	18.7	8	0.6	130
06DTMMI-30A	170	<1	21	<10	132	426	<0.5	208
06DTMMI-31A	N.A.	N.A.	N.A.	N.A.	N.A.	N.A.	N.A.	N.A.
06DTMMI-32A	330	<1	13	<10	10.8	44	1.1	136
06DTMMI-33A	550	<1	<1	<10	9.3	10	<0.5	66
06DTMMI-34A	820	<1	2	<10	7.3	<3	<0.5	125
06DTMMI-35A	110	<1	10	<10	44.5	79	<0.5	32
06DTMMI-37A	150	<1	33	<10	70	47	<0.5	111
06DTMMI-38A	130	<1	17	<10	38.7	58	1	25
06DTMMI-36A	150	<1	13	<10	45.1	118	<0.5	40
06DTMMI-39A	120	<1	17	<10	47.5	121	1.3	32

ANALYTE	W	Y	Yb	Zn	Zr
DETECTION	1	5	1	20	5
UNITS	PPB	PPB	PPB	PPB	PPB
06DTMMI-01A	<1	8	1	20900	<5
06DTMMI-02A	39	669	41	10200	373
06DTMMI-03A	1	268	21	3990	77
06DTMMI-04A	2	2260	170	730	114
06DTMMI-05A	<1	714	52	1550	80
06DTMMI-06A					
06DTMMI-07A	1	1030	67	10000	95
06DTMMI-08A	4	1430	64	3300	322
06DTMMI-09A	<1	124	6	3330	14
06DTMMI-10A	<1	93	4	2710	9
06DTMMI-11A	<1	377	28	11200	68
06DTMMI-12A	<1	282	17	3650	50
06DTMMI-13A	<1	828	45	1010	22
06DTMMI-14A	<1	219	9	540	110
06DTMMI-15A	<1	636	35	1540	82
06DTMMI-16A	<1	678	27	2460	147
06DTMMI-17A	<1	751	43	2950	43
06DTMMI-18A	<1	428	26	5000	73
06DTMMI-19A	<1	56	4	6310	35
06DTMMI-20A	<1	134	8	224252	41
06DTMMI-21A	2	519	40	34500	111
06DTMMI-22A	2	823	54	6690	37
06DTMMI-23A	1	124	10	7300	138
06DTMMI-24A	<1	154	11	24400	25
06DTMMI-25A	1	341	23	29200	79
06DTMMI-26A	<1	146	10	24700	42
06DTMMI-27A				N.A.	
06DTMMI-28A				N.A.	
06DTMMI-29A	<1	958	70	4810	52
06DTMMI-30A	8	662	43	15600	433
06DTMMI-31A	N.A.	N.A.	N.A.	N.A.	N.A.
06DTMMI-32A	1	413	19	2950	38
06DTMMI-33A	<1	27	2	1790	27
06DTMMI-34A	<1	63	4	750	22
06DTMMI-35A	<1	314	14	1520	46
06DTMMI-37A	<1	1030	58	1450	94
06DTMMI-38A	<1	541	24	1040	59
06DTMMI-36A	2	390	15	1770	60
06DTMMI-39A	1	605	27	1380	72

Appendix F: Till Geochemistry Data

MMI Sample #	Ag	Al	As	Au	Ba	Be	Bi
Units	ppm	ppm	ppm	ppm	ppm	ppm	ppm
06DTMMI-01A	0.25	57300	7	-99	650	0.9	1
06DTMMI-02A	0.25	49200	2.5	-99	4780	1.6	1
06DTMMI-03A	1	58200	30	-99	3460	1.9	1
06DTMMI-04A	0.25	49500	28	-99	3150	1.7	1
06DTMMI-05A	0.25	40100	26	-99	3190	1.4	1
06DTMMI-06A	0.25	51700	26	-99	2230	1.5	3
06DTMMI-07A	0.5	52300	26	-99	5320	1.9	2
06DTMMI-08A	0.25	52800	22	-99	2210	1.6	1
06DTMMI-09A	0.6	61600	11	-99	3100	2.3	2
06DTMMI-10A	0.5	57100	17	-99	3800	1.7	1
06DTMMI-11A	1.3	60500	29	-99	4380	2.2	1
06DTMMI-12A	1.3	54100	20	-99	3320	1.9	1
06DTMMI-13A	1	55200	24	-99	2330	3.1	1
06DTMMI-14A	0.25	55700	37	-99	3740	2.2	1
06DTMMI-15A	0.5	56200	23	-99	2180	2.6	1
06DTMMI-16A	0.25	52200	19	-99	2290	2	1
06DTMMI-17A	0.7	59000	32	-99	2760	3.4	1
06DTMMI-18A	0.7	62200	10	-99	4000	2.5	1
06DTMMI-19A	0.5	54200	20	-99	3140	1.4	1
06DTMMI-20A	4.3	41200	41	-99	1550	1.9	1
06DTMMI-21A	0.7	52000	20	-99	3300	1.9	2
06DTMMI-22A	0.6	56000	43	-99	4040	2.2	2
06DTMMI-23A	0.25	58400	16	-99	2710	1.9	1
06DTMMI-24A	1.4	55700	27	-99	4010	2.3	1
06DTMMI-25A	0.7	53600	27	-99	4270	2.5	1
06DTMMI-26A	0.25	57800	6	-99	2290	1.6	1
06DTMMI-27A	0.25	68200	20	-99	2790	2.3	1
06DTMMI-28A	0.8	56600	20	-99	3050	2	1
06DTMMI-29A	0.25	49400	27	-99	2200	1.8	1
06DTMMI-30A	0.25	55300	9	-99	2510	1.9	1
06DTMMI-31A	0.25	56900	23	-99	1880	1.7	1
06DTMMI-32A	0.6	53900	15	-99	1890	1.7	1
06DTMMI-33A	0.25	54600	6	-99	1540	1.4	1
06DTMMI-34A	0.25	55300	12	-99	3180	1.7	1
06DTMMI-35A	0.25	50800	30	-99	2740	1.8	1
06DTMMI-37A	0.25	49800	26	-99	840	1.9	1
06DTMMI-38A	0.25	59700	38	-99	2150	2.1	1

MMI Sample #	Ca	Cd	Co	Cr	Cu	Fe	Hg
Units	ppm	ppm	ppm	ppm	ppm	ppm	ppm
06DTMMI-01A	14200	4.7	7	6	69	12000	-99
06DTMMI-02A	1600	0.6	3	78	17	8000	-99
06DTMMI-03A	4600	11.9	10	86	74	29100	-99
06DTMMI-04A	1300	0.25	48	82	47	103500	-99
06DTMMI-05A	600	0.25	19	70	53	171000	-99
06DTMMI-06A	1300	0.7	7	73	30	38300	-99
06DTMMI-07A	3000	4.2	9	78	45	28500	-99
06DTMMI-08A	4300	0.6	7	62	33	28300	-99
06DTMMI-09A	4900	1.1	5	84	33	21300	-99
06DTMMI-10A	6100	1.2	6	63	32	21400	-99
06DTMMI-11A	6700	1.3	5	92	78	28800	-99
06DTMMI-12A	7600	1.3	5	68	44	24500	-99
06DTMMI-13A	18300	2.2	11	103	66	44800	-99
06DTMMI-14A	3400	0.5	10	94	56	46400	-99
06DTMMI-15A	6800	1.4	9	85	50	34200	-99
06DTMMI-16A	4700	0.7	6	76	52	33300	-99
06DTMMI-17A	17400	1.6	15	117	80	37700	-99
06DTMMI-18A	2800	0.25	2	79	19	14400	-99
06DTMMI-19A	8200	2.4	6	69	16	28000	-99
06DTMMI-20A	28000	49.3	5	37	53	26100	-99
06DTMMI-21A	4700	3	6	70	45	26300	-99
06DTMMI-22A	3800	3.4	9	82	84	35800	-99
06DTMMI-23A	3400	1.7	4	73	25	22500	-99
06DTMMI-24A	8500	7.6	17	79	86	40700	-99
06DTMMI-25A	5400	3.6	5	105	47	36600	-99
06DTMMI-26A	9900	3.7	5	58	23	21000	-99
06DTMMI-27A	1200	0.7	4	116	32	27400	-99
06DTMMI-28A	3600	1.7	7	82	43	29600	-99
06DTMMI-29A	2500	1.2	9	69	41	30800	-99
06DTMMI-30A	3400	1.3	7	71	23	13600	-99
06DTMMI-31A	10800	0.25	6	68	19	34300	-99
06DTMMI-32A	8100	1.9	7	58	30	25600	-99
06DTMMI-33A	13000	0.5	6	54	19	27500	-99
06DTMMI-34A	5700	0.5	4	75	22	22200	-99
06DTMMI-35A	2800	0.9	6	79	36	33800	-99
06DTMMI-37A	5800	0.25	11	47	21	37800	-99
06DTMMI-38A	4300	1	11	73	39	37700	-99

MMI Sample #	K	Mg	Mn	Mo	Na	Ni	Pb
Units	ppm	ppm	ppm	ppm	ppm	ppm	ppm
06DTMMI-01A	13700	4300	251	3	17900	53	8
06DTMMI-02A	19500	5300	42	5	1400	33	112
06DTMMI-03A	21800	6400	323	13	2700	110	87
06DTMMI-04A	20500	4700	2240	12	1800	39	63
06DTMMI-05A	15000	3600	548	21	800	35	60
06DTMMI-06A	19400	6200	300	11	1600	40	129
06DTMMI-07A	20600	6100	200	11	2400	63	164
06DTMMI-08A	19200	6100	218	9	4500	42	217
06DTMMI-09A	26600	6500	148	4	2900	38	85
06DTMMI-10A	21700	5400	146	5	5300	41	81
06DTMMI-11A	25600	8200	50	8	1600	53	356
06DTMMI-12A	21600	7400	71	7	2300	50	1600
06DTMMI-13A	19900	5600	846	9	2700	107	187
06DTMMI-14A	21400	5600	356	18	800	81	192
06DTMMI-15A	20000	5700	559	12	3200	85	160
06DTMMI-16A	18700	5600	279	12	3000	55	209
06DTMMI-17A	23600	6000	714	9	5000	111	144
06DTMMI-18A	28400	6100	47	4	1100	36	49
06DTMMI-19A	17600	5400	239	8	2600	56	242
06DTMMI-20A	13300	3900	344	13	6400	32	49900
06DTMMI-21A	20600	6000	140	9	1900	59	864
06DTMMI-22A	23900	6800	257	13	1300	76	1280
06DTMMI-23A	21700	6300	106	5	3000	35	311
06DTMMI-24A	23700	6500	253	23	1600	154	890
06DTMMI-25A	20600	5900	184	16	600	68	807
06DTMMI-26A	20200	6000	210	6	8300	31	89
06DTMMI-27A	24000	6900	89	11	1100	47	240
06DTMMI-28A	21100	7200	147	9	1600	53	159
06DTMMI-29A	19500	6600	221	8	1100	54	133
06DTMMI-30A	24700	9400	40	6	700	50	69
06DTMMI-31A	23400	8900	161	9	4000	34	41
06DTMMI-32A	21100	6900	179	8	4700	45	58
06DTMMI-33A	20400	7000	1775	7	7100	28	26
06DTMMI-34A	20600	6600	117	6	2100	30	44
06DTMMI-35A	18600	6300	155	11	1200	56	137
06DTMMI-37A	19900	11000	752	5	1900	39	25
06DTMMI-38A	22400	10800	433	10	2500	65	83

MMI Sample #	S	Sb	Se	Sr	Ti	V	Zn
Units	ppm	ppm	ppm	ppm	ppm	ppm	ppm
06DTMMI-01A	5200	8	-99	410	1700	82	1460
06DTMMI-02A	1600	10	-99	56	3800	606	171
06DTMMI-03A	600	11	-99	92	3200	543	915
06DTMMI-04A	1200	11	-99	51	2900	433	306
06DTMMI-05A	1100	19	-99	26	1900	569	333
06DTMMI-06A	600	10	-99	48	4000	447	312
06DTMMI-07A	1100	8	-99	62	3500	473	499
06DTMMI-08A	400	7	-99	103	3500	373	394
06DTMMI-09A	400	6	-99	69	3500	366	208
06DTMMI-10A	500	5	-99	117	3400	343	275
06DTMMI-11A	1500	8	-99	51	3700	533	623
06DTMMI-12A	700	6	-99	66	3700	395	723
06DTMMI-13A	600	5	-99	97	3000	489	635
06DTMMI-14A	500	12	-99	39	3200	450	435
06DTMMI-15A	500	6	-99	91	3200	410	460
06DTMMI-16A	600	5	-99	89	3400	393	369
06DTMMI-17A	800	5	-99	148	2900	456	503
06DTMMI-18A	300	2.5	-99	34	3800	375	381
06DTMMI-19A	1000	2.5	-99	78	3200	334	937
06DTMMI-20A	2000	9	-99	154	2000	364	18600
06DTMMI-21A	500	8	-99	54	3300	403	817
06DTMMI-22A	500	13	-99	42	3900	488	1130
06DTMMI-23A	400	2.5	-99	70	3700	429	458
06DTMMI-24A	700	8	-99	53	2900	390	1680
06DTMMI-25A	600	9	-99	45	3500	829	1840
06DTMMI-26A	1100	5	-99	196	2900	276	748
06DTMMI-27A	800	7	-99	41	3800	577	438
06DTMMI-28A	400	6	-99	51	3500	368	842
06DTMMI-29A	300	7	-99	38	3800	336	515
06DTMMI-30A	1300	7	-99	32	3600	384	428
06DTMMI-31A	700	5	-99	131	3500	309	333
06DTMMI-32A	400	6	-99	129	2900	312	483
06DTMMI-33A	900	2.5	-99	186	2800	269	240
06DTMMI-34A	600	5	-99	67	3500	407	206
06DTMMI-35A	500	8	-99	51	3300	440	446
06DTMMI-37A	500	2.5	-99	57	2600	119	209
06DTMMI-38A	500	6	-99	75	3400	302	522

Appendix G: Terrestrial Cosmogenic Nuclide Data

Sample #	Latitude (o)	Longitude (o)	Elevation (m.a.s.l.)	Sample Thickness (cm)	Density (g/cm2)
06YUK-1	62.76	129.70	1436	2.3	2.7
06YUK-3	62.77	129.65	1496	2.5	2.7
06YUK-4	62.77	129.65	1506	2.5	2.7
06YUK-5	62.77	129.65	1508	2	2.7

	Shielding Correction (topography and snow)	Erosion Rate (cm/yr)	Concentration Be10 (atoms/g)	+/- (atoms/g)
06YUK-1	0.951	0.0003	170260	4046
06YUK-3	0.964	0.0003	358174	8394
06YUK-4	0.958	0.0003	243960	5837
06YUK-5	0.956	0.0003	537304	22902

	Thickness Scaling	Production Rate Muons (atoms/g/yr)	Internal Uncertainty (yr)	Exposure Age (yr)	External Uncertainty (yr)	Production Rate Spallation (atoms/g/yr)
06YUK-1	0.9808	0.331	228	9339	862	18.37
06YUK-3	0.9792	0.338	468	18962	1795	19.54
06YUK-4	0.9792	0.339	314	12673	1181	19.58
06YUK-5	0.9833	0.34	1343	29050	3044	19.66

	Desilets et al. (2003-2005)		Dunai (2001)		Lifton et al. (2005)		Lal (1991)/Stone (2000)	
	Age (yr)	External Uncertainty (yr)	Age (yr)	External Uncertainty (yr)	Age (yr)	External Uncertainty (yr)	Age (yr)	External Uncertainty (yr)
06YUK-1	9897	1192	9801	1176	9354	954	9574	865
06YUK-3	20086	2488	19824	2444	18864	1974	19452	1805
06YUK-4	13406	1631	13254	1606	12665	1304	12995	1186
06YUK-5	30808	4111	30352	4031	28773	3289	29820	3074

	Age (no erosion) (yr)	External Error (2o precision) (yr)	Internal Error (2o precision) (yr)
06YUK-1	9453	225	1054
06YUK-3	18665	440	2085
06YUK-4	12690	305	1417
06YUK-5	27840	1194	3274

Age (erosion corrected) (yr)	External Error (2o precision) (yr)	Internal Error (2o precision) (yr)
9684	473	2215
19591	967	4604
13108	650	3027
29978	2772	7621